TOOL POSITIONING ALGORITHMS FOR IMPROVED MACHINING OF TRIANGULATED SURFACES

A thesis submitted in fulfillment
of the requirement for the award of the degree of

DOCTOR OF PHILOSOPHY

Submitted by

RAVINDER KUMAR DUVEDI

Registration No.: 950808011

Under the supervision of

Dr. Sanjeev Bedi
Professor
Dept. of Mech. & Mechatronics Engg
University of Waterloo
Waterloo, Ontario
Canada

Dr. Ajay Batish
Professor & DoCA
Mechanical Engineering Department
Thapar University
Patiala
India

DEPARTMENT OF MECHANICAL ENGINEERING
THAPAR UNIVERSITY, PATIALA-147004, PUNJAB, INDIA

September – 2015

Dedicated to

Their Lordships Sri Sri Radha Krishna

for giving me wonderful company of family,

friends and mentors

CERTIFICATE

I, Ravinder Kumar Duvedi hereby certify that the work presented in this thesis report entitled **"TOOL POSITIONING ALGORITHMS FOR IMPROVED MACHINING OF TRIANGULATED SURFACES"** in fulfillment of requirement for the award of degree of **Doctor of Philosophy** submitted in Mechanical Engineering Department, Thapar University Patiala, is an authentic record of my own work carried out under the supervision of **Dr. Sanjeev Bedi** (Professor, Department of Mechanical and Mechatronics Engineering, University of Waterloo, Ontario, Canada) and **Dr. Ajay Batish** (Professor and Dean of Contemporisation and Accreditation, Mechanical Engineering Department, Thapar University, Patiala) from July 2009 to July 2015. The matter presented in this thesis has not been submitted either in part or full to any other University or Institute for the award of any other degree.

Ravinder Kumar Duvedi

Registration No.: 950808011

Date: September 28, 2015

It is certified that the above statement made by the student is correct to the best of our knowledge and belief.

Date: 26/Sept/2015.

Dr. Sanjeev Bedi
Professor
Deptt. of Mech. & Mechatronics Engg
University of Waterloo, Waterloo, Ontario
Canada
Supervisor

28/9/15.

Dr. Ajay Batish
Professor & DoCA
Mechanical Engineering Department
Thapar University, Patiala
India
Supervisor

ACKNOWLEDGEMENT

I am grateful to the Almighty God for giving me the opportunity and strength to serve the cause of education and enabling me in digging a few concepts presented in this thesis work which may be helpful in some way for the welfare of humanity.

It gives me immense pleasure to have an opportunity to express humble feelings of gratefulness and submit my acknowledgements for those who helped me earn this day. First and foremost, I wish to express my deep sense of gratitude with reverence towards my supervisors **Dr. Sanjeev Bedi** (Professor, Department of Mechanical and Mechatronics Engineering, University of Waterloo, Ontario, Canada) and **Dr. Ajay Batish** (Professor and Dean of Contemporisation and Accreditation, Mechanical Engineering Department, Thapar University, Patiala), for their valuable guidance and inspiration in pursuance of this work. Despite their busy schedule, they always spared time for me. Their able and valuable guidance always kept me on the right track. I shall remain grateful to my supervisors for providing me remarkable support throughout this thesis work. I am highly obliged to Dr. Ajay Batish for enabling me get the opportunity to work with Professor Sanjeev Bedi under a Thapar University and University of Waterloo collaborative research program. His encouragement is the only reason I could prepare myself for this across the continent PhD project. I am highly indebted to Dr. Sanjeev Bedi for his support provided for getting Canadian Commonwealth Fellowship during December 2010 to July 2011 which enabled me work in his close association in 5-axis machining lab in University of Waterloo, Canada. This opportunity enriched me with many thoughts while working in the great research environment in his association at university of Waterloo, Canada, where I could get the glimpse of the genius research ideas Prof. Sanjeev Bedi has nurtured for long. His systematic approach and unconditional support provided to me around the clock is the only reason for the successful accomplishments achieved during the course of this thesis work. It is great pleasure working with him and he is the reason I shall cherish this work forever during my lifetime. For me it is the beginning of research and I wish for continuous guidance from Prof. Sanjeev Bedi for my future research endeavors. I shall remain grateful to him forever.

I am very grateful to Dr. Stephen Mann, Associate Professor, Computer Science Department, University of Waterloo, Canada for his expert support extended in form of critical review of the developments carried out during this work as well as by the way of his expert ideas

provided to me in the area of CAD, CAM and geometric modeling. I am grateful to him for allowing me the use of the multi-axis graphical NC simulator developed by him which has been extensively used for verification of the program codes developed during this work.

I feel extremely blessed to have great company of friends and colleagues in Thapar University who supported me in many ways during this thesis work. I am very thankful to Dr. S. K. Mohapatra, Senior Professor & Head, Mechanical Engineering Department, Thapar University for his extended help provided for getting the required resources for this work as well as excellent academic environment and encouragement throughout this thesis work.

I am grateful to Dr. V. K. Jadon, Professor, Mechanical Engineering Department, Chitkara University, Rajpura, Punjab, for his constant mentoring and guidance. I am very thankful to Dr. Sandeep Sharma, Assistant Professor, Mechanical Engineering Department, Thapar University for his encouragement and sincere advice given time to time which kept me focused during the present thesis work. I express my sincere gratitude to Mr. A. S. Jawanda, Associate Professor, Mechanical Engineering Department, Thapar University for his being a great teacher, colleague and friend to me. I express my sincere thanks to Dr. Rajneesh Bassi (PhD student of Prof. Sanjeev Bedi) for his support both technical as well as for making us feel at home in the beginning of this PhD work during my stay in Canada in 2010-11. The company of Mr. A. S. Jawanda and Dr. Rajneesh Bassi, during our stay at University of Waterloo, Canada is memorable. Their motivation and support in the form of ideas in the area of CAD were of great help.

I am very thankful to all my colleagues in Mechanical Engineering Department and Central Workshop, Thapar University for their help and support, especially Dr. J. S. Saini, Mr. Supreet Bhullar, Mr. Sumit Sharma, Dr. Tarun Nanda, Mr. Devender Kumar, Mr. Daljit Singh, Mr. Sohan Lal, Mr. Gian Singh (Retd.), and Mr. Lalit Kumar for their encouragement and support extended during this work.

I am also grateful to the Dr. Prakash Gopalan, Director, Thapar University, for his motivating words and providing the resources required to accomplish this research work. My sincere thanks are also due to Dr. Sushil Mittal, Deputy Director, Thapar University and Dr. O.P. Pandey, Professor and DoRSP, for giving me constant encouragement and co-operation in pursuit of this thesis work.

I am indeed indebted to my parents, Sh. S. K. Duvedi and Mrs. Leela Duvedi who have been very generous and exceptionally supportive for my studies since my childhood. The values they have imbibed in me along with their moral support have made me reach this mild stone. I am also thankful to my parent in-laws, Sh. Dharam Pal Shrama and Mrs. Sudesh Sharma for encouraging and supporting me during this work. I acknowledge my heartiest gratitude to my loving wife Ms. Monika Sharma, without whose untiring support, enduring patience and continuous motivation I could not complete this work successfully. I owe special thanks and love for my little angles Vrinda Sharma and Rit Pragya Dwivedi for having a lot of patience waiting this very day. I really regret troubling them by my long working days. I express my sincere thanks to my brothers Mr. Rajiv Duvedi, Mr. Raheesh Duvedi, and sisters-in-law Ms. Mukti Sharma and Ms. Rituka Sharma for their support provided in many ways during this work.

I also thank all my fellow friends, colleagues, all my B.E. and M.E. students and relatives who directly or indirectly helped me during this thesis work. Last but not the least, I wish to express my thanks to all those who remained behind the screen but whose work has been quoted and consulted in the present research.

Ravinder Kumar Duvedi **Dated: 28 September, 2015**

ABSTRACT

Multipoint 5-axis machining (MPM) with a radiused end mill is ideal for efficient machining of sculptured surfaces. Multipoint tool positioning using radiused end mill cutter is challenging especially when the input part geometry is taken in parametric form. Known methods use optimization techniques to determine the orientation of the tool axis relative to an orthogonal coordinate system. These optimization methods result in higher order transcendental equations that have many solutions, are ill behaved and lack robustness.

This thesis presents a method for multipoint machining of sculptured surfaces that is robust, reliable and can be implemented in an environment that is usable in industry. The method is based on a new concept in which the tool positioning is divided into two steps. In the first step the tool is dropped along a fixed axis onto the part surface and in the second step the tool is rotated onto the part surface in a manner that maintains the first point of contact. This sub-division of the tool positioning method into two steps reduces the complexity of the resulting equations. To further simplify the mathematical model, the surface of the part is modeled as a series of connected triangles. The triangulation allows the piecewise representation of the surface to any desired accuracy, thereby simplifying the toolpath generation equations. The impact of the simplification of the part surface definition is that at each tool position numerous checks involving faces, edges and vertices have to be done. Although the number of computations increases, their complexity reduces.

The proposed method is called, Drop and Tilt Method (DTM). The detailed concept of DTM approach is presented in chapter 3 and the solutions of the mathematical model are obtained using a symbolic algebra package. This implementation is used to develop and test the toolpaths for a number of test parts. These test parts are validated in simulation and by machining of sample parts.

In the next step a new method for numerical implementation of DTM, that does not require a symbolic environment, is developed. The numerical DTM method uses a Bisection algorithm in conjunction with the generalized tool drop algorithm and tilt about pseudo-insert axis algorithm to determine the 5-axis tool position. The numerical DTM method is computationally faster compared to the original analytical DTM method. The complete mathematical model used for numerical implementation of Drop and Tilt method is presented

in chapters 4 and 5 along with sample toolpaths developed for test models that are used to validate the proposed model in simulation and with machined samples.

The edge-torus tangency found in the numerical implementation is computationally expensive and thus, an efficient method for edge-torus tangency is developed. The developed edge-torus tangency model is presented in chapter 6 along with the testing and validation of this new edge-torus tangency model.

Overall, the DTM method is computational simple and efficient method for generating the toolpaths for 5-axis machining of the triangulated models. The accuracy of the developed 5-axis tool positioning method is tested in simulation and by actual machining of various test parts using DMG 80-P Hi-Dyn 5-axis tilt-rotary table CNC machine. The simulations and machining results confirm that the method is suitable for industrial use.

CONTENTS

LIST OF PUBLICATIONS AND PATENTS FILED

1. Duvedi R.K., Bedi S., Batish A., Mann S. (2014) A multipoint method for 5-axis machining of triangulated surface models, Computer-Aided Design, Elsevier, 52:17–26, **DOI: 10.1016/j.cad.2014.02.008**
2. Duvedi R. K., Bedi S., Batish A., and Mann S. (2015) Numeric Implementation of Drop and Tilt Method of 5-Axis Tool Positioning for Machining of STL surfaces, International Journal of Advanced Manufacturing Technology, Springer-Verlag London, 78:1677–1690, **DOI: 10.1007/s00170-014-6636-3**
3. Duvedi R. K., Batish A., Bedi S., Mann S. (2015) Scallop Height of 5-axis Machining of Large Triangles with a Flat End Mill, Presented at 11th International CAD conference 2014 at HKUST, Hong Kong and published in Computer Aided Design and Applications, Taylor and Francis, Published online: 30 April 2015, **DOI: 10.1080/16864360.2015.1033334**
4. Duvedi R. K., Batish A., Bedi S., Mann S. (2015) A method for simplifying edge-torus tangency in drop-tilt method for 5axis machining of triangulated surfaces, Accepted for the plenary presentation at the 4th International Symposium on NC Machining (CNCM 2015, http://cncm2015.ust.hk/index.html), June 3-5, 2015 at Hong Kong University of Science and Technology, HK, China.
5. Duvedi R. K., Bedi S., Batish A., and Mann S. (2015) The Edge-Torus Tangency Problem in Multipoint Machining of Triangulated Surface Models, International Journal of Advanced Manufacturing Technology, Springer-Verlag London, Published online 18th July, 2015, DOI 10.1007/s00170-015-7532-1

INDIAN PATENTS APPLIED

S. No.	Inventors	Applicant	Name & Title of Patents	Application reference number
1	1.Ravinder Kumar Duvedi 2.Dr. Sanjeev Bedi 3.Dr. Stephan Maan 4.Dr. Ajay Batish	Thapar University, P.O Box 32, Patiala-147004, India	Drop and tilt method of tool positioning for 5-axis machining of triangulated surfaces	064/DEL/2014 filed on 18/04/2014

ABBREVIATIONS USED

2D : Two Dimensional

3D : Three Dimensional

AIM : Arc Intersect Method

APT : Automatically Programmed Tool

CAD : Computer Aided Design

CAM : Computer Aided Manufacturing

CNC : Computer Numeric Control

CC : Cutter Contact

CL : Cutter Location

CSG : Constructive Solid Geometry

DTM : Drop and Tilt Method

MPM : Multipoint Machining Method

NC : Numerical Control

NURBS : Non-Uniform Rational B-Spline Surface

PAM : Principle Axis Method

PEM : Penetration Elimination Method

RBM : Rolling Ball Method

STL : Stereo Lithography

LIST OF FIGURES

LIST OF TABLES

CHAPTER 1
INTRODUCTION

1.1 INTRODUCTION

Sculptured surfaces form an integral part of our lives. The shape of the automobiles bodies, artistic furniture items, toys, fashion accessories, electronic items, automobiles are some of the examples of objects which are generally found rich with sculptured surfaces/features. In addition to the aforesaid parts, dies and moulds used for manufacturing such parts also have sculptured shapes. The 3-dimensional (3D) models of parts with sculptured surfaces can be developed mathematically or by reverse engineering. Mathematically defined surfaces are based on a mathematical formulation and the reverse engineered surfaces are used to model physical artifacts. In the automotive industry both methods are used. There are several techniques available these days to mathematically model complicated sculptured surfaces in the 3D CAD environment. In reverse engineering, the sculptured surfaces are developed manually using clay before they can be digitized. The digitized data is then used to model the surface in a 3D CAD system. For most manufacturing processes, like machining, rapid prototyping etc., the sculptured surfaces must be represented using 3D models.

The most commonly used method for creation/realization of the sculptured products is through either using multi-axis machining method to crave such part shapes directly from raw stock or by first creating the dies for such parts shapes. In either case the machining of accurate sculptured shapes is of foremost importance and is discussed in details in the subsequent sections.

1.2 MACHINING OF SCULPTURED SURFACES

The accurate and efficient machining of complex sculptured surfaces cannot be achieved with the traditional manual machining methods. In recent years computer numeric control (CNC) technology has been used in the manufacturing industry to machine complex sculptured surfaces with desired accuracy and repeatability. The main advantages offered by CNC machining are: significant reduction in manufacturing time; relatively simple setup procedure; improved accuracy and repeatability of machining; and the ability to machine parts without using complicated machining fixtures.

A typical CNC machining system basically consists of three main components namely: CNC machine tool (also known as CNC machining centers); CNC control system; and NC part program. Whereas the CNC machine tool uses high precision drives for accomplishing accurate motion of cutting tool with respect to the part, the CNC control system uses the electronic and electrical systems for interface with various components of CNC system namely computer and the electrical drives. The CNC controller also acts as an interface between the human operator and the machine tool to monitor, actuate and control the functions of a CNC machining center.

To accurately machine the desired sculptured shape from the raw material stock, with the optimal use of available resources, the user of CNC technology must have access to two most important components of CNC systems, namely: the multi-axis machining center which can be used for machining of sculptured surfaces and an accurate NC part program. These two aspects are discussed in detail below.

1.2.1 Multi-axis machining center

The most common CNC machining centers used in modern day manufacturing industries are 3-axis and 5-axis machining center. A typical 3-axis CNC machining center is a vertical milling center which can move a cutting tool along three mutually orthogonal directions relative to the part to be machined. The movement of the tool can be controlled by synchronized motion of the three machine drive axis. Though 3-axis CNC machining centers have been generally used for machining of complex engineering parts, in recent times the use of 5-axis machining centers has increased. The main advantage of 5-axis machining centers is the additional ability to tilt the tool about two of the machine axis. Many researchers have used the flexibility of 5-axis machines to generate tool positioning data which enables the cutter to achieve the closest possible proximity to the desired machined surface. Thus, the key advantage in 5-axis machining is that the toolpaths result in a wider strip around the trajectory of the point of contact that meet the user specified machining tolerance. This reduces the number of passes required to machine the entire part surface. 5-axis machining centers can machine the desired sculptured surface faster compared to a 3-axis machine particularly in finish machining and in certain cases the machining time can be reduced by as much as 80% [1, 13]. While the use of 5-axis CNC machining centers offers the advantage of efficient machining of complex sculptured surfaces at the same time the development of NC

toolpath data for accurate and efficient 5-axis machining of sculptured surfaces is a great challenge [63-69].

It is almost impossible to generate an absolute error free sculptured surface with any type of multi-axis machining strategy. Although 5-axis machining techniques are capable of providing relatively better surface machining properties than 3-axis machining systems [41, 54, 106], but they require more complicated machine tool and CNC control logics for executing the 5-axis tool positioning. Moreover, the determination of toolpath information for 5-axis machining is complicated especially for machining of compound surfaces which need to be machined with complex cutter shapes like radiused end mill cutters or profiled tools to achieve better machining accuracy and efficiency.

1.2.2 NC part program

NC part program is a code for a typical CNC controller. The CNC controller decodes the NC part program and actuates necessary control functions on the CNC machining center. A typical NC part program contains two types of commands. The first set of commands are used for initializing the machine settings or activating/executing the necessary auxiliary control functions of the CNC system like control of spindle rotation, control of feed rate for various machine drives, setting the tool geometry information, tool change, and coolant control etc. The second important set of commands in an NC part program is called cutter location (CL) data or simply toolpath data. The toolpath data is a sequential collection of information about the position and/or orientation of the cutting tool with respect to the part surface and it is used to move the drives of a CNC machining center to locate the cutting tool relative to the workpiece to perform the desired machining operation.

The toolpath data for machining of sculptured surfaces cannot be created manually, and a number of automated toolpath algorithms have been developed over last few decades for efficient machining of the required 3D part model. For a selected precision machine tool (3-axis or 5-axis) and predetermined machining parameters (for work piece and tool material combination like feed rates and cutting speeds), the accuracy of the finish machined part primarily depends on the accuracy of the CL data or toolpath data. The machined surface can never be more accurate compared to the toolpath data used to machine it. In turn, the accuracy of the toolpath data can never be better than the accuracy of the 3D part data and the accuracy of automatic mathematical algorithms used to generate it. In addition there are

certain key issues that have direct implication on determination of accurate and efficient toolpath data, as well as on the precise execution of toolpath data on a multi-axis machining center which includes: cutter geometry, toolpath footprint patterns or toolpath topologies, dynamic stability of machine tool elements including the cutting tool, surface finish or machining tolerance requirements, type of machining operation whether roughing, semi-finishing or finishing etc. The roughing and semi finishing machining operations do not require high surface finishes and the objective of such operations is the high material removal rate within the permissible rigidity of the machine tool and the cutting tool. At the same time, the requirements from the finishing toolpath data are comparatively stringent particularly in terms of surface finish and overall time required for finishing operation. In the present work the focus is for development of efficient toolpath data for 5-axis finish machining, thus the issues pertinent to the 5-axis finish machining are highlighted in the following sections.

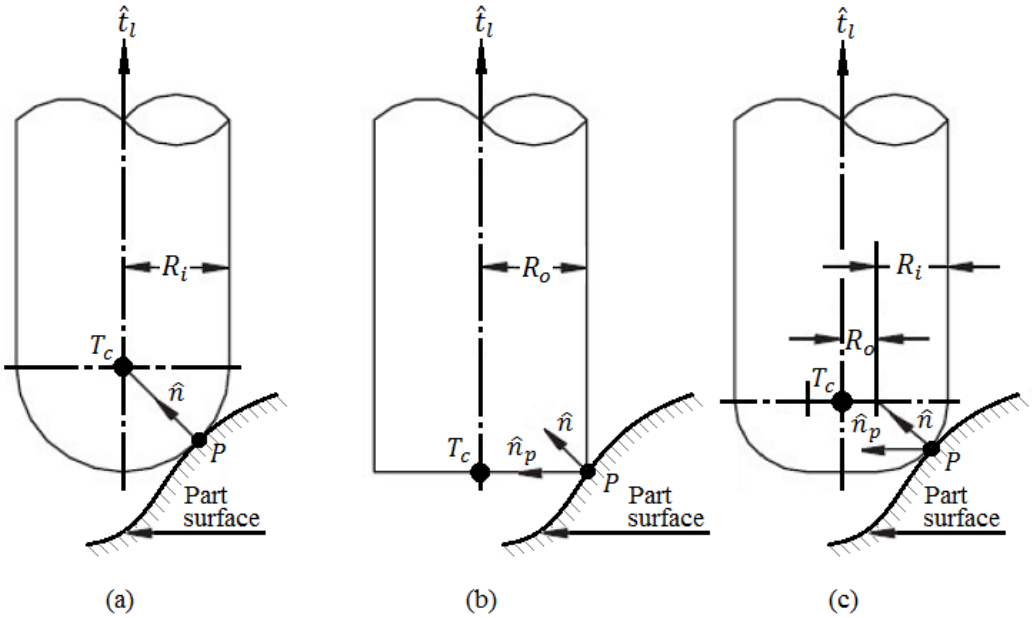

Figure 1.1: The concept of cutter contact (CC) point and cutter location (CL) point for: (a) ball end mill, (b) flat end mill, (c) radiused end mill cutter.

1.3 CUTTER CONTACT (CC) AND CUTTER LOCATION (CL) POINTS

The choice of correct toolpath computation method, for determining toolpath data for finish machining of the sculptured surfaces, is the driving factor for the accurate determination of the cutter contact (CC) and cutter location (CL) positions. The CC point by definition is the location of contact between the machining surface of a cutting tool and the part surface, whereas the CL point denotes the location of a suitable pre-identified point on the cutting tool (generally on the tool axis) which is used as reference for positioning and/or orientating the cutting tool. Figure 1.1 shows the concept of CC point and CL point for most commonly used tool shapes for sculptured surface machining, which are: a ball nosed, flat and radiused end

mill cutters. Point T_c is the CL point, P is the CC point and the vectors $\hat{t}_l$, $\hat{n}$, $\hat{n}_p$, R_i, and $R_o$denotes the retract direction of tool or tool-axis direction vector, the surface normal at CC point, the direction vector representing the projection of surface normal on a plane normal to tool-axis, the radius of ball end mill or corner/ minor radius for radiused end mill and radius of flat end mill or offset/ major radius for radiused end mill respectively. The parameters R_i, and R_o are also known as insert radius and radius of center of radiused end mill, and represent the radius of minor and major circles of the torus that models the cutting surface of the radiused tool. The cutter shapes of a ball, a flat and a radiused end milling cutters commonly used in surface machining applications are shown in figure 1.2.

(a) **(b)** **(c)**

Figure 1.2: Geometry of a tool used for surface machining: (a) ball nosed end mill, (b) flat end mill, and (c) a radiused end milling cutters.

The accurate determination of CC points is instrumental for finding the gouge free CL points. The CL points, which are also known as tool locations or tool positions, are strung together in a logical order to form the toolpath. Thus the objective of the toolpath planning strategies is to determine a string of CL points corresponding to CC points, which should result in accurate machining of the desired part surface. The accurate determination of CC and CL point data for particular cutting tool geometry depends directly on the accuracy of representation scheme used for 3D part model and the type of mathematical model used for computation of the toolpath data. The types of 3D part data formats and the toolpath planning methods available are discussed in the following sections.

1.4 PART MODEL DATA FOR TOOLPATH PLANNING

There are several data formats that are being used to represent the 3D part model information within a commercial CAD (computer aided design) packages, but for NC toolpath planning the features of the complex data formats are not needed. The available CAD data formats are first translated into simpler data formats to be used by toolpath algorithms or CAM (computer aided manufacturing) packages. Generally the CAM packages/ toolpath algorithms make use

of three kinds of data formats for generating the toolpath data for machining of sculptured surfaces and these are discussed below:

1.4.1 Parametric surface patches

For most industrial objects the precise machining of part surfaces with good surface finish is important. To achieve this, most of the toolpath algorithms use the mathematical representation of the sculptured surfaces for precise computation of the CC and CL points. Most sculptured surfaces are composed of several non-parametric and parametric patches joined together to form a 3D object. The non-parametric surfaces include the plane surface patches (triangular/ rectangular), cylindrical or spherical surfaces, surfaces of revolution etc. The parametric category includes surfaces such as Hermite, Bezier and Non-uniform rational B-spline surfaces (NURBS) etc. These types of surfaces make use of geometric handles called control points to shape the geometry of the part surface. The designer can manipulate these control point handles to build the desired surface. The various parametric or non-parametric surface patches can be put together with C_0 (positions), or C_1 (gradients), or C_2 (curvature) continuities to represent a curved surface. The surface continuity allows different surface patches to be joined together edge-to-edge with position, slope, and second derivative etc. continuity at all point along the edge. These geometric continuities require the corner points, gradient vectors, and twist vectors to match between the constituent patches. Thus the mathematical model, used to represent the parametric sculptured surfaces is quite complicated and it is the input used for computation of toolpath data for such surfaces.

1.4.2 Free-form surfaces

Free-form surfaces are reverse engineered from physical models. The surfaces or objects are crafted manually and the developed part surface is scanned and digitized to create a cloud of points that lie on the surface. This set of point cloud can be directly used for computation of CC and CL points for NC toolpath generation [70-75]. Though the 3-axis toolpath computation for point cloud data is very efficient, the accuracy of the toolpath data is dependent on the density of the scanned data set and the noise in the collected data. High point densities are required for computation of accurate toolpaths. The point cloud data is not directly suitable for 5-axis machining because noise in the data can cause abrupt change in tool position and orientation.

The scanned geometry is processed to generate either parametric compound surface/s that fit the scanned data points or are converted into a tessellation and the STL (Stereo Lithography) format is used to store them. A number of CAD applications support the development of freeform surfaces directly from the scanned point cloud data. These can be stored in parametric, non-parametric surface/s or faceted formats and can be translated as required by the downstream applications such as NC toolpath generation.

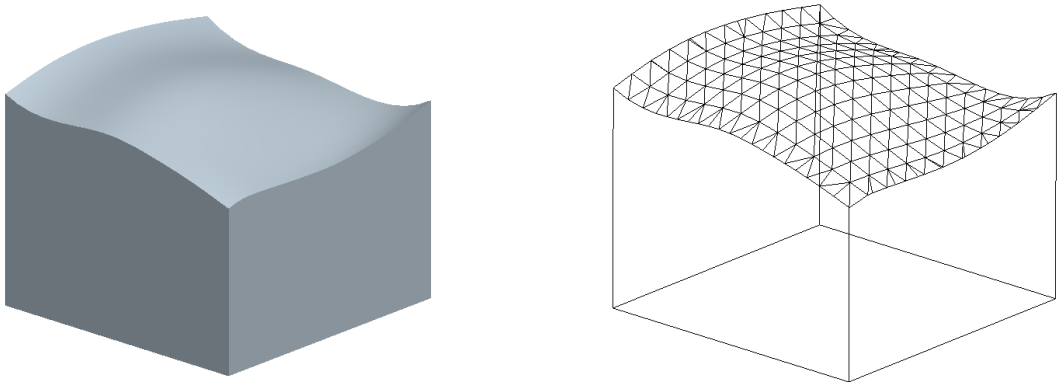

(a) (b)

Figure 1.3: (a) A freeform surface developed in CAD environment, and (b) corresponding STL representation.

1.4.3. Triangulated representation of sculptured surfaces

The sculptured surfaces can be suitably represented by tessellation in STL format. The tessellations or the triangulated meshes approximate the part model using the planer facets of varying sizes. The STL (also known as tessellated data) format is commonly used in rapid prototyping and many other reverse engineering applications. In STL data format the object is represented as a collection of connected triangles that share a common edge and touch each other along common vertices. The method ensures that the triangles do not touch each other at any other point. Since a planar surface is used to model a curved object, the model deviates from the original. However, by increasing the number of triangles that model an object the deviation can be reduced or controlled. Figure 1.3 (a) shows a 3D part model developed in CAD environment, having a freeform surface on its top face, and figure 1.3 (b) shows the STL model for the same part.

Most STL generators can produce models to user defined accuracy. Although the translation of 3D CAD data into STL data format filters out most of the associated CAD information, it can express the geometric details of the 3D part shape in a simple and accurate form [6, 33, 41]. The STL file has the information about the points representing the three vertices of the planer triangular patches and the direction of the unit surface normal vector in a direction pointing outwards from the front face. Because of its simplicity and wide application in

reverse engineering applications, the STL data format can be generated for all CAD models. Although the faceted representation of a 3D part model is never exact, it can help reduce the computational complexity of NC toolpath algorithms. Many NC toolpath planning approaches for 3-axis and 5-axis machining have been investigated which use the faceted part model data [12, 18, 20, 30-69, 117-118, 120].

1.5 GOUGING AND INTERFERENCES IN MULTI-AXIS MACHINING

An ideal toolpath should be free of tool gouging, interference and collision. Checks must be performed to detect and avoid gouging, interference, and collisions; especially in 5-axis machining to ensure the accurate and safe execution of machining operation [1, 19-20, 54, 114, 119-120].

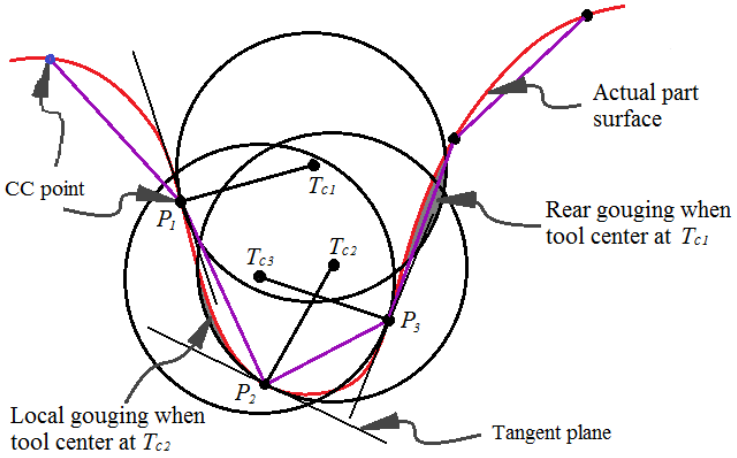

Figure 1.4: Gouging resulting from tool offset in concave region of a parametric surface.

There are three possible ways in which a cutting tool may gouge the design part surface, which are classified as local gouging, rear gouging and global gouging [19, 54]. The local gouging occurs when a cutting tool plunges into the design surface at the CC point beyond a user specified tolerance. One common reason responsible for local gouging is the inaccurate mathematical model used to find the CC point. The rear gouging is caused when the tool plunges the workpiece on the side diametrically opposite to the CC point. The rear gouging in a concave region of a parametric surface machined with a ball end milling cutter is shown in figure 1.4.

The global gouging is caused when the non-cutting surface (or shaft) of the tool penetrates the work surface [20, 54, 117-120]. The toolpath data must be free from these three types of gouging for accurate machining of workpiece. The global gouging can be avoided in 3-axis machining to an extent while its identification is a challenge in case of 5-axis machining. The

gouge free toolpath determination for complex mathematical/ parametric representation of 3D part models is difficult because these methods do not take into account the surface geometry around the CC point. The inability to integrate the tool positioning and gouge avoidance techniques together for toolpath generation is also one of the reasons for tool gouging the design part surface [54, 120].

To generate an ideal toolpath information one should carefully consider the removal of possible tool gouging and interferences. There are a number of techniques available for identification of tool gouging and interferences. The feasibility cone method and configuration space method are considered to be one of the most effective methods for global gouge and collision avoidance [20]. In 5-axis toolpath planning methods the local gouging is identified by approximating the parametric surface under tool shadow close to first CC point by triangular facets. Several techniques for collisions detection and avoidance are discussed and compared by Tang [120] in his review work.

1.6 TOOLPATH FOOTPRINT PATTERNS FOR SCULPTURED SURFACE MACHINING

One of the important criteria which directly affect the efficiency of finish machining of sculptured surfaces is the appropriate selection of the toolpath footprint pattern. In typical 3-axis or 5-axis machining operation, the toolpath footprint pattern describe the direction of motion of the rotating end milling tool as it carves the part out of the raw stock efficiently as well as with the required surface finish [20, 23]. For identifying a toolpath footprint a region, typically a polyhedron that engulfs the part, to be machined is identified by the user. This region is projected onto a plane perpendicular to the tool axis (typically perpendicular the z-axis).

The typical footprint pattern shapes which are generally used are contour parallel, contour offset, iso-planer, spiral, raster, space filling curves and zigzag [6, 12, 20, 23, 85]. A lot of work has been carried out to examine the effect of footprint patterns on machining efficiency and it has been established that the selection of the footprint patterns is governed by the overall shape of the design surface, the feed directions of the cutting tool, machining feed rate, the geometry of the cutting tool and the surface finish requirements [6, 8-12, 15, 17, 20-25, 30, 34, 38, 41, 43, 45-49, 51-53, 56-58, 61, 64, 68, 79, 82-86, 88-90, 104, 115, 117-118]. In a study published by Makhanov [23], the author has tested various forms of toolpath

patterns for sculptured surface machining and has reported that it is difficult to identify a single toolpath footprint pattern which can ensure simultaneously machining efficiency as well as good surface finish.

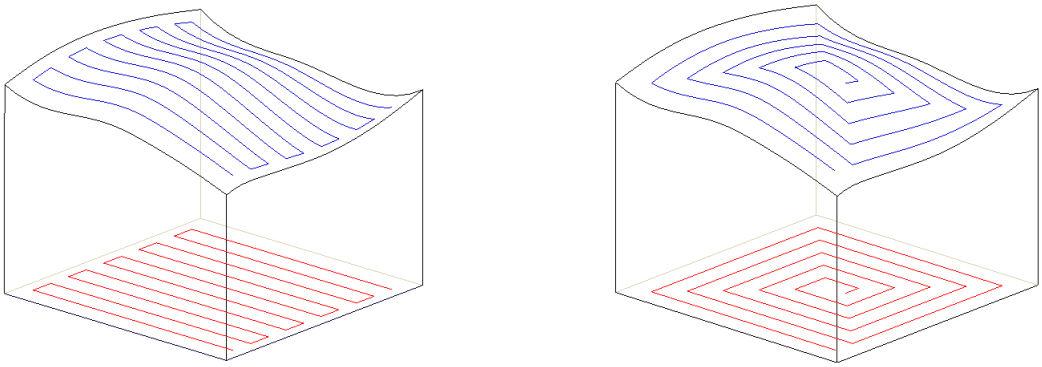

(a) (b)

Figure 1.5: Common toolpath footprint patterns used for sculptured surface machining (a) Zigzag pattern (b) contour pattern

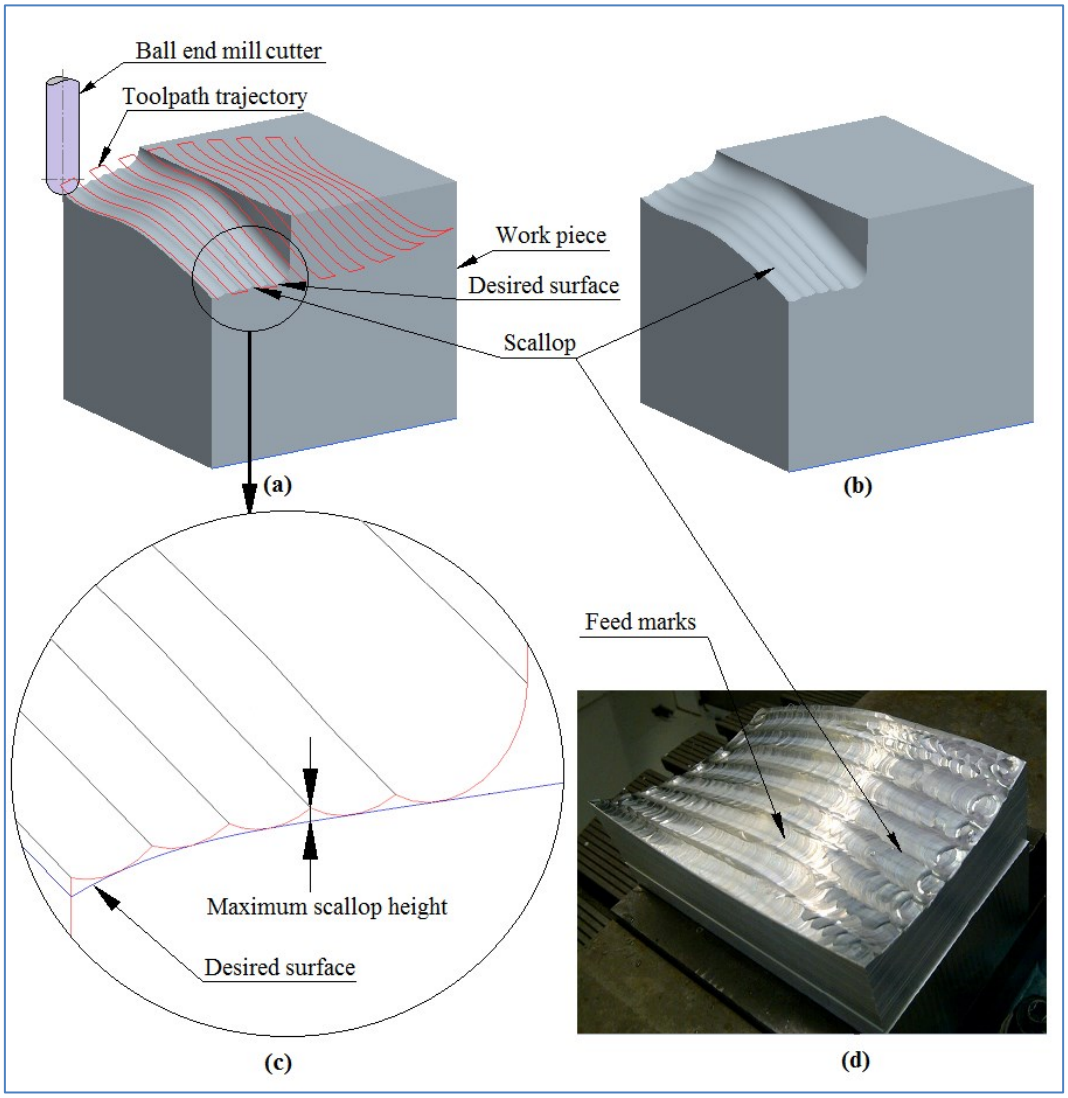

Figure 1.6: (a) Scallops generated by a ball nosed end mill with a zigzag pattern, (b) simulation of a part surface after five machining passes, (c) the scallop compared with the required part surface, and (d) scallops and feed marks on a part surface machined by a radiused end milling cutter [65].

It is desirable that the selected toolpath footprint pattern should generate the maximum surface finish, engage the cutting tool with uniform thickness of uncut material for avoiding fluctuation of cutting forces, should have minimum direction changes of the moving tool, and it should ensure minimum tool retractions. The zigzag and contour parallel toolpath pattern ensure minimum direction changes while moving the cutting tool in a chosen feed direction and this is the reason that most of 3-axis and 5-axis application for sculptured surface machining use the zigzag pattern or the contour parallel pattern as reported by Lasemi et. al. [20] and Kim and Choi [85]. The typical zigzag and contour parallel patterns are shown in figure 1.5. The spiral toolpaths ensure the minimum tool retractions and can ensure relatively better surface finish [64, 68, 83, 115], but the number of direction changes of the cutting tool slow down the overall machining process.

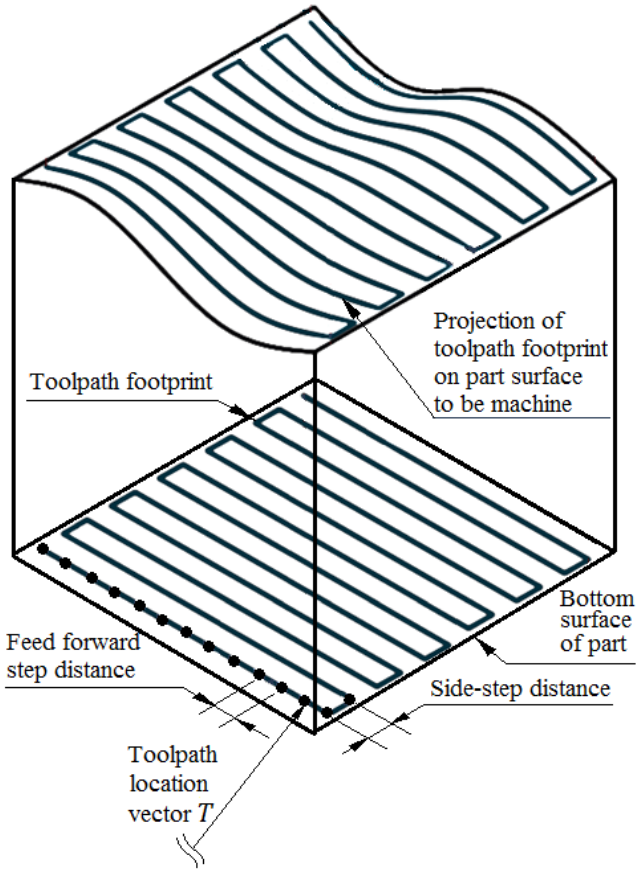

Figure 1.7: The zigzag toolpath pattern [63]

For selected cutting tool geometry, the surface finish obtained from an end milling operation depend upon the scallop height and the surface roughness generated by the feed marks left by the cutting tool while moving along the feed direction. As the tool moves along the toolpath, it leaves some material un-machined, which lies between two neighbouring tool passes. This un-machined material is known as a scallop. The uncut material or the impressions of the cutting edge of the tool between two feed-forward position causes feed marks. The typical

scallop height pattern while machining a sculptured surface with a ball end milling cutter in 5-axis machining simulation is shown in figure 1.6(a), (b) and (c), while the figure 1.6(d) shows the scallops and feed marks generated by a radiused end milling cutter in 5-axis machining [65]. The machined surface will always contain scallops between tool passes. The scallop heights are a function of the step-over distance as shown in figure 1.6(c). The magnitude of the surface roughness is measured along the feed direction is always much less than the scallop height generated if seen across the feed direction. In most cases scallops must be removed manually with hand polishing, which is a very tedious and time-consuming task. Thus it is very important to minimize the scallops especially in finish machining.

The discretization of a zigzag toolpath in side-steps and feed-forward steps is shown in figure 1.7. The decrease in side-step value will increase the number of machining passes while the decrease in feed-forward distances will increase the toolpath length within a particular toolpath direction. The side-step distance is a function of the curvature of the designed part surface and the curvature of the effective cutting edge of the tool when using a flat end mill or radiused end mill cutter. In 5-axis machining it is possible to match the effective curvature of the cutting edge of tool with the curvature of part surface under the cutting tool by choosing the proper cutter orientation, thus one can use wider side-steps in 5-axis machining compared to 3-axis machining. Similarly adaptive feed-forward discretization can help achieve higher machining feed rates without compromising the surface finish. Thus for a selected toolpath strategy, one can choose the side-step and feed-forward values to ensure a balance between surface finish and machining time.

Now, once the footprint pattern is defined along with the side-step and feed-forward discretization, the next step is to determine the gouge free CC points and thereafter the CL points for each of the toolpath footprint locations for the selected cutter geometry.

1.7 CUTTER GEOMETRY FOR MACHINING OF SCULPTURED SURFACES

The quality of a machined part is affected by the geometry of cutting tool used for 3-axis or 5-axis machining. In 5-axis machining the cutting tool remains in the close proximity to the desired part surface thereby removing more of the uncut material over the designed surface. The scallop height has a direct relation with the cutter geometry and the side-step between two machining passes. Suitably selected cutter shape can significantly reduce the scallop height even with large side-step and help reduce overall machining time [20, 41, 50, 58, 77-81].

The commonly used end milling cutters for sculptured surfaces machining are: ball nosed, flat end, and radiused end milling cutter. These three tool geometries are shown in figure 1.1 and 1.2. Each of these tool shapes has its merits and limitations for machining of sculptured surfaces. Out of these tool geometries, the ball end milling cutter is able to generate better surface finish for the part models having sharp changes in surface curvatures or geometry of the surface features [58, 62, 77]. This tool shape has better access to the narrow concave regions for material removal compared to the flat and radiused end milling cutter of the same diameter [58, 77]. A number of 3-axis and 5-axis tool positioning algorithms are developed for machining of parametric and non-parametric sculptured surfaces using ball end milling cutter [10, 30, 35, 41, 43, 46, 48-49, 51-53, 56-58, 61-62, 64, 71, 73, 74, 82, 98, 102, 112, 113, 115]. The toolpath planning for sculptured surfaces using ball end mill cutter is computationally easy, and one can get gouge free toolpaths using part information in faceted form of suitable accuracy [41, 43, 51, 57-58]. The limitation of ball end milling is that it needs large number of machining passes to minimize the scallops produced in surface machining operations, thus the machining operations with ball end milling cutters is not efficient. Using larger diameter ball end milling cutter can help reduce the scallop height and the machining passes in certain cases, but such a tool will be ineffective for machining of sharp features of sculptured part. Also the ball end milling tool cannot help in improving the machining efficiency even if used with 5-axis machining system, because the effective cutting edge of the ball end milling cutter does not change its shape with change in orientation of cutting tool with respect to part surface and in all orientations it remains spherical. Thus no benefit of tilt axes is achieved using ball end milling cutter. This is the reason the use of ball end milling tool for 5-axis machining is restricted to accessing the machining regions not accessible in 3-axis machining [67] and to avoid the scratch marks on machined surface caused by the zero cutting velocity region at bottom of the tool axis of a ball end mill cutter in 3-axis machining [61, 74, 82]. The benefit of 5-axis machining, which enables the cutting tool to achieve better proximity to the designed part surface at the CC points, can only be realized using flat end milling and radiused end milling cutters. Because of this reason, the flat end and/or radiused milling cutters are preferred for 5-axis machining. However, limited numbers of studies are conducted for positioning of flat and radiused end milling tools for 5-axis machining of faceted surfaces [6-7, 20, 34, 38, 50, 54, 63-69].

The flat and radiused end milling cutters are more effective compared to ball end milling cutter, in improving the efficiency and surface finish especially in case of 5-axis machining

of sculptured surfaces [20, 23-24, 43, 58, 62-63, 65- 69, 77-78, 89-90, 110]. In a comparative study of scallops produced by ball, flat and radiused end milling cutters, reported by Bedi et al. [77], it is shown that the scallops height produced by radiused and flat end milling cutter of same diameter are quite small compared scallops produced by ball end milling cutter.

It is also reported by Bedi et al. [77] that the 5-axis machining using radiused end milling cutter produces better surface finish along feed direction and smaller scallop height is achievable with relatively much wider side-step value. The merits of radiused end milling cutter over ball nosed and flat end milling cutters for 3-axis and 5-axis machining of sculptured surfaces is demonstrated by several other authors as well [1-8, 14, 41, 43, 58, 62, 78, 91]. A comparison of the side step value, cut width/ machine strip width for same scallop height produced by a ball and a radiused end mill cutter is shown in figure 1.8.

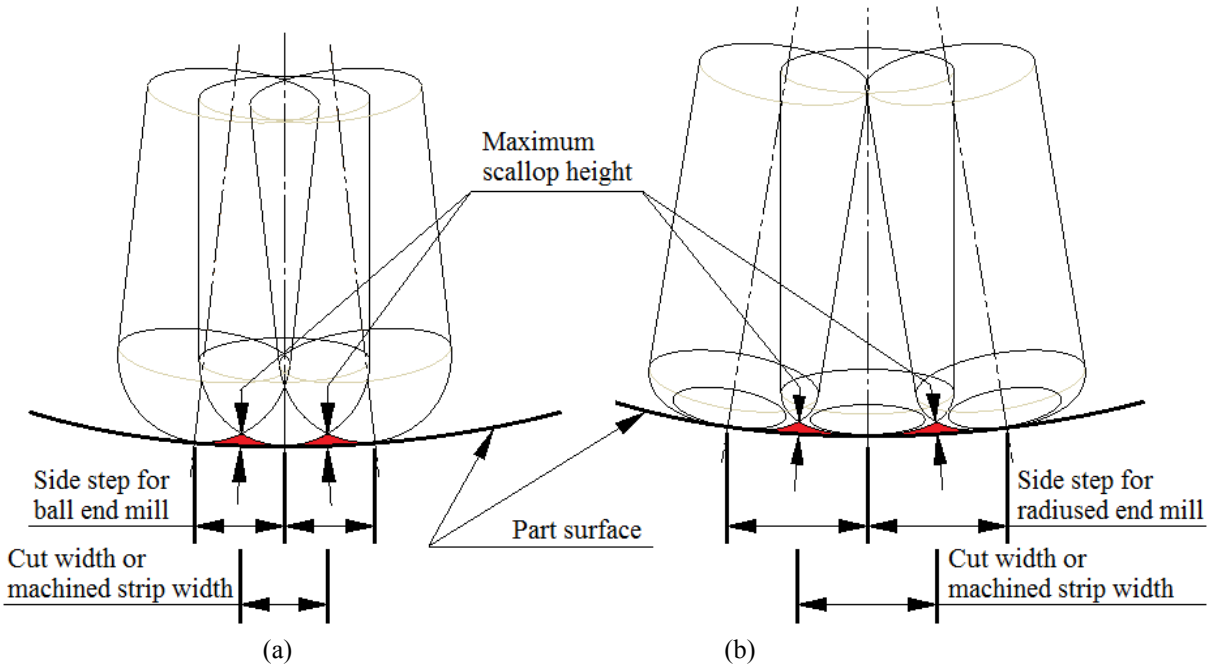

Figure 1.8: Comparison of machined strip width for equal scallop height while machining with: (a) a ball end mill, and (b) a radiused end mill

In addition the multipoint 5-axis tool positioning methods developed for radiused end milling cutter has opened a new horizon for precise and efficient machining of complex sculptured surfaces. The multipoint machining methods can help achieve much wider side-steps for 5-axis machining of sculptured surfaces for a predetermined surface tolerance, which was not known until a few years back [1-8, 14, 91]. But most of these multipoint tool positioning methods use parametric surfaces for finding the CL data, which makes these methods very complicated and computationally inefficient.

As discussed in section 1.4.3, the 3D part data represented in planer faceted format can be used to generate the gouge free toolpath data for sculptured surface machining. It is computationally simple and efficient compared to using mathematical representation of the part models. In literature faceted models have been used for toolpath generation but their use has been limited to 3-axis machining only and in most cases for ball end milling tool [30-69]. A few methods for toolpath planning using other tool shapes like flat or radiused end mill cutters have also been proposed [6, 13, 31, 33, 34, 38, 41, 50, 54, 58, 62]. These methods are also mostly restricted to 3-axis machining [20]. In certain cases a limited study has been carried out to explore the use of flat end mill cutter for 5-axis machining [34, 38, 50, 54].

1.8 TOOL POSITIONING METHODS FOR SCULPTURED SURFACE MACHINING

To generate the sculptured surfaces out of raw stock, the NC toolpath data must be created for various machining passes, including roughing, semi-finishing, finishing and undercut removal (also known as pencil cut or corner cut) [41]. The rough cut is executed with a larger sized flat end mill cutter to eliminate the excessive raw material generally using 3-axis machining methods. Subsequently, several semi-finish cuts are executed with ball or radiused end milling tools for reaching closest to the final desired part surface. A layer of uncut material is left on the finally required surface after the semi-finish cuts, which is removed in finishing cut. The finishing cut is the final and most important step in machining operations. The finishing cut takes longest time compared to other machining passes because it is executed using a large number of passes with a ball end-mill cutter to remove the final thin layer of material left over after the semi-finish cuts using 3-axis machining [41]. In certain cases, a pencil cutter or a very small diameter ball end mill cutter can be used for removing the uncut material from corners or undercut regions or the edges of a sculptured surface. Recently, 5-axis machining is preferred for finish machining. The finishing passes executed using 5-axis machining systems are more efficient compared to 3-axis machining.

The tool positioning methods used for 3-axis or 5-axis machining of sculptured surfaces can be categorized into two basic types [20, 41, 95], which are discussed below:

1.8.1 Parametric or offset tool positioning methods

In this method the NC toolpath data is generated along constant parametric curves on the parametrically defined surface. The CL data is determined by offsetting the parametric part surface [116-118]. Though this technique has advantage of using the actual surface

information for CL data creation, but this method cannot be used for development of toolpath data for sculptured surfaces composed of multiple parametric patches [112, 119] because the process of offsetting the different patches may result in self-intersections or gouging. The major limitation of these methods is the generation of toolpaths which are free from concave gouging [8, 54] as shown in figure 1.4**.**

Alternately, the offset surfaces generated from the actual parametric surfaces within the commercial CAD packages can be used for computation of tool positioning information. But the creation of offset surface for compound parametric surface is itself very complicated and computationally expensive process. Also, offsetting of multiple trimmed surfaces can cause self-intersections and global intersections. The uniformly offset surfaces can be easily determined for toolpath creation for ball end mill cutters [33], thus a number of surface offset methods have been proposed for machining with ball end milling cutter [20].

The iso-parametric toolpath data cannot ensure the uniform sidesteps toolpaths in Cartesian space. Some studies have focused on generating uniformly spaced Cartesian space toolpath data for parametric surfaces. This requires determining the intersection of offset parametric surface and the vertical planes to generate the offset curves. These offset curves are then used for tool positioning. This procedure is computationally expensive.

1.8.2 Cartesian space machining

The Cartesian space machining method can be used to determine the gouge free toolpath data using the intersection curves generated by a series of vertical section planes with the designed part surface [21]. This can generate the CC points that lie in a plane but the CL point may wander in the Cartesian space. For generating CL points that lie in one plane of Cartesian space the vertical planes must be intersected with the offset of the part surface, a much more complex process from the mathematical perspective. Additionally it requires additional algorithmic logic to avoid gouging, as identified earlier.

Z-map is another popular Cartesian space toolpath planning method [7, 9-10, 27] used to determine the gouge free NC toolpath data directly from data obtained as a result of digitization of sculptured surfaces using 3D scanning techniques. The accuracy of the toolpath data determined from Z-map method directly depends upon the density of the data

points, but higher point cloud density need larger memory space and processing time for accurate implementation of the Z-map Method.

The faceted/tessellated/STL data format can also be used for determining the toolpath data for sculptured surface machining using Cartesian space machining. The toolpath generation for Cartesian space machining is relatively simple using STL/faceted data because in this case the CL points are computed from the polyhedral surface elements only, which are facets, edges and vertices of the faceted model [51, 58]. This method, however, requires gouge checking to be incorporated within the tool positioning method to avoid undercutting in concave surfaces. The implementation of the Cartesian space method, using triangulated meshes of planer facets, requires the solution of linear simultaneous equations [41, 51]. Unlike the parametric toolpath planning method, in this method a sequence of CC points is not used. This method uses a pattern, called the toolpath footprint to define the X–Y components of the CL point trajectory. Tool position computations are used to determine the Z-height for the CL points. This method is computationally simple and is used mostly for toolpath generation for 3-axis machining; while the application of this method for 5-axis machining of faceted sculptured surfaces is limited to ball and flat end mill cutter shapes only [63].

Figure 1.9: Flat facets appearing on the STL part machined using a ball-nosed end mill.

Though the toolpath planning for faceted surfaces is computationally simple compared to using the parametric surfaces as discussed in section 1.8.1, however, the accuracy of the toolpaths generated from a faceted model depends largely on the accuracy of the triangular meshes used to approximate the actual part model. For achieving good accuracy of the computed CL data, the finer triangular meshes should be created to ensure the minimum surface deviation of the approximated faceted model with respect to the actual part model. This, however, increases the number of computations required to produce the toolpath and

increases the computation time. On the other hand if the size of the STL data file is small for ease of data storage and subsequently for efficient generation of cutter location/toolpath data, the surface approximation is poor and the actual flat facets can be seen on the surface of machined part as in figure 1.9.

The most fundamental challenge encountered in tool positioning for parametric surfaces is the computational complexity of the mathematical models used to determine the gouge free CC and CL locations, particularly for 5-axis machining. The computational complexity of such tool positioning algorithms increases further when using flat or radiused end mill tools. Finding the most effective tool-tilt angles is a critical issue for 5-axis tool positioning because one has to simultaneously check for the possibilities of tool gouging at second point on the part surface along with keeping an eye on configuration space of the machine tool to avoid the possibility of tool interference with moving machine parts. Thus the 5-axis tool positioning is a multi-objective problem, which gets little more complicated if one has to develop the toolpaths for higher order mathematical surfaces which need to be cut with tools of higher order geometry like radiused end milling cutter. The approximations used for simplification of the mathematical model of the overall problem of 5-axis tool positioning can yield solutions which may not result in desired surface finish and required machining efficiency. Thus even though the parametric definition of the part model data is one of the most precise representation, but it's use for determination of gouge and interference free 5-axis tool positioning for flat and radiused end mill cutters is very difficult [1, 7, 20, 27, 23, 91, 120].

1.9 MOTIVATION FOR THE PRESENT RESEARCH WORK

The greatest challenge for the optimal use of 5-axis CNC machining technology is the computation of gouge-free tool positioning data to position the cutting tool in closest possible proximity of the designed part surface. 5-axis toolpath planning has been addressed by several research initiatives in the early 90's. Rao et al. [2, 3] and Bedi et al. [4] developed the Principle Axis Method (PAM) which determines the principle curvatures of the parametric part surface at the point where the tool has to be positioned and matches the minimum curvature to the maximum curvature of the tool thereby determining the direction of tilt and brings the tool into close proximity of the design surface. Gouge detection is done as a secondary step. Subsequent to the Principle Axis Method, the Multi-Point Method (MPM) was developed. MPM integrates gouge checking with the positioning and inclination process

as reported by Warkentin et al. [1, 5]. In MPM method the tool is positioned at a point on parametric surface and is inclined until it touches a second point on the parametric surface. The inclination of the tool is formulated as an optimization problem for tool rotated about two orthogonal axes. This optimization problem poses computational challenges in the determination of the second point of contact. To address the computational issue the Rolling Ball Method (RMB) was developed by Gray et al. [6]. The RBM method uses triangulated part model to simplify part geometry. It further uses a sphere to approximate the local part surface and the tool is positioned within it. This method has difficulty crossing sharp edges and single vertices of triangulated part surface as reported by Gray et al. [7]. Subsequently, Gray et al. [7] developed an improved version of the RBM method called Arc-Intersect Method (AIM). The RBM generates conservative tilt angles to ensure gouge-free tool positions, whereas AIM directly positions the tool to contact the surface. Like RBM, the AIM is also an area-based method that generates gouge-free tool positions without the use of secondary gouge-check and correction algorithms. The AIM method uses computer's graphics hardware for tool position calculations and was tested on triangulated surfaces. In AIM the concept of shadow grid points is used which are the points computed on the projected shadow of the cutting edge of the tool around the first CC point on the part surface. The 5-axis tool orientation of the toroidal cutter is determined using each of the grid points under tool shadow, which makes it computationally slow as well as ineffective for determining the global interferences in certain cases as discussed by Hosseinkhani et al. [8].

Hosseinkhani et al.[8] introduced another tool positioning strategy for 5-axis machining called the penetration–elimination method (PEM). PEM used a set of evenly distributed sampling points as the representation of the part surface. In PEM the concept of quantitative gouging is used in conjunction with numerical root-finder algorithms to find the optimized tool orientations for each CC point. To enhance the efficiency of the computational process the authors dynamically detects the ineffective grid points and remove them for determining the 5-axis tool orientation. The accuracy of the 5-axis tool positioning and orientation greatly depends on the density of the grid points which represents the actual parametric surface. Thus PEM method cannot assure absolute gouge avoidance. A comparison of toolpath data developed from PEM and AIM show that the two methods give identical solution in determining the tool orientation, but PEM method is computationally more efficient compared to AIM method.

One of the key problems identified with the multipoint NC toolpath computation methods is that they are very complicated and computationally expensive. The prime factor that complicates the computation of the tool position in MPM is the use of higher order algebraic or parametric representation for input part models and the optimization method used to find the second point of contact [1-29]. In summary multipoint 5-axis machining method offer the advantage of reduced machining time while ensuring better surface finish of the machined parts. At the same time, the gouge free 5-axis toolpath data cannot be generated efficiently due to computational complexity of the available methods especially using radiused end milling cutter. The magnitude of computational complexity in 5-axis tool positioning can be reduced significantly by using planer faceted 3D part models compared to mathematically defined higher order 3D part model representation scheme. The faceted models/ triangular meshed part models can be easily generated with required surface tolerances using tessellation algorithms available within most commercial CAD modelers, or customized subroutines can be developed to approximate the parametric or mathematically defined surface models with planer triangular meshes [63, 65, 69].

The available 5-axis tool positioning algorithms developed for faceted models can generate toolpath data for ball and flat end milling cutter only [20, 34, 38, 50, 54] and these algorithms are not capable of ensuring the multipoint tool positioning. Thus an opportunity was identified for development of an efficient, gouge free and multipoint 5-axis tool positioning method for machining of faceted parts with a generalized radiused end milling cutter. The generalized radiused end milling cutter can suitably represent the tool geometry of a flat as well as a toroidal/ radiused end mill cutter.

1.10 OBJECTIVES OF THE RESEARCH WORK

Considering the above-mentioned need for multipoint 5-axis tool positioning algorithms for machining of faceted/ STL/triangulated meshed surfaces, the following objectives were identified for the research work undertaken:

1. Development of automatic efficient 3-axis tool positioning algorithms for the gouge free machining of triangulated surfaces using generalized radiused end mill.
2. Expansion of 3-axis tool positioning strategy to 5-axis tool positioning for the gouge free machining of triangulated surfaces using generalized radiused end mill.
3. Testing and validating tool positioning algorithms by actual machining.

1.11 INPUT PARAMETERS CONSIDERED FOR PRESENT THESIS WORK

In order to achieve the objectives outlined in section 1.10, the following key input parameters were identified.

(i) 3D part model data

(ii) Tool geometry information and

(iii) Toolpath footprint pattern.

These parameters are required for automated tool positioning algorithms to determine the multipoint NC toolpath. The parameters are user specified. To develop a new approach for gouge free 3-axis and multipoint 5-axis tool positioning the following forms of the above mentioned three inputs have been identified.

1.11.1 Part model data input in the form of triangular faceted format

It is observed from published literature that the 3D part models represented in planer triangular facets/ STL data format have been successfully used for 3-axis toolpath planning for different types of end milling cutters geometries [12, 30, 32-33, 35-36, 39-49, 51-53, 55-62, 64, 68, 70-75]. The 3-axis NC tool positioning methods for faceted part models use different ways of dropping a tool along a predetermined tool axis orientation until the tool touches the part surface at a gouge free CC point [12, 30-69, 70-75]. The determination of the tool center (CL) corresponding to the point of contact (CC point) between the faceted part and the tool surface is the key to determine the 3-axis toolpath data [13, 20, 30, 33, 40-49, 51, 58, 63, 65-66]. In a published work by Yau et. al.[41], the authors have reported that the 3-axis NC toolpath generation for faceted surfaces can be far more efficient than direct toolpath generation from the parametric surfaces. Thus, it is evident from the published literature that faceted sculptured part models have been reliably used for toolpath generation for 3-axis machining but the work with respect to 5-axis tool-positioning is in infancy. Moreover the developed 5-axis tool positioning methods for faceted surfaces are computationally intensive, time-consuming and limited to flat end milling cutter only [34, 38, 50, 54].

A planer triangular facet is the simplest mathematical entity that can be used to represent part of a complex surface defined in a 3D space. The 3D part geometry can be easily translated into triangular faceted format using available robust tessellation algorithms or else custom subroutines can be developed to translate the mathematically defined surfaces into planer faceted formats [20, 63, 65, 69]. The commercial CAD systems can also reliably convert part model geometry into faceted data format known as STL format with user specified accuracy

[58-69]. Therefore in this work we have used the part input geometry in the form of planer triangular faceted/ STL format for development of efficient algorithms for determination of gouge free multipoint toolpath data for 5-axis machining.

1.11.2 Tool geometry in the form of generalized radiused end mill

The second important aspect considered in the present work is the choice of the appropriate tool shape required for surface machining [58, 76-81]. Several authors have studied the effect of geometric shape of the milling cutter for sculptured surface machining with respect to factors like tool wear, vibration characteristics, effect of cutting directions, step-over distance, effective cutter feed, speed, and required surface tolerances [76-82]. As discussed in section 1.7, the toroidal/radiused end mill offers better surface machining characteristics particularly for curved surface machining because it can machine wider cut width per machining pass and smaller scallop height are achievable compared to other two tool types for both 3-axis and 5-axis machining [58, 77].

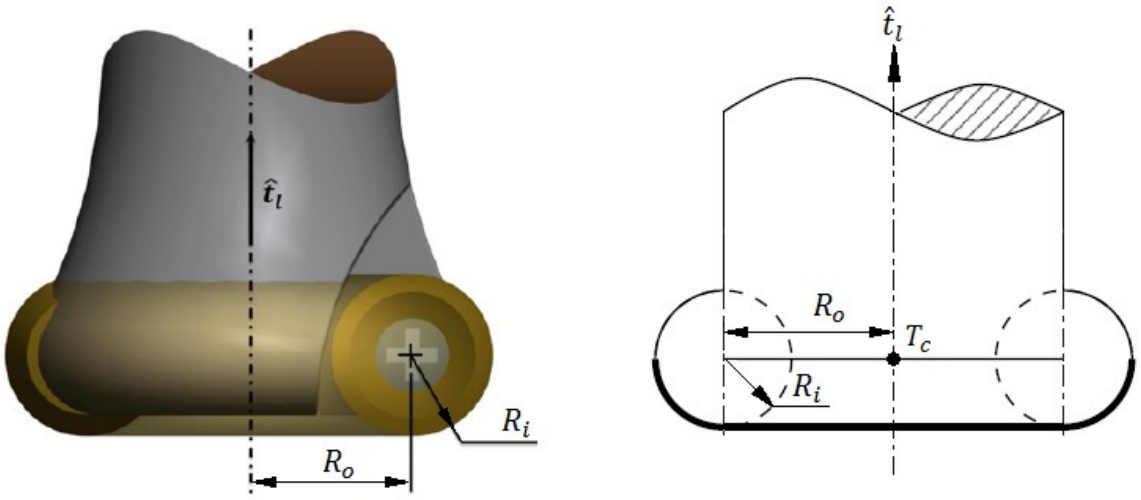

Figure 1.10: (a) 3D model of an industrial radiused end mill cutter, and (b) geometry of a generalized radiused end mill.

The radiused end mill provides a smooth surface finish much like a ball end mill and has excellent cutting capability along its entire cutting edge [1-2, 5-7, 13, 15, 20, 41, 58, 77]. Moreover the radiused end mill can be thought as the generalization of the geometric shape for ball and flat end milling cutter as well [63, 65]. Figure 1.10 (a) shows 3D model of a typical insert based industrial radiused/ toroidal end mill cutter. Figure 1.10 (b) shows the geometry of a generalized radius end mill in which the cross-section of the cutting edges of a radiused end mill cutter is shown by the dark boundary towards tool bottom. In figure 1.9 (b), the cutting edge of the rotating tool is represented by a circle of radius R_i called as pseudo-insert circle [1-8, 14, 63, 65-67, 69]. The center of pseudo-insert circle is offset from the tool

axis by a distance R_o known as major radius or simply offset radius of a toroidal end mill. For $R_i = 0$ and $R_o > 0$ the radius end mill models a flat end mill, whereas if $R_o = 0$ and $R_i > 0$ it models a ball end mill [63].

Though the radiused end mill tools are capable of achieving better results for sculptured surface machining, few studies have been undertaken for 5-axis tool positioning on compound surfaces represented in STL/faceted format. The work done for 5-axis tool-positioning is either limited to flat end mills or require the higher order approximation of the triangulated surface as reported by [6, 12, 19-20, 34, 38, 50, 54]. The above discussion establishes the need for development of gouge free 5-axis NC tool positioning algorithms for generalized radiused end mill for faceted surfaces.

1.11.3 Toolpath footprint pattern

The third important input is the toolpath footprint pattern. It is a sequence of discrete locations that directs the tool movement, through which the tool axis will pass for 3-axis machining of the part surfaces and to be used as a reference for determining the first CC point in 3-axis tool drop which is in turn used for finding the multipoint 5-axis tool positioning in the present study. The discrete footprints are taken in a plane perpendicular to the tool approach direction and defined within the boundary of the projected part surface. Generally the XY plane is taken as the footprint plane. The shape of the toolpath footprint describe the motion of the tool over the designed part surface and it controls the surface finish achievable from the machining operation [9-12, 15, 17, 20-21, 23-24, 30, 38, 43, 46, 51, 53, 61, 79, 82-86, 89-90].

As discussed in section 1.6, the zigzag and contour parallel patterns are the preferred toolpath footprint patterns for 3-axis and 5-axis machining, and are mostly used for machining of industrial sculptured parts [20]. Although our work on the development of tool positioning algorithms for 5-axis machining with generalized radiused end mill cutter is independent of toolpath footprint pattern and any type of toolpath footprint pattern suitable for Cartesian space tool positioning can be used with the developed algorithms. For demonstrating the capability of the developed 5-axis tool positioning algorithms the zigzag and circular contour parallel footprint pattern is mostly used for toolpaths generation for various test parts in this work.

1.12 OUTLINE OF THE RESEARCH WORK

The objective of the present research work was to develop a computationally efficient, gouge free and multipoint 5-axis tool positioning approach for generalized radiused end mill for faceted surfaces. The work undertaken has evolved from the work reported in the area of multipoint 5-axis machining initiated by Warkentin et al.[1, 5, 14], Gray et al. [6-7], Manos et al. [51], Patel et al. [58] and Bedi et al.[77]. The foundation step of the present work is the generalization of 3-axis tool positioning approach for radiused end mill for faceted surfaces which has been derived from Patel et al.[58]. In the first phase of this work, the generalized 3-axis tool positioning approach was implemented first in Maple^{TM} [63] and subsequently in Visual C++ programming environment [65]. The implementation of the developed approach in Visual C++ is quite fast and accurate in terms of computation of tool positioning data, and the developed algorithms can work well with any kind of toolpath strategy. The details of the generalized 3-axis tool positioning approach have been published in Duvedi et al. [63, 65]. The accuracy of 3-axis tool positioning algorithm was verified using customized 3-axis NC simulator developed by Mann et al. [93] as well as in the customized Maple^{TM} simulation environment similar to the one used for demonstrating graphical simulation for the 5-axis tool positioning published by Duvedi et al. [63, 65-67].

Subsequently the generalized 3-axis tool positioning method was extended to 5-axis tool positioning. This development can be categorized into the following main sections:

(i) Development of an analytical model for a new scheme for 5-axis tool positioning of a toroidal/radiused end mill on triangulated surfaces called “Drop and Tilt Method” or “DTM” method (Duvedi et al. [63]).

(ii) Numerical implementation of DTM method for 5-axis tool positioning (Duvedi et al. [65]).

(iii) Development of a new mathematical model to determine the edge-torus tangency to improve the computational efficiency of the DTM approach (Duvedi et al. [69]).

The detailed description of the work done during this thesis work is presented in different chapters and organized systematically as listed in the next section.

1.13 ORGANIZATION OF THESIS

From the study carried out in this work, the thesis has been organized in the following sections:

Chapter 1 Introduction: Introduction of automated NC tool positioning for 3-axis and 5-axis machining of faceted surfaces, research goals, contributions and outline of thesis is presented in this chapter.

Chapter 2 Background and Literature Review: Background and relevant literature reviewed till date for the automated NC toolpath planning and tool positioning for 3-axis and 5-axis machining of faceted sculptured surfaces is discussed in this chapter [1-120]

Chapter 3 Analytical model of Drop and Tilt method of 5-axis tool positioning: In this chapter the mathematical model developed for the 5-axis tool positioning of generalized radiused end mill over faceted sculptured surface using drop and tilt method (DTM) is discussed along with its implementation using commercial solver Maple^{TM}.

Chapter 4 Generalized 3-axis tool positioning: In this chapter the mathematical concept of generalized 3-axis tool positioning algorithm for radiused end mill cutter over faceted surfaces is presented which serves as the basis for numerical implementation of DTM for tool positioning for 5-axis machining [63, 65].

Chapter 5 Numerical Implementation of DTM Model: This chapter details the numerical implementation of the DTM algorithm for 5-axis tool positioning of radiused end mill for faceted surfaces [65].

Chapter 6 A new approach for edge-torus tangency: The determination of the point of edge-torus tangency is computationally most difficult part in numerical implementation of DTM algorithm. In this chapter a new methodology developed for determining the edge-torus tangency is presented [69].

Chapter 7 Conclusion of the research work: This final chapter summarizes the conclusions of the research work undertaken along with the future scope of work done for 5-axis tool-positioning of radiused end mill for faceted surfaces.

CHAPTER 2
BACKGROUND AND LITERATURE REVIEW

The previous chapter provided an introduction to 5-axis machining. It was shown that the multipoint class of machining method offer special advantage over single point methods; in producing a wide strip of machined surface, that meets user specified tolerance. These strips result in up to 80% saving in machining time as compared to 3-axis methods. Even with these advantages 5-axis methods have not gained in popularity and remain obscure. This chapter presents a review of literature related to 3-axis and 5-axis NC toolpath planning or tool positioning for machining of parametric and faceted sculptured surfaces. The focus of the review is to identify the unique strengths and shortcomings of the existing methods. Also as identified in chapter 1, special attention has been given to literature related to various multipoint machining methods to identify clearly the opportunity for extending the work to allow indirectly take advantage of benefits offered by MPM methods.

2.1 BACKGROUND

The accuracy of the toolpath data generated using automated computer programs depends upon the geometry of 3D part model, the geometric shape and size of the cutting tool, the type of machining system (whether 3-axis or 5-axis etc.), the toolpath footprint pattern, the feed forward and side step discretization of toolpath pattern, cutting/ machining speed, feed rates, the tool's velocities between consecutive CL points, the accepted scallop height of the machined part etc.[12, 17, 20, 23, 117, 118, 120]. Toolpath planning is done in the light of identified parameters. Toolpath planning involves the computation of the tool positioning data (CL data) for a given toolpath footprint location and for the selected tool shape and size.

For NC toolpath planning, the input part data can be used either in parametric or faceted/ tessellated/STL format. The computation of gouge free tool positioning using sculptured surfaces in parametric form is well established, but is a very complicated and computationally expensive approach [20, 33, 38, 41, 43, 58, 63]. It is well known that the triangulation of the local region of parametric design surface under tool shadow is considered as one of the efficient as well as computationally effective method for tool positioning for 3-axis and 5-axis finish machining. This logic is being used in most commercial CAM packages as discussed by Lauwers et al. [38], and Lu et al. [54]. At the same time, it has been proven by published literature that computation of gouge free NC toolpath is relatively simple using

faceted representation of the 3D sculptured part geometry compared to parametric compound surfaces as reported by Lasemi et al. [20], Lauwers et al. [38], Yau et al. [41], Bedi et al. [51] and Patel et al. [58].

Toolpath planning also depends on the tool positioning methods. The tool positioning algorithms can be divided mainly into three categories namely: roughing, semi-finishing and finishing [41]. Most of the rough machining or bulk stock removal, and semi-finish operations, are carried out using 3-axis machining. The present work does not focus on development of the 3-axis tool positioning for roughing and semi-finishing operations because these methods use considerably larger values of surface tolerances for toolpath planning and such methods are well established [41]. Although, roughing removes around 80% of the unwanted material while taking only 25% of the total machining time. Over 50% of the total machining time is spent in finish machining and the remaining 25% is spent on hand polishing etc. Since the largest time is spent in finish machining, 5-axis method focused on finish machining are discussed. Multipoint methods offer some additional advantages compared to single point 5-axis machining methods. Thus the concepts of multipoint 5-axis machining methods proposed by several authors is explored with a view to identify the scope for further development to enhance the accuracy as well as efficiency of the tool positioning of a generalized radiused end milling cutter for finish machining of faceted/ STL sculptured surfaces.

The toolpath data for CNC machining should be free from local gouging, rear gouging, global gouging and the interferences caused by tool holder and work holding devices as discussed by Jun et al. [19], Lasemi et al. [20], Balasubramaniam et al. [31], Lu et al. [54], You and Chu [86], Choi et al. [114] and Tang [120]. In the review work by Lasemi et al. [20] the authors reported that out of several methods of gouge and collision avoidance the feasibility cone method and configuration space method are said to be effective [20]. There are several techniques available for interference detection between tool and the workpiece, and are discussed in a review of work related to collisions detection and avoidance by Tang [120]. The interference detection algorithms can be used to generate the interference free tool positioning either by finding the limits for tool approach/tool orientation in 5-axis machining or by indicating the possible interferences during machining simulations and applying the correction in the developed toolpath data. However, Hu et al. [119] have analyzed sources of obstacles in 5-axis machining and developed a new methodology for determining the obstacle

free tool-orientations for 5-axis machining in the toolpath generation stage only. This new method of toolpath planning has collision avoidance integrated in it and it can ascertain the collisions in early stage of toolpath generation and eliminate it thereby saving time.

Another important factor to be considered during computation of NC toolpath data is the control of cusp height or the scallop height. The scallop height is the function of feed forward and side feed discretization of toolpath footprint in Cartesian space. The accurate determination of scallop height for each pass in 5-axis machining is not an easy task. Determination of optimized feed forward and side feed values to maintain a predetermined surface tolerances level, particularly for faceted surface models is a challenging task. Ideally the machined surface should have scallop height within specified tolerance and should be gouge free [20]. The aim of the present work is the development of gouge free multipoint tool positioning algorithms which are independent of type of tool footprint pattern and the magnitude of feed forward or side step distances. Thus logic related to scallop height control can be easily integrated with the developed algorithms. The concepts of automatic selection of the tool geometry and size, feed forward and side step distances for generation of efficient toolpath data for user defined scallop height is not considered in the scope of present work and is suggested for future work.

For the comprehensive review of the published work related to machining of triangulated sculptured surfaces, the literature surveyed has been organized in the following sections:

1. Multipoint 5-axis tool positioning methods.
2. Sculptured surface data for automatic toolpath planning.
3. Tool positioning techniques.
4. Tool geometry.
5. Toolpath footprint pattern.

After the presentation of literature survey for the above mentioned areas, the conclusions have been presented in the last section of this chapter.

2.2 MULTIPOINT TOOL POSITIONING METHODS FOR 5-AXIS MACHINING

The 5-axis tool positioning for manufacturing of sculptured surfaces ideally should be such that the cutting edge of a radiused end mill cutter tangentially touches the part surface. This proximity results in the machined surface being close to the design surface [1-8, 14]. The

developments of multipoint 5-axis machining methods were initiated in early 90's for the accurate machining of parametric surfaces, and Principle Axis Method (PAM) was one of early methods developed by Rao et al. [2-3].

In PAM [2-4], the principle curvature of the parametric surface is determined at CC point for a radiused end mill cutter. This method uses the minimum curvature of part surface and its direction to tilt/rotate the tool to position its cutting edge closer to the designed parametric surface. The gouge elimination in PAM is carried out in a secondary step. The problem with PAM is that gouge detection cannot be integrated with the tool positioning which makes the implementation of this method very complicated. The concept developed in PAM has laid the foundation for the evolution of Multi-Point Method (MPM) of 5-axis machining developed by Warkentin et al. [1, 5, 14]. In MPM method first the location of a CC point is determined on the parametric surface and then the tool is tilted along the feed direction by matching the geometry of the cutting edge of radiused end mill cutter with the region of the part surface under its shadow to make it touch the designed surface at a second point. The determination of a second point of contact on the parametric surface in MPM is modelled as an optimization problem to determine tool tilting about two axis of rotation that result in two tangential contacts of tool with the part surface. This computation involves high order transcendental equation and is ill behaved and lack robustness. In MPM, gouge detection is integrated within tool positioning and inclination process.

The above multipoint machining methods as such are not suitable for machining of multi-patch sculptured surfaces which are commonly encountered in industrial application. This is because the generation of 5-axis toolpath data for moving the cutting tool across the common boundary between two parametric surface patches poses computational challenges. Thus for machining of multi-patched parametric surfaces the toolpath data for each surface patch has to be created separately, which is a hindrance in 5-axis machining. Gray et al. [6] have extended the concept of 5-axis multipoint machining for faceted/triangulated surfaces by developing a new method for tool positioning called rolling ball method (RBM). The RBM method does not use a direct method for positioning of radiused end milling tool to determine the second point of contact on the faceted surface. Rather for a given toolpath footprint, RBM uses the approximation of the local curvature of the STL surface under tool shadow with a spherical envelop and the radiused end milling tool is tilted until it touches this spherical envelop. This tilt angle value is recorded as the 5-axis tool orientation. The implementation of

RBM methods is also not straight forward, and it has certain limitations that it cannot be used for 5-axis tool positioning for certain cases like crossing sharp edges and raised vertices of the faceted surface. Thus Gray et al.[7], developed another approach for multipoint 5-axis tool positioning called the arc-intersect method (AIM) which is an improved method compared to RBM. Both RBM and AIM are area-based tool positioning methods. In AIM the concept of shadow grid points is used which are the points computed on the projected shadow of the cutting edge of the tool around the first CC point. The 5-axis tool orientation of the toroidal cutter is determined using each of the grid points under tool shadow, which makes it computationally slow as well as ineffective for determining the global interferences in certain cases as discussed by Hosseinkhani et al. [8].

Hosseinkhani et al. [8] have introduced another multipoint tool positioning strategy referred as penetration elimination method (PEM). It is reported that PEM is 7.5 times faster than AIM method while offering the same results for 5-axis tool orientation. PEM use a set of uniformly located sampling points as the representation of the part surface. In PEM authors used the concept of quantitative gouging along with numerical root-finder algorithms to find the 5-axis tool inclinations for each CC point. The efficiency of the computational process is enhanced by removing the ineffective grid points in determining the 5-axis tool orientation. The accuracy of the 5-axis tool positioning and orientation greatly depends on the density of the grid points which represents the actual parametric surface. Thus PEM method cannot assure of absolute gouge avoidance.

He and Chen [91] has recently presented a multipoint-machining approach called middle-point error control method for multipoint positioning of radiused end mill cutter on mathematically defined surface. In this method first the shape of error distribution curve and it asymmetry is determined for the preselected value of surface tolerance, followed by the rotation of cutter about the roll angle to make the error distribution curve symmetrical and simultaneously the cutter is moved from the surface. Further the tool tilt angle is determined which gives two CC points on the part surface.

The determination of tool positioning using the multipoint machining methods discussed above is very difficult owing to the fact that all of the stated methods need the solution of higher order simultaneous equations. The foremost computational barrier in the implementation of these methods is the mathematical representation of algebraic or

parametric surfaces which need to be solved along with the 4^{th} order mathematical model representing the geometry of radiused end milling cutter [1-29, 91]. Thus the computational complexity of these methods has imposed a big barrier for implementation of these methods for real industrial applications.

2.3 SCULPTURED SURFACE DATA FOR AUTOMATIC TOOLPATH PLANNING

A sculptured surface by definition is the collection of interconnected and bounded parametric patches put together with blending and interpolation functions [78, 95, 96, 97]. For the automatic development of toolpath data for multi-axis machining, the input geometry of the sculptured part models/surfaces can be used in the one of the following formats:

(i) Mathematically defined compound parametric sculptured surfaces.

(ii) Sculptured surfaces represented by a set of point cloud data

(iii) Faceted/ STL representation of sculptured surfaces/ 3D part model

The above mentioned data representations have their own advantages and disadvantages in generation of toolpath data, and these are discussed below:

2.3.1 Mathematically defined compound parametric sculptured surfaces

Generally CAD systems use some form of mathematical (analytical, parametric, or non-parametric) representation 3D part model data. Dragomatz and Mann [12], Lasemi et al. [20], Jensen and Anderson [117], and Hatna et al. [118] have presented a review of literature related to toolpath generation and multi-axis machining of mathematically defined sculptured surfaces. Dragomatz and Mann [12], have presented the review of the papers published from year 1988 to 1994, while Jensen and Anderson [117], and Hatna et al. [118] have reviewed the research work in the areas of finish machining of sculptured surfaces and CNC milling of pockets respectively from year 1994 to 1997. Byrne et al. [18] presented the review of the development of cutting technology with focus on developments which has been noticed in the area of cutting tools, tool materials, workpiece materials, machine tools, the process conditions and manufacturing environment since the foundation of CIRP (for the period from 1941 to 2003). Later Lasemi et al. [20] presented the review the research work related to various issues of multi-axis machining of freeform surfaces with a focus on developments related to toolpath determination, and effective cutter geometry, which are published from 1997 to 2008. It is clear from the review work published on NC toolpath planning that a large amount of work related to toolpath planning and tool positioning has been is done for the parametric surfaces.

Dong et al. [9] developed roughing toolpaths for sculptured parts using contour map approach with an aim to reduce the rough machining time using a flat end mill cutter. The authors reported the gain in the efficiency for rough machining operation but achieved at the cost of tool positioning accuracy. Lai and Wang [10] reported that the Cartesian method of generating NC toolpath data for machining of compound sculptured surfaces has problems generating gouge free toolpath data. Thus the authors developed a surface offset method for 3-axis toolpath generation using a ball nosed cutter for machining of complex sculptured parts composed of analytical CSG (constructive solid geometry) primitives and parametric surface elements. The analytical and parametric surface elements are offset separately. To enhance the computation efficiency the NURBS surface elements were triangulated before they were offset. The CL points were determined as the location center of the ball nosed cutter directly from the offset surface for parallel toolpaths.

You and Chu [11] presented toolpath generation method for roughing machining of solid models which may be composed of planar patches, general quadratic surface elements, B-spline surfaces and other compound surfaces. The 3D solid model data is translated into a 2D grid which is then used to find the NC toolpath data. The developed toolpath is not free of tool interference, thus is not suitable for finish machining operations. In an attempt, Rao et al. [15] developed a method where toolpath planning and tool positioning is integrated together for machining of parametric surfaces with the radiused end mill cutter. Although the developed method reduces the number of machining passes significantly, it is not a completely gouge free method. Furthermore the computational time required to determine the toolpath data is high. Fard and Feng [24] reported that curvature matched toolpath planning methodologies for freeform surfaces are not able to generate gouge free toolpath data because these methods do not consider the global surface geometry around the CC point. Thus the authors developed a new approach to determine maximum machining strip width at CC point for a flat end mill and optimal feed directions using toroidal surface inscription technique. The developed method has limitations in convex regions as well as the scallop height control measure is not integrated in the algorithm. Zhou et al. [25] developed a mathematical model for computation of tool envelope for 5-axis tool positioning using theory of rigid body motion. The tool envelope surface is used for generating the grazing points which then can be used for toolpath simulation and verification for 3-axis and 5-axis machining.

Fard and Feng [26] have presented a new approach for finding the 5-axis tool orientation for a flat end mill for machining of sculptured surfaces for a given feed direction. The proposed method uses two criterions for finding 5-axis tool orientation namely: maximum material removal at CC point and cutter orientation which will gives minimum toolpath length. Lin et al. [27] developed a uniform chord error method for accurate surface interpolation of cutter in 5-axis machining of freeform surfaces. The developed method determines the consecutive CC points in a way that ensures the chordal error between two adjoining CC locations to remain within predefined tolerance. The machining error for the accurate determination of intermediate CC points is found from the trimmed lengths of the simulated grass model. Gilles et al.[28] developed a 5-axis toolpath strategy such that the cutting forces encountered by the inserts of the radiused end mill cutter are dynamically balanced by sharing the cutting load between outer-front and inner-rear side of cutter inserts as seen with respect to the cutter feed direction. This method does not make use of curvature matching method for tool positioning with respect to the designed surface, rather tool is kept lifted from front side. This ploughing toolpath strategy is still able to give better surface finish with respect to iso-planar toolpaths, but overall it takes longer to finish the toolpath compared to the other curvature matched machining techniques. This method cannot ensure minimizing tool gouging, and maximization of cutting strip width because the proximity of the cutting edge of tool to the design surface is not ensured.

Kim et al. [29] have presented a gouge free 5-axis toolpath planning method for parametric surfaces for flat and radiused end mill cutters, based on combination of two methodologies namely hyper-osculating circles and two-contact configuration. The developed method takes very long time to generate the 5-axis toolpath data and hence is not computationally efficient alternative. Cho et al. [32] has reported the development of a toolpath planning approach for multi-patch sculptured surfaces. The developed method generates the toolpath data in parametric plane with minimum CL points for a user defined machining tolerance. The authors reported that the developed method can generate continuous toolpaths capable of machining different parametric surface patches, while a new error analysis method is used to find the forward and side-step discretization which is used for minimizing the number of tool positions to machine the entire composite parametric surface. Chen et al. [37] reported that the 3-axis machining methods are not capable of efficient machining of complex sculptured parts and the addition of two discrete rotational degrees of freedom to the 3-axis CNC machine can help machine such complex shapes in a comparatively better way. Thus the

authors presented a method for determining the toolpath for 3½½-axis machining of sculptured surfaces. In the developed method the complete surface is automatically subdivided into number of patches with defined patch boundaries. For each patch the suitable machining orientation is determined and then the 3-axis NC toolpath data is determined for machining of each sub-divided patch separately. In a way authors proposed a method to achieve the benefit of 5-axis machining but with a 3-axis CNC machine tool, but this method is time consuming compared to machining of sculptured surfaces on a 5-axis CNC machine.

In the isoparametric toolpath planning method reported by Broomhead and Edkins [108], the cutter contact points are specified along isoparametric curves. The isoparametric curves are approximated by linear segments. The drawback of this method is that the larger size of the linear segments may results in under-cuts on the parametric sculptured surfaces of the model. This is one of the reason why the absolute gouge avoidance is not possible using parametric toolpath planning. Chen and Ravani [109] have presented offset method for toolpath planning for a ball nosed end mill. The developed method is conceptually similar to the Cartesian method, and it used an offset surface generated from the original part surface which has offset distance equal to the tool radius. The center of the cutting tool travels along the offset surface to machine the part, and the toolpath is calculated by identifying tool passes on the offset surface. The advantage of this method is that one can find a tool trajectory parallel to X-axis in which the tool moves only along the Y- and Z-axis. The self-intersections toolpath that leads to over-cut or cavities of under-cut must be detected and corrected while implementing the offset surface method. Uniform offset work only for ball end milling cutter while non-uniform offsets are required for other tool geometries.

Cho et al. [111] developed a toolpath methodology for machining multi-patched surfaces, using parametric planes to machine the part surface with smallest number of CL points for required accuracy level using a ball end mill cutter. Choi et al. [112] have reported the development of a compound surface modelling method suitable for interactive surface design system and presented a method for finding CL data for a ball nosed end mill for compound parametric surfaces. Lee [115] has reported the development of a spiral toolpath methodology based on contour offset technique for constant scallop height using high speed finish machining for parametric surfaces. The developed method works well for machining of steeper as well as flat areas and ensure the minimum tool retraction for efficient surface machining. The developed method is suitable for ball end milling cutters only.

The tool positioning or cutter location determination is a challenge when input part geometry is used in mathematical/ parametric form. The tool positioning algorithms for such surfaces first determine the CC location and then iteratively check/ adjust tool height for tool gouging. Thus these methods are generally called cutter contact (CC) methods of toolpath planning [12, 20, 23, 41, 58, 62].

2.3.2 Sculptured surfaces represented by a set of point cloud data

The other method of machining surfaces discussed in literature is to use point cloud data captured using 3D scanning technologies. The point cloud in such case represents the data points captured from the surface geometry of the scanned part and is stored in a systematic order with respect to a user defined 3D coordinate system. The accuracy of the point cloud data is purely dependent on the accuracy of part surface, the scanning technique used and the part orienting fixtures used to present the part in front of the scanning devices.

Several authors have developed methodologies to use the point cloud data to determine the NC toolpath data [30, 69, 70-75]. The toolpath generation using point cloud data is computationally very simple and efficient for a ball end milling cutter. The density of the scanned data points is an important concern in its use for toolpath planning. Improper selection of point cloud density will cause tool gouging in the gap regions between neighbouring points. Although the density of points can be increased to achieve the desired surface finish, but the problem of tool plunging into the work piece cannot be avoided completely.

Kawabe et al. [71] used a 3D-coordinate measuring system to measure a sculptured surface and fit a surface through the scanned data. The surface is used to generate 3-axis NC toolpath for machining using ball end milling cutter. Feng and Teng [72] reported that the interference avoidance for toolpath generated from point cloud data required high point cloud density. The authors proposed the use of very small toolpath segments as an alternative to avoid need for high density data points and to control machining errors. This however it significantly reduces the machining feed rates and leads to premature tool wear as the tool remains in contact with very small uncut chip thickness. In continuation Teng et al. [73] reported the development of a machining area segmentation method for 3-axis toolpath generation for a ball end mill to machine the surfaces represented with point cloud data. The machining area

segmentation is carried out on the basis of the geometric complexity of data points for efficient and gouge-free machining of such areas with a ball end mill of different sizes in order to control the machining errors. The developed method can only be used if the high density data points are available and this method does have problem with sharp corners.

Chui et al. [74] used point cloud data for 5-axis toolpath planning for ball end milling cutter. In the first step a triangular mesh is constructed from the scanned data which is subsequently used to generate the toolpath data. The accuracy of the 5-axis toolpath generated depends greatly on the fineness of the grid used for meshing and the method used to select the points from the scanned data. The developed toolpath data is not suitable for machining tiny features which will be filtered out in the mesh generation step and the vertical features cannot be captured. Makki et al. [75] used the digital scanned point cloud data from a non-contact device for 3-axis and 5-axis toolpath planning, but the proposed method use only ball end milling cutter. Cho and Yang [110] have used Z-map method for determining the 5-axis orientation for a flat end mill for machining of free form surfaces. The tool-axis is inclined in the plane of feed motion of the tool and the direction vector representing the orientation of tool axis in the feed plane is found using the Z-map of the local region of the parametric surface around the CC point, such that the tool bottom rides on the freeform surface.

Though the toolpath computations are relatively easy and fast when using point cloud data, the methods lacks accuracy of tool positioning and the developed toolpath is not free from gouging. Moreover the density of the point cloud data and tool diameter have direct relationship with the toolpath accuracy and generating a toolpath for a smaller diameter cutter with larger spacing between the scanned data points will result in unacceptable parts.

2.3.3 Sculptured surfaces represented triangulated facets/ STL data

The third alternative form of 3D part data representation found in literature is the faceted/ STL data format [20]. STL models are being used in a number of industrial applications, which include: rapid prototyping, multi-axis NC toolpath generation, graphics, CAD and finite element analysis [20, 41, 58]. The 3D CAD models and 3D point cloud data can be converted to the faceted/STL format using commercial CAD packages with user defined surface tolerance. The approximation of part geometry using 1^{st} order triangulated facets in STL models reduces the computational complexity of tool positioning compared to using the higher order analytical or parametric surface models and does not suffer from gouging as in

toolpath generation using point cloud data for 3-axis and 5-axis machining [13, 20, 35, 41, 58, 63]. The data in STL models is sufficient for development of toolpath generation for many machining applications [6-8, 12, 30-69, 91].

Hwang and Chang [13] presented a method for toolpath generation for sculptured surfaces taken in tessellated form for a flat and radiused end mill cutters for 3-axis roughing and finish machining. The authors used the region rejection criteria to select the triangulated facets in the CC region under tool shadow and then used them to determine the CL point efficiently. It is claimed that the developed method is capable of machining any compound sculptured surface. Vickers [30] developed a method for tool positioning of a ball end milling cutter for machining of marine propeller blades using the polyhedral approximation of curved surfaces of marine blade shapes. The author used the Polyhedron to model the part and a zigzag toolpath is generated for machining the faceted surface with a ball end mill cutter. Balasubramaniam et al.[31] has used the tessellated model created in ACIS geometric modeler for 5-axis roughing toolpath planning, which is said to be relatively easier compared to using the feature recognition method used for toolpath planning for parametric surfaces. Toolpath data for roughing 5-axis machining for several part models is successfully generated for a flat end milling cutter.

Zhou et al. [39] have proposed the use of STL models as the common data format for: machining simulation studies for interference and collision avoidance, predict the machining accuracy, studies for optimization of machining conditions and storing the output from the simulation studies for further investigation. Ahn et al. [42] reported the advantages of use of STL data for a web based automatic NC toolpath generation algorithm for micro machining applications. The authors reported that the data transfer between different CAD CAM systems is stable and efficient using STL format, particularly for implementation of web based applications. The CAD data for certain applications like molar prosthesis is generated in STL format and used for accurate machining as reported by Bu et al.[48].

The STL models generated from surface models are incomplete in terms of gaps and overlap between the facets generated on the boundaries of the model. Thus the generation of offset CL surfaces for such incomplete meshes cannot be used as such for accurate NC toolpath generation, because of wrong offset directions and increase in size of small gaps during offsetting, which may exist between boundary edges. Thus Kim and Yang [49] has developed

a method to for offsetting of incomplete meshes for 3-axis and 5-axis machining, but such offset methods are useful only for machining with a ball end milling cutter. Tapie et al. [59] developed a method for extracting information about the machining areas using the method of topological decomposition for complex parts like forging dies, modeled in STL format. The topology considered in the reported work is the orientation of part shapes compared to axis of the cutting tool and the toolpath trajectory to be followed during machining.

The quality of machined parts is affected by several factors which include deformations incurred by workpiece, tool wear/deformation/deflections while machining, thermal deformations, and inaccuracies in the machine tool etc. Two methods can be used to enhance the accuracy of the machined part, namely: mapping the tool–workpiece displacement and applying the dimensional error compensation in the finishing toolpath. Sortino et al. [60] developed an approach for development of finishing toolpath capable of accommodating the subsequent anticipated machining errors. The new toolpath approach is based on adaptation of the geometrical 3D CAD model in STL form which is used to generate trajectories by CAM software. The first workpiece is machined using toolpath generated from commercial CAM package, which is then scanned optically. The point cloud data of the scanned part is compared with the original STL part model to determine the displacement vectors, which are used to find a compensated workpiece model, which is intern used as a reference to develop the final compensated NC toolpath for actual production of parts.

Azzam et al. [61] have reported that there is a direct relationship between mesh refinement in STL and the surface quality of machined surface in 5-axis machining. Thus finer mesh will offer a better surface finish and effect of flat facets on machined surface is minimized. This, however increases the toolpath generation time. Lin et al. [70] has developed a methodology for generating triangulated meshes from 3D scanned point cloud data. They first developed a set of parallel section curves using curve fitting algorithm and then used a triangulation algorithm to generate the triangular meshes to model the original design surface. The triangulated data is then offset to create NC toolpath for 3-axis machining for a ball nosed end mill. Hwang [102] developed the method of triangulation of parametric surface and then generated the toolpath data for machining of the triangulated surface using a ball end mill. The author proposed that it is computational simpler as well as efficient method for determining the toolpath data compared to finding the toolpath data from parametric surfaces. The toolpath generation method can be easily extended to other tool shapes as well.

It is clear from the above discussion that a triangular mesh generated with suitable tolerance/ surface accuracy can reduce computational complexity and increase the efficiency of the toolpath generation for sculptured surface machining.

2.4 TOOL POSITIONING TECHNIQUES

In this section the tool positioning methods used for 3-axis and 5-axis machining of faceted surfaces are explored. The 3-axis tool positioning techniques have been extensively researched for faceted models [12, 20, 30, 32, 33, 35-36, 39-49, 51-53, 55-69, 100-101], whereas the work in the area of 5-axis machining is limited [31, 38, 50, 54]. Lasami et al. [20] have presented the review of the published literature related to CNC machining of freeform surfaces. The authors have discussed in detail the advances in methodologies for toolpath planning and other requirements for machining of sculptured surfaces like tool shapes, part geometry format, machining method like 3 or 5-axis.

The available 3-axis toolpath generation approaches for machining of sculptured surfaces can be classified into two categories namely: the cutter contact (CC) methods and the cutter location (CL) methods. In the cutter contact (CC) methods, the first step is to locate the cutter contact (CC) point between part surface and the tool, which is later used to determine the gouge free tool position. In the CL surface approach, also known as offset surface approach, the offset surface is generated from the designed part surface and then using certain suitable toolpath footprint pattern the toolpath is constructed. Most of the CL surface methods use the uniform surface offset techniques and are suitable for toolpath planning for ball end milling cutter only [36].

The CL method offers smooth NC toolpath compared to CC surface method. The toolpath data obtained from CL approach is better particularly for high speed machining (HSM) because it allows better smoothing of cutter load and for even chip thickness [116]. But the computation of accurate CL surface is a challenge, especially for compound parametric surfaces. The use of other surface representation such as a faceted/meshed/STL surface or a Z-map model for computation of CL surface is relatively simple and a computationally efficient alternative. The Z-map is a discrete non-parametric surface representation of part surface which contains the information about the Z-height of regular grid points taken on part surface in a 2D array. Choi and Jerard [116] have explained the procedure for determining

CL-surface for Z-map surfaces. The authors have indicated that the Z-map data is insufficient for toolpath generation for most precision machining operations as it suffers from the same deficiencies as a point cloud data which are discussed earlier.

Faceted or triangulated models can be used for creating CL surface data as discussed by Park [36] which seems to be an efficient alternative for 3-axis machining. However, implementation of this technique for generating gouge free toolpath data for 5-axis machining is quite difficult. For convenience the literature survey for 3-axis and 5-axis toolpath planning methods is discussed separately as presented below:

2.4.1 3-axis tool positioning methods

3-axis toolpath methods are of two types namely: offset surface and those which use "drop the tool" concept. The determination of 3-axis toolpath, particularly for faceted models, comprises of varying ways of dropping an end mill cutter along a predetermined tool-axis direction until the tool touches the part surface at a contact point called CC point. The tool center corresponding to the CC point is taken as the CL point and is stored as a part of the toolpath data. The faceted surfaces/ part models are approximate representation of the original part surfaces. The level of accuracy used in creating the approximate faceted models will be reflected in the toolpath generated and the final machined part. But as discussed earlier in section 2.3.3, the faceted surfaces can offer a balance between accuracy of the toolpath generated and the reduction in the computational complexity of the mathematical model used for generating the toolpath.

The first method that used surface offsetting was the polyhedral offset method. The tool positioning for complex sculptured surfaces represented by an approximating polyhedron are developed by Duncan and Mair [98]. The developed toolpaths were generated using tool location (CL points) for a ball end milling cutter which is located tangentially to triangular facets such that the cutter contact (CC) point is located on the centroid of a facet. The final toolpath is developed as a systematic collection of such CL points obtained from all facets.

Hwang and Chang [13] presented a tool positioning approach for tessellated surfaces using a flat and radiused end mill cutters for 3-axis roughing and finish machining. The developed method finds the tool position from the CC points determined on cutting edge of a tool vertically positioned on the triangulated part. Jun et al.[35] have presented a curve based

surface offset approach for 3-axis machining of faceted models with ball end milling cutter using an analytical method. The approach developed for finding the accurate surface offset model is capable of handling concave as well as convex regions for gouge free toolpath generation. These toolpaths can be more suitably machined on the machining center with NURBS interpolator, but this method can generate the toolpath data for a ball end milling cutter only.

Yau et al. [41] have reported a unified method for 3-axis tool positioning for the cutter geometries defined by generalized APT (Automatically Programmed Tools) cutter shape for machining of faceted surfaces. First the CC point is determined between a vertically projected generalized APT tool on a faceted surface, which is then used for finding the cutter location. Authors demonstrate that the toolpath generation is more efficient using faceted models compared to using parametric surfaces. Chuang and Yau [43] have presented a z-level contour toolpath generation approach for 3-axis machining of triangular faceted surfaces using fillet end mill. Authors reported that the z-level machining methods need accurate CL surface for their implementation, which are generally generated either by surface offset techniques or using a high-density z-maps data. These two surface offset methods are computationally expensive and require large amount of memory space. Therefore, the authors developed a new toolpath approach where the contour of the projected region of the tool is identified on the faceted surface, and then the vertices of facets in the contour region are offset along the direction which is normal to the edges of the facets falling in the contour region. The amount of offset is found from cutter size and the part surface and the offset of the contour region is then used to find the CL data for filleted end mill.

Kim and Yang [44] have introduced a method for 3-axis toolpath generation which is based on offset of triangulated meshes for a generalized APT cutter and a cutter shape defined by a parametric curve. The offset cutter location (CL) surface for the triangulated meshed surface is generated using a curve defining the cutter geometry and the offsets of the vertices of the facets along the multiple surface normals of triangulated facets through each of the vertices. The offset CL surface is used to find the toolpath data for the given tool shape geometry. A similar method for 3-axis toolpaths for machining of STL models is developed by Bu et al. [48], which use a vertex-based entity offset algorithm for computing the roughing and finishing toolpath for a flat and a ball end mill cutter. Kim and Yang [49] developed a method

of 3-axis and 5-axis toolpath generation based on uniform offset of incomplete triangular meshes for machining with a ball end mill.

Chen and Shi [52] developed a technique for generating 3-axis toolpaths for a ball end mill cutter using offset meshed surfaces. In the developed method first a triangulated meshed surface is developed form original freeform surface, which is used later for generating an offset meshed surface by offsetting the vertices of facets of meshed surface along the facet normals. The gap between the offset vertices thus generated, is connected using new triangulated planer facets. The offset faceted surface is then sliced with series of parallel planes to generate the planar toolpaths for 3-axis machining, but these toolpaths are suitable for machining with ball end mill cutter only.

Manos et al.[51] presented the ball-drop method for generating the spiral toolpaths for 3-axis machining of pseudo-symmetrical ornamental part models taken in STL format. The developed toolpaths are suitable for machining on a milling lathe with a rotary axis and two translational axes. To determine the gouge free tool location, the ball end mill is dropped along a direction normal to the axis of rotation of the pseudo-symmetric part such that the tool just touches the triangulated surface at a CC point farthest from axis of the rotating part. The mathematical model used to find the farthest CC point and hence the corresponding CL point for the dropping ball end mill, tests separately each of the facets, edges and vertices falling under the tool shadow, for every tool footprint location on the spiral path. In an extension of the ball-drop method, Patel et al. [58] developed a “drop the tool” approach for finding the gouge free 3-axis vertical tool positioning for a generalized geometry of radiused end mill for machining of STL models. The generalized radiused end mill cutter encompasses the shape of ball and flat end milling cutters as shown in figure 1.2 in chapter 1. At each toolpath footprint location, the valid CC points are identified from each element of triangulated facets found under the shadow of the vertically dropping tool namely: all facets, the three edges of each facet and the three vertices of each facet. The highest of all valid CC points for a given tool footprint location is taken as the gouge free CC location and then the corresponding CL position is determined.

The CL surface computation for 3-axis machining of STL surface is a computationally simpler and efficient approach. An offset CL surface is developed by Bolaños et al. [62] for 3-axis machining using a generalized radiused end mill cutter which encompasses the

geometric shape of a ball, flat and radiused end mill. The authors have reported that the use of CL surface for toolpath computation is far more efficient compared to ball drop method when the number of triangles are relatively higher. Huertas-Talón et al. [64] used the surface offset method to study surface triangulation. They reported that the accuracy of the 3-axis machining of STL surfaces measured in terms of the surface finish is directly related to the accuracy of input STL data in addition to the accurate selection of the toolpath information. Choi [84, 85] focused on development of toolpath algorithms based on surface offset techniques capable of machining free-form surfaces within a predetermined surface tolerance. The toolpath are developed using the mathematical definition of the part surface. Also, Austin et al. [99] provide a discussion on the use of triangulated models for toolpath planning and the accuracies required in triangulated models for gouge-detection in CNC machining.

Qu and Stucker [100] developed a 3D offset approach for developing an offset meshed surface for an STL model. They have developed a method of offsetting the vertices, instead of facets to generate the offset surface that can be used for toolpath planning. Kim and Yang [101] have reported development of a method for generating constant scallop height toolpaths form STL surfaces using CL surface deformation approach. The toolpaths generated using their approach has been tested and verified by graphical simulations and by actual machining. The machining results demonstrated that better quality of machined surface is achievable using the developed method compared to that of mesh slicing, when the machining time is taken as a constraint.

The most common method of parametric surface machining is the offset surface method. Some variations exist in surface offset methods proposed by various authors as discussed above. Iso-parameter, Cartesian and Z-map techniques have been used by various researchers for parametric surface machining while Cartesian and Z-map techniques are also used for machining of faceted surfaces. It is evident from the discussed literature that STL models have been reliably used for toolpath generation specially for 3-axis machining. Several other authors have also developed the 3-axis tool positioning strategies for various tool shapes like ball, flat, radiused, conical end mill cutters [43, 44, 56, 58, 64, 101]. Most of the 3-axis tool positioning methods cannot be extended or usable for multipoint 5-axis machining of triangulated surfaces because the surface offset methods were developed for ball end mills. As long as the center of the ball is on the offset surface the tool axis orientation does not impact the surface finish. When surface offset was extended to flat and radiused end mills the

offset surface is for a specific tool axis direction and size of tool. Varying tool axis orientation or size of the cutter changes the offset surface. Thus surface offset techniques cannot be generalized and cannot ensure the tool positioning accuracy and gouge avoidance, required for multipoint 5-axis machining. For this thesis work we have selected to build on the "drop the tool" technique.

2.4.2 5-Axis Tool Positioning Methods

There are four main categories 5-axis tool positioning method for faceted surface, which are: (1) trial and error; (2) minimization of objective function; (3) curvature matching, and (4) tool drop method. Few researchers have studied 5-axis tool positioning methods for faceted surface machining. Furthermore, the proposed methods for 5-axis machining of faceted models generate toolpaths for flat end milling cutters only [34, 38, 50, 54]. A brief history of 5-axis machining methods is given in chapter 1 and is not repeated here. The observations from the study of literature related to 5-axis tool positioning methods used for faceted as well as for non-faceted non-parametric surface models are presented below:

The rolling ball method (RBM) evolved by Gray et al.[6], uses part input data in faceted format to approximate the local curvature of the surface. The surface curvature is then used to find the inclinations of a radiused end milling tool for 5-axis positioning. The RBM method does not directly use the faceted surface for toolpath planning rather uses it for surface approximations.

Jun et al.[19] have presented a method for optimization and smoothing of orientations of a flat end milling cutter for 5-axis machining. The developed method is based on a machined surface error analysis technique and takes into account the three types of gouging (local, rear and global) as well as kinematic limits of machine structure to determine an optimal local tool orientation in C-space considering minimization of scallop height as an objection function. The globally optimized and smoothened 5-axis tool orientations are selected based on closest alternate tool orientations in the C-space and the machined surface geometry adjacent to the CC point.

Balasubramaniam et al. [31] developed 3D graphics hardware based global visibility approach for 5-axis roughing toolpath planning for machining of tessellated parts with a flat end mill cutter. The developed method uses the depth buffer of 3D graphics hardware to

identify the tool positions (CC points) which is taken as the location of the centroid of the very fine triangles on tessellated part. The authors reported that a flat end mill cutter may have infinite 5-axis orientations for every CC point and identifying a single optimum solution can be computationally expensive. The developed approach used a three step procedure, namely: visibility determination, posture definition, and a path interpolation. Depth buffer method is used for visibility analysis to find directions from where a CC point in a predetermined machining region is visible to an observer positioned away from the part to be machined. The visibility cone is formed using the set of all possible visible directions for a accessing a particular point in the machining region on the part surface. A concept of 'access profiling' is used to determine the tool diameter and the tool orientation that can be used with the visibility cone formed in the previous step to access the particular point without interference. The posture definition step is then implemented to determine the valid tool orientations for every CC point identified inside machining region. Further the path interpolation step used a graphical simulation and path correction scheme to select the tool postures which avoid the possible interference with the part surface while interpolating between different tool positions. The set of final interference free tool positions are then used to as the toolpath data for 5-axis machining.

Xu et al.[34] proposed a 5-axis tool positioning method for faceted surfaces where a flat end mill cutter located at a CC point is inclined in a plane containing feed direction and surface normal. The amount of tool tilt for 5-axis tool positioning is determined by the constraints imposed by three factors, namely, kinematic limits of the 5-axis machine, gouging, and orientation smoothing between successive CC points in iso-planar toolpath. The developed tool positioning method is suitable for a flat end milling tools and is specific to a specific machine tool. Lauwers et al. [38] have developed a method for computation of tool inclinations for 5-axis positioning, which is based on the curvature matching of a triangulated model with the curvature of effective cutting edge of a flat end mill tool. The gouge elimination is controlled using adjustment of tool-tilt angles and tool retractions.

In an iso-planner 5-axis machining method for faceted models with flat end mill cutter, proposed by Kiswanto et. al.[50], first the CC points are determined as the points of intersection of series of parallel planes passing through the faceted surface. These CC points are used as origin of a right handed local coordinate frame whose direction vectors are defined by the surface normal vector through CC point, a feed forward direction vector and

the unit vector representing their cross product. The direction vectors through the local coordinate frame at every CC points can be used to determine the constant or varying optimal 5-axis tool inclinations. The tool gouging is eliminated later using the concept of tool lifting for the final 5-axis tool inclination for every CC point.

Lu et al. [54] have developed a 3D C-space method for generating 5-axis finishing toolpaths for faceted parts to be machined with a flat end mill cutter. The CC points are determined on the intersection of the boundary surfaces developed from the tessellated surface based on the machining tolerances and the drive plane used to direct the motion of a flat end mill cutter. The CC points are then used to determine an intersection curves. The local curvature of such intersection curves is determined using a method proposed by Lauwers et al.[38], which use a spline to develop an interpolation curve through the intersection of drive plane of the tool and the design surface. The step-over distance for the tool is maximized using the Curvature Matched Method. A C-space determined for each CC point is used to find the optimum tool tilt angles and the tool lift at CC point using the penalty function method which takes into account the machine tool kinematics to ensure gouge free tool positioning. This method use a minimization of tool travel distance concept to smoothen tool inclinations using the upper and lower surface boundaries which define the scallop surface and the gouging tolerance for each tool positioning. The authors have reported that the proposed method of tool positioning is computationally intensive and time-consuming.

Jensen et al. [78] proposed a technique for 5-axis toolpath planning which determines the cutter position and orientation data for a radiused end mill cutter for machining of the parametric surface using curvature matching technique, while the triangulated model of the parametric part surface is used in the later step for gouge and interference elimination. The proposed method works in conjunction with an algorithm for automatic selection of three tool geometry parameters: cutter radius, corner radius and cutter length. The authors developed an objective function for reducing the machining errors and maximizing the material removal rate. The geometry parameters of the radiused end milling tool are found using curvature matching with the region of part to be machined, whereas length of the tool is found using global interference detection.

It is clear from the literature reviewed that use of faceted surfaces for 3-axis and 5-axis NC toolpath planning possess many advantages which include: faceted surfaces are easy to

model, readily available, possess the accuracy desired for most industrial machining applications, and can be used for accurate tool positioning and gouge avoidance. Though some disadvantages do exist in using faceted surfaces, for example, gaps may occur in facet boundaries if the translator or tessellation algorithm used is poor. In case of stringent accuracy requirements very fine triangulated facets have be generated for the part surface in which case the data generated may need large amount of memory space, and large number of computations may be required and it may take longer time to determine a single tool position in such cases. These are minor issues considering the capabilities of today's computers. Moreover, it is clear from literature reviewed that the flat and radiused end milling cutters are the preferred tool geometries for 5-axis machining, whereas in some cases the ball end mill is preferred to access the hidden and inaccessible regions for 5-axis machining [38, 82]. As discussed above, the methods of 5-axis tool positioning, for compound sculptured surfaces modeled using triangular facets, are studied for flat end mill cutter only. Thus, there is a need for development of a direct method for generation of gouge free tool positioning data for a generalized radius end milling cutter for faceted surfaces.

2.5 TOOL GEOMETRY

The quality and efficiency of the machining process depends upon the accuracy of the tool geometry among other things [58, 76-81]. The shape of the milling cutter affects factors like tool wear rate, tool chatter, cutting directions, step-over distance, effective cutter feed, speed, and required surface tolerances [76-82]. The most commonly used tools for surface machining applications, particularly used for machining of sculptured surfaces are ball, flat and radiused (also known as filleted or toroidal) end mill cutters [1-9, 13-16, 20, 23, 30-81, 87, 92, 102-104, 108-120]. Generally the methods used for tool positioning treat each shape cutter separately, particularly for 5-axis tool positioning [63]. The geometry and the size of the cutting tool for surface machining application greatly depends upon the work material properties, material removal rate, geometry and topology of the surface to be machined as well as the types of machining operation used like 3-axis or 5-axis machining. Moreover the cutters used for roughing and finishing operations may have different geometry as well as sizes [41, 58].

Spence et al. [16] developed a simulator for predicting the behavior of 3-axis milling operations using ball and flat end milling cutters. The developed simulator can represent the machining process graphically and model the FEM analysis for the machining process to

detect the tool and part deflection. Mehta et al. [76] conducted an experimental study on face milling cutters to predict the relationship between tool wear and machine tool vibrations. It is revealed that the increase in frequency of vibration in machine tool increases the tool wear rates. Thus for finishing operations, the tool wear rate can be reduced if the machine vibrations are controlled in terms of frequency and the amplitude. This can be ensured to an extent by use of radiused end milling cutter by using the toolpath data which can ensure dynamic balance of cutting forces by proper selection of tool orientation angle with respect to part surface especially in 5-axis machining as reported by Gilles et al. [28].

The flat end milling tool is used extensively in manufacturing industries for 5-axis machining of sculptured surfaces. It is primarily because of the reason that this tool shapes has best material removal capability for near flat regions of sculptured surfaces as explained by Lauwers et al.[38]. But determination of optimum 5-axis tool positioning and orientation of flat end milling cutter for faceted sculptured surfaces is challenging because there can be several possible tool orientations at the CC point and it is difficult to identify the best orientation out of several possible alternate solutions as discussed by Xu et al.[34] and Lauwers et al.[38].

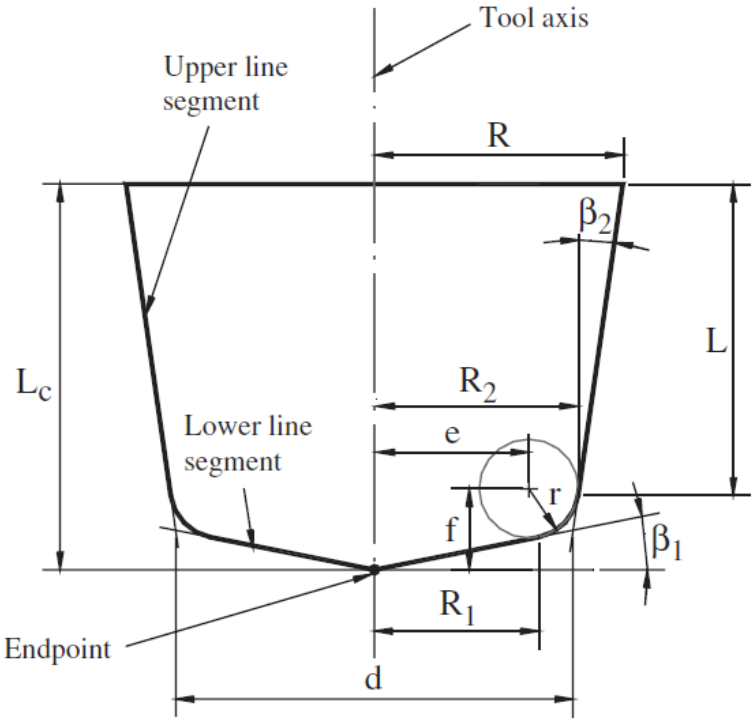

Figure 2.1: Generalized APT cutter geometry [41]

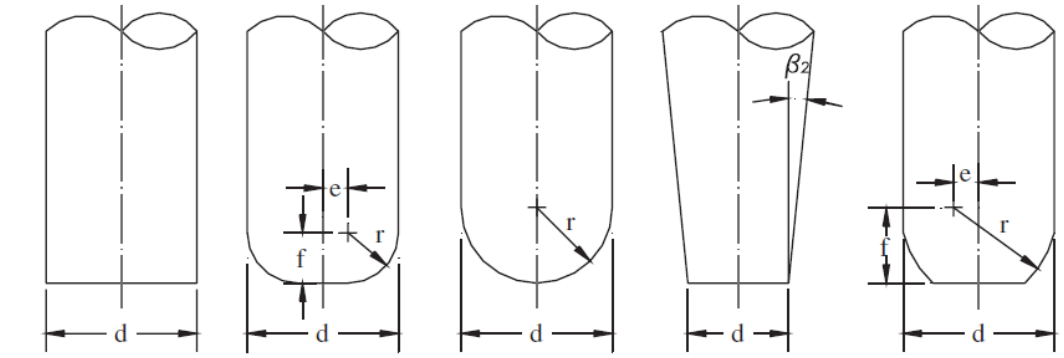

(a) $r=e=f=\beta_1=\beta_2=0$ (b) $e=(d/2-r)$, $f=r$, $\beta_1=\beta_2=0$ (c) $e=\beta_1=\beta_2=0$, $d=2r$, $f=r$ (d) $r=f=e=\beta_1=0$, $\beta_2>0$ (e) $\beta_1=\beta_2=0$, $e<0$, $f<r$, $r>|e|+d/2$

Figure 2.2: Common end milling cutter geometries based on APT definition [41]

Yau et. al.[41] developed a unified approach for determination of CL data for 3-axis machining of faceted models for various end milling cutter geometries defined by a generalized APT cutter. The geometry of the generalized APT cutter along with geometric parameters used to define its shape is shown in figure 2.1. The APT tool is a generalization in the sense that multiple tool shapes can be represented by suitable selection of key parameter values to be used in the mathematical model of APT tool geometry. The figure 2.2 shows the common end milling cutter geometries which can be derived from a generalized APT cutter.
Patel et al.[58] discussed a new methodology for optimal tool shape selection for 3-axis end milling of faceted surface models. The authors compared the material removal, depth of tool penetration and surface finish produced at various sections of faceted sculptured surfaces using 3-axis machining with ball, flat mill and radiused end mill cutters. The authors reported that no single tool geometry is capable of giving the best results for all regions of the faceted sculptured model which may have flat, inclined, convex and concave regions.

Bedi et al. [77] compared the machining results numerically and by performing machining on aluminum, for surface roughness along and across feed directions produced by ball nosed, flat, and radiused end milling tools. The study demonstrated that the radiused end milling tool generates smaller scallops across the feed direction compared to a ball end mill and low surface roughness due to feed marks compared to flat end milling tool. Moreover, considering zero corner radius in case of a flat end mill will generate inaccurate estimate of surface properties like scallop height and surface roughness. It is suggested that the radiused end mill cutters having small corner radius will be able to give the best properties for machined surface results in terms of smaller scallop heights and low roughness along the feed direction.

5-axis sculptured surface machining with a ball end mill cutter cannot realize the advantages of the change in tool shape as it is inclined with respect to the part surface and the curvature of the effective cutting edge in this case is the same as in 3-axis machining. Furthermore, the cutting speed at the tool bottom is zero. This results in tool rubbing against the part surface rather than cutting it. A flat end mill cutter has better cutting characteristics but it is physically impossible to get a sharp corner/ cutting edge of the tool. Use of a radiused end mill is a better alternative compared to using a ball or a flat end milling tool, as reported by Jensen et al.[78]. Senatore et al. [79] compared the step over distance and the quality of machined surface for a ball and a radiused end milling cutter for 3-axis machining. It is found that for same outer radius of the two tool types, the radiused end mill gives better machining results as well as wider step over distance. Thus the overall machining time will be less using a radiused end mill tool.

Accurate cutter shape information is necessary for precise and efficient machining of sculptured surfaces. As a step for accurate modelling of cutting tool geometry, Khan and Tandon [80-81] developed a NURBS and sweep surfaces based technique to model the 3D geometry of a multipoint rotary milling tool. The developed tool model can represent a family of multi-profile milling cutters used for machining of sculptured surfaces. Chen et al. [103] have explored the relation of machining efficiency in 3-axis machining with feed direction, cutter geometry, and surface geometry. Chung et al. [113] developed an approach for modelling swept surfaces for ball and flat end milling tools to represent the 3-axis machining simulations, which can be used for virtual comparison of the machining results from the two tool shapes.

It is clear from the literature reviewed that the toroidal/ radiused end mill offers better surface machining characteristics for 5-axis machining of sculptured surfaces, where it can achieve wider cut width per machining pass while generating relatively smaller scallop heights [1-2, 5-7, 13, 15, 20, 41, 58, 77]. Also, the geometry of a radiused end milling cutter can be considered as the geometric generalization for ball end mill and a flat end mill cutter. The geometry of cutting edge of a flat end mill is identical to a radiused end mill cutter in the sense that the corner radius of a flat end mill cutter cannot be zero [77]. The corner radius in case of a roughing flat end mill may range in a few microns, and from a few microns to fraction of microns for a very fine finishing flat end milling cutter compared to a relatively

larger corner radius in case of radiused end milling tool. Also the bottom of a ball end mill is not completely spherical, rather it has a very small flat region at the tool bottom to prevent the zero cutting velocity region, thus it can be thought of a radiused end mill with very large insert radius (R_i) compared to the offset radius (R_o) of the radiused end mill cutter as shown in figure 1.1 and 1.9. This generalization of three tool shapes will be used for development of a unified tool positioning approach for 5-axis tool positioning for machining of faceted surfaces.

2.6 TOOLPATH FOOTPRINT PATTERN FOR FINISH MACHINING OF FACETED SCULPTURED SURFACES

The tool footprint or toolpath pattern greatly influences the machining accuracy of sculptured surfaces. The toolpath footprint pattern locations are used to find the tool position information. The toolpath footprint is the pattern followed by the moving tool to cover the entire region of the part surface for removal of excess material. The toolpath pattern affects the magnitude of scallop height, machining time and overall stability and efficiency of machining operation [20, 23]. Manos et al. [51] has reported that the most common toolpath generation methods are isoparametric, Cartesian, offset surface, feed forward, and side-steps method. The authors added that, in addition to describing a tool's route, the toolpath generation methods must also guarantee minimum deviations between the desired and actual machined part surface.

Chen and Shi [52] reported that the parallel toolpaths are suitable for controlling the feed rate for smooth machining of freeform surfaces. Lee et al. [53] have developed an improved drive surface based method to determine unevenly placed, constant scallop height, CL-paths for 3-axis machining for ball end milling cutter using the curvatures determined from the meshed model. Yang and Feng [56] developed a methodology for iso-planer CL toolpaths for finish machining. The toolpath are determined within a user defined tolerance zone used, which is used to develop two faceted offset surfaces from the original design surface, where one of the faceted offset surface represents the under-cut limit while other represent the over-cut limit. The triangulated meshed offset surfaces are generated by offsetting the facets, edges and vertices, and further Z-map method is used to remove the self-intersections between offset elements. The developed method is suitable only for ball end milling cutter for 3-axis machining.

The iso-planar toolpath does not perform well for machining of flat regions of freeform surfaces due to redundant machining paths. To resolve this issue, Li et al. [57] developed a new 3-axis toolpath generation methodology to remove the unevenness of conventional iso-planar toolpaths as observed in 3D space. The input part geometry is used in faceted form and a method of least-squares conformal map (LSCM) parameterization is used to unfold the triangular facets of 3D part model on a 2D plane. The iso-planer cutter contact paths are then determined using principal component analysis (PCA) method, which are later translated back to 3D toolpaths. The developed method is tested using 3-axis CNC machining using a ball end milling cutter for toolpaths having scallop height of the magnitude of 0.5 mm which seems to be very course for most engineering applications.

Huertas-Talón et al. [64] used spiral toolpath pattern for development of 3-axis toolpath data for machining of STL surfaces with a ball end mill cutter. The spiral toolpath pattern does not leave the impression of direction changes and can help achieve higher machining feed rate as well as surface finish. The author reported that accuracy of the machined surface is directly related to the toolpath footprint pattern used for toolpath generation in addition to the accuracy of input STL data. Xu et al. [68] have developed a methodology for non-self-intersecting spiral offset toolpath patterns for machining of faceted surfaces. The proposed methodology is said to be suitable for non-convex surface and is relatively better compared to the conventional projection method. The developed spatial offset toolpaths has been improved using a corner rounding method based on transition arc to prevent the uncut regions.

Lacalle and Lamikiz [82] have discussed about the selection of optimal toolpaths and cutting parameters (like feed, speed and surface tolerances) for sculptured surface machining using high speed 3-axis milling using ball-end milling tools and 5-axis using ball or flat-end mills. The toolpath footprint pattern is a key for efficiency and accuracy for milling of free form shapes as reported by Marshall and Griffiths [83]. The authors compared five toolpath topologies spiral (collapsed boundary), spiral (scaled boundary), zigzag (workpiece parallel sweeps), zigzag (isoparametric parallel sweeps) and space filling curves. The spiral toolpaths are suitable for pockets, pocket boundaries and sides, while the zigzag and space filling curves can be applied for machining of general shapes. Authors developed a method to identify the toolpath strategy that is applicable to general features, general shapes, should be able to generate the toolpath data for machining within required tolerances and efficiently.

The authors concluded that the zigzag (workpiece parallel and contour parallel) paths are better suited for milling of general features and surfaces.

Huang and Oliver [104] have discussed parameterization of the surface to determine the step size while maintaining the machining errors within a desired tolerance. The linear feed-forward tool motion between two tool positions is used to determine the deviation between the actual straight line toolpaths and the desired surface. The step-over increments, which are the distance between the adjacent toolpaths in the side-step direction, are used to determine the height of cusps that remain after the machining process. Thus, the toolpath is basically recognized as a set of tool positions for the tool to traverse and interpolate into a smooth path movement. Hence, the method of determining the tool positions is a factor that can affect the finish quality of the machined parts.

The methodology used for tool positioning for machining of faceted surfaces is independent of toolpath data [58]. Thus independent study can be performed for tool positioning determination and for determining the most efficient toolpath footprint pattern. The identification of suitable toolpath footprint pattern is the key to efficiently machine the designed part surface with required surface finish [8-12, 15, 17, 20-25, 30, 38, 41, 43, 45-49, 51-53, 61, 64, 79, 82-86, 88-90]. For defining a typical toolpath footprint for machining, first the faceted models a rectangular region defining the part boundary can be identified. This rectangular region is then projected on a plane normal to tool axis, which is generally perpendicular the z-axis. The footprint patterns may have several shapes like zigzag, raster, contour parallel or space filling curves, and which are selected based on the feed directions of the cutting tools and the surface finish requirements. The most commonly used footprint patterns are the zigzag pattern or the contour parallel pattern as reported by Lasemi et. al.[20] and Kim and Choi [85]. The toolpath footprint pattern is discretized into small steps called feed-forward step and side-step, which are important factor in toolpath planning because the machine movements are discretized into finite piecewise motions based on these two values. At each point on the toolpath footprint a gouge free tool position is determined. Thus the desired toolpath data comprises of information about the position and orientation of the tool moving between consecutive tool positions along the toolpath footprint [58, 63]
The DTM method developed in this thesis work for 5-axis tool positioning of a generalized radiused end mill cutter on faceted surfaces is independent of toolpath footprint pattern and any type of toolpath footprint pattern can be used with this method [63, 65-66, 69]. Toolpath

planning is not the focus of this thesis work and further investigation is required to integrate the developed tool positioning method with a toolpath planning algorithms. For demonstrating the capability of the developed 5-axis tool positioning algorithms the zigzag footprint pattern is mostly used for toolpaths generation for various test parts presented in this thesis work.

2.7 CONCLUSIONS OF THE LITERATURE REVIEWED

The 5-axis machining methods are efficient and capable of generating better machined surface properties for sculptured surfaces compared to 3-axis machining methods especially using a radiused end milling cutter. For a user specified surface finish, the 5-axis finish machining of sculptured surfaces can be accomplished with larger side-step values using a radiused end milling tool. Thus the finish machining process gets executed in lesser number of machining passes which can save a lot of machining time. The merits of radiused end milling tool are well-established for 3-axis and 5-axis sculptured surface machining [20, 34, 58, 77, 65]. Moreover the radiused end milling cutter can be used as the geometric generalization of a ball and a flat end milling tool [62].

The multipoint 5-axis tool positioning methods can provide toolpath data that can make significant difference in terms of the efficiency gain and the surface properties that can be achieved compared to other 5-axis tool positioning methods. At the same time, the computation of gouge-free tool positioning data for 5-axis multipoint machining of complex sculptured surfaces in parametric form is a great challenge, because it need solution of higher order simultaneous transcendental equations. The computational complexity of the mathematical procedure increases multi-fold with increase in the order of the part surface model and the tool geometry in determining the multipoint 5-axis toolpath data. One possible and feasible solution to tackle the computational complexity of 5-axis multipoint tool positioning is the use of faceted representation of the 3D part/surface model.

It is observed from the published literature that the studies related to 5-axis machining of sculptured surfaces using radiused end milling cutter are limited to parametric surfaces only. The multipoint machining method developed for machining of faceted surfaces using a radiused end milling tool is the RBM method, and its extension call AIM method developed by Gray et al.[6, 7]. The implementation of these two 5-axis multipoint machining methods is

quite complicated. Although some other authors have developed 5-axis toolpath algorithms for faceted models, but their methods are limited to flat end mills [34, 38, 50, and 54].

It is also observed from the literature reviewed that three kinds of approximations are being used in 5-axis toolpath generation algorithms, which are: (i) approximations of the part surface under the tool shadow around the first point of contact (may be with grid of points on the part surface or triangulation of region close to CC point or use of triangulated data for the entire surface), (ii) approximations used for simplification of mathematical logic to avoid the local and global gouging of the cutting tool into the part surface, and (iii) the use of path smoothing functions to avoid the abrupt fluctuations in the computed toolpath data required for smooth interpolation of tool through the computed CL points while moving in the feed forward direction. Setting-up higher precision requirements for each the three aforesaid computational steps will significantly reduce the efficiency of the tool positioning algorithm, while accepting a reasonable tolerance in the three levels of approximations mentioned above can commute to a non-acceptable magnitude of computational error in some or other form. An alternate idea is to use the discretization of the input surface into faceted data and use this faceted data as an absolute reference to generate the toolpath data for a generalized radiused end mill cutter.

The review of literature presented in this chapter establishes the need for development of gouge free 5-axis multipoint tool positioning method for generalized radiused end mill for machining of faceted surfaces. The developed method must be computationally accurate and efficient. Furthermore, it should be easily adopted for industrial use.

The main issue with the available MPM methods is that the tool rotation is done about two orthogonal axes. This results in a transcendental equation which must be solved while ensuring tangency and contact of tool with the part surface. In this work the search for two points of contact is broken into two steps. In first step, the tool is dropped along a user specified tool axis direction onto the part surface, and for this fixed tool axis direction a first contact (CC) point is determined using a generalized 3-axis tool positioning approach which is based on the ‘drop the tool’ method developed by Patel et al. [58]. The second step is based on a unique observation, that if a radiused end mill is rotated about the axis of the pseudo-insert at the first contact point, it does not loose its contact with the initial point. So in this step the tool is tilted about the axis of the pseudo-insert at the first contact point until it

touches the part surface at a second point. This observation is the basis of the work presented in this thesis.

Thus, in this thesis work a generalization of the "3-axis drop the tool" concept proposed by Patel et al. 58 is developed and is extended for 5-axis tool positioning. In the generalized tool drop approach, a generalized radiused end mill is made to approach the designed part surface along any predetermined tool-axis orientation to determine a gouge free CC point on faceted part surface. The first CC point thus determined is used as a reference to search for the best 5-axis tool orientations with in the anticipated range for tool tilt angle. The tool tilt angle determined for 5-axis tool positioning ensures the identification of gouge free second point of contact between tool and part surface [63, 65, 69]. The tool positioning methods developed in the course of this thesis work is gouge free as well as free of global tool interferences. The new methodology developed for machining for faceted surfaces using a generalized radiused end milling cutter has been named as drop and tilt method (DTM) of 5-axis tool positioning [63, 65] and is presented in detail in the next chapters of this thesis work. In the developed tool positioning approach the local gouging is avoided by the 3-axis generalized "drop the tool" algorithm, while the global gouging is taken care of by the "Drop and Tilt" algorithm while determining the tool-tilt angle for 5-axis tool positioning. The interferences caused by the tool holder and work holding devices need special attention and are not considered in the present work.

The detailed methodology of the DTM method is presented in the chapter 3 along with the result obtained from the developed method. The generalization of the "3-axis drop the tool" concept is presented in the 4th chapter. The implementation of the DTM method was initially tested in Maple^{TM} symbolic algebra environment. For implementation of DTM method using a standalone solver a new numerical DTM approach was developed which is efficient compared to original analytical DTM approach. Thus in chapter 5, the numerical implementation of the DTM method is presented along with the simulation and machining results of some of the test parts. The edge-torus tangency is the most complicated step in implementation of numerical DTM method. Thus a new edge-torus tangency method was developed to enhance the computational efficiency of the DTM method and is presented in chapter 6 along with the simulation results. The conclusion derived from the work done during this thesis work is presented in chapter 7 along with scope for future work.

CHAPTER 3

DROP AND TILT METHOD OF 5-AXIS TOOL POSITIONING

3.1 INTRODUCTION

The important criterion for 5-axis toolpath planning for faceted/STL models are discussed in the chapter 1 and 2. In published literature the faceted models have been used to generate accurate toolpaths for 5-axis machining of sculptured surfaces suitable for industrial applications. Literature surveyed also shows that radiused end milling cutters have better 5-axis finish machining capabilities compared to a ball or a flat end mill, but the computational complexity of 5-axis multipoint tool positioning of a radiused end mill is a challenge [1-8, 14, 20, 77].

In this work an innovative idea for 5-axis multipoint machining is proposed and demonstrated. Most methods to date try to find the multiple contact points in a single step. Finding the tangency points is difficult with higher order surfaces, at the same time finding the multiple points of contact makes the problem very challenging. If the process of multipoint tool positioning is to be simplified then an alternate technique is required. It is proposed to divide the multipoint tool positioning into independent steps. Initially one point of contact is found and then the other contact point is determined. Second this work identifies an axis of rotation which guarantees the contact between the tool and the part surface for multipoint tool positioning.

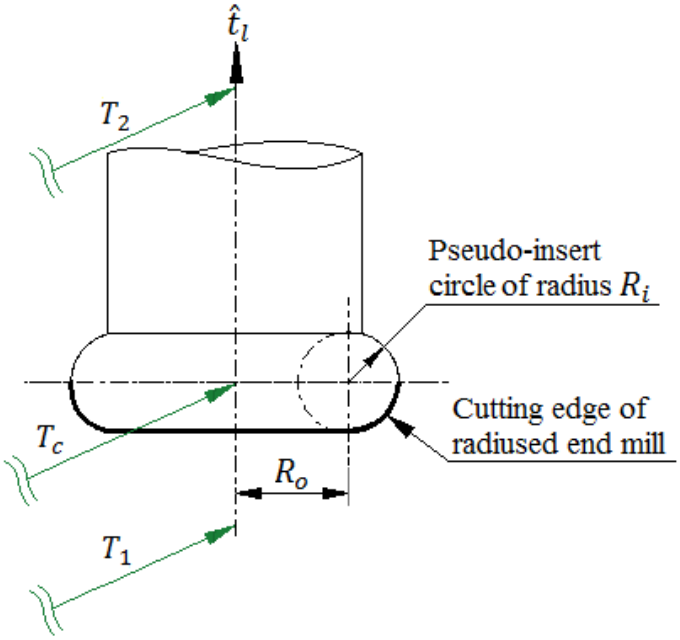

Figure 3.1: Generalized radiused end mill [65]

The first contact point can be found using any known 3-axis method for determining CC or CL point. The search for the second point must ensure that the contact is maintained at first point. In this work a radiused end mill represented as a torus is used for its excellent cutting characteristics. A torus is generated by the rotation of a circle of radius R_i around the circumference of another circle of radius R_o as shown in figure 3.1. This circle of radius R_i is called pseudo-insert circle for a generalized radiused end mill. The circular cutting edge of the radiused end mill is shown in figure 3.1. Note if we consider $R_i = 0$ then the radius end mill models a flat end mill, whereas considering $R_o = 0$ it models a ball-nose end mill.

The toolpath footprint pattern and the tool positioning information are two important and integral component of 5-axis toolpath planning. The tool footprint information which includes path pattern, side-step and feed forward discretization is specified by the user and is known before proceeding to compute the tool positioning information. In this work a zigzag toolpath pattern is used. This path pattern is discretized into points and the tool position is determined at each point. For a given point the tool is aligned to the default axis and positioned to touch the part surface. The toolpath is constructed by moving the tool between consecutive CL points. These choices do not restrict the validation of the tool positioning method and it can be applied to other tools, regions and footprints.

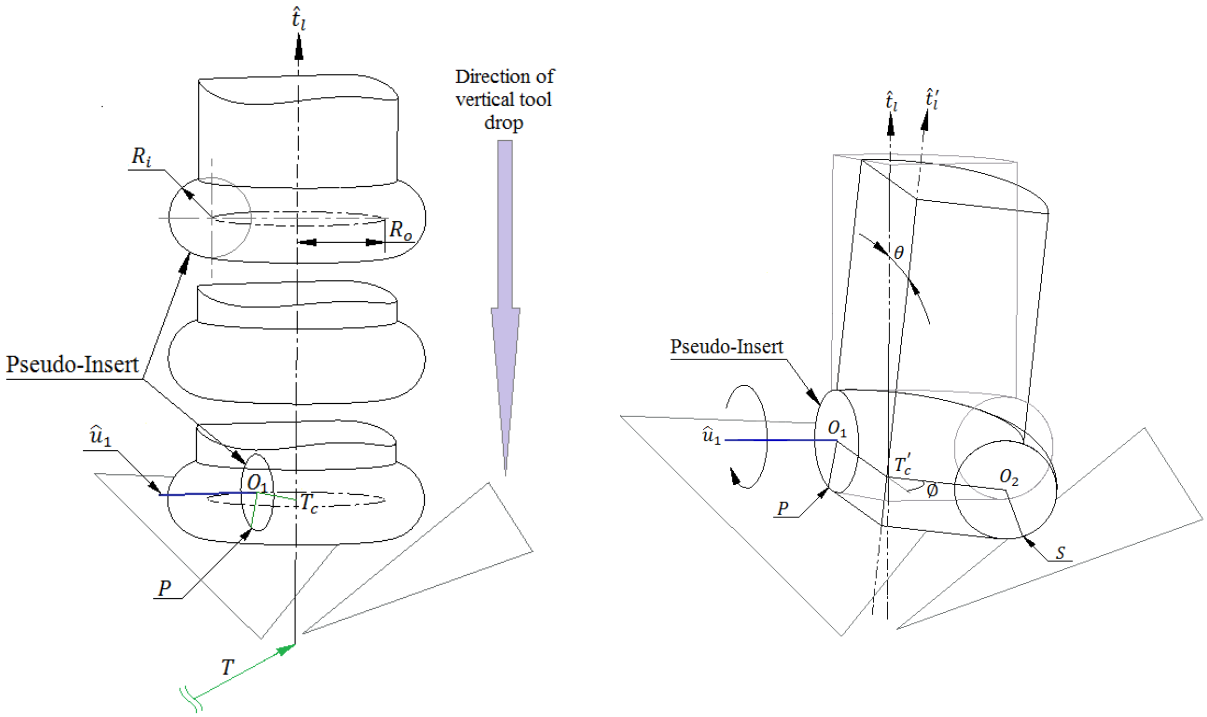

(a) **(b)**

Figure 3.2: (a) Vertical drop of toroidal tool on STL surface, (b) toroidal tool rotated about center of pseudo-insert [63]

The 3-axis tool drop method developed by Patel et al. [58] is used to determine a point of contact P between a radiused end-mill and a triangulated surface. The pseudo-insert located at the point of contact P has a special characteristic. If the tool is rotated about the center of pseudo-insert the tool will retain its contact with point P. The pseudo-inset axis $\hat{u}_1$ and center at O_1 are shown in figure 3(a) and 3(b). The tool will tangentially touch the faceted surface at this point of contact. As the radiused end mill is rotated about the perpendicular line passing through the center of the first pseudo-insert circle at O_1 (denoted by the direction vector $\hat{u}_1$) as shown in figure 3.2(b), the tool will maintain the tangency at P as it tilts more towards the part surface. The tilting tool will contact the triangulated surface at a second point S as shown in figure 3.2(b). The first point of contact may lie on a triangular facet, or an edge, or a vertex of the STL surface. Similarly the second point of contact for the rotating radiused end mill can also lie on a facet, or an edge, or a vertex of one of the triangulated facet of the part. This concept called "Drop and Tilt method" is explored in this thesis.

The analytical model of DTM was implemented using Maple^{TM} symbolic algebra environment. The detailed mathematical model used in DTM method is presented here along with the test results. The developed 5-axis toolpaths were simulated and machined successfully on DMU-80P tilt-rotary 5-axis machine.

3.2 DROP AND TILT METHOD

To determine the first point of contact P for a given tool footprint location, the tool at a given footprint location is dropped along a user defined tool axis $\hat{t}_l$ (typically the z-axis). As the tool drops over a particular triangular facet $\Delta P_1P_2P_3$, it may come in contact with the interior of facet, or any of the three edges or the any of three vertices. The highest point of contact where the cutter tangentially touches the triangulated model gives the tool position. The first contact point denoted by point P is as shown in figure 3.2(a). The point P and the tool axis $\hat{t}_l$ define a plane. The intersection of the cutting surface of the tool (a torus) with this plane is a circular arc of radius R_i with center at O_1 as shown in figure 3.2(b). The parent circle of the circular arc is called the pseudo-insert and the arc represents the cutting edge of the radiused end mill. At P the center of the tool is located at T_c which is R_o distance away from O_1 and lies on tool axis.

It must be observed that if the tool is tilted about an axis passing through the center of the pseudo-insert and perpendicular to the plane of the pseudo-insert, $\hat{u}_1$, the contact point on the

part surface will remain unchanged whereas the contact point on the pseudo-insert will move along its arc. The tool remains tangential to the surface. This observation is exploited and the tool is tilted about the pseudo-insert axis $\hat{u}_1$ until it touches a second point S on the triangulated model. The center of the tool and the direction of its axis describe the tool position at the point T on a zigzag toolpath. In figure 3.2(b) the new location of tool center and the rotated tool axis are defined by vectors T_c' and $\hat{t}_l'$.

```
     FindPointOfContact(Tool, STL, METHOD)
1    S = -infinity # initialize contact point to below STL surface
2    for each triangle Tri of STL-Surface
3        Find point of contact cS between tool and plane of Tri
4        If cS is inside Tri and cS higher than S then
5            S = cS
6            next
7        Endif
8        for each edge E of Tri
9            Find point of contact cS between tool and line of E
10           if cS on E and cS higher than S then
11               S = cS
12           Endif
13       End
14       For each Vertex V of Tri
15           If tool contacts V and V higher than S then
16               S = V
17           End if
18       End
19   End
20   Return S

FindTwoPointsOfContact(Tool, STL)
1a   P = FindPointOfContact(Tool, STL, DROP)
2a   S = FindPointOfContact(Tool, STL, ROTATE)
```

Figure 3.3: Pseudo-code for finding two points of contact. Given a tool and an triangulated data file, the two points of contact *P* and *S* are determined by first dropping the tool onto the part surface (giving *P*) and then point *S* is determined by rotating the tool around the pseudo-insert axis.

The process to find the second point of contact is similar to that used for finding the first point of contact. The only difference is that to find the first point of contact, the tool is dropped onto the faced part, whereas, the entire faceted part data is processed for a second time while determining the second point of contact which is found by rotating the radiused end mill around the pseudo-insert at the first point of contact. Mathematical details for these calculations are found in Sections 4 and 5.

The developed 5-axis tool positioning method is able to generate the gouge-free tool position for the following reasons:

(i) The tool drop concept used to determine the first point of contact picks-up the highest point of contact between the tool and the triangle set thereby ensuring that the un-rotated tool does not gouge the triangle set.

(ii) When the radiused end mill is rotated around a pseudo-insert, it is ensured that there is no gouging at the first point of contact.

(iii) For the rotated radiused end mill cutter, the smallest angle of rotation that yields a second point of contact between the tool and the triangle set thereby ensuring that the rotated tool does not gouge the triangle set is chosen as the maximum possible gouge-free tool tilt angle.

The proposed idea is implemented in two stages:

1. In stage one the tool is dropped along a line rooted in the toolpath footprint through a point T and oriented along a user defined direction $\hat{t}_l$. As the tool descends, each of the triangular facets is checked (investigated) independently to determine the highest point of contact where the tool dropping is tangential to the facet and does not gouge it. To determine this gouge free tool location a two-step process is followed for each facet in the surface.

- In step one, the location of the tool as it touches the interior of planar face of the triangle, $\Delta P_1P_2P_3$, is determined. If the contact point is inside the bounds of the triangular facet at height h, then the tool will not be tangent to the edges or vertices of $\Delta P_1P_2P_3$ at a point higher than h. Therefore, the subsequent steps required to test the edges or the vertices of the facet $\Delta P_1P_2P_3$ are skipped, and line 6 of pseudo-code in figure 3.3 is executed. A similar statement is true about the rotating tool.
- In the second step, the locations of the tool as it touches the three edges or three vertices of the triangle $\Delta P_1P_2P_3$ are determined. If the tool is tangent to an edge at a height h, it is still possible for the tool to be tangent to a vertex at a point higher than h, so if the tool is not tangent to the interior of $\Delta P_1P_2P_3$, then we must check all its edges and all its vertices for the highest contact point. A similar statement is true about the rotating tool.

The gouge free tool locations calculated for all the triangular facets are compared and the highest tool location is selected as the gouge free location for the part at the given point T. After dropping the tool and computing the point of contact P, the corresponding center of pseudo-insert O_1, and the pseudo-insert axis $\hat{u}_1$ are determined. The second stage of the

process is to find the magnitude of tool rotation that will allow it to touch the faceted surface at a second point S.

2. In the second stage the tool is rotated about the pseudo-insert axis $\hat{u}_1$ located at O_1. As the tool rotates each of the triangular facets is checked (investigated) independently to determine a second contact point where the tool is tangential to the facet and does not gouge it. To determine this gouge free tool rotation, the two-step tool drop procedure similar to stage 1 is repeated for each facet.

- In step one, the tool is rotated about $\hat{u}_1$ until it touches the planar face of the triangle $\Delta P_1 P_2 P_3$. If the contact point is inside the bounds of the triangular facet $\Delta P_1 P_2 P_3$ then the angle of rotation is noted and the subsequent step is skipped.
- In the second step, the tool is rotated until it touches the three edges and the three vertices of the triangle $\Delta P_1 P_2 P_3$. If the contact points are inside the edge or the tool touches the vertices of triangle under consideration then the smallest angle of rotation is selected as the gouge free tool inclination.

The gouge free tool inclinations calculated for all the triangular facets are compared and the smallest angle of rotation is selected as the gouge free orientation of the tool at the given point T.

This method of 5-axis tool positioning is independent of machine configuration and toolpath strategy and positions the tool directly on the triangulated surface. To handle triangle sets of the part sizes generally found in industry, bucketing and other techniques are required to make the proposed algorithm efficient.

3.3 LOCATION OF PSEUDO-INSERT AT FIRST POINT OF CONTACT

In this section the mathematical formulation used for determining the first points of contact is presented. The first stage uses the 3-axis tool drop method to identify the position of pseudo-insert at first point of contact. Let h be the distance of the tool center T_c from the selected point T on the toolpath footprint along the tool axis $\hat{t}_l$. As the tool descends its point of contact with each facet of the model is determined and the highest point of contact gives the location and orientation of the pseudo-insert as described above. Though it is possible to find points of contact between the STL triangular facets and the tool that are either on the top or inside of the torus representing the tool, but such cases are not considered in implementation

of analytical DTM model to focus on the evaluation of multipoint tool positioning where the initial points of contact are found on the radiused corner of the tool (whether from the facet or edges or the vertices). Thus the cases wherein the dropping tool first touches the triangulated part surface tangentially on the radiused corner of the cutting edge (figure 3.1) are of primary interest and used to find the second point of contact or the 5-axis tool inclination.

The mathematical model used to determine the first point of contact, herein named as point P, between the dropping radiused tool with a triangular facet is broken into three steps. In the first step the point of contact of the descending tool with the inside plane of the triangle is determined as follows:

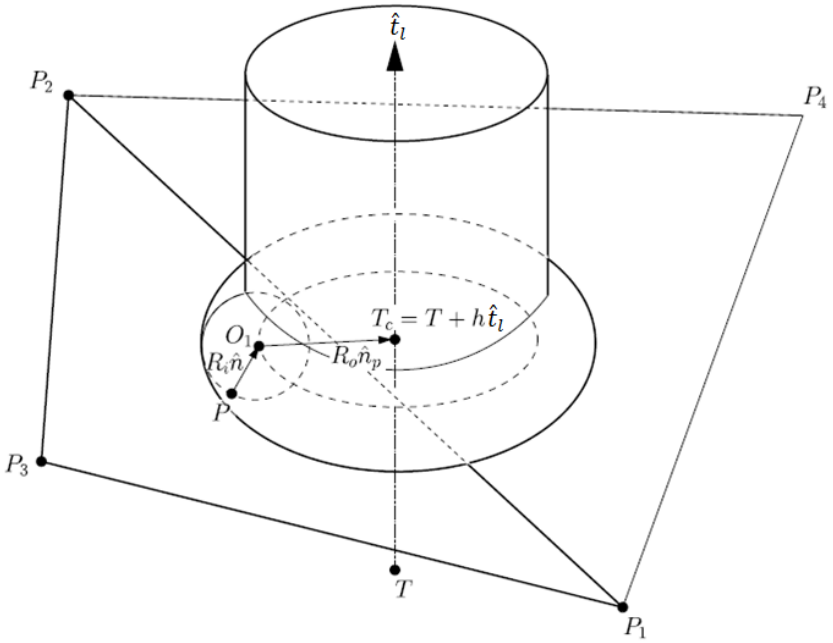

Figure 3.4: Location of first point of contact P between a toroidal tool and a triangular facet $\Delta P_1P_2P_3$

3.3.1 3-axis contact point with a triangular facet

The location of tool center T_c of a dropping radiused end mill as it touches triangular facet $\Delta P_1P_2P_3$ during its descent along the axis $\hat{t}_l$ can be represented as shown in figure 3.4. For a radiused end mill to be tangent to a facet $\Delta P_1P_2P_3$ at point P, the location of tool center T_c can be determined using following two equations, where the first equation relates the tool center T_c to the toolpath footprint location T and distance (height) h up to the point of contact (where h is yet to be determined), and the other equation based on the tangent triangle. These equations are as given below:

$$T_c = T + h.\hat{t}_l \qquad 3.1$$

And, $T_c = P + R_i.\hat{n} + R_o.\hat{n}_p$ 3.2

Where, $\hat{n}$ is the surface normal for triangulated facet $\Delta P_1P_2P_3$ and is given by:

$\hat{n} = [(P_2 - P_1) \times (P_3 - P_1)]/|(P_2 - P_1) \times (P_3 - P_1)|,$

P is a point on the plane of the triangular facet $\Delta P_1P_2P_3$ that can be parameterized as:

$P = P_1 + s.(P_2 - P_1) + t.(P_3 - P_1)$,

Where, $(0 \leq s, t \leq 1)$, and $\hat{n}_p$ is the projection of surface normal $\hat{n}$ in a plane perpendicular to tool axis $\hat{t}_l$ and is given by:

$\hat{n}_p = [\hat{n} - \hat{t}_l \cdot (\hat{n} \cdot \hat{t}_l)]/|\hat{n} - \hat{t}_l \cdot (\hat{n} \cdot \hat{t}_l)|.$

The above simultaneous equations can be solved for s, t and h. If value of s and t is such that they lie between 0 and 1, along with another constraint that $(0 \leq s + t \leq 1)$ then it is a valid solution for point of contact with triangular facet $\Delta P_1P_2P_3$. In addition, to the tool center location T_c and first point of contact P, the center of pseudo-insert O_1 can also be computed as given below.

$O_1 = P + R_i.\hat{n}$

If a valid contact point is found within the bounds of facet under consideration then the next two steps are skipped, and next triangular facet is selected for calculation until all triangles in model are processed. If it is the last triangular facet the computation move to stage 2 for determination of tool orientation as presented in section 3.4. If, however, no valid point is found within the bounds of the facet, then the three edges and the three vertices are evaluated to find the valid point of contact of dropping tool with them using the procedure given in next two steps.

3.3.2 3-axis contact point with an edge

The contact points between the descending tool and the three edges of the facet are determined considering one edge at a time. To determine the contact point between the edge (P_1, P_2) and the descending tool, a cylindrical envelope is imagined around the edge. The cylindrical envelope defined by vector Cyl_1 will pass through the center of pseudo-insert located at O_1 as shown in figure 3.5, which is given as:

$O_1 = Cyl_1 = P + R_i.(\hat{u}.\cos\alpha + \hat{v}.\sin\alpha)$

Where, $(\hat{u}, \hat{v}, \hat{w})$ are unit direction normals of a local coordinate frame at P_1 given by:

$\hat{w} = (P_2 - P_1)/|(P_2 - P_1)|$

$\hat{u} = (\hat{t}_l \times \hat{w})/|(\hat{t}_l \times \hat{w})|$

$\hat{v} = (\hat{w} \times \hat{u})/|(\hat{w} \times \hat{u})|,$

Where P defines an edge through vertices $(P_1,\ P_2)$ given by:

$P = P_1 + s.(P_2 - P_1)$, for $(0 \leq s \leq 1)$

The center of torus representing the tool T_c can be written in two forms as given below:

$$T_c = T + h.\hat{t}_l \quad (3.3)$$

$$T_c = P + R_i.\hat{n} + R_o.\hat{n}_p \quad (3.4)$$

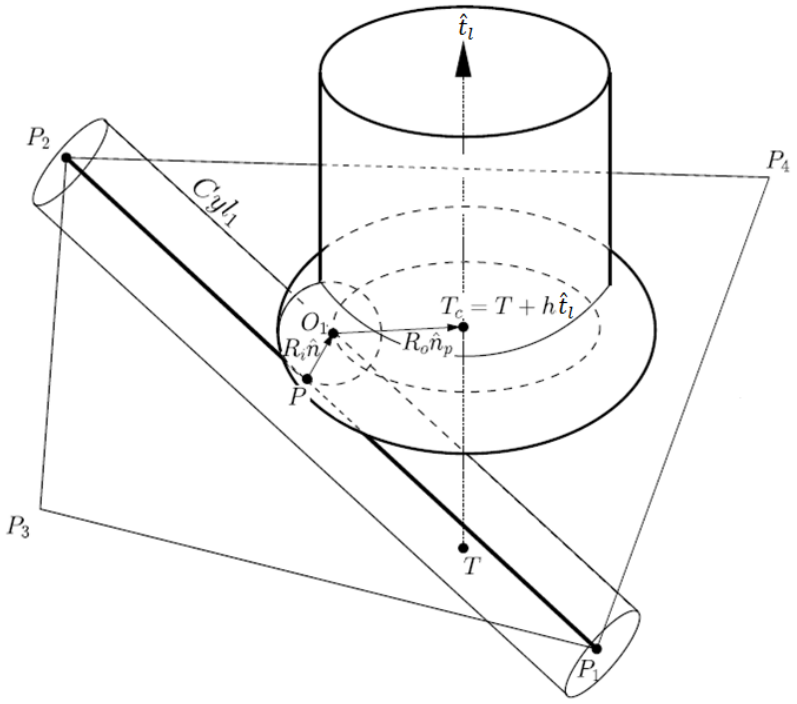

Figure 3.5: Location of first point of contact of toroidal tool in vertical configuration with an edge

The above simultaneous equation can be solved for s, α and h. If value of s lies between 0 and 1, then the contact point lies within the limits of the edge $\overline{P_1P_2}$. From these parameters the tool center location T_c, the point of contact P and the center of pseudo-insert O_1 can be determined for an edge.

Note that in the implementation of present methodology, if the edge $\overline{P_1P_2}$ is parallel to tool axis direction $\hat{t}_l$, then we skip this edge test, and detect any tangencies in the vertex tests. Also, if the tool drops on a horizontal edge, the tool is not rotated since tool effectively already have two points of contact. Further, since such an edge typically lies between two

faces (on our toolpath), not rotating tool on such an edge reduces the machine motions as the radius end mill transition between faces.

The contact points (if any) are determined for each edge of triangulated facet $\Delta P_1P_2P_3$ independently. Any number of edges may result in valid contact points. The highest of the valid contact points is selected as the edge contact point. In case we find a valid point of contact with the edges of facet under consideration or not, under both conditions we still evaluate the possibility of having valid point of contact with the three vertices of the facet $\Delta P_1P_2P_3$ and move to the next step.

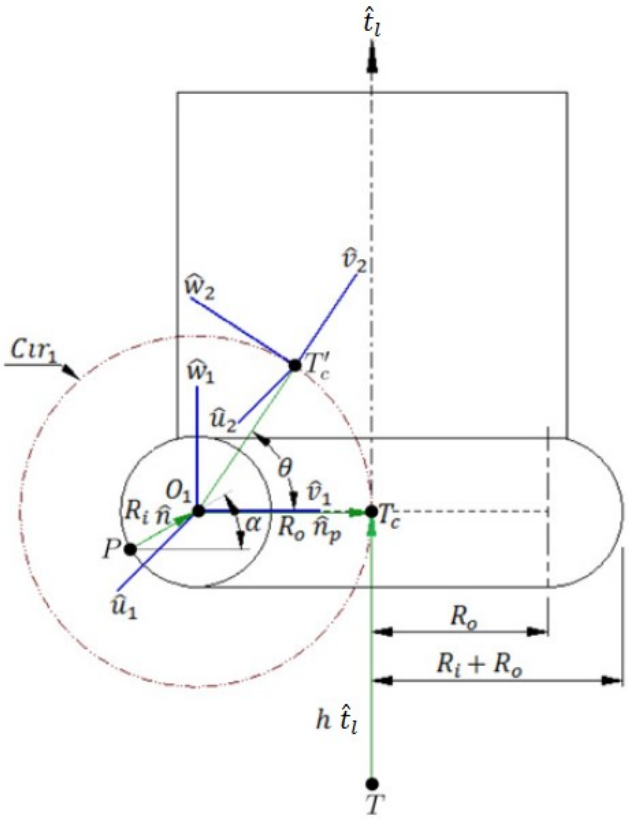

Figure 3.6: Location of first point of contact of toroidal tool with a vertex *P*

3.3.3 3-axis contact point with a vertex

In this step, the contact points between the descending tool and the vertices of the facet $\Delta P_1P_2P_3$ are determined. As the tool descends onto a vertex P, there are three possibilities depending on the shortest distance between the vertex and the axis of tool descent. The shortest distance between tool axis and the vertex P is given by:

$$\left|\hat{t}_l \cdot \left(\vec{P}_t \cdot \hat{t}_l\right) - \vec{P}_t\right|,$$

Where, $\vec{P}_t = P - T$

Case 1: $(R_i + R_o) \leq \left|\hat{t}_l \cdot \left(\vec{P}_t \cdot \hat{t}_l\right) - \vec{P}_t\right|$: in this case vertex P lies away from tool and the descending tool will not touch vertex P.

Case 2: $0 \leq \left|\hat{t}_l \cdot \left(\vec{P}_t \cdot \hat{t}_l\right) - \vec{P}_t\right| \leq R_o$: in this case P lies under the flat region of the radiused end mill and will not touch the cutting edge of pseudo-insert. There are infinite ways of inclining the tool when it encounters such situations. For simplicity, the tool is not inclined at such tool positions in this work.

Case 3: $R_o \leq \left|\hat{t}_l \cdot \left(\vec{P}_t \cdot \hat{t}_l\right) - \vec{P}_t\right| \leq (R_i + R_o)$: in this case the vertex will touch the cutting edge on the pseudo-insert. To determine the tool location as it descends onto a vertex P along $\hat{t}_l$ at toolpath footprint location T (as shown in figure 3.6), the following simultaneous equations must be solved.

$$T_c = T + h.\hat{t}_l \quad 3.5$$

$$T_c = P + R_i.\hat{n} + R_o.\hat{n}_p \quad 3.6$$

Or, combining equation 3.5 and 3.6, we have

$T + h.\hat{t}_l - P - R_i.\hat{n} - R_o.\hat{n}_p = 0,$

Where, $\hat{n} = \hat{n}_p.\cos\alpha + \hat{t}_l.\sin\alpha$, and $\sin\alpha$ and $\cos\alpha$ terms are defined as:

$\sin\alpha = \{(T_c - P).\hat{t}_l\}/R_i$

$\cos\alpha = \sqrt{1 - (\sin\alpha)^2}$

$\hat{n}_p$ is the direction vector passing through vertex P and perpendicular to tool axis $\hat{t}_l$ as shown in figure 3.6 and is given by:

$\hat{n}_p = \left[\hat{t}_l \cdot \left(\vec{P}_t \cdot \hat{t}_l\right) - \vec{P}_t\right] / \left|\hat{t}_l \cdot \left(\vec{P}_t \cdot \hat{t}_l\right) - \vec{P}_t\right|$

The above simultaneous equation can be solved for α and h. Knowing these parameters the tool center location T_c and the center of pseudo-insert O_1 can be determined for a vertex as given below:

$O_1 = P + R_i.\hat{n}$

Any, all or none of the vertices of facet $\Delta P_1P_2P_3$ may result in valid contact points. The highest of the valid contact points is selected as the final contact point. If no valid contact point is found then the facet does not touch the tool as it descends and then the next triangular facet is considered. This process is repeated until all facets have been processed at which point the computation moves to stage two as described in section 3.4.

The above three steps are applied to all the triangular facets in the model and for the given point on the toolpath footprint the gouge free tool contact position P as well as the center of pseudo-insert O_1can be determined which will be used in finding the 5-axis tool rotation as explained in the next stage.

3.4 THE SECOND POINT OF CONTACT AND 5-AXIS TOOL ORIENTATION

After finding the first point of contact of tool with faceted surface and the location of center of pseudo-insert, in the second stage the tool is tilted about the pseudo-insert axis. As the tool rotates, its point of contact with each facet is determined. The point of contact with the smallest rotation determines the final location and orientation of the tool. The procedure to determine the point of contact with a triangular facet as the tool is rotated about the pseudo-insert axis is broken into three steps, wherein the logic for finding the second point of contact with a triangular facet, or an edge or a vertex is established and is explained below:

3.4.1 5-axis contact point with a triangular facet

In the first step, the second point of contact S, between the rotating tool and the inside of the triangular facet $\Delta S_1S_2S_3$ is determined, as shown in figure 3.7. Under certain circumstances the second point of contacts can be found on the same triangulated facet on which first point of contact has been obtained. The second point of contact S lies on a pseudo-insert with center O_2. The following two equations for O_2 allows us to find S:

$$O_2 = S + R_i.\hat{n}_2 \quad (3.7)$$

$$O_2 = Cir_1 + R_o.(\hat{u}_2.\cos\emptyset + \hat{v}_2.\sin\emptyset) \quad (3.8)$$

Where, $S = S_1 + s'.(S_2 - S_1) + t'.(S_3 - S_1)$, with $(0 \leq s',\ t' \leq 1)$,

and, $\hat{n}_2$ is the surface normal for triangular facet $\Delta S_1S_2S_3$, which is given as:

$\hat{n}_2 = [(S_2 - S_1) \times (S_3 - S_1)]/|(S_2 - S_1) \times (S_3 - S_1)|$

and Cir_1 is the trajectory of the tool center T_c as the tool is rotated about pseudo-insert axis O_1 which is shown in figures 3.6 and 3.7 and is given by:

$$Cir_1 = T_c' = O_1 + R_o.(\hat{v}_1.\cos\theta + \hat{w}_1.\sin\theta) \quad (3.9)$$

A local right hand coordinate system with unit direction vectors ($\hat{u}_2,\ \hat{v}_2,\ \hat{w}_2$) is defined at rotated tool center T_c' which moves on locus of Cir_1 as shown in figures 3.6 and 3.7, and its direction normals are given by:

$\hat{u}_2 = \hat{u}_1$

$\hat{v}_2 = \hat{v}_1.\cos\theta + \hat{w}_1.\sin\theta$

$\hat{w}_2 = (\hat{u}_2 \times \hat{v}_2)/|\hat{u}_2 \times \hat{v}_2|$

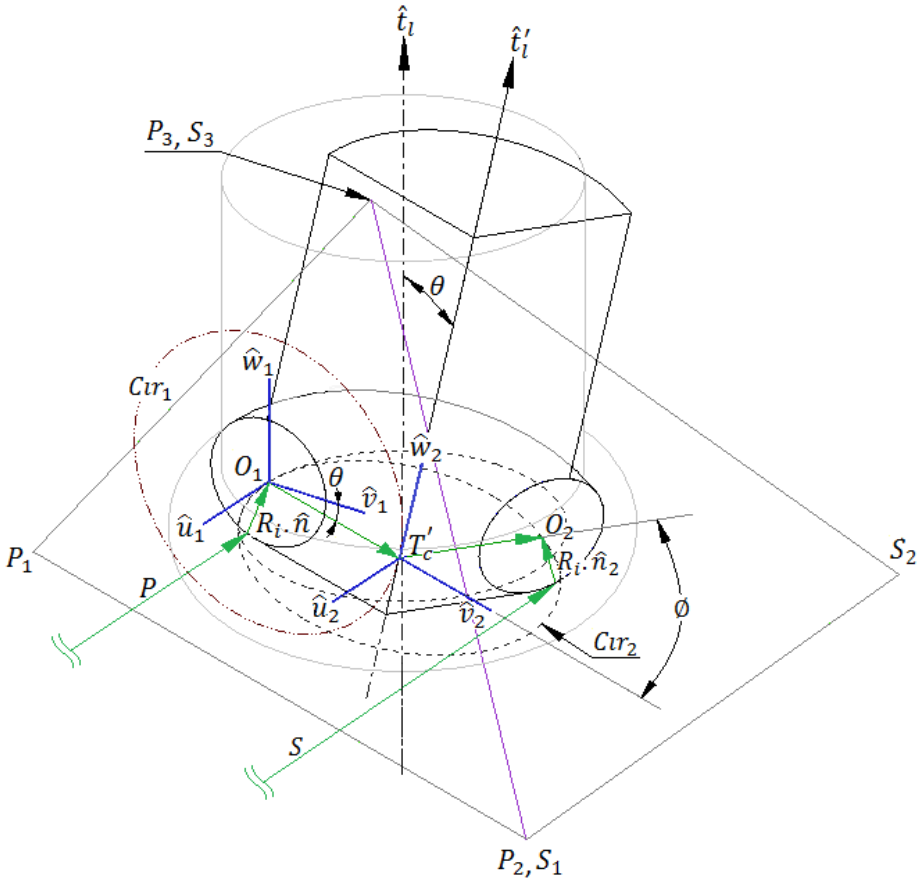

Figure 3.7: Location of second point of contact of radiused end mill and a triangular facet

Also set of direction normal ($\hat{u}_1,\ \hat{v}_1,\ \hat{w}_1$) define a local right hand coordinate system at the center of pseudo-insert $\vec{O}_1$, as shown in figures 3.2, 3.6 and 3.7. These three directions normal are given as:

$\hat{w}_1 = \hat{t}_l$

$\hat{u}_1 = (\hat{n} \times \hat{t}_l)/|\hat{n} \times \hat{t}_l|$

$\hat{v}_1 = (\hat{w}_1 \times \hat{u}_1)/|\hat{w}_1 \times \hat{u}_1| = \hat{n}_p$

In addition to the above equations the surface normal at the second point of contact must be normal to the tool surface and perpendicular to the major circle of the torus. This condition is given by:

$$(\hat{v}_2.\cos\emptyset - \hat{u}_2.\sin\emptyset)\cdot\hat{n}_2 = 0 \qquad 3.10$$

The non-linear simultaneous equations 3.7, 3.8 and 3.10 can be solved for four variables namely two angles θ, and $\emptyset$, and two scalars s' and t'. If the values of s' and t' lie between 0 and 1, along with another constraint that $(0 \leq s' + t' \leq 1)$ then the solution represents a valid second point of contact. Out of all the valid solution for the second point of contact, the one which gives minimum value of tool axis rotation θ is selected as the final solution. If a valid second point of contact exists then next two steps are skipped for the facet under consideration and next facet is selected for computations. Otherwise the solution from present facet is discarded and next step is executed where we evaluate the three edges and three vertices of the facet to find the valid second point of contact, if any.

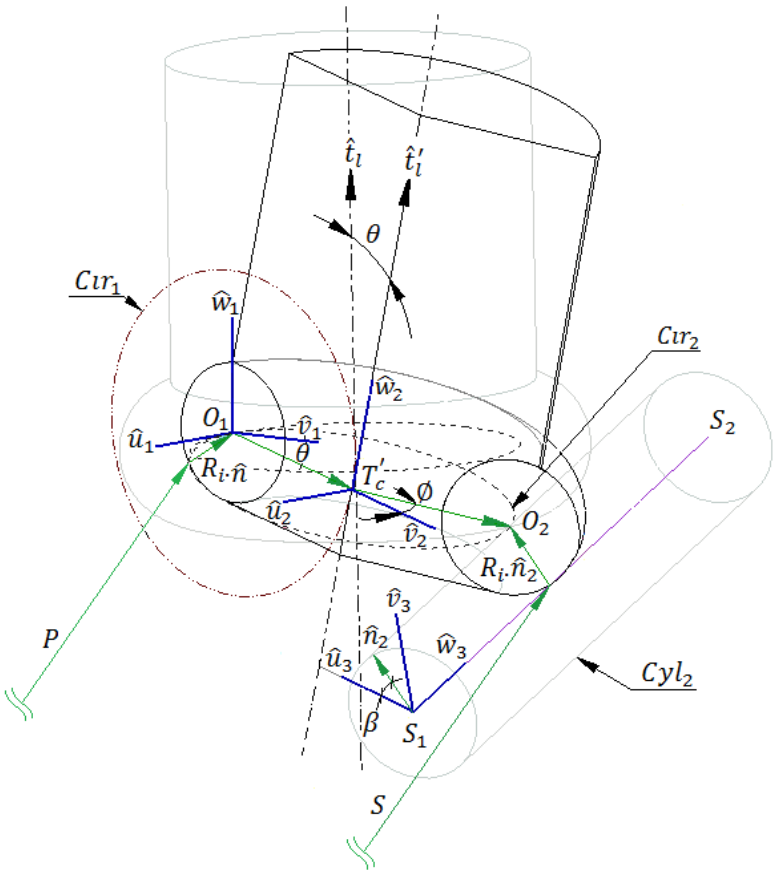

Figure 3.8: Location of second point of contact with radiused tool and an edge

3.4.2 5-axis contact point with an edge

In this step the contact points between the rotating tool and the three edges of the facet $\Delta S_1 S_2 S_3$ are determined. Any number of edges may result in valid contact points. The smallest of the tool axis rotations for the valid contact point on edges of the triangulated facet is selected. If a valid point/s of contact or even if no valid contact point is found from three

edges, still we execute and test the possibility of vertices of the facet touching the rotated tool to give a valid second point of contact.

The contact point between the edge $(S_1,\ S_2)$ and the rotating tool, such that it will just touch the edge of faceted surface tangentially at point S will exist when:

$O_2 = T_c' + R_o.(\hat{u}_2.\cos\emptyset + \hat{v}_2.\sin\emptyset)$

Or, $O_2 = \ Cyl_2 = S + \ R_i.\hat{n}_2$ 3.11

Where, S is the second point of contact between the radiused tool and a new edge $(S_1,\ S_2)$.

Under certain circumstances the second point of contacts can be found on the same edge on which first point of contact has been obtained. The vector S can be defined in terms of a scalar s' as:

$S = S_1 + s'.(S_2 - S_1)$, where $(0\ \leq s' \leq 1)$

And, the direction normal vectors $(\hat{u}_2,\ \hat{v}_2,\ \hat{w}_2)$ and vector T_c' represent the similar entities as derived in the previous steps from direction normals $(\hat{u}_1,\ \hat{v}_1,\ \hat{w}_1)$ defined at O_1 and are shown in figure 3.8.

The direction normal $\hat{n}_2$ through S helps defining an imaginary cylinder Cyl_2 of radius R_i through edge $(S_2 - S_1)$ as axis and is given by:

$\hat{n}_2 = \hat{u}_3.cos\,\beta + \hat{v}_3.sin\,\beta$

Where, a local coordinate system $(\hat{u}_3, \hat{v}_3, \hat{w}_3)$ at S as shown in figure 3.8 is given as:

$\hat{w}_3 = (S_2 - S_1)/|S_2 - S_1|$

$\hat{u}_3 \ = \ (\hat{t}_l' \times \hat{w}_3)/|\hat{t}_l' \times \hat{w}_3|$

$\hat{v}_3 \ = (\hat{w}_3 \times \hat{u}_3)/|\hat{w}_3 \times \hat{u}_3|$

Where, $\hat{t}_l'$ represents the rotated tool axis about $\hat{u}_1$, given by:

$\hat{t}_l' = \ \hat{v}_1.sin\,\theta - \hat{w}_1.cos\,\theta$

The equation 3.11 ensures that the point S on the edge $(S_2 - S_1)$ is R_i distance away from the center of the torus at O_2, but it does not ensure tangency of vector $\hat{n}_2$ to circle Cir_2 through T_c' at O_2. To ensure this tangency the normal $\hat{n}_2$ at S must be perpendicular to tangent to circle Cir_2 through T_c' at O_2. The perpendicularity of direction normal $\hat{n}_2$ to tangent to circle $Cir_2 = (\hat{v}_2.\cos\emptyset - \hat{u}_2.\sin\emptyset)$ is ensured by following equation:

$(\hat{v}_2.\cos\emptyset - \hat{u}_2.\sin\emptyset)\cdot\hat{n}_2 = 0$ 3.12

The equation 3.11 and 3.12 can be solved for angles $\theta,\ \emptyset,\ \beta$ and scalar s'. If value of s' lies between 0 and 1, then the contact point lies within the edge and it is accepted as a valid solution, otherwise the solution is discarded. For all valid solutions from the edges of the facets, the solution which offers minimum value of tool axis rotation θ is accepted as the valid solution for toolpath location and orientation. Then we move to the next step to evaluate the possibility of rotated tool touching any of the three vertices of the facet under consideration at a valid second point of contact such that the tool orientation angle is less than what we get from the edges in this step.

3.4.3 5-axis contact point with a vertex

In this stage the contact position of the rotating tool and the vertices of the facet $\Delta S_1S_2S_3$ are computed. Any number of the three vertices may have valid contact with rotated toroidal tool. Out of all touching vertices, the one which offers the smallest angle of rotation θ is selected. If no valid contact point is found then the facet does not touch the tool as it rotates and the other remaining facets in the model can be evaluated for the current tool footprint location.

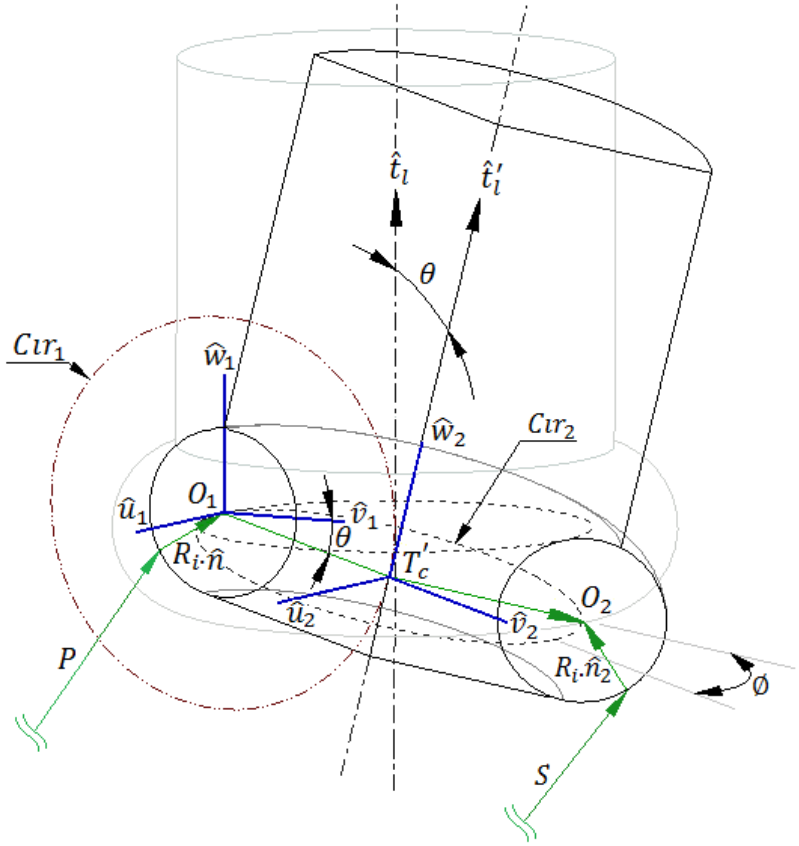

Figure 3.9: Location of second point of contact with toroidal tool and a vertex on STL surface

As the tool rotates by an angle θ about the axis of pseudo-insert at first point of contact $\hat{u}_1$ onto a vertex S, the new orientation of the tool axis, as shown in figure 3.9, is given by:

$\hat{t}_l' = \hat{v}_1 . \sin\theta - \hat{w}_1 . \cos\theta$

There are three possibilities depending on the distance of point S from the projection of rotated tool center T_c' on a plane containing bottom of toroidal tool, which is given by:

$|(T_c' - \hat{t}_l' . R_i) - S|$

Where, T_c' can be found as mentioned in equation 3.9.

Case 1: $(R_i + R_o) \leq |(T_c' - \hat{t}_l' . R_i) - S|$: In this case the vertex will not touch the rotated tool.

Case 2: $0 \leq |(T_c' - \hat{t}_l' . R_i) - S| \leq R_o$: In this case the vertex S lies under flat region of rotated radiused end mill and following equation can be solved to find out the angle of rotation θ such that the vertex S lies in the plane containing the bottom of rotated tool:

$\{(T_c' - \hat{t}_l' . R_i) - S\} . \hat{t}_l' = 0$

Case 3: $R_o \leq |(T_c' - \hat{t}_l' . R_i) - S| \leq (R_i + R_o)$: In this case the vertex S will touch the cutting edge on the pseudo-insert of rotated tool when:

$O_2 = T_c' + R_o . (\hat{u}_2 . \cos\emptyset + \hat{v}_2 . \sin\emptyset)$ 3.13

and, $O_2 = S + R_i . \hat{n}_2$ 3.14

where $\hat{n}_2$, is direction normal from vertex S pointing towards circle Cir_2.

Equations 3.13 and 3.14 have five variable parameters, which are $\hat{n}_{2x}$, $\hat{n}_{2y}$, $\hat{n}_{2z}$, θ and $\emptyset$. Thus two additional equations are required to solve for the five variable parameters. The equation 3.14 ensures that vertex S on triangulated surface is R_i distance away from the center of the torus, but it does not ensure that direction normal $\hat{n}_2$ is perpendicular to tangent to Cir_2 at O_2. The tangent to circle Cir_2 at O_2 is given by $(\hat{v}_2 . \cos\emptyset - \hat{u}_2 . \sin\emptyset)$, and the perpendicularity of direction normal $\hat{n}_2$ to tangent to circle Cir_2 at O_2 is ensured by following equation:

$(\hat{v}_2 . \cos\emptyset - \hat{u}_2 . \sin\emptyset) \cdot \hat{n}_2 = 0$ 3.15

Also the vector $(T_c' - O_2)$ has to be normal to rotated tool axis $\hat{t}_l'$. Thus another equation can be written as:

$(T_c' - O_2) . \hat{t}_l' = 0$ 3.16

Or, $\{T_c' - (\vec{S} + R_i.\hat{n}_2)\}.\hat{t}_l' = 0$ 3.17

The non-linear simultaneous equations 3.13, 3.14, 3.15 and 3.17 can be solved for five variables to find the 5-axis tool position for all three vertices (one at a time) of triangular facet under consideration. For all valid solutions, the solution which offers minimum value of θ is taken up as the final solution for toolpath location and orientation. Thus final position of T_c' and hence orientation of rotated tool axis $\hat{t}_l'$ can be determined.

3.4.4 Boundary element triangles

If the tool is dropped on a boundary element triangle, potentially the tool will be rotated off the edge of the surface. However, in an industrial implementation, machine kinematics will limit the rotation of the tool. Further, if we construct the footprint to lie inside the shadow of the surface, then we can treat boundary element triangles as any other triangle in the STL file and not as special cases.

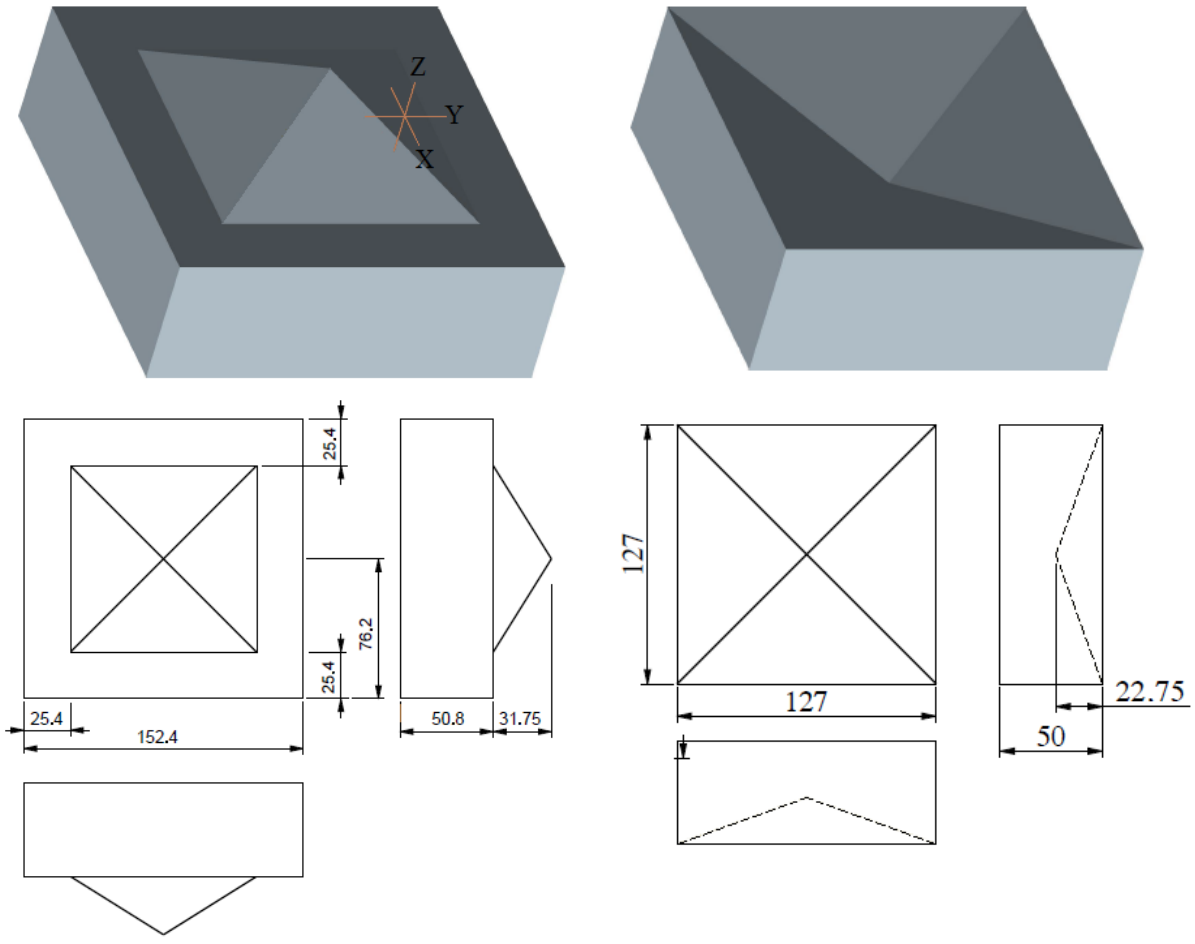

(a) **(b)**

Figure 3.10: The CAD model of (a) convex pyramid part and (b) inverted (concave) pyramid part

3.5 IMPLEMENTATION AND TESTING

The algorithm presented in sections 3.2 to 3.4 requires the solution of linear and non-linear simultaneous equations. To test the proposed DTM concept of 5-axis tool positioning, the developed algorithm is implemented in Maple™ symbolic algebra environment. Maple™ offers a programming and plotting environment, which was also used to test and validate the toolpath results from the algorithm before actual machining.

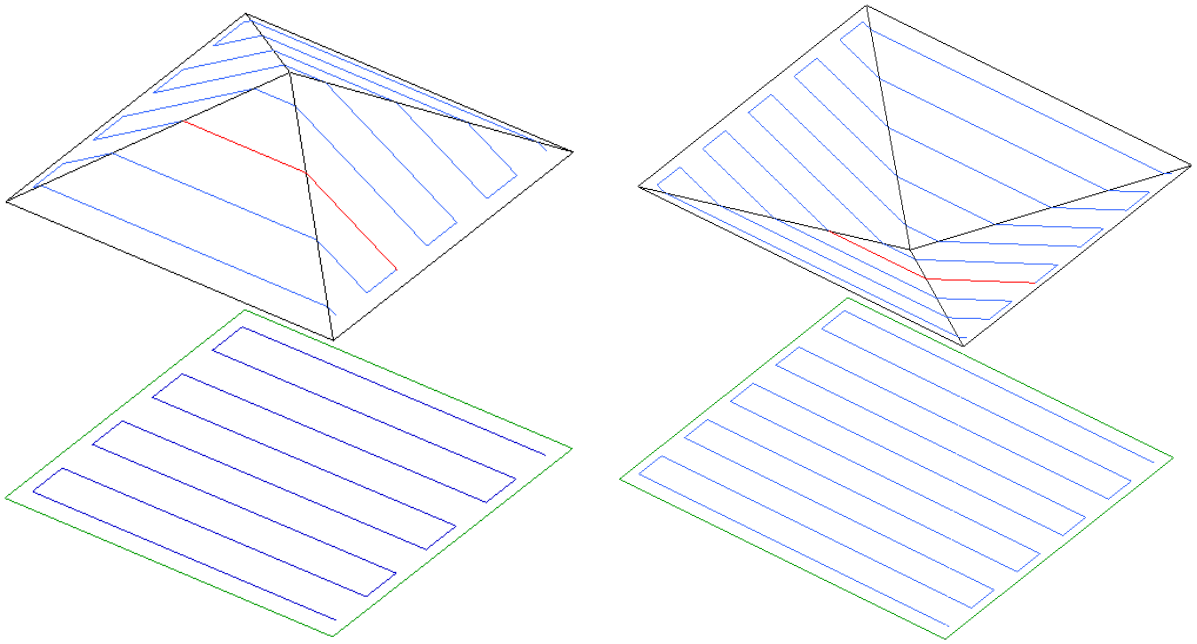

(a) **(b)**

Figure 3.11: The CAD model of test part shapes with zigzag toolpath pattern for (a) convex pyramid and (b) inverted (concave) pyramid [63]

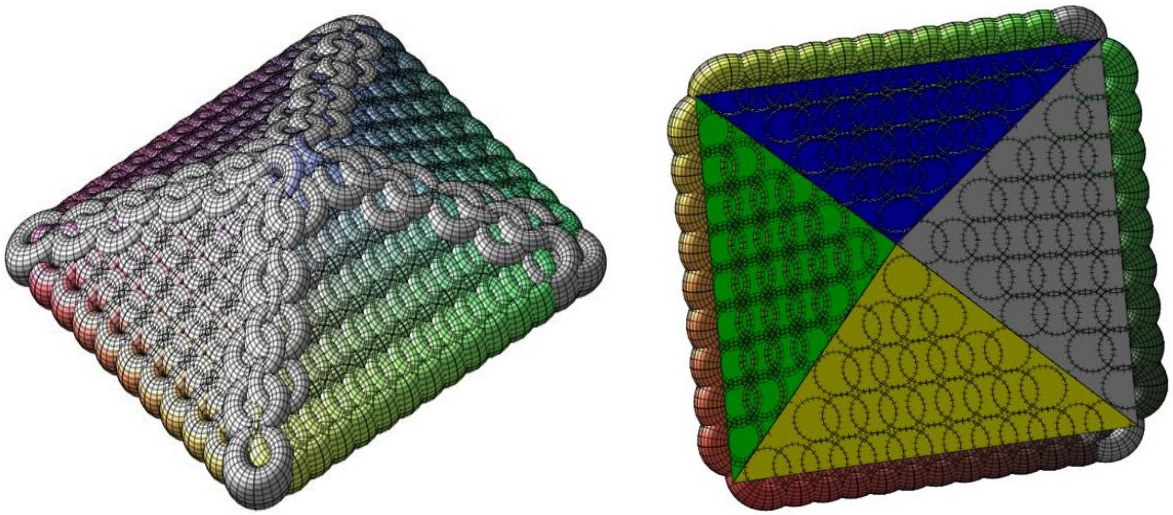

(a) **(b)**

Figure 3.12: Simulation results of the toolpath for machining a pyramid (convex part shape). (a) view from above and (b) view from bottom [63]

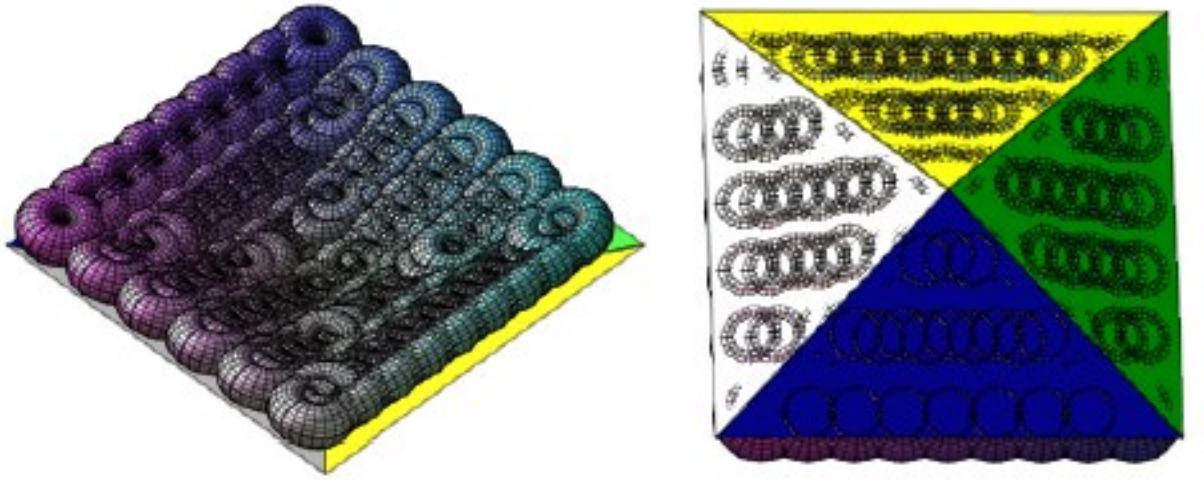

(a) (b)

Figure 3.13: Simulation results of the toolpath for machining an inverted (concave) pyramid, (a) view from above and (b) view from bottom [63].

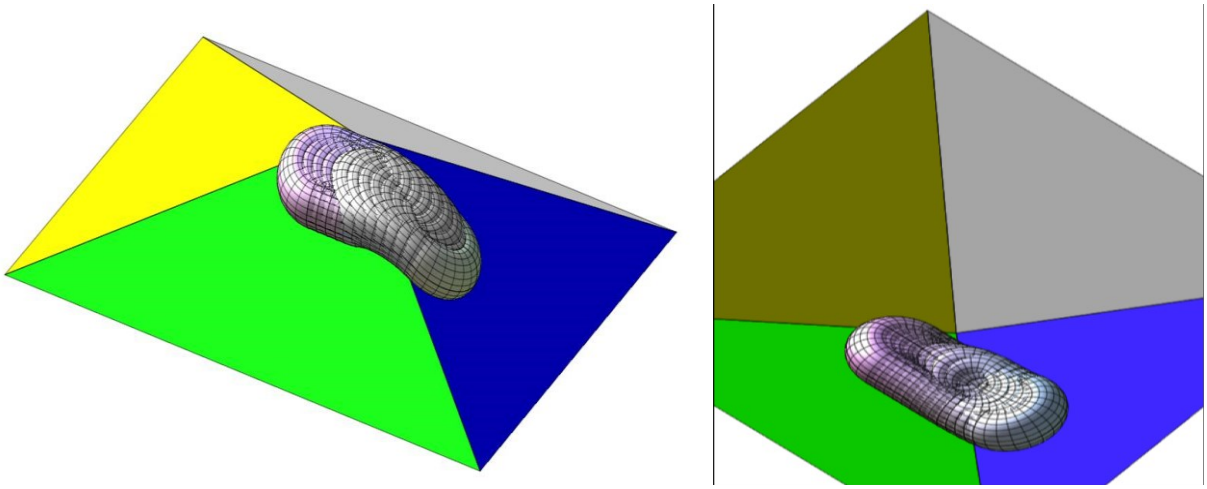

(a) (b)

Figure 3.14: Simulation of a segment of the toolpath as the tool crosses an edge of (a) a pyramid and (b) an inverted (concave) pyramid [63]

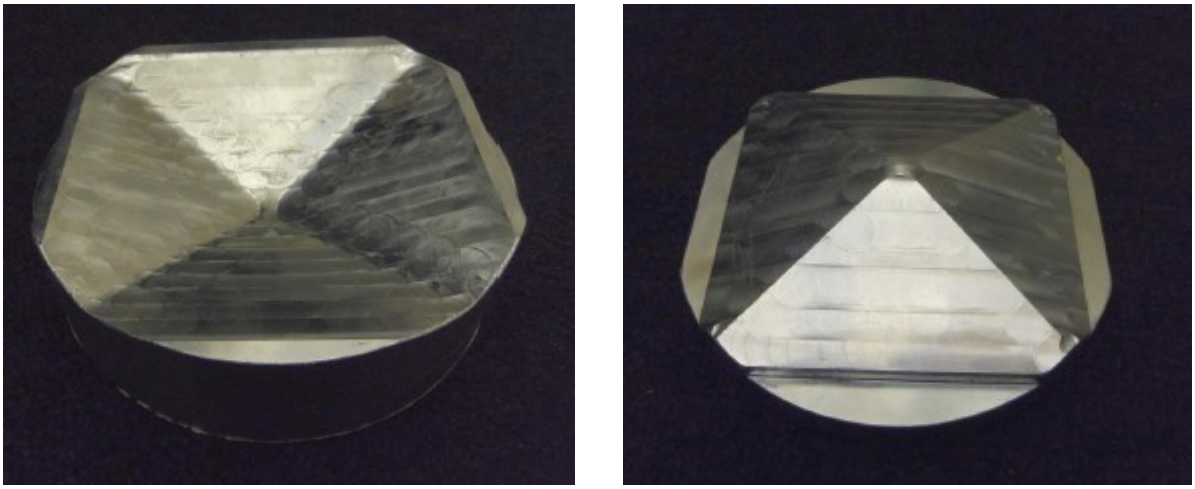

(a) (b)

Figure 3.15: A photograph of (a) an inverted pyramid and (b) a pyramid, machined on a DMG 80-P Hi-Dyn tilt-rotary table simultaneous 5-axis CNC machine [63]

An industrial STL surface will have thousands of triangles or more. However, for DTM algorithm, the tool will be in contact with at most two triangles at any time. In implementation of DTM approach each triangle in the tool shadow has to be tested to find the first point of contact and all triangles in the part have to be tested in the second step to find the second point of contact. Thus there are computational issues associated with larger numbers of triangles while using the Maple^{TM} solver (since each triangle in the tool shadow has to be tested to find the first point of contact and tested again to find the second point of contact), therefore the basic operation of the algorithm can be verified with part models having a smaller number of triangles.

The two adjacent triangles were not inadequate to test issues related to dropping the tool on edges and vertices, nor would two triangles be sufficient to test the second point of contact when rotating the tool. Instead, as a proof of concept, the algorithm was tested on a four triangle pyramid and a four triangle inverted pyramid models of size shown in figure 3.10(a) and (b). This was sufficient to test our algorithm as the tool moved over faces, edges and a vertex.

The first part model having convex rectangular pyramidal shape, shown in figure 3.10(a), is selected to show that the algorithm works on convex parts and can handle edges and vertices accurately, while the concave pyramid part model, shown in figure 3.10(b), is used to verify the capability of the DTM method for positioning a radiused end mill as it traverses in a region between multiple triangular facets.

A plot of the toolpath with a zigzag toolpath footprint used to determine the required NC toolpaths for both the pyramidal parts is as shown in figure 3.11(a) and (b). Note that the footprint is inside the shadow of the pyramid, avoiding issues with boundary element triangles. These two test part shapes were selected to demonstrate the capability of DTM approach to machine convex as well as concave regions of the triangulated part shapes. The tool parameters used for the radiused end milling cutter taken are $R_o = 6.5$ mm and $R_i = 6.0$ mm. The NC toolpath data was generated from the developed DTM approach for two test parts taking feed forward step of 0.5 mm and the side-step value of 10 mm respectively. The developed 5-axis toolpath data for the two sample pyramidal test parts was verified using a customized simulation environment developed in Maple^{TM} graphics in which the tool is represented by a torus and the plot shows every tenth position of the tool (torus) from the

generated NC toolpath as shown in figures 3.12, 3.13 and 3.14 respectively. When seen from the bottom, as shown in figure 3.12(b) and 3.13(b), the tool outline indicates that there is no gouging of the part in both convex as well as concave part geometries.

To examine the developed toolpath in a better way, a portion of the toolpath where the tool starts on the surface of one triangle and transitions across the common edge to a second triangle has been shown in figure 3.14 for both the part models. When machining the convex pyramid, the edges were sharp with no gouging and the vertex crossed without gouging as shown in figure 3.15(a). As the tool crosses the edge it was expected to roll along the edge from one facet to the next. This is shown in figure 3.14(a).

For crossing an edge of the inverted (concave) pyramid, the algorithm resulted in a tool inclination that aligned the tool axis to the facet normal as was expected. As the tool moves towards the edge the second contact point moves from one triangular face into the neighboring face. As the tool crosses an edge it was anticipated that the second point of contact would make the tool stand-up into a vertical position and then as the tool moves further into the second facet, it would start inclining towards the normal of the second facet. The tool behaved as anticipated as observed from the simulation results in figure 3.14 (b).

Once the verification of the toolpath data using the simulation developed in Maple^{TM} graphics was successful, these toolpaths developed for both part shapes were tested by machining on a DMG 80P 5-axis machine with a simultaneous rotary-tilt table. The tool dimensions taken were R_i = 6 mm and R_o = 6.5 mm. The feed forward step was 0.5 mm and the side step was 10 mm. The machined parts are shown in figure 3.15(a) and 3.15(b). The machined parts matched the simulation closely in both the cases. In case of convex part shape, the machined part had sharp edges and the scallops between adjacent passes were negligible. The tool smoothly traversed over the raised edges as well as the vertex of the pyramid without gouging. Note the excess material near the tip (apex) of convex pyramidal part is left after machining. It is possible to remove this excess material but it would require extra passes. Similarly, it was observed during machining of concave part model that the algorithm has the capacity to position the tool such that the tool-axis is aligned to the facet normal. Moreover as the tool crossed the region of an edge in a concave region, the tool moved without gouging the faced surface, but un-machined material near the edges was seen in the concave region as expected. Near the bottom of the inverted pyramid the tool has the

potential of touching any of the four faces of the concave pyramid during its dropping phase and during its tilting phase. The DTM algorithm is capable of processing this section successfully.

3.6 CONCLUSIONS

The drop and tilt method presented above can be used to determine the multipoint 5-axis tool positioning and orientations for machining of triangulated surfaces using a radiused end mill. Overall the results obtained from Maple^{TM} graphics simulation environment and the machined surfaces have been found to be satisfactory, which demonstrate the capability of the DTM method to successfully handle the multiple triangles, edges and vertices of a faceted model.

It is to be noted that while a radiused end mill is a generalization of a ball-nose tool, in the case of a ball-nose tool the developed 5-axis tool positioning method will be able to determine only a single point of contact, since rotating around the pseudo-insert of a ball-nose tool (a sphere) does not change the effective curvature of the cutting edge of the tool and hence what is being machined.

It is observed from the earlier work on multipoint machining methods [1], that the cusp profile for multipoint machining is W-shaped, which differs from the U-shaped cusp profile of 3-axis machining. Between the two contact points, the cusp height is small enough for most engineering applications, but the cusp rises sharply beyond the contact points. The impact of this cusp shape is that a larger side step can be used while still meeting engineering tolerance requirements. While we have not investigated the cusp height for our method, we expect that it will be similar to that of this earlier work on multipoint machining.

Our method rotates around the pseudo-insert. Alternate rotations are also possible, but the optimal rotation likely depends on the particular goals of the machinist, such as minimizing cusp height, maximizing step forward, reducing cusp deviation. Optimizing for various goals is topic of future study.

Finally, the DTM method in the form presented in this chapter is based on solving linear/non-linear simultaneous equations. While these equations can readily be solved in Maple^{TM}, the solution time is long and severely restricts the number of triangles that can be used. The STL

file for an industrial parts will have thousands or more triangles, and the Maple™ implementation would require hours to generated a toolpath for such triangle set, an unacceptable amount of time in an industrial setting. Thus, stand-alone software using robust solvers are needed to make our method practical for industrial uses. A simple method for solving these equations analytically is challenge. Therefore, in the next phase of this thesis work a numerical approach is developed for implementation of DTM method using a generalized tool-drop methodology which works within an iterative procedure to determine the accurate as well as an efficient solution for 5-axis tool positioning. The stand-alone application program for implementation of the numerical DTM method is developed in Visual C++ environment. The entire procedure for generalized tool drop method is presented in chapter 4, while the details of numerical implementation of DTM method are presented in chapter 5 along with the simulation and the machining results.

CHAPTER 4
GENERALIZED TOOL DROP METHOD

4.1 INTRODUCTION

The DTM method of 5-axis tool positioning is discussed in chapter 3 and it was shown that the computational accuracy of DTM method is sufficient for the most industrial applications; however, some computational hurdles remain for its use in industrial applications. The DTM method presented in chapter 3 was implemented within a symbolic algebra package, Maple™. In this implementation the vector equations presented in chapter 3 are developed symbolically for each tool position and each triangle. This symbolic development of equations cannot be captured in a programming language such as C or C++ because such programming languages work with numbers and not symbols. Symbolic environment such as Maple™ are more flexible but harder to program. These systems have not found wide use in industrial applications where as the application programs developed in programming languages such as C or C++ have wider commercial use. Another advantage of C like programming languages is the speed of execution. The complied programs in environments like C or C++ etc. run faster and are ideal when large numbers of computations have to be performed.

For the efficient implementation of the DTM approach it has to be ideally implemented as a stand-alone application in a C++ type programming language. The development of a DTM approach that does not rely on symbolic computations is presented in this chapter. The key idea behind this approach is based on the 3-axis tool positioning method developed by Patel et al. [58], wherein the tool was dropped along the Z-axis onto a triangulated model of the part. The tool stops when it encounters the first point of contact (the highest point). This method guarantees a gouge free tool position at all points along the toolpath. In the proposed DTM method, named as numerical DTM method, the tool axis is tilted about the axis of the pseudo-insert at the first point of contact and the tool is dropped again. If the tilted tool axis results in touching the triangulated surface at two or more points the DTM tool position is considered found, otherwise the process is repeated. The concept is shown in figure 4.1. As this method depends on generalizing Patel et al.'s 3-axis method, the first step is the development of a new generalized tool-drop approach for determining a gouge free point of contact between a radiused end mill and a triangulated/STL surface. In the new tool drop algorithm, the highest point of contact is determined from all planer facets, edges and the

vertices lying under the projected tool shadow on the triangulated part surface and stored as the gouge free first point of contact.

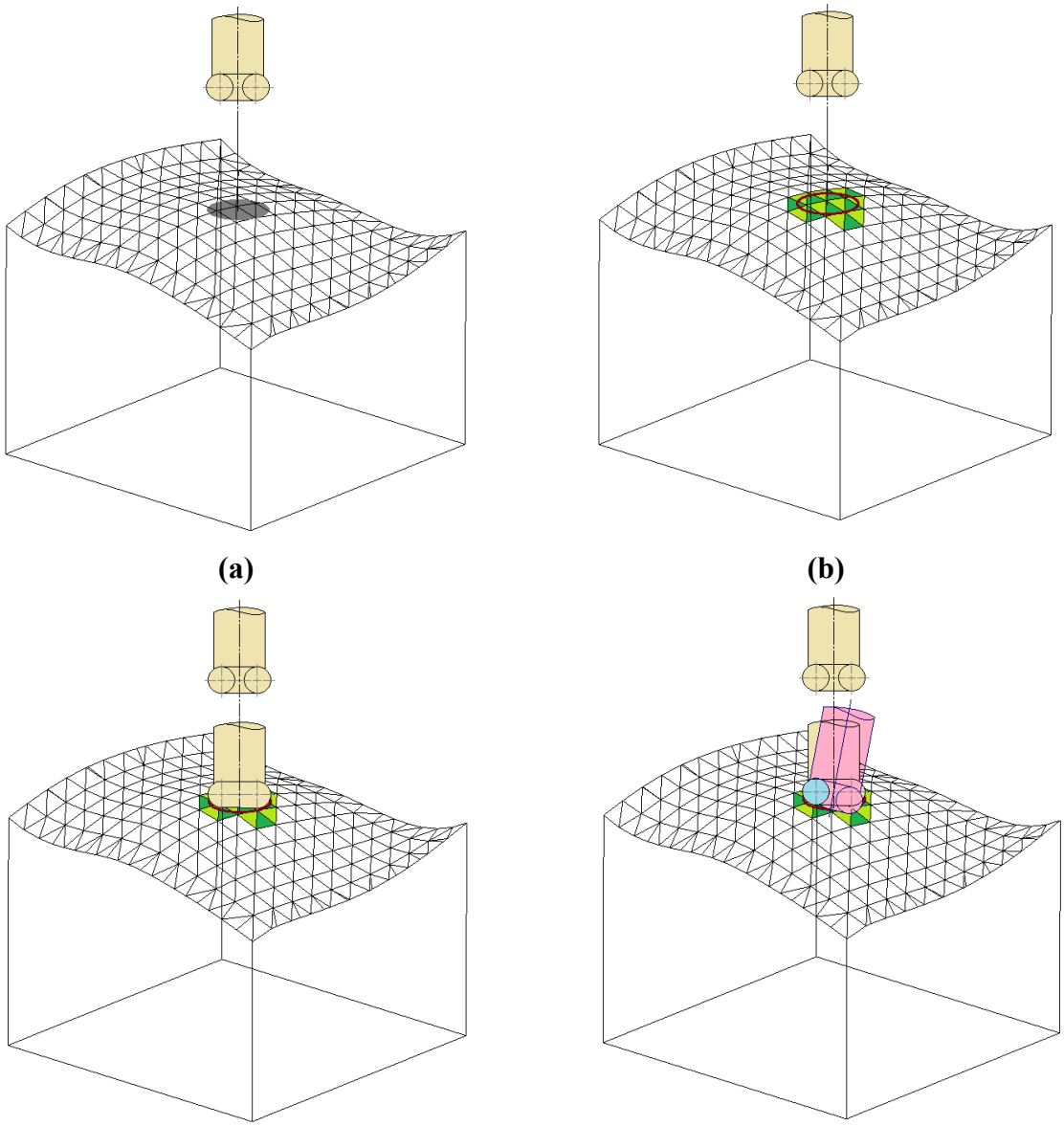

Figure 4.1: (a) Tool shadow projected on STL surface, (b) selection of triangles under tool shadow, (c) dropping tool finds the highest point of contact with triangulated surface, and (d) tool rotation about the highest point of contact to find maximum possible 5-axis tool tilt.

Similar to DTM method, in the numerical DTM method, the location of first point of contact is used to find the center of a pseudo-insert circle O_1 and a unit direction vector, $\hat{u}_1$, normal to the plane of pseudo-insert circle is determined. The location of center of the pseudo-insert O_1 and the unit direction vector $\hat{u}_1$, is used in the second step to determine the 5-axis tool orientation as presented in the next chapter.

4.2 GENERALIZED TOOL POSITIONING ALGORITHM

For evaluation of the toolpath generated from the zigzag and contour footprints the toolpath pattern is discretized into a set of points T_1 that lie on the footprint curve and by a point T_2 offset from T_1 in the direction $\hat{t}_l$. As the tool, a radiused end mill, descends on the triangulated surface, the contact points will lie in the tool shadow or projection of tool taken along the tool axis direction as shown in figure 4.1(a). Thus the algorithm first identifies all triangular facets that lie in the tool shadow, as shown in figure 4.1(a) and (b). To determining the first point of contact, the tool is dropped along Z-axis and to identify the set of triangular facets which will yield the highest point of contact with the dropping tool, the tool shadow radius is taken equal to tool radius $R_i + R_o$. Similarly, it is ideal to identify the set of triangular facets that may lie under the tool projection taken on a plane perpendicular to the direction of tool drop to determine the correct value of tool-tilt angle in the second step.

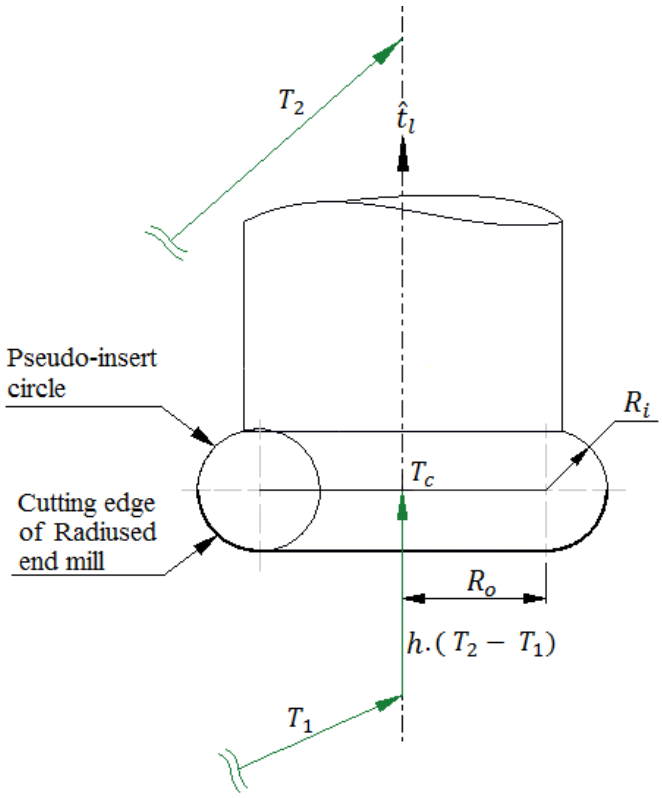

Figure 4.2: Concept of tool drop for first point of contact

The dropping tool can contact the triangles in its shadow within: the bounds of a triangular facet; or any of three edges; or any of the three vertices. For finding the first point of contact between the dropping tool and triangular facets the algorithm analyzes all selected triangles that lie in its projected shadow. Out of all possible solutions the one which gives the highest location of tool center relative to the footprint reference point T_1on tool axis $\hat{t}_l$, is recorded as the gouge free tool location as point T_c along with the corresponding point of contact P, as

shown in figure 4.2. Also, it is important to record whether the highest point of contact P is obtained from a facet or facet entity (edges or vertices of facet), for the purpose of determining 5-axis tool positioning subsequently.

As discussed earlier, the tool drop algorithm need to test all facet under tool shadow to determine the gouge free point of contact. The tool drop algorithm begins by selecting a triangular facet and check whether a descending tool will touch it inside the facet boundary or along an edge or at a vertex. As the computations required to find the point of contact with respect to facet are simple and if valid point of contact is found within the bounds of the facet, the algorithm moves to test the next triangular facet or if no more facets remain to the next step. If a valid contact is not found from a facet, the algorithm analyzes the three edges and the three vertices of the facet. The algorithm processes all triangles under tool shadow to selects the highest point of contact as the gouge free cutter contact point P and then determine the corresponding tool center location T_c for the given tool footprint position T_1. The three key steps of the algorithm namely: the triangle check; the edge check; and the vertex check are described in the following sections.

4.2.1 Triangle check

Let the triangular facet under consideration be $\Delta P_1P_2P_3$ and let $\hat{n}$ be the unit surface normal of facet. The tool is dropped on to the plane of the triangle and the contact point is determined. The dropping tool may or may not contact the facet within its bounds depending upon the orientation of facet with respect to tool drop direction $\hat{t}_l$. The triangle check involves three distinct cases as given below:

(i) $\hat{\boldsymbol{n}} \cdot \hat{\boldsymbol{t}}_{\boldsymbol{l}} = \mathbf{0}$**: The surface normal of the facet is perpendicular to the tool axis**

First we check whether the tool axis is perpendicular to the surface normal of the triangular facet (or tool axis is parallel to the plane of triangular facet). For such facets the tool cannot touch the inside of the facet as it will first touch one of the edges or vertices of facet depending upon the position of the facet vertices with respect to tool axis. Thus for such cases we skip the step to find the point of contact with the facet, rather directly proceed to compute the location of first point of contact with respect to the three edges and the three vertices of the facet as described in appendix B and C.

(ii) $|\hat{\boldsymbol{n}} \times \hat{\boldsymbol{t}}_{\boldsymbol{l}}| = \mathbf{0}$**: The surface normal of the facet is parallel to the tool axis**

When the tool axis is parallel to the surface normal of the triangulated facet (or the tool axis is perpendicular to the plane of triangular facet), a facets under tool shadow can touch the flat bottom of the tool or the radiused cutting edge of the tool can touch an edge/vertex of such a facet. A triangular facet can touch the flat bottom of the radiused end mill only when the tool axis passes through the facet boundary, or when one or more of the three facet vertices lie under the flat bottom region of the radiused end mill. Thus in this case the algorithm first identifies facets that can touch the flat bottom of tool and then proceed to determining the tool center location (or a reference point for 5-axis tool positioning along feed direction) from such facets. Otherwise the algorithm directly proceeds to test the point of contact with respect to the edges or vertices of such facets. The mathematical model developed to determine the point of contact and the location of the tool center with respect to a facet having its surface normal parallel to tool axis which touches flat bottom of the radiused end mill is described in appendix A.1.

(iii) $\hat{\boldsymbol{n}} \,.\, \hat{\boldsymbol{t}}_{\boldsymbol{l}} \neq \mathbf{0}$ **and** $|\hat{\boldsymbol{n}} \times \hat{\boldsymbol{t}}_{\boldsymbol{l}}| \neq \mathbf{0}$**: Triangular facet inclined to the tool axis**

In this case, a point of contact can be determined between the radiused cutting edge of the dropping radiused/toroidal end mill and the inclined plane of the facet. The validity of point of contact can be evaluated by determining whether it lies within the bounds of the triangular facet or not. If the point of contact determined in this case is not located within the facet boundary then the algorithm proceeds to check the tool contact with respect to the three edges and the vertices of the facet under consideration. The mathematical procedure to compute the point of contact and the location of the tool center with respect to an inclined facet are given in appendix A.2.

4.2.2 Edge check

An edge $\overline{P_1\, P_2}$ lying under tool shadow can have three possible orientations with respect to tool axis, which are processed in a sequence of three steps given below:

(i) $|(\boldsymbol{P_2} - \boldsymbol{P_1}) \times \hat{\boldsymbol{t}}_{\boldsymbol{l}}| = \mathbf{0}$**: The edge parallel to the tool axis**

The line defining such an edge will pass through the tool. An edge is limited by its vertices, and a tool dropping on such an edge will rest on one of the vertices. Thus for

such cases, the solution for tool contact will be obtained when algorithm processes the vertices of such an edge.

After assuring that the edge under consideration is not parallel to the tool axis, the shortest distance of the edge from the tool axis, D_e, is determined as given below:

$$D_e = \frac{(P_2 - P_1) \times \hat{t}_l}{|(P_2 - P_1) \times \hat{t}_l|} \cdot (P_1 - T_1) \qquad 4.1$$

If $D_e \leq R_i + R_o$, then the edge will touch the dropping tool and the algorithm proceeds to the next steps. Else, select the next edge of the facet under consideration, until all edges are tested for determination of first point of contact and tool location.

(ii) $(\boldsymbol{P_2 - P_1}).\hat{\boldsymbol{t}}_{\boldsymbol{l}} = \mathbf{0}$**: The edge normal to the tool axis with** $\mathbf{0} \leq \boldsymbol{D_e} \leq \boldsymbol{R_i} + \boldsymbol{R_o}$

These edges are further classified into two types based on whether: (a) $0 \leq D_e \leq R_o$, or (b) $R_o < D_e \leq R_i + R_o$.

The edges which are normal to tool axis with $0 \leq D_e \leq R_o$ will touch the flat bottom of the radiused end mill and will have a line contact with the tool bottom. The mathematical models used for finding the location of the tool center for such edges are given in appendix B.1.

On the other hand, the edges on the triangulated surface having $R_o < D_e \leq R_i + R_o$ will touch the radiused cutting edge of toroidal tool, and will maintain a point contact with the toroidal tool. The point of contact is recorded if it lies within the bounds of the edge as given in appendix B.2.

(iii) $(\boldsymbol{P_2 - P_1}).\hat{\boldsymbol{t}}_{\boldsymbol{l}} \geq \mathbf{0}$**: The edge inclined to the tool axis with** $\mathbf{0} \leq \boldsymbol{D_e} \leq \boldsymbol{R_i} + \boldsymbol{R_o}$

The contact point between the radiused end mill cutter and the line defining the edge is determined and the validity of the point of contact is checked to ensure that it lies within the bounds of the edge. It is one of the most complicated step in implementation of numerical DTM as the edge-torus tangency derivation results in an 8^{th} order equation, though with rearrangement of terms it can be reduced to a 4th degree in our case. In this work we have solved this equation using the bisection method. The derivation details of the procedure used is given in appendix B.3.

Whether, a valid point of contact is determined from the edges of the facet under consideration or not, the algorithm analyses the three vertices (one at a time) to check if the valid point of contact can be obtained from them.

4.2.3 Vertex check

When the radiused end milling tool is dropped along tool axis $\hat{t}_l$ on a vertex P lying under tool shadow, it can touch the vertex either on the flat bottom part of tool or the radiused corner of the tool depending upon the shortest distance of vertex from tool axis. When the tool axis $\hat{t}_l$ passes through a point T_1 on toolpath footprint projection on XY-plane, the shortest distance D_v of vertex P can be found using the equation given below:

$$D_v = |(P - T_1) \times \hat{t}_l| \qquad 4.2$$

If $D_v \leq R_i + R_o$, then the vertex will definitely touch the dropping tool. If this condition is met then proceed to the next steps, else select the next vertex of the facet under consideration, until all vertices are tested. There are two cases to consider for every vertex under tool shadow as given below:

(i) **$0 \leq D_v \leq R_o$: Vertex touching the flat region of radiused end mill**

In this case the tool center location is determined as the tool sits on the vertex. For determining the 5-axis tool positioning and orientation such vertices have been classified into two types based upon the value of D_v as vertex with $D_v = 0$ or $0 < D_v \leq R_o$. The mathematical procedure used to determine the tool center and other variable used for 5-axis tool positioning for such cases are given in appendix C.1 and appendix C.2.

(ii) **$R_o < D_v \leq R_i + R_o$: Vertex touching the radiused corner of a toroidal end mill**

For such vertices the 3-axis location of tool center can be determined, as the location of the vertex is the point of contact between tool and triangulated surface. The numerical implementation of multipoint method can be applied in this case similar to the facet and edge which are inclined to tool axis, as stated above. The derivation details are given in appendix C.3.

The generalized 3-axis algorithm used for finding the gouge free point of contact for a tool dropping on the triangulated facets under tool shadow is implemented in Visual C++. The 3-axis tool drop code is passed the facet information in the form of coordinates of vertices and facet normal. This code returns the location of tool center, the point of contact (where ever possible) and the information about the surface entity whether facet or edges or vertices from where the solution for highest tool center location is determined. The information containing the highest tool center location out of all triangulated facets under tool shadow for a predetermined tool footprint location is taken as the final output and is used as input for 5-axis tool positioning algorithm.

The mathematical approach used for determining the first point of contact, tool center and orientation of pseudo-insert to be used for 5-axis tool positioning is explained in the appendix A, B and C.

4.3 VALIDATION OF TOOL DROP ALGORITHM

The developed tool drop algorithm is implemented as a stand-alone application developed in visual C environment. This algorithm was tested on: a flat; a cylindrical; a spherical and pyramidal test parts. 3-axis tool positioning over facets, edges and vertices were checked by designing specific toolpath footprints. The tool positioning for 3-axis machining was also tested for triangulated surfaces with a variety of insert dimensions. Checks were made to ensure that the algorithm worked when the tool touches the facets, or edges or vertices on its flat bottom or along the radiused corner. The developed 3-axis toolpaths were tested using a custom 3-axis graphical simulator [92]. As the graphical simulations have been checked these 3-axis toolpaths were not machined. The results obtained from the simulations proved that the tool drop algorithm was able to position the tool over the machined surface accurately as desired in 3-axis machining.

The sole purpose of development of the generalized tool drop algorithm is for its use in 5-axis tool positioning in the numerical implementation of drop and tilt method. The details of numerical implementation drop and tilt method of 5-axis tool positioning is presented in the chapter 5.

CHAPTER 5
NUMERICAL IMPLEMENTATION OF DROP AND TILT METHOD

5.1 INTRODUCTION

A new algorithm referred to as numerical implementation of DTM or numerical DTM algorithm was introduced in the last chapter. The new method avoids the use of symbolic computations required to generate the simultaneous non-linear equations required to solve the multipoint tangency problem. To find the second point of contact numerical DTM algorithm uses the concept of tool axis rotation about the axis of pseudo-insert along with the generalized tool drop algorithm (discussed in chapter 4). This chapter presents the method used to determine the second point of contact for multipoint 5-axis tool positioning.

The developed algorithm is implemented in Visual C++ environment. The toolpaths generated using this method are initially validated in a custom graphical simulator developed in Maple^{TM}, and finally by actual machining on DMU -80P-HiDyn tilt-rotary 5-axis machine. The subsequent sections of this chapter present the complete details of the numerical implementation of DTM method.

5.2 NUMERICAL DTM CONCEPT

In the proposed method, the tool is first dropped along a predefined orientation of tool axis to find the 3-axis tool position *P* as shown in figure 5.1(a). Once the point of contact *P* is known, the plane passing through the contact point and tool axis is used to find the pseudo-insert, its center and the axis of rotation defined by a line passing through the center of pseudo-insert and perpendicular to the plane containing pseudo-insert. Second, the tool axis is rotated about the pseudo-insert axis such that the first point of contact between tool and surface is retained. The new tool axis orientation determined in the second step is then used to drop the tool again onto the triangulated surface. As the tool descends along the new axis, it will definitely come in contact with the model surface, but it may happen that the descending tool touches another part of the surface before it touches the first point of contact. In the first instance when the descending tool touches the first point of contact the tool axis is rotated (tilted) further as shown in figure 5.1(b). In case the tool touches another point as shown in figure 5.1(c), then the tool axis rotation (tilt) is reduced. The tool axis rotation (tilt) is bracketed between an *over* and an *under* rotation and the difference between the two is reduced using the bisection method as shown in figure 5.1(d). The process is stopped when a

specified tolerance in terms of the descend distance for the first and second point of contact is reached. The details of the proposed method are presented next followed by its implementation and testing.

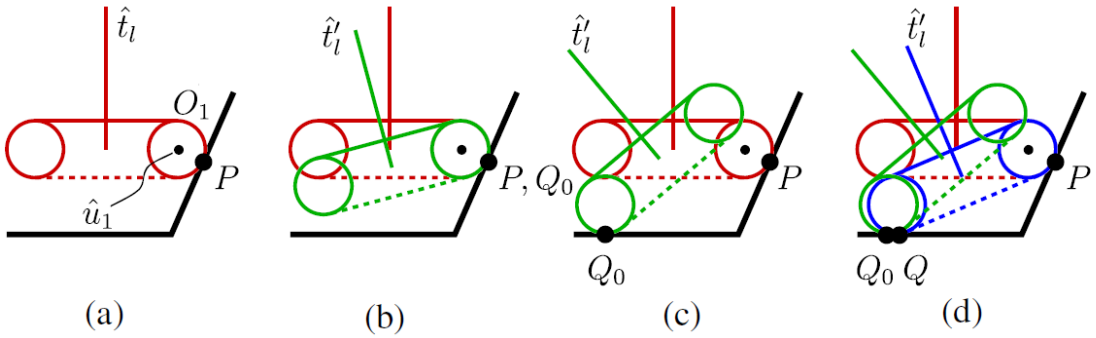

Figure 5.1: Tool positioning algorithm. (a) Drop tool to find point of contact *P*. Rotate tool around $\hat{u}_1$ (pointing out of the page), drop again, and find point of contact Q_o. (b) If Q_o= *P*, rotate by larger angle and drop again. (c) If point of contact Q_o differs from *P*, then perform binary search until (d) we find tool position tangent at two points, *P* and *Q* [65]

Thus the problems need to be solved for multipoint tool positioning are (a) how to compute the initial gouge free point of contact for the dropped tool; (b) which axis to rotate the tool around; and (c) how far to rotate around this axis.

The bisection method begins by dropping the tool at point T_1 in a default direction, $\hat{t}_l$, usually [0,0,1], and finding the first point of contact P. Point P might be on the toroidal part of the tool or on the flat bottom. The main focus of this work is rotating radiused end mill tool around pseudo-insert axis, so we performed no rotation when the tool contacts an edge or vertex of the STL file on the flat bottom. Thus, in the following, we assume that P is on the toroidal part of the tool as illustrated in figure 5.1(a). From P, the location of center of pseudo-insert O_1 and the pseudo-insert axis $\hat{u}_1$ can be computed. Next, the tool axis is rotated about the pseudo-insert axis $\hat{u}_1$ by the largest angle permitted (see Section 5.2.1). The tool is then dropped along the rotated tool axis $\hat{t}'_l$. The rotation of the tool around $\hat{u}_1$ at P ensures that, when dropped a second time, the tool will either come in contact with P or with a second point of contact. Regardless, let Q_o denote the point of contact when dropping the tool along $\hat{t}'_l$. If $P = Q_o$(figure 5.1(b)) and a larger rotation is still possible, then a larger rotation is used to find a second point of contact. If the angle of rotation is the maximum rotation allowed and P still equals Q_o, then only a single point of contact exists and the process stops. Otherwise, $Q_o \neq P$ (figure 5.1(c)) and the two angles made by P and Q_o bracket the angle

where two simultaneous points of contact exist; in this case, we use the bisection method to find these two points of contact, P and Q (figure 5.1(d)).

At each of these footprint locations, a point T_1 lies on the footprint curve and another point T_2 is offset from T_1 in the tool axis direction $\hat{t}_l$, usually [0,0,1]. The radiused end mill is assumed to be dropped at a predetermined toolpath footprint location along the tool-axis $\hat{t}_l$ on the triangulated surface and the first point of contact P, between the tool and the triangulated surface is determined along with the location of tool center T_c. As the tool descends on the triangulated surface, the first contact point P will lie in the tool shadow or projection of tool taken along the tool axis direction as shown in figure 4.1(a). Depending upon the orientation of tool axis for the dropping tool, the tool can contact a triangle either on its face or along its edge, or at its vertices. For finding the first point of contact between the dropping tool and triangular facets, the algorithm analyzes all selected triangles that lie in the tool shadow. Out of all possible solutions the one that gives the highest location of tool center T_c relative to the point T_1 on tool axis is recorded as the gouge-free tool location. The three key components, the triangle check, the edge check, and the vertex check, are used in the determination of the gouge free first point of contact. The detailed mathematical model for tool drop algorithm is presented in chapter 4.

Method used for finding the second point of contact for determining the 5-axis tool position uses the following steps;

Step 1: Determine pseudo-insert center O_1 and axis of rotation $\hat{u}_1$ at first point of contact P.

Step 2: Rotate tool axis about pseudo-insert axis $\hat{u}_1$ taking the center of O_1, as pivot of rotation

Step 3: Drop tool along new tool axis $\hat{t}_l'$ to find second point of contact Q_o

Step 4: If $Q_o = P$, then rotate tool axis by a large angle and return to Step 3. If the new angle of rotation is becoming larger than the permitted limit, then there exists only single point of contact.

Step 5: Use the bisection method to determine the angle of rotation of the tool axis that results in two points of contact

5.2.1 Maximum rotation angle

After dropping the tool a check is done to find, if the first point of contact is on the toroidal part of the tool. If so, then rotate the tool axis around the center of the pseudo-insert at first

point of contact, and drop the tool again along the new tool axis to find the second point of contact as shown in figure 5.1(b), (c) and (d). The module used to determine the 5-axis tool position and orientation data based on the bisection method discussed above repeatedly calls the tool drop algorithm until a valid 5-axis tool position is determined. There are three limits on the maximum possible tool rotation angle: geometric, machine kinematics, and user defined. The maximum angle of rotation will be the minimum of these three values.

The limitations due to machine kinematics manifest in limiting the rotation of the machine's rotary axis. If the algorithm requires a rotation beyond the capability of the machine's rotary axis, in such case the machine tool would encounter an axis overrun and stop executing the NC program. Such cases should be avoided. In addition, there is a geometric constraint on how far we may rotate tool axis around the center of the pseudo-insert. As shown in figure 5.2, if the tool is tangent to a facet at P, then the tool can be rotated by a maximum angle of magnitude $\emptyset$ as shown in figure 5.2(a), where O_1 is the center of the pseudo-insert and R is the point where the circle of the pseudo-insert is tangent to the bottom of the tool. As shown in figure 5.2(b), a rotation by $\emptyset$ will align the flat bottom of the tool with the facet; and any further rotation would cause gouging.

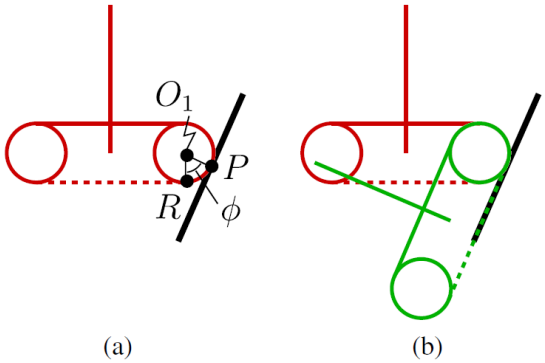

Figure 5.2: Tool can be rotated by a maximum angle of $\emptyset$ without causing gouging. (a) unrotated tool; (b) tool after rotation of $\emptyset$ (*green*), the maximum rotation without gouging, the flat bottom of the tool aligns with the plane of the facet [65]

5.2.2 Step 1: Determination of first point of contact, tool center, center of pseudo-insert and axis of rotation

The tool is dropped along the predetermined tool axis direction $\hat{t}_l$ and the first point of contact P and tool center location T_c is determined using generalized tool drop method elaborated in chapter 4. The point of contact P is used to determine the center of pseudo-insert O_1 as well as the tool rotation axis $\hat{u}_1$. Also the location of the reference toolpath footprint points T_1 and T_2, is required for determining the references for rooting the tool-axis in 5-axis DTM algorithm. As shown in figures 5.3, 5.4, 5.5, and 5.6, the tool rotation axis $\hat{u}_1$

is normal to the plane containing the pseudo-insert and passes through the center of pseudo-insert. The location of the center of pseudo-insert O_1 is given by:

$$O_1 = P + R_i.\hat{n}, \qquad 5.1$$

where, $\hat{n}$ is the unit surface normal through the point of contact. It is the facet normal in case the first point of contact is determined from triangulated facets inclined to tool axis. When the first point of contact in tool drop is found on radiused corner of the tool from edges normal to tool axis, an inclined edge or a vertex, then $\hat{n}$ is determined using equation B.12, B.26 and C.10 given in appendix B and C respectively.

As shown in figure 5.3, 5.4, 5.5, and 5.6, a coordinate frame $(\hat{u}_1, \hat{v}_1, \hat{w}_1)$ is defined at O_1 and is given as:

$\hat{w}_1 = \hat{t}_l$

$\hat{u}_1 = (\hat{n} \times \hat{t}_l)/|\hat{n} \times \hat{t}_l|$

$\hat{v}_1 = (\hat{w}_1 \times \hat{u}_1)/|\hat{w}_1 \times \hat{u}_1| = \hat{n}_p$

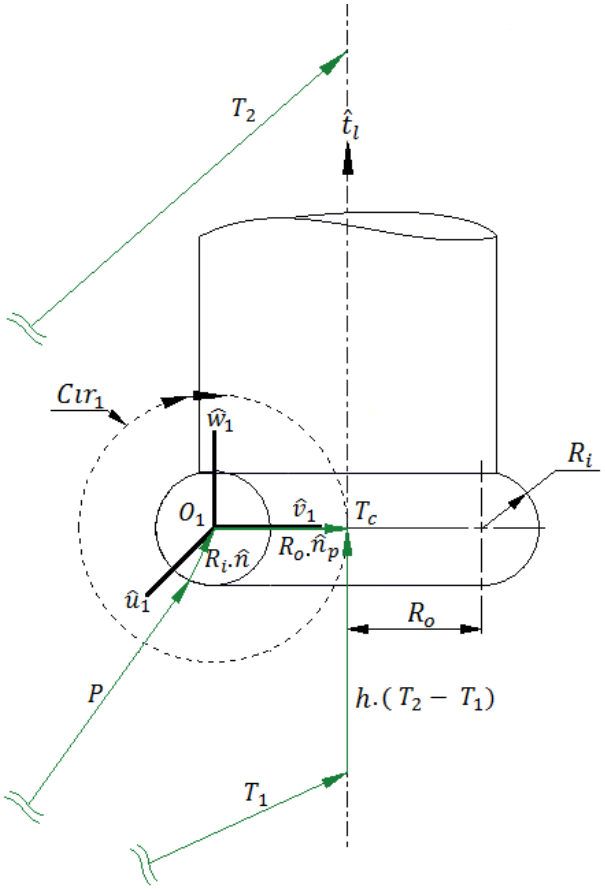

Figure 5.3: Location of pseudo-insert at first point of contact between tool and STL surface on radiused corner of tool

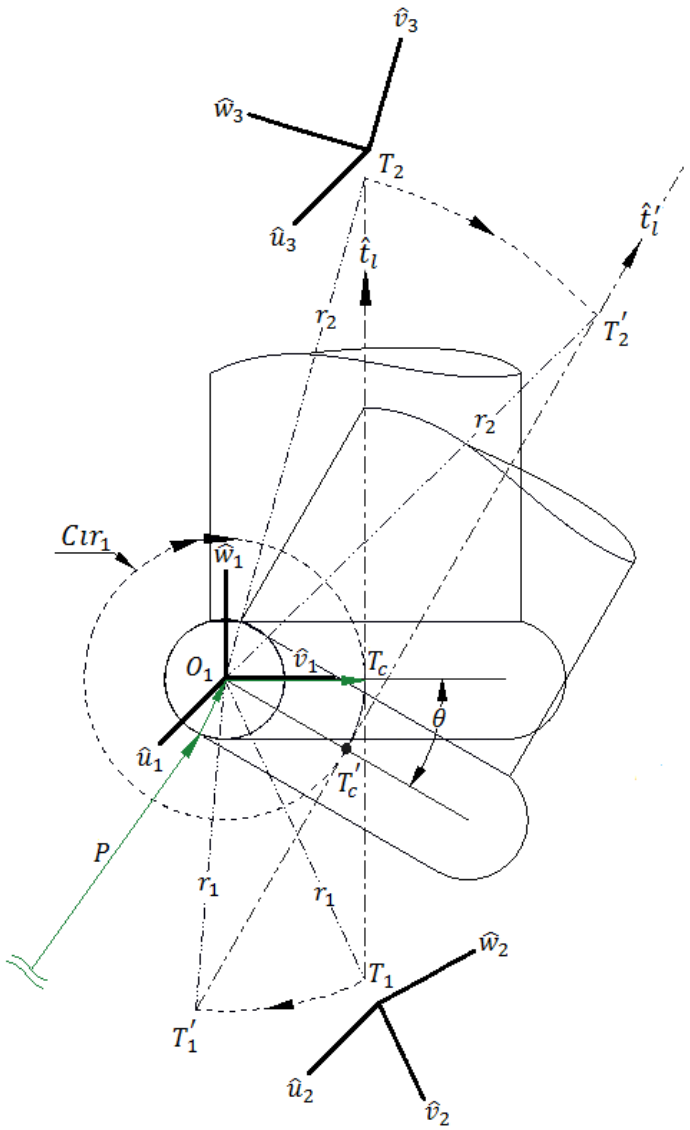

Figure 5.4: Radiused end mill rotated about center of pseudo-insert O_1

5.2.3 Step 2-4: Rotation of tool axis about pseudo-insert axis

Next the tool axis is rotated about pseudo-insert axis $\hat{u}_1$ up to maximum machine limit say angle θ such that the tool center can be moved closer to the surface to be machined as shown in figure 5.4. The angle θ in a tilt-rotary machine corresponds to the A-axis angle, while the orientation of unit normal $\hat{u}_1$ will be finally used to define the value of C-axis angle for proper positioning of tool with respect to the workpiece.

This imaginary rotation of the tool about axis $\hat{u}_1$ taking pseudo-insert center O_1 as the center of rotation will ensure the tangency of the toroidal tool with the STL surface at the first point of contact P. Such rotation will move the tool center T_c to a new location T_c' on a circle defined by Cir_1 as shown in figure 5.4, and given by:

$$Cir_1 = T_c' = O_1 + R_o.(\hat{v}_1 \cos\theta + \hat{w}_1 \sin\theta) \quad 5.2$$

Similarly, after rotation of tool about $\hat{u}_1$, tool axis $\hat{t}_l$ moves it to $\hat{t}_l'$ as shown in figure 5.4 which is given as: $\hat{t}_l' = (T_2' - T_1')/|(T_2' - T_1')|$ 5.3

Where the vector T_1' and T_2' are the rotated positions of vectors T_1 and T_2 lying on tool axis respectively, when they are rotated about O_1, and are given as:

$$T_1' = O_1 + r_1.(\hat{v}_2 \cos\theta + \hat{w}_2 \sin\theta) \quad 5.4$$

$$T_2' = O_1 + r_2.(\hat{v}_3 \cos\theta + \hat{w}_3 \sin\theta) \quad 5.5$$

Where,

$r_1 = |(T_1 - O_1)|$

$\hat{u}_2 = \hat{u}_1$

$\hat{v}_2 = (T_1 - O_1)/|(T_1 - O_1)|$

$\hat{w}_2 = (\hat{u}_2 \times \hat{v}_2)/|\hat{u}_2 \times \hat{v}_2|$

$r_2 = |(T_2 - O_1)|$

$\hat{u}_3 = \hat{u}_1$

$\hat{v}_3 = (T_2 - O_1)/|(T_2 - O_1)|$

$\hat{w}_3 = (\hat{u}_3 \times \hat{v}_3)/|\hat{u}_3 \times \hat{v}_3|$

As shown in figure 5.4, the vectors T_c and T_c' both lie on a circle Cir_1, as well as the vectors $T_1$and T_1' also lie on a circle of radius r_1 having center at O_1. Thus if rotated tool does not strike any other part of STL surface the parametric height of T_c' above T_1' should be same as the parametric height of T_c above T_1 represented by h in equation A.4 in Appendix A.

Thus for rotated tool following equation holds:

$$Cir_1 = T_c' = T_1' + h.(T_2' - T_1') \quad 5.6$$

Where, h is the same scalar parameter as presented in equation A.4.

In case the tool touches another part of triangulated surface the parametric height of tool center T_c'' above T_1' represented by h_1, will be greater than h. Where T_c'' represents the tool center height when it is dropped along new orientation of tool axis $\hat{t}_l'$ rooted at point T_1'. The tool orientation direction $\hat{t}_l'$ is obtained using the rotated tool reference points represented by

the vector T_1' and T_2'. The location of tool center T_c'' with respect to T_1' can be obtained using the generalized tool drop algorithm and is given by:

$$T_c'' = T_1' + h_1.(T_2' - T_1') \qquad 5.7$$

Where, $0 \leq h_1 \leq 1$

The value of parameter h_1 calculated from equation 5.7 will always be equal to or greater than parameter h represented in equation A.4 as well as in equation 5.6. This is because of the reason that the dropping tool can touch at higher region of triangulated surface other than initial point of contact and stopped. For valid first point of contact, the value of parameter h_1 cannot be smaller than h, as it results in the tool penetrating below the first point of contact. In case the value of parameter h_1 is more than h the angle of rotation must be reduced to find the appropriate tool inclination that will result in gouge free multipoint contact.

The presented method iteratively determines the tool axis where $h = h_1$. The number of iterations can be large, so to limit it we use the condition $|h - h_1| = \Delta_{Bisection}$ to stop the iterations. The variable $\Delta_{Bisection}$ represents a user specified tolerance.

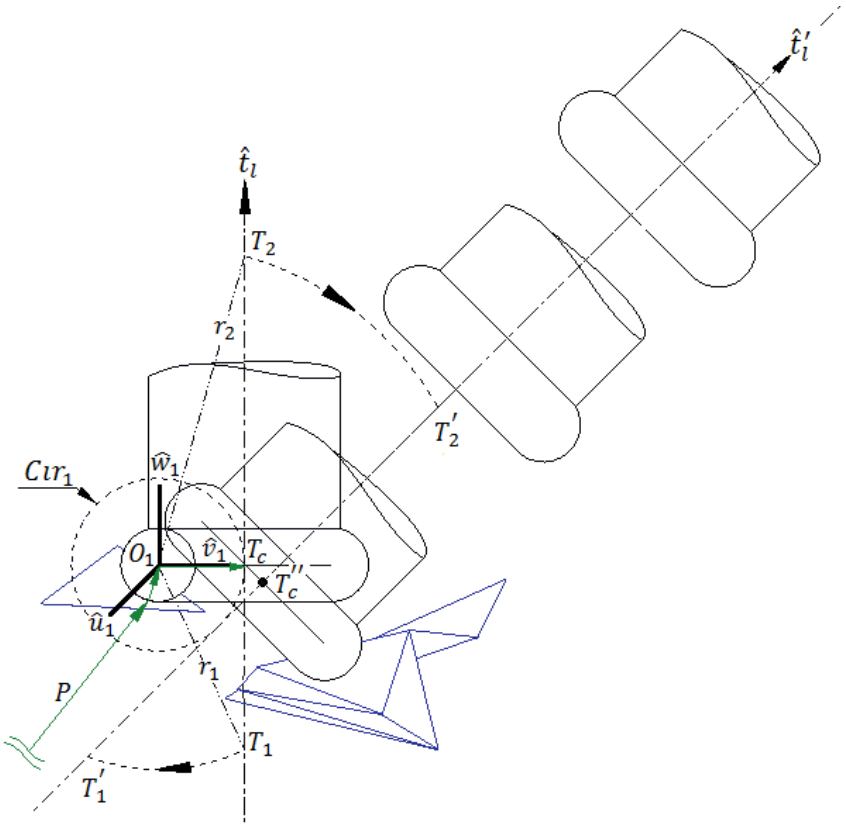

Figure 5.5: Tool drop along rotated tool-axis $\hat{t}_l'$

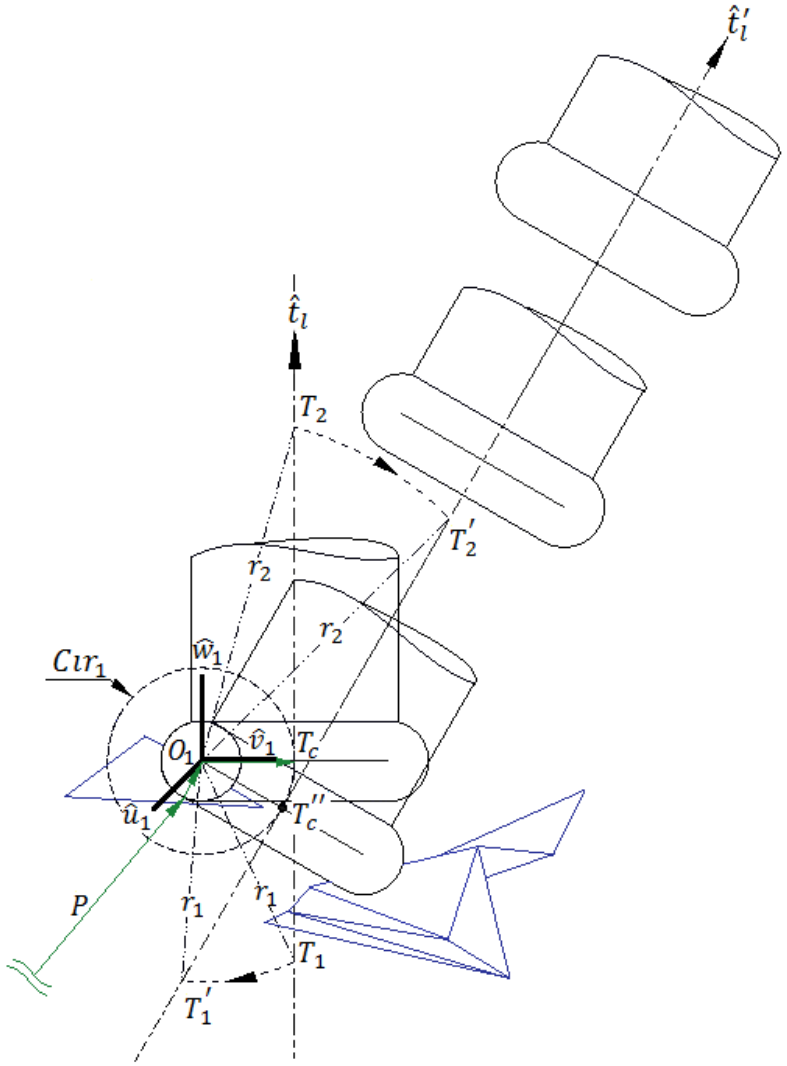

Figure 5.6: Tool drop along tool-axis $\hat{t}_l'$ which is at lesser inclination than in figure 5.5

5.2.4 Step 5: Bisection Method of determining angle of rotation of tool axis

The tool rotation that ensures retention of the first point of contact with STL surface while it also touches the STL surface at other location simultaneously is the desired solution for multipoint machining. The bisection method uses the following two steps iteratively to determine the angle of rotation for 5-axis tool positioning algorithm:

Case 1: When $|\boldsymbol{h} - \boldsymbol{h_1}| > \Delta_{Bisection}$

In this case, the rotated toroidal tool is no more tangent or in contact with the STL surface at P rather it touches the STL surface at higher location of tool center with respect to rotated reference tool footprint point T_1' as shown in figure 5.5. In this case the tool rotation angle is reduced to half, and the new tool drop axis orientation $\hat{t}_l''$ is determined with respect to initial tool axis orientation $\hat{t}_l$ as given below:

$$T_1'' = O_1 + r_1.(\hat{v}_2 \cos(\frac{\theta}{2}) + \hat{w}_2 \sin(\frac{\theta}{2})) \quad 5.8$$

$$T_2'' = O_1 + r_2.(\hat{v}_3 \cos(\frac{\theta}{2}) + \hat{w}_3 \sin(\frac{\theta}{2})) \quad 5.9$$

and, $\hat{t}_l'' = (T_2'' - T_1'')/|(T_2'' - T_1'')| \quad 5.10$

Thus in this case a tool axis orientation in the middle of $\hat{t}_l$ and $\hat{t}_l'$ is tested, and tool is dropped along $\hat{t}_l''$ to determine the new tool center location h_1 and hence $|h - h_1|$.

Case 2: When $|h - h_1| \leq \Delta_{Bisection}$

In this case, the bisection limits for angle are changed between $\frac{\theta}{2}$ and θ , and angle value in the middle of this range is selected, whereas if $|h - h_1| > \Delta_{Bisection}$ the bisection limits for angle are changed between 0 and $\frac{\theta}{2}$. The above concept is demonstrated through figures 5.5 and 5.6.

The bisection process is continued until the difference between the two extreme limits of angle θ in a step is less than 0.0001 radians in this work. Using the final value of angle θ the location of vectors T_1'', T_2'' and $\hat{t}_l''$ are determined. Using the above stated methodology, the 5-axis toolpath data is recorded for all points along the selected toolpath footprint.

5.3 IMPLEMENTATION OF NUMERICAL DROP AND TILT METHOD

The above algorithm was implemented as a stand-alone Visual C++ programming environment and within the Maple™ symbolic algebra package. The module used to determine the 5-axis tool positioning data based on the bisection method discussed above in section 5.2.4 repeatedly calls the tool drop algorithm until a valid 5-axis tool position is determined. To control the bisection algorithm, rather than comparing P to Q_o as suggested in section 5.2.4, one can compare the height that the tool is dropped along the two axes; if the height is the same then $P = Q_o$, otherwise $P \neq Q_o$.

Bucketing was used to avoid testing triangles that were far away from the tool. In 3-axis tool drop the tool shadow diameter is taken equal to maximum tool diameter [41], but for 5-axis tool positioning, the tool shadow has to be larger, as the radiused end mill may twist as it is dropped along the rotated tool axis. For simplicity and efficiency, the algorithm proposed by Yau et al. [41] has been implemented with radius of tool shadow in 3-axis tool drop equal to

$(R_i + R_o)$, while for 5-axis tool positioning algorithm the radius of tool shadow has been taken equal to $(2R_i + R_o)$.

In CNC machining of sculptured surfaces, the toolpath is designed to machine the part to a tolerance specified by the user. In our method, there are two tolerances: one is the tolerance used to generate the STL file (which should be half the tolerance required by the user), the other is the tolerance governing the bisection method used by our method. These two tolerances are related. In our work, we chose the tolerance of the bisection method to be half of the user defined tolerance, as suggested by Lauwers et al.[38]. The user defined tolerance is typically 0.1mm for steel parts [65].

5.4 TEST CASES

The developed numerical implementation algorithm for "DTM" approach has been successfully tested for various aspects using customized Maple^{TM} graphics simulation environment on four test parts. Also the accuracy of the toolpath developed using the new approach has been verified by actual machining of these four test parts on DMU-80P 5-axis machine with simultaneous tilt-rotary table.

The first two part shapes considered were identical to the one used in the study of DTM method, which are, inverted (concave) pyramid and convex pyramid part shapes having four triangles. The geometry of the convex and concave pyramidal faceted part models are shown in chapter 3 in figure 3.10(a) and 3.10(b) respectively.

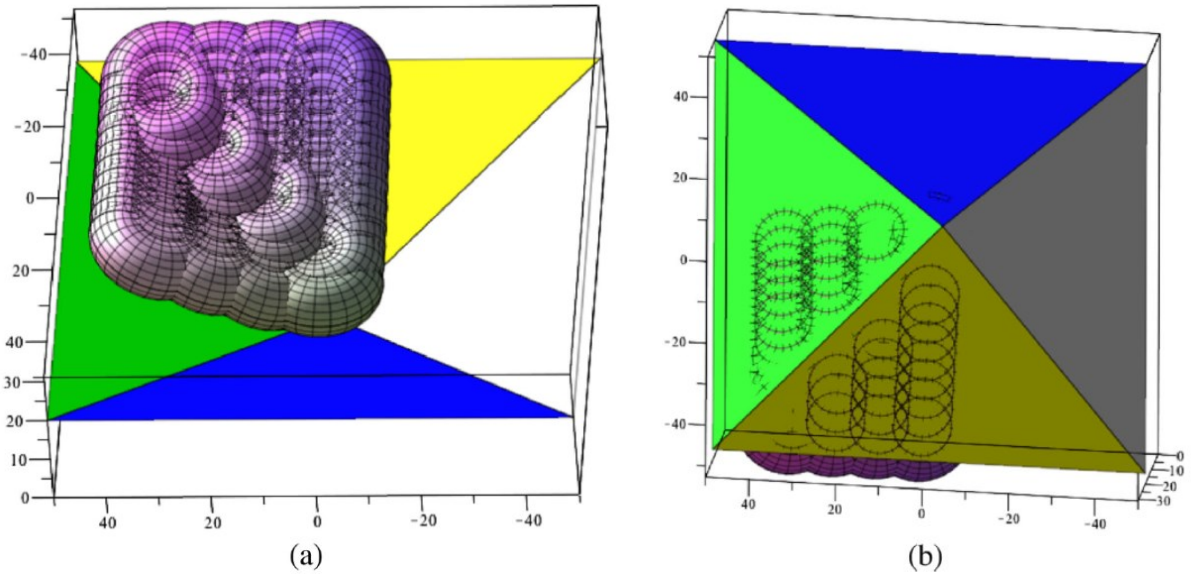

Figure 5.7: Simulation results of 5-axis toolpath data for an inverted pyramid part (concave part with 4 facets), (a) top view showing torus at the various tool locations, and (b) bottom view [65]

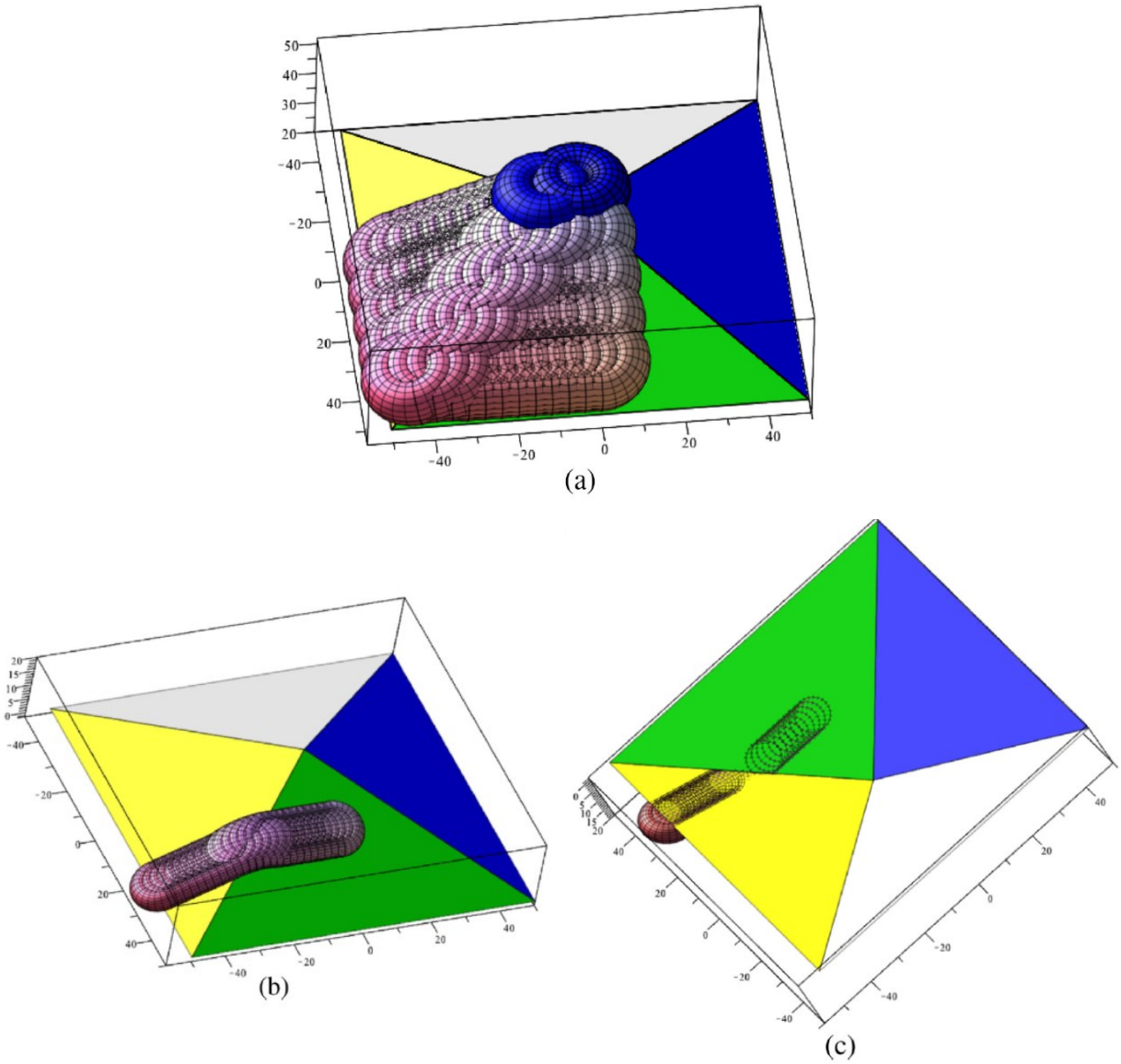

Figure 5.8: Simulation results of 5-axis toolpath data for a rectangular pyramid part (convex part with 4 facets), (a) top view of toolpath simulation results for the quarter section of convex a pyramid. Simulation of a single toolpath as the tool crosses an edge of the convex pyramid, (b) top view and (c) bottom view[65]

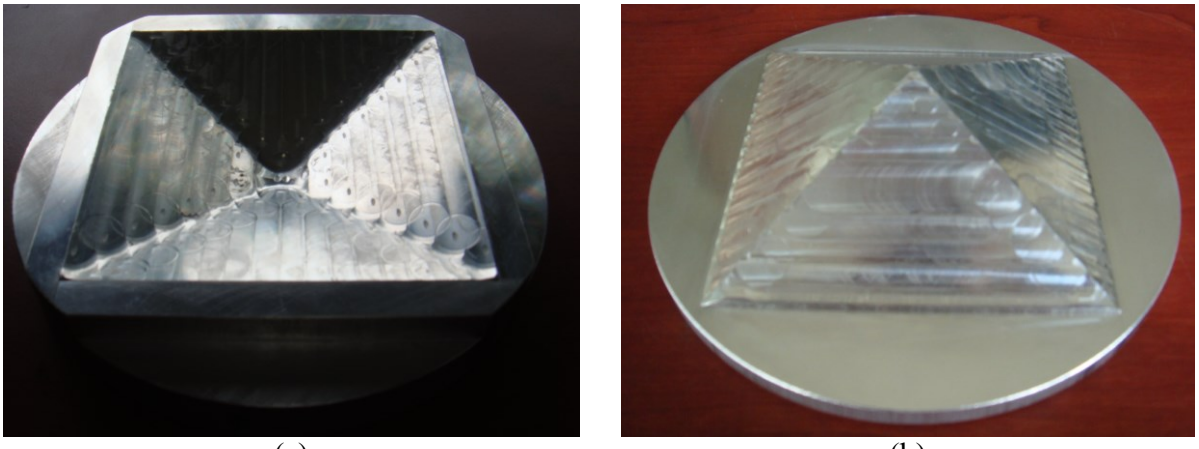

Figure 5.9: 5-axis machining results for pyramidal test parts on DMG 80-P Hi-Dyn tilt-rotary table simultaneous 5-axis CNC machine, (a) concave (inverted) pyramid part, (b) convex pyramid part

The concave pyramidal part was used to evaluate the parameter selection within the algorithm which included: maximum number of iterations in the bisection method; the acceptable error height; and the acceptable angle between two tool axis orientations used by the bisection algorithm. The concave (inverted) pyramid part does not result in contact with edges or vertices but validates the multiple triangle edge crossing and vertex crossing situations for concave geometries. The size of the triangles in concave pyramid model are chosen so that the triangles were large enough that the tool would traverse along them with the flat bottom of the tool tangent to the triangle facet; the slope of the triangles was chosen to be large enough to have easily distinguishable triangles, but small enough that the part could be machined by a typical 5-axis milling machine. The toolpath for the parts selected in the study was created for a tool with dimensions $R_o = 6.7$mm, $R_i = 6$mm. The tool positions for the concave pyramidal part shapes were generated 4 mm apart with a side step of 10 mm. The toolpath was simulated in Maple^{TM} graphics. The graphical simulation for the developed toolpath is shown figure 5.7 both in a top and bottom views. In the top view, it can be seen that as the tool moves across an edge, the tool axis gradually moves from being normal to the green face, to being vertical, and to being normal to the yellow face. The bottom view shows the contact between the tool and the part surface. When the tool lies on a face, the contact is a circle; as the tool crosses an edge, the contact is two points, one on each face. (These circles are visible because of the way Maple^{TM} renders the triangles. The circles vanish as we zoom into the part). This inverted pyramid model was also used in testing the analytical DTM model (demonstrated in chapter 3), where a 5-axis toolpath was made, simulated, and the part was actually machined. The simulation results from the analytical DTM algorithm matched with the actual machining results closely as presented in section 3.5 of chapter 3. The new simulation results from numerical DTM algorithm matched the results shown in chapter 3. The inverted pyramid test part was also machined using the new 5-axis toolpath generated using numerical DTM algorithm. The machined inverted pyramid part shown in figure 5.9(a) matched the simulation results (from DTM and numerical DTM method) as well as the earlier machined part.

The second part that we tested was a convex pyramid part whose geometry is shown in figure 3.10(a). We selected this part to validate the ability of the algorithm to deal with edges and vertices. The pyramid is made of four triangles connected at the apex. The test part illustrates that the developed algorithm can satisfactorily deal with convex parts; large triangles; more than one triangle in the shadow of the tool; one triangle surrounding the shadow of the tool; a

contact point on an edge; both contact points on an edge; and the contact point on a vertex. The 5-axis toolpath for the convex pyramid part was created for a toroidal/radiused tool with dimensions R_o = 6.7mm and R_i = 6mm. The tool positions were generated 4 mm apart with side-step value of 10 mm. The toolpath was simulated in Maple^{TM} graphics. The top view of the graphical simulation of 5-axis toolpath is shown figure 5.8(a). In this view, the tool position in blue color corresponds to situation when the tool is in contact with a vertex. In this case, the tool does not rotate. In figure 5.8(b), part of one tool pass with feed forward step of 2 mm is shown in top view. In this figure, as the tool moves across an edge, the tool axis gradually rolls over the edge. Figure 5.8(c) shows a bottom view of the pass, showing the contact between the tool and the part surface. When the tool lies on a face, the contact is a circle; as the tool crosses an edge, the contact is initially a semi-circle, until the first point of contact of the dropped tool is on the edge, at which point the contact between the tool and the part is confined to the edge. Eventually, the first point of contact of the dropped tool moves to the next face, and we again have a (semi-)circle of contact. The convex pyramid test part was machined using the 5-axis toolpaths generated from numerical DTM method, and the machined part is shown in figure 5.9(b). This convex pyramid part was also used in testing the analytical DTM algorithm presented in section 3.5 of chapter 3. The simulation as well as 5-axis machining results for this part model for the 5-axis toolpaths generated from numerical DTM algorithm match the results of analytical DTM results shown in chapter 3.

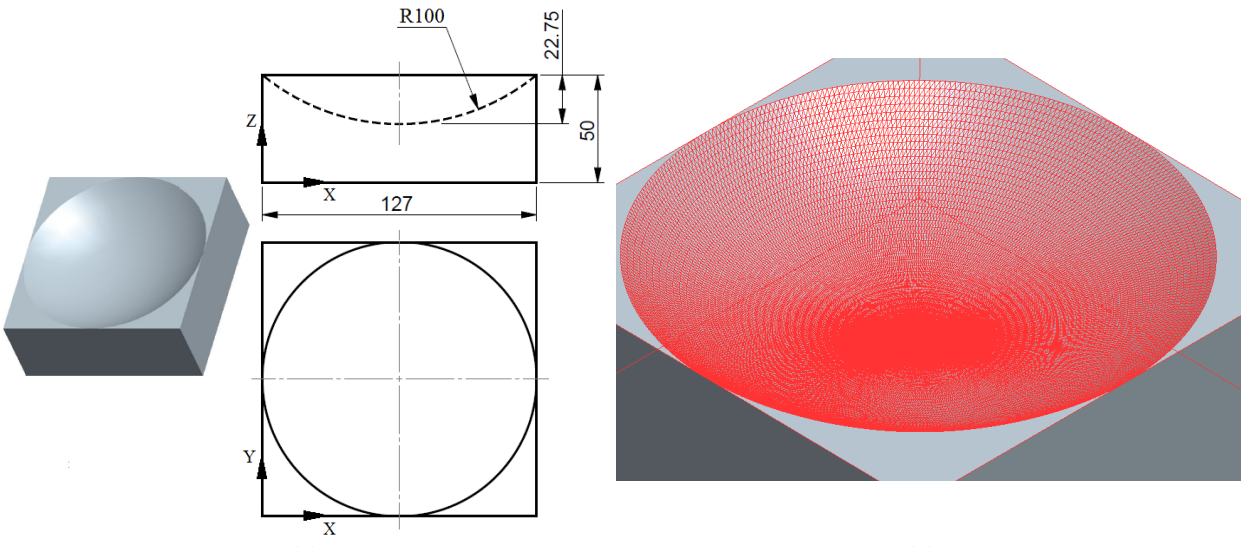

Figure 5.10: (a) Geometry of the spherical test part, (b) STL model of the spherical test part showing the higher mesh density at spherical bottom and less mesh density towards outer regions

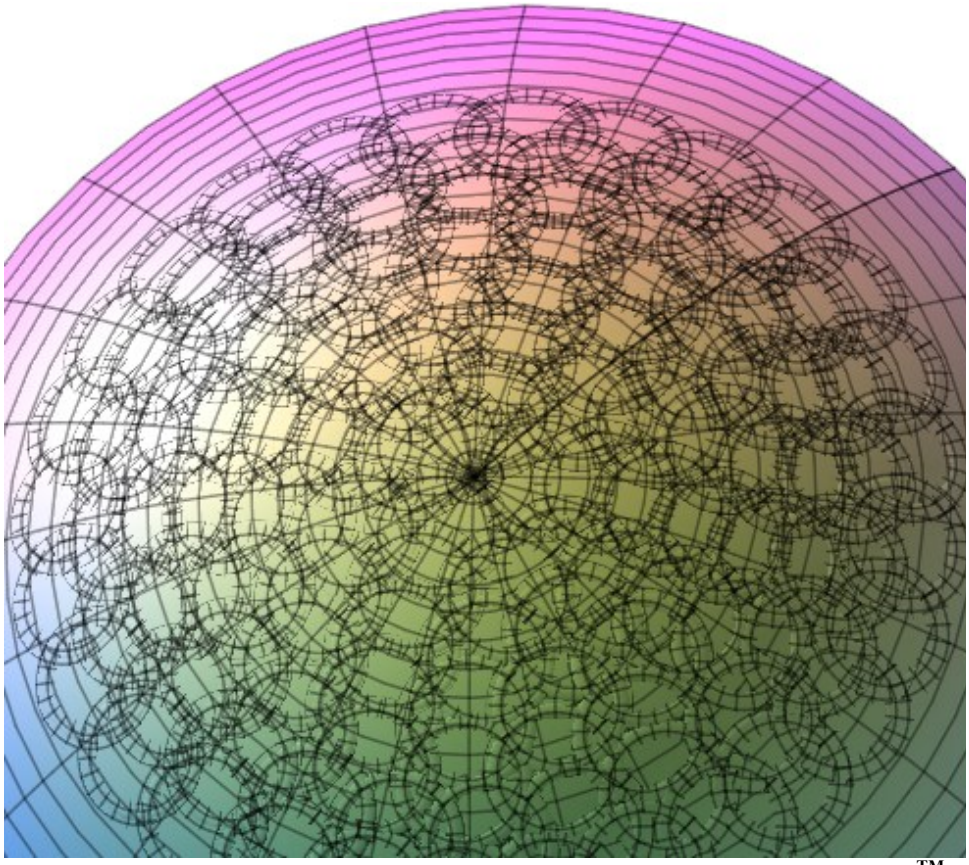

Figure 5.11: Simulation results of 5-axis toolpath for spherical model in Maple™

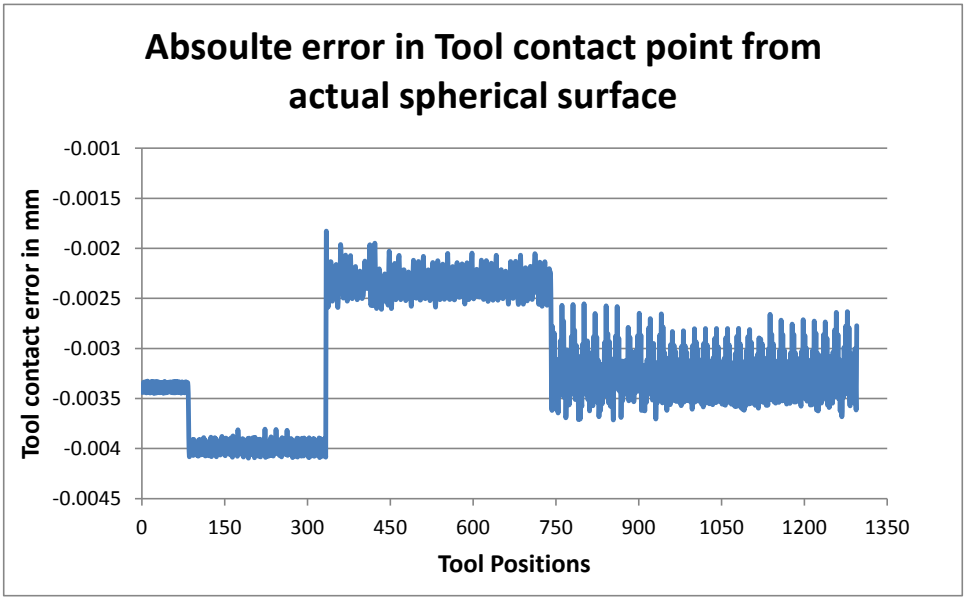

Figure 5.12: Absolute error in location point of contact *P* obtained from 5-axis algorithm from actual spherical surface for 1294 tool positions for four passes measured in mm

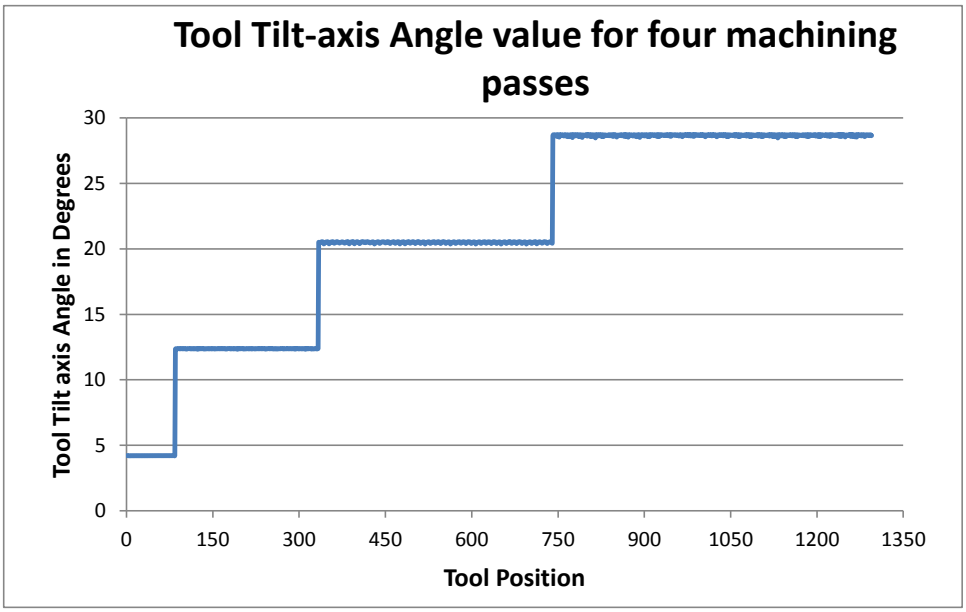

Figure 5.13: Tilt-axis (or A-axis) angle value calculated from 5-axis algorithm for four machining passes for 1294 tool positions for sphere machining

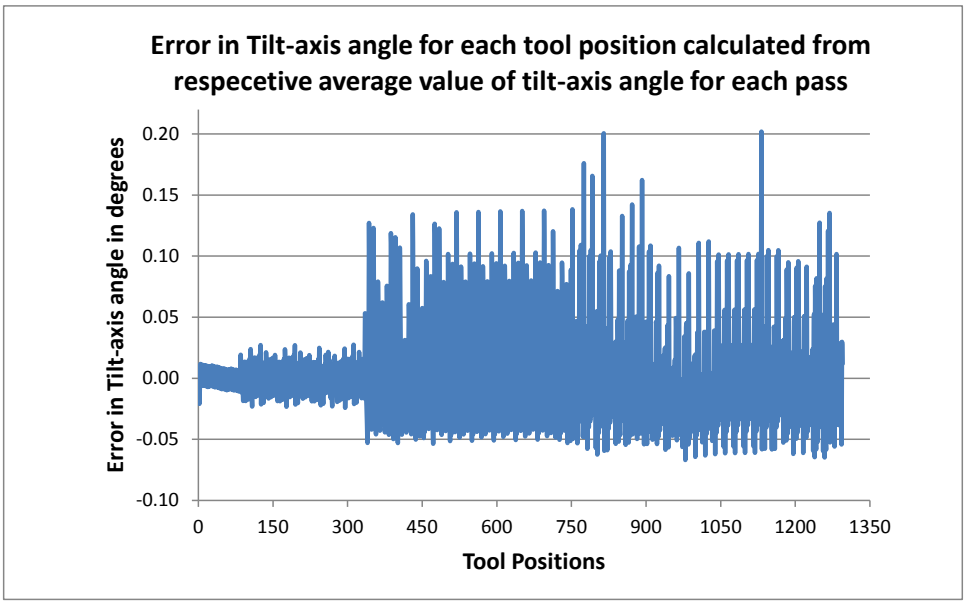

Figure 5.14: Error in computation of A-axis angle measured from the mean A-axis angle for different passes for sphere machining

Figure 5.15: 5-axis machining results for spherical test part [65]

The third part, which is a spherical faceted surface with 28814 facets, was designed to check the ability of the algorithm to deal with a large number of small triangles and its geometry is shown in figure 5.10. As the theoretical solution to 5-axis tool position at any point is known, this part helped in debugging and refining the algorithm. This part surface is machined with a toolpath whose footprint comprised of concentric circles. The toolpath for this part was constructed for a radiused end mill tool with dimensions $R_o = 6.7$mm, $R_i = 6$mm and a circular contour offset toolpath with variable side step and 0.5 mm feed forward step. The developed 5-axis toolpath had 1294 positions and the simulated toolpath is shown in figure 5.11. In the bottom view of simulation, the tool contacts the triangulated surface at multiple points of contact. The circular impressions of the tool disappear as we zoom into the part. This shows the generated tool positions are gouge free. For the spherical part (model without triangulations) the actual 5-axis tool positions (cuter contact points) and the tool tilt angle (tool axis inclination with the vertical reference) were determined analytically, and compared to the results obtained from the numerical DTM method. Figure 5.12 shows the positional error in point of contact P obtained from numerical DTM method with respect to the actual spherical surface for 1294 tool positions for four passes (measured in mm). The positional error in the initial set of tool passes is relatively very less as shown in figure 5.12, which is because of the reason that these tool passes are for region of sphere near the bottom where the triangulation is very fine and the fine meshes are located very close to the actual surface in the STL model. The positional error in point of contact in the later tool positions is higher and this is attributed to the course triangular meshes in the spherical regions located away from bottom of the part. The overall range of the positional error observed in this case is very less compared to the required machining tolerances in 5-axis machining for industrial parts.

The horizontal lines in figure 5.13 shows the tool-tilt angle value for four tool passes of the spherical part, which look very consistent in this plot and match the desired value. The results of difference between the tool-tilt angles for each tool position with the mean tool-tilt angle for a particular tool pass is plotted to determine the accuracy of numerical DTM algorithm, which is shown in figure 5.14. The figure 5.14 shows the similar pattern as we get in figure 5.11, where the accuracy of tool-tilt angle are best for the first two tool passes compared to the outer tool passes (represented by the later tool positions in the plot). The results for initial tool positions (for point of contact and tool-tilt angle) which correspond to first tool pass demonstrate the accuracy of numerical DTM algorithm (figure 5.12 and 5.14), while the higher magnitude of the errors from mean value visible in the results for other tool passes are

because of the increase in the size of triangular meshes for spherical regions which are away from the bottom of the spherical part. The figure 5.15 shows the machined spherical test part using the developed 5-axis toolpath, which confirms the simulation results.

Table 5.1: Control points of biquadratic Bezier surface (shown in figure 5.16)

(0.0, 0.0, 65.0)	(0.0, 76.2, 100.0)	(0.0, 152.4, 85.0)
(50.8, 0.0, 50.0)	(50.8, 76.2, 95.0)	(50.8, 152.4, 65.0)
(101.6, 0.0, 85.0)	(101.6, 76.2, 70.0)	(101.6, 152.4, 85.0)

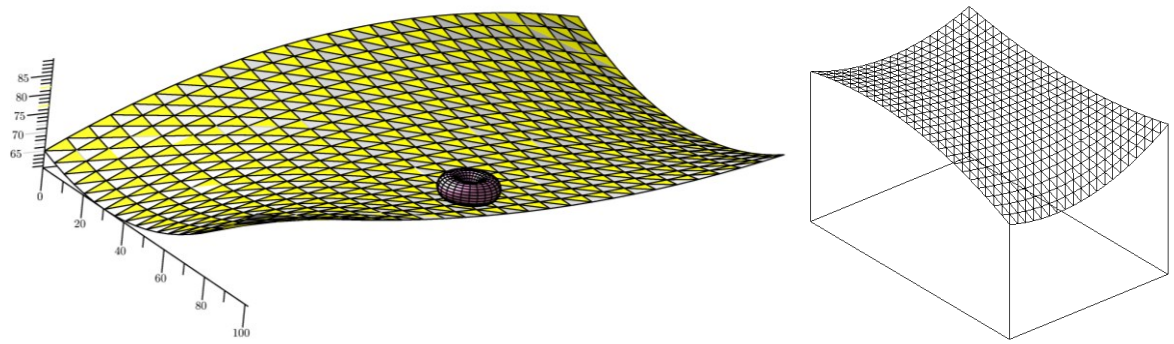

Figure 5.16: Triangulated biquadratic Bezier test part [65]

The fourth test part selected to verify the accuracy of the developed method is a biquadratic Bezier patch with concave, convex, and inflection regions, which is shown in figure 5.16. The control points for this Bezier surface are given in Table 5.1. The Bezier patch has been triangulated on a 21 × 26 grid and the geometry of the triangulated model surface with 1000 facets is shown in figure 5.16. A zigzag toolpath was used to machine the part with tool parameters $R_o = 6.7$mm and $R_i = 6$mm. The spacing between the passes was 12 mm and the feed forward distance was 1 mm for the first three passes and 2 mm for others. Figure 5.17(a) and (b), shows top and bottom views of the tool positioned along the toolpath, where only every 16^{th} tool position has been shown for clarity. In the bottom view, the toroidal cutting edges can be seen as circles. The generated toolpath considers multiple small triangles for each tool position. The machined part, shown in figure 5.18, shows that the feed forward distance of 2 mm gave results which are adequate to verify the algorithm. The test toolpath comprised of 825 tool positions. (The tool marks at either side of the part are due to our use of a simplistic entry/exit strategy and can be avoided with the use of a proper strategy).

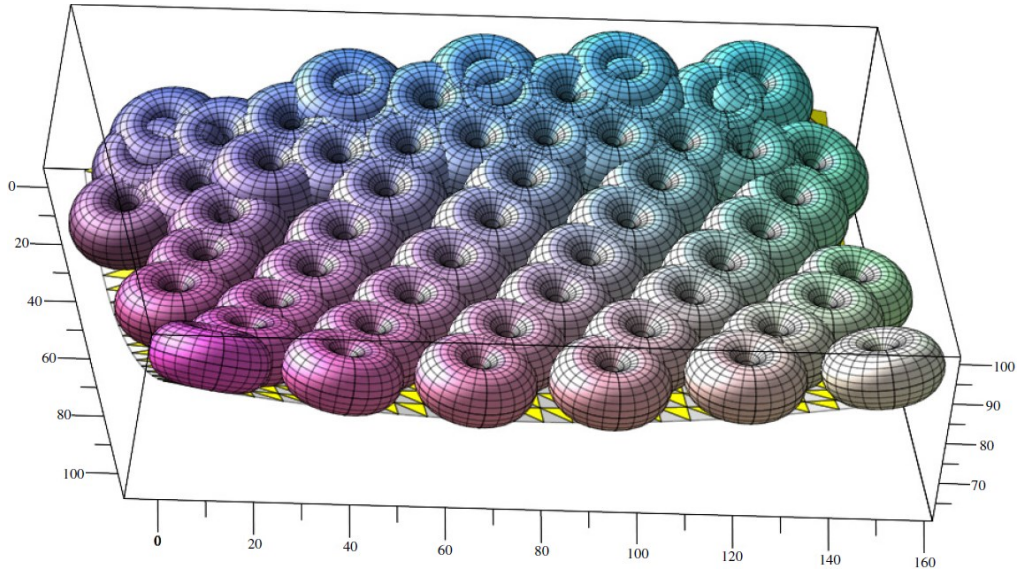

(a)

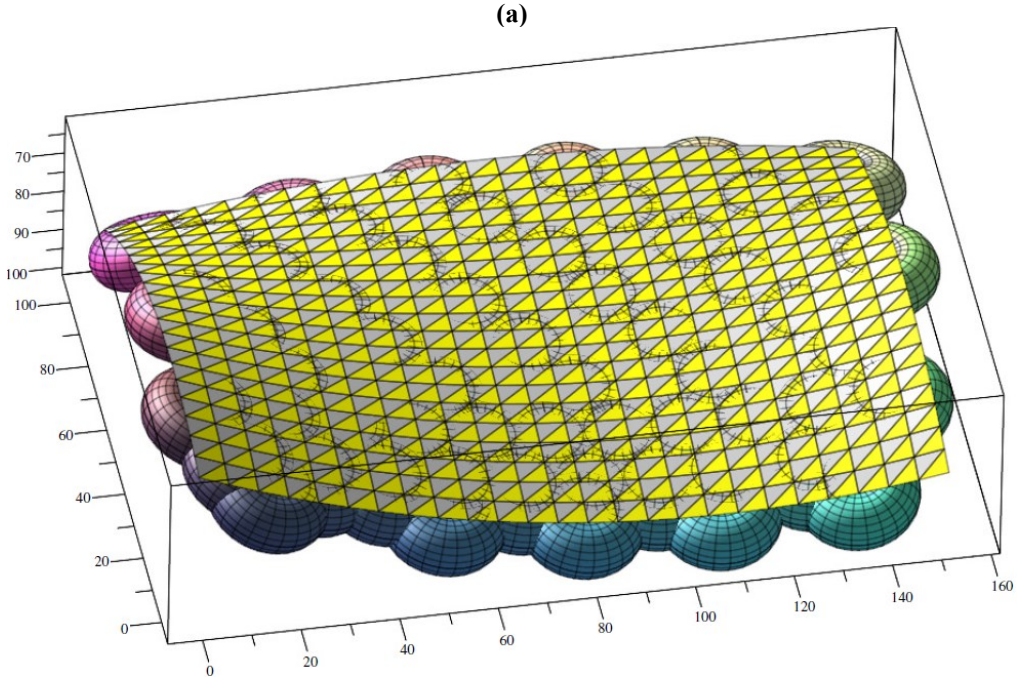

(b)

Figure 5.17: Simulation results from Maple™ graphics for bi-quadratic Bezier surface showing: (a) the top views of 5-axis toolpath, and (b) the bottom views of 5-axis toolpath [65]

(a) **(b)**

Figure 5.18: Results of 5-axis machining of the bi-quadratic Bezier test part [65]

5.5 SUMMARY

The developed algorithm is capable of generating gouge free toolpath for a radiused end mill for machining of a part models taken in triangulated format, where the tool has multiple points of contact with the triangulated surface. It is found that the numerical DTM algorithm no longer needs mathematical solvers for its implementation.

The tool drop method used in the numerical implementation of DTM method tests whether the tool comes in contact with the face, or edges, or vertices of a triangle. Care must be taken when implementing these intersections, primarily to avoid testing the edges multiple times (since testing edges are significantly more expensive to test for contact compared to faces or vertices). The generalized tool positioning method used in this work, to determine the point of contact between an edge and a torus needs the solution of 8^{th} order equations. Thus various approaches can be used to reduce the number of required edge checks, such as testing all faces first, and then only testing those edges that are higher than the highest point of contact with the faces.

Overall, the numerical implementation of DTM algorithm is quite accurate and generates gouge free tool positioning data. It does not require solving systems of nonlinear equations like analytical DTM approach. And it is computationally faster compared to the Maple™ implementation of analytical DTM method. At the same time, there are certain shortcomings that can be worked upon to enhance the computational efficiency of the numerical DTM in the form presented in this chapter. These short comings appeared in terms of: the computations with respect to tool positing over an edge are quite complicated and is a one of the biggest hurdle for overall computational efficiency of numerical DTM method. Another drawback of the numerical DTM approach is that for checking the global gouging and tool interference during 5-axis tool positioning the algorithm in the present form need to check all triangular facets.

CHAPTER 6
A NEW METHOD FOR EDGE-TORUS TANGENCY FOR MULTIPOINT MACHINING

6.1 INTRODUCTION

The tool-drop algorithm based DTM method is presented in chapters 3, 4 and 5. The cutter contact (CC) points obtained on the radiused end mill can lie on the triangular facet (plane), or edge (line) or vertex of the triangulated surface. As discussed in chapter 4, the mathematical models for the triangle and vertex checks are simple to implement. However, the edge check is complex [6, 13, 33, 41, 58, 63, 65]. The edge-torus tangency equations as developed in chapter 4 and 5 result in 8^{th} order equation. Various approaches [13, 33, 41, 58] are required to select the correct solution and researches have investigated various methods of reducing the number of edge checks required. The solution methods for the 8^{th} order equation are time consuming computationally.

Thus, the critical challenge in using a radiused end mill for toolpath generation for triangulated surface is the accurate and efficient determination of cutter contact point with respect to an edge of the triangulated surface. While carrying out our study on 5-axis tool positioning of radiused end milling cutter on STL surfaces [63, 65], we found shortcomings in the available methods. This led to the need for development of a comprehensive simple, faster, accurate and generalized method for solving the edge-torus contact/tangency problem suitable for 5-axis tool positioning. This chapter presents the shortcomings and a new generalized 3D approach to determine the edge-torus tangency that can be used in the DTM method.

6.2 LITERATURE REVIEW AND DRAWBACKS OF AVAILABLE EDGE-TORUS TANGENCY METHODS

We studied four algorithms [13, 33, 41, 58] for finding the contact between an edge and a radiused end milling cutter such that the edge and radiused end mill are tangent to each other. Hwang and Chang [13] presented a method to generate point of contact of radiused end mill with respect to an edge of the STL surface for 3-axis vertical machining in which the radiused end milling cutter is transformed into a flat end mill of radius R_o touching a cylinder of radius R_i where the edge under consideration represented the axis of the cylinder. The resulting higher-order implicit equation is solved using Newton–Raphson search. The

average number of iterations reported was five in their tests. The implementation of the mathematical model proposed by Hwang and Chang [13] is not easy for 5-axis tool positioning, because it would require a number of geometric transformations for each edge on triangulated surface before we get the solution for point of contact between the edge and the radiused end mill.

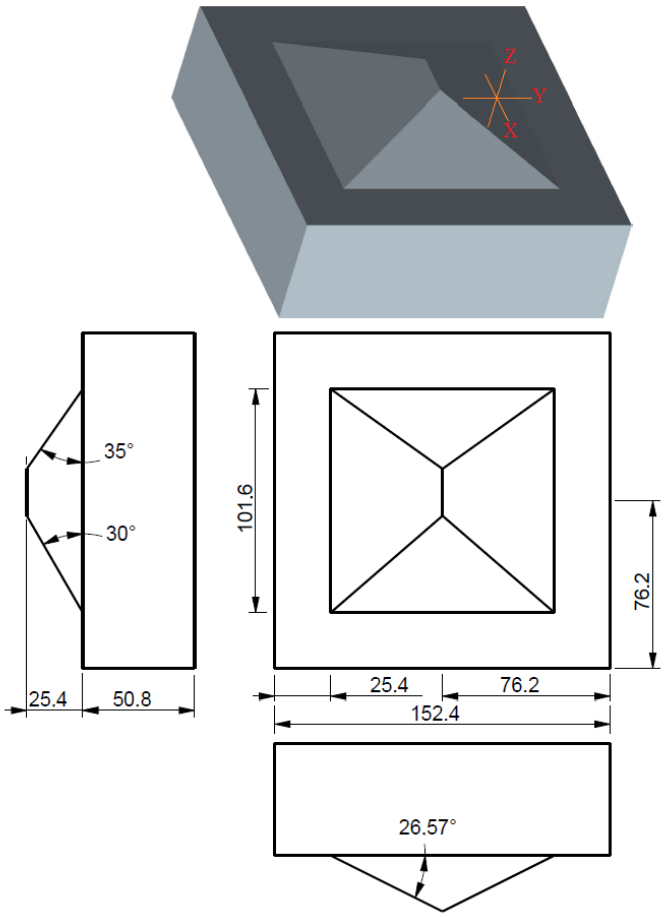

Figure 6.1: The dimensions of pyramidal test part used to test the accuracy of the edge-torus tool positioning algorithm proposed by Chuang et al. [33]

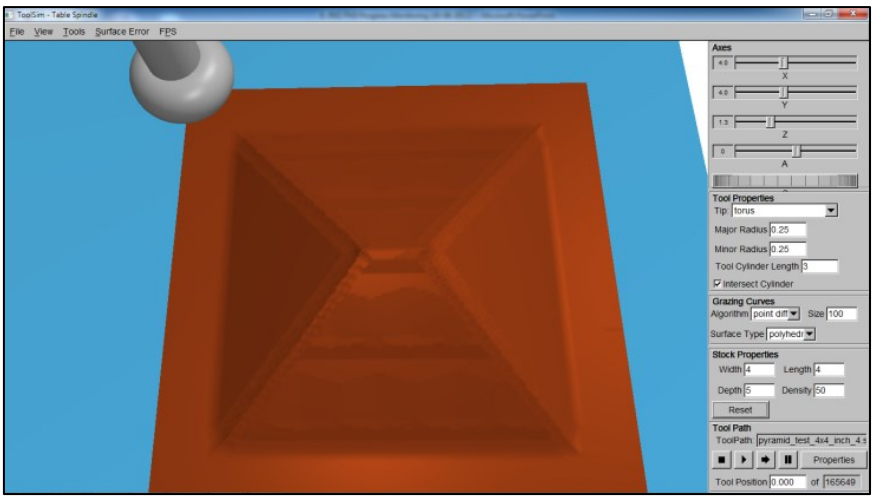

Figure 6.2: Machining simulation of faceted pyramid model machine with 3-axis vertical toolpath with toroidal end mill ($R_i = R_o = 6.35$ mm) using the edge-torus tangency model of Chuang et al. [33].

Chuang et al. [33] developed a geometric approach to determine gouge free cutter location data for radiused end mills for 3-axis vertical milling of triangulated surfaces. The authors simplified the procedure for edge-torus tangency developed by Hwang and Chang [13], wherein a vertical section plane, which is parallel to tool axis and contains the edge under consideration, cuts the body of radiused end mill. The profile of the sectioned surface generated on radiused end mill is approximated with an ellipse, which is used to determine the cutter contact position.

When implementing the method of Chuang et al. [33], it is found that the vertical approximation of the toroidal section with an ellipse was inaccurate. Figure 6.2 shows an example of machining a pyramid shape with their method using an NC toolpath for a radiused end mill $R_i = R_o = 6.35$mm. The dimensions of the pyramidal part are as shown in figure 6.1. The resulting toolpath was tested in a custom 3-axis vertical milling simulator developed by Mann et al.[92]. The simulation showed that the tool gouges the part as the tool crosses an edge; this gouging is visible in figure 6.2. Viewing the simulation, we noticed sharp changes in tool orientation near the edges. These changes can be attributed to inaccuracies in the edge-torus tangency computation.

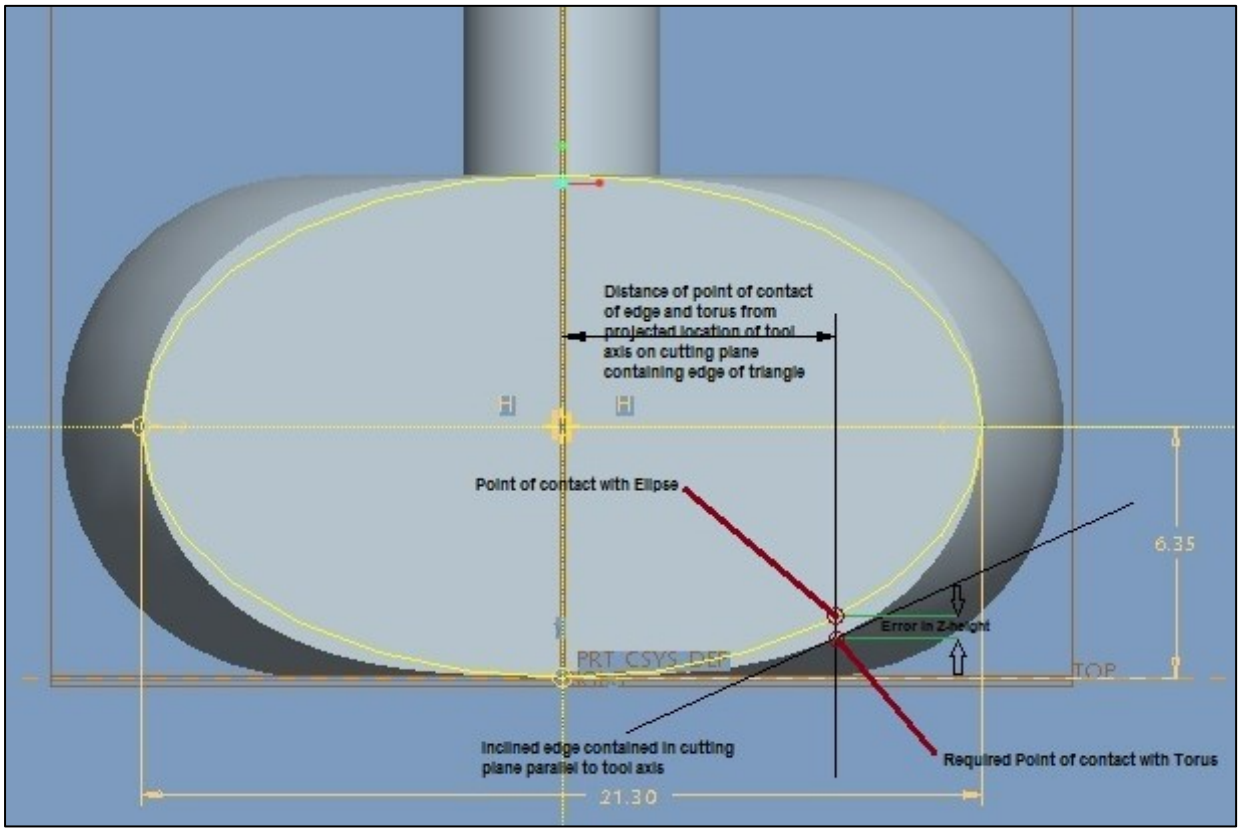

Figure 6.3: Reason for overcutting at edges with Chuang et al.'s method [33] (cutting plane distance from tool axis is equal to major radius of torus in 3D CAD model)

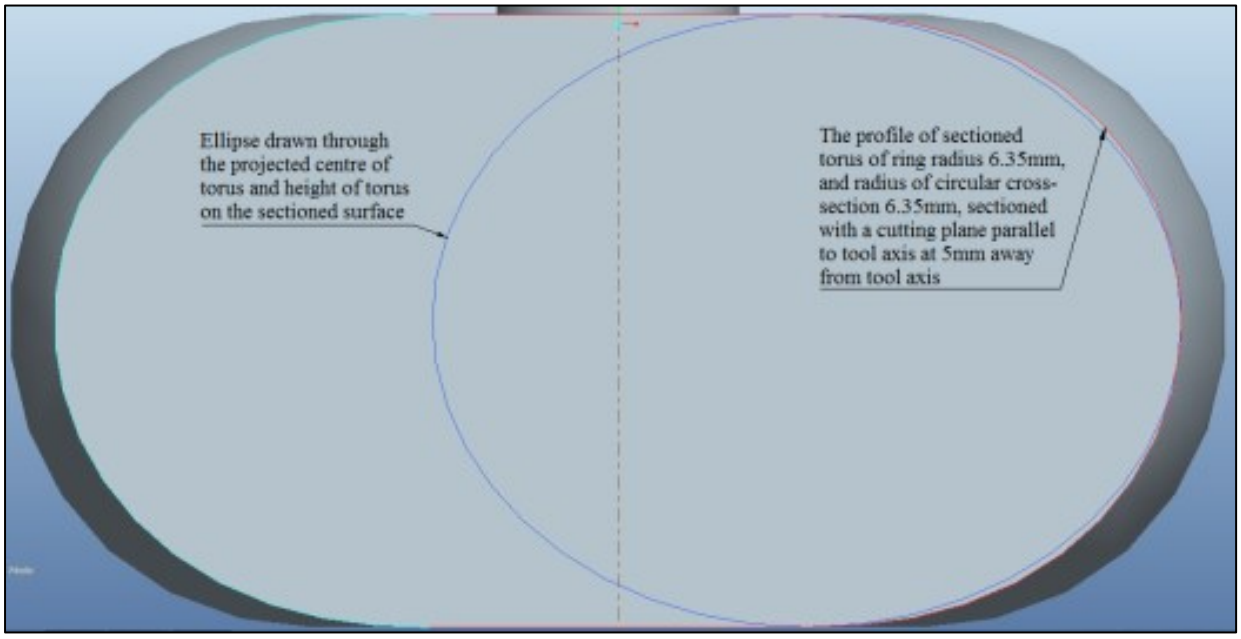

Figure 6.4: Reason for overcutting at edges with Chuang et al.'s method [33] (cutting plane distance from tool axis is less than major radius of torus in 3D CAD model)

To investigate the reasons for the inaccuracy in the Chuang et al. [33] edge-torus algorithm, a 3D model of sectioned toroidal tool was created in Pro-E CAD environment. The figure 6.3 shows the cross section of a sectioned surface generated by a plane parallel to tool axis and containing the edge for which the point of tangency is to be found. An ellipse drawn on the sectioned surface, by taking the extreme vertical and horizontal end positions of the sectioned surface is shown in figures 6.3 and 6.4. It is clear from the figures that the cross section generated by the cutting plane parallel to tool axis does not generate an exact elliptical contour in either case. The reason for overcutting is clear from the lower quarter part of the ellipse and sectioned surface as visible in figure 6.3 and 6.4. For a given distance from tool axis projected on the plane of intersection, the inclined edge will have a point of contact at lower height on actual sectioned profile on torus compared to the elliptical profile of Chuang et al. [33]. The difference in z-height or vertical height between two points of contact (actual CC point and the one found using Chuang et al.[33] method), is the cause for the overcutting on the edge and the sharp changes in tool orientation encountered by toroidal tool while machining over an edge of the triangulated surface.

Yau et al. [41] have also developed a method for locating the tangency of a toroidal tool with an edge of a triangulated surface for 3-axis machining. Their approach used the Newton-Raphson method to find the numerical solution for the vertical orientation of the tool-axis of

a radiused end mill and edge having an arbitrary orientation. This method is computationally expensive and is not suitable for 5-axis tool positioning in the proposed format.

The multipoint 5-axis tool positioning methods (MPM) for machining of triangulated surfaces for radiused end milling cutter are known as rolling ball method (RBM) [6] and arc-intersect method (AIM) [7]. The RBM method has problems with finding accurate tool positions when crossing the edges and raised vertices of a facet, while the AIM method, which is improved version of RBM, approximates the toroidal tool as a sphere to locate a second point of contact for generating a multipoint tool positioning. These two methods approximate the triangulated surface under to tool with a set of discrete points (exploiting the z-buffer of graphics card) and avoid the determination of tool positioning using the three elements of triangulated facets like facets itself, their edges and vertices respectively. Since they employ approximate and discrete data, some error in the tool positions is introduced.

Patel et al. [58] have presented a generalized solution for edge and torus tangency for 3-axis tool positioning for machining of faceted surface models. The edge check is performed to determine if the tool touches an edge tangentially within the limits of the vertices defining the edge using a generalized vector algebra approach. The final equation derived for edge-torus point of contact is an eighth order equation, which need to be solved using numerical methods. Compared to other methods this approach is easier to implement and gives an accurate result for edge-torus contact position. The problem with this method is that large number of iterations is required to get the solution for the point of contact with sufficient precision [65]. For example, while machining over an edge of the pyramid model shown in figure 6.1 (details discussed in section 6.5), Patel et al.'s method took 24 iterations to achieve an accuracy of 0.03 mm, while a new method described in this chapter in section 6.3 took only five iterations to achieve the same accuracy.

For implementation of DTM method (as discussed in chapter 3), we used another approach for determining the point of contact between edge and radiused end mill, but it needs a commercial mathematical solver like Maple^{TM} to determine the accurate solution from the complicated mathematical model [63]. An accurate solution gains more significance when the model is used in 5-axis tool positioning. A small error in orientation can result in large deviation between the desired contact point and the actual contact point. Any error in the solution results in an abrupt change in the tool position as well as orientation, which is

undesirable for achieving surface properties like surface finish. However, while the improved accuracy is beneficial, the method's use of a commercial mathematical solver makes it impractical for most industrial purposes.

Thus a simpler mathematical approach for finding accurate results for edge-torus contact that is fast and can be used for NC tool positioning in 5-axis machining is needed. The details of the new developed model for edge-torus tangency have been discussed in the next section.

6.3 A NEW APPROACH FOR FINDING THE POINT OF CONTACT AT EDGE-TORUS TANGENCY

This section presents a new methodology for finding the solution for the point of tangency between an edge and a radiused end mill. The developed method models the radiused end milling tool as a solid of revolution generated by a rotating circular pseudo-insert of radius R_i, which rotates about the axis of the tool (also known as the major radius of the torus) [63, 65, 69], as shown in figure 6.5. The contact point on the tool lies on a minor circle (pseudo-insert) of the torus that defines the tool's cutting surface as shown in figure 6.5.

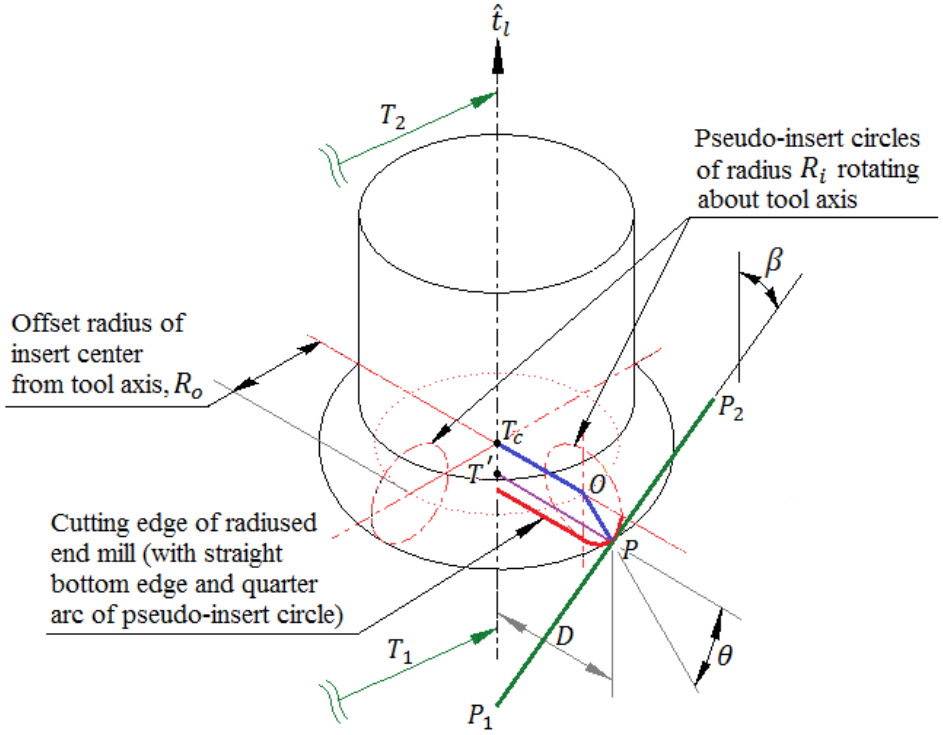

Figure 6.5: An edge touching the radiused corner of a radiused end mill cutter

The developed method makes use of following two main steps:

1. The first step is the classification of the edge based on the angle between the edge and the tool axis in a plane perpendicular to the shortest vector between them.

2. The second step is that any edge/line tangent to the radiused end milling cutter will always touch the circle of pseudo-insert tangentially on its outer lower quarter circumference shown in red in figure 6.5.

In the proposed method, the cutting edge of the tool has two components. The circular component describes a torus and the flat component describes a flat disc. The center of the torus defined by the circular component is taken as the tool center, as shown in figure 6.5. The tool center T_c moves along a line, the tool axis $T_a = T_1 + t.\hat{t}_l$, where, $\hat{t}_l$ is a unit direction vector along $(T_2 - T_1)$.

If an edge $\overline{P_1P_2}$ is tangent to the radiused end mill at position P as shown in figure 6.5, and T' is the projection of point P onto the tool axis, then the point P, O, T_c and T' will lie on a plane passing through tool axis T_a. Moreover this plane will also contain the circle of pseudo-insert located with its center at O. The vector $(T' - P)$ is always orthogonal to the tool axis and vector $(O - P)$ is orthogonal to vector $(P_2 - P_1)$ as shown in figure 6.5. Thus T' is given as:

$$T' = T_1 + \hat{t}_l.(P - T_1) \quad 6.1$$

where, $\hat{t}_l = (T_2 - T_1)/|T_2 - T_1|$

If one can determine the magnitude of distance D between point P and point T' given by $|T' - P|$, then the exact location of point P and point T' which are lying on lines $(P_2 - P_1)$ and $(T_2 - T_1)$ respectively, can be determined. Thus, the key element in the proposed new methodology is to determine the distance D between the point of contact of edge $\overline{P_1P_2}$ on the cutting edge of tool to the axis of the radiused end mill.

The distance D between edge $\overline{P_1P_2}$ and tool axis T_a depends on the angle θ between the vectors $(T_c - O)$ and $(O - P)$ as shown in figure 6.5.

Here, $|T_c - O| = R_o$ 6.2

and, $|O - P| = R_i$ 6.3

The projection of vectors $(T_c - O)$ and $(O - P)$ taken on a plane perpendicular to tool axis passing though the tool center T_c can also be given by $|T' - P|$. Thus, the logic to determine

angle θ is the key to determine the value of distance D and the vectors P and T_c, and hence the edge-torus tangency and is presented here.

The distance D is given by:

$$D = |T' - P| \quad 6.4$$

Also the distance D can be obtained as:

$$D = R_o + R_i \cos(\theta) \quad 6.5$$

The values of position vectors D, P and T_c are obtained as follows:

(i) Compute the shortest distance D_e between the edge $\overline{P_1P_2}$ and the tool axis T_a.

(ii) Determine angle of inclination β of the edge $\overline{P_1P_2}$ with respect to the tool axis T_a.

(iii) Select the mathematical model relating angle θ with angle β and shortest distance D_e. The edge–tool axis combination results in four cases.

(iv) Use value of angle θ to find distance D and hence position vectors P and T_c

The detailed procedure followed for edge torus solution is explained given below.

6.3.1 The shortest distance between an edge and the tool axis

The shortest distance D_e of the edge $\overline{P_1P_2}$ from tool axis defined by vector $(T_2 - T_1)$ can be determined as:

$$D_e = \frac{(P_2 - P_1) \times (T_2 - T_1)}{|(P_2 - P_1)||(T_2 - T_1)|} \cdot (P_1 - T_1) \quad 6.6$$

As long as the shortest distance of the line segment $\overline{P_1P_2}$ from tool axis is less than equal to $(R_i + R_o)$ it will touch the radiused end mill. Moreover, the edges having distance more than $(R_i + R_o)$ from the tool axis are not considered for further analysis since they will not touch the tool. The shortest distance between the edge and the tool axis lies along the vector

$$\hat{S}_d = \frac{(P_2 - P_1) \times (T_2 - T_1)}{|(P_2 - P_1)||(T_2 - T_1)|} \quad 6.7$$

6.3.2 The angle of inclination of edge with respect to tool axis

To find the solution for angle θ, the edge $\overline{P_1P_2}$ is categorized based on its slope given by angle β with respect to tool axis T_a, which is given by:

$$\beta = \cos^{-1}\left[\frac{(P_2-P_1).(T_2-T_1)}{|(P_2-P_1)||(T_2-T_1)|}\right] \quad 6.8$$

Depending upon the angle β the solution procedure for edge-torus tangency is divided into following four categories:

(A) Edge parallel to tool axis, $(\beta = 0)$

(B) Edge normal to tool axis, $(\beta = \frac{\pi}{2})$ with $(0 \leq D_e < R_o)$

(C) Edge normal to tool axis, $(\beta = \frac{\pi}{2})$ with $(R_o \leq D_e \leq R_o + R_i)$

(D) Edge inclined to tool axis such that, $(0 < \beta < \frac{\pi}{2})$ and $(0 \leq D_e \leq R_o + R_i)$

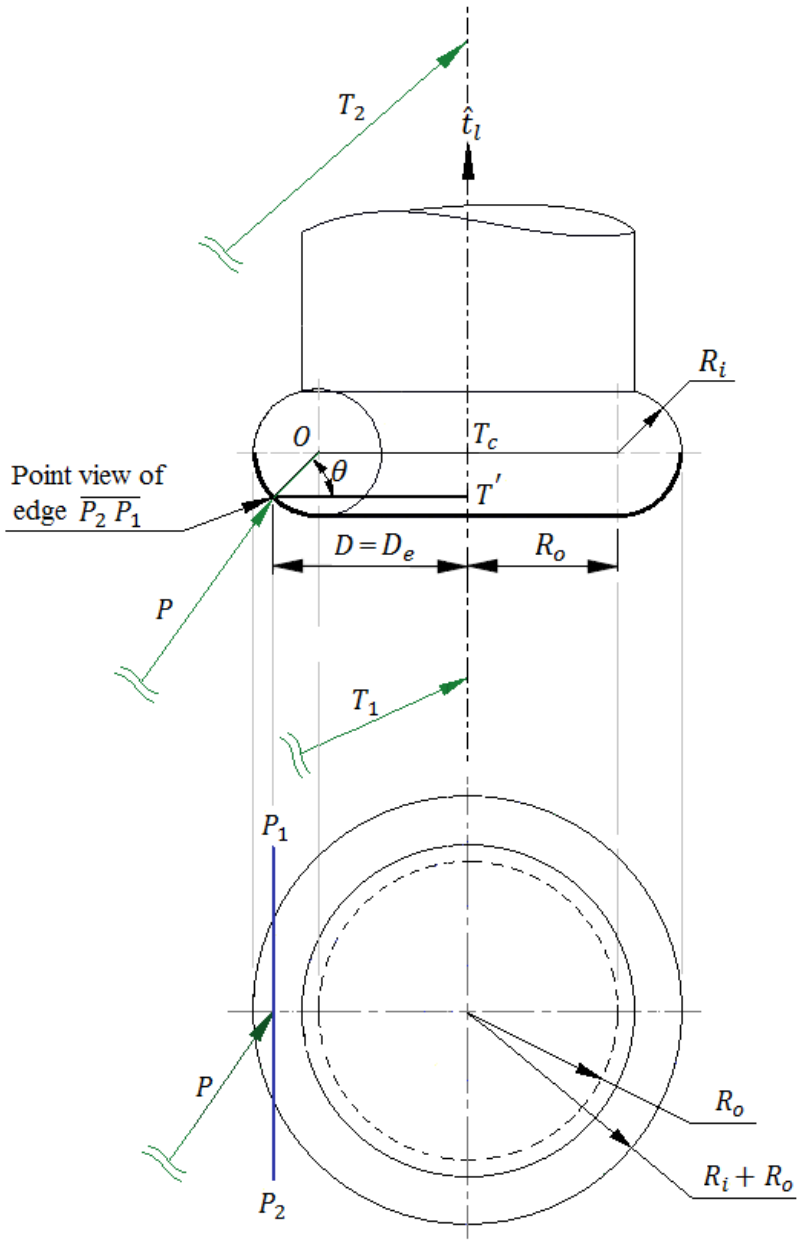

Figure 6.6: Category C: an edge normal to tool axis when $(R_o \leq D_e \leq R_o + R_i)$

Category A: When ($\beta = 0$), the edge is parallel to the tool axis. As the tool descends along the tool axis the first point on the edge it will touch is the vertex. This case is not considered any further as the computation of the tool contact is determined from either of the vertices of the edge. This procedure is explained in chapter 4.

Category B: When ($\beta = \frac{\pi}{2}$) with ($0 \leq D_e < R_o$), the edge is normal to the tool axis and the edge will have line contact with the flat bottom of the radiused end milling cutter or it will have two solutions for the point of contact with circular pseudo-insert of tool. The contact point is not found at the pseudo-inserts. Rather, in this case, the location of point T' can be found by using the projection of any one of the vertices of edge onto the tool axis, as given below:

$$T' = T_1 + \hat{t}_l.((P_1 - T_1).\hat{t}_l) \quad 6.9$$

where, $\hat{t}_l = (T_2 - T_1)/|T_2 - T_1|$

The point T' can be further used to find the point of contacts on circular tool bottom using:

$$(T' - P).(T' - P) = R_o^2 \quad 6.10$$

where $P = P_1 + \text{s}.(P_2 - P_1)$. The above equations will yield two solutions for P. Further, the location of the tool center T_c can be found as:

$$T_c = T' + \hat{t}_l.R_i \quad 6.11$$

Category C: When ($\beta = \frac{\pi}{2}$) but with ($R_o \leq D_e \leq R_o + R_i$), the edge is again normal to tool axis, but there is a unique point of contact between the edge and the radiused corner of the tool. Here, the shortest distance D_e between edge and tool axis will be equal to the distance D between point of contact P and tool axis as shown in figure 6.6. Thus, the value of D can be used to determine the location of point of contact P.

Category D: The most common situation for determination of point of contact is when an edge is inclined to tool axis such that ($0 < \beta < \frac{\pi}{2}$) and ($0 \leq D_e \leq R_o + R_i$). Such edges are referred here as *inclined edges*. In this method, the edge inclined to the tool axis is transformed into a coordinate system having a plane parallel to the tool axis. Thus, the point of contact P simultaneously lies in this plane as well as is tangent to the lower quarter of pseudo-insert circle.

For an inclined edge with $(0 < \beta < \frac{\pi}{2})$ the solution procedure is divided into four cases depending on the value of shortest distance D_e between edge $\overline{P_1P_2}$ and tool axis T_a as listed below:

1. $D_e = 0$
2. $D_e = R_i + R_o$
3. $0 < D_e < R_o$
4. $R_o \leq D_e < R_i + R_o$

Cases 1 and 2 are special cases; cases 3 and 4 are of more interest.

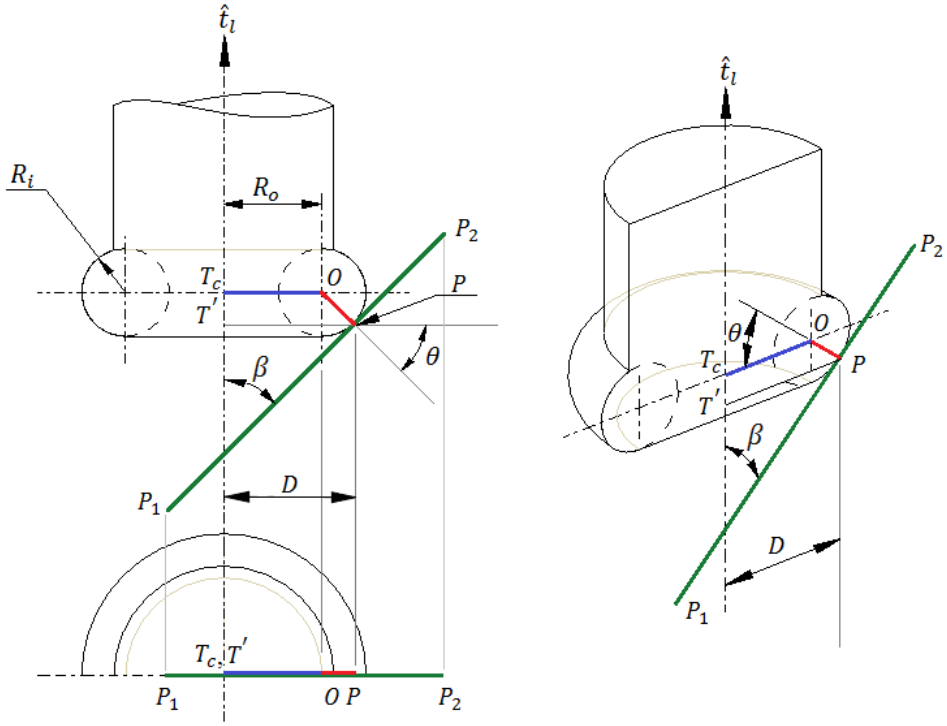

Figure 6.7: Category D, case 1: the figure shows the point of contact of an edge inclined to tool axis and passing through it when $(D_e = 0)$

Case (1): When $D_e = 0$, the tool axis and the edge $\overline{P_1P_2}$ are co-planar, and their common plane divides the radiused end mill into two equal halves. The contour of sectioned surface at the point of contact with the edge will be a circular arc as shown in figure 6.7. Thus the edge is basically contained in the plane of the pseudo-insert. It is evident from the geometry of the sectioned surface through the point of contact that the angle θ will be equal to the inclination of the edge with respect to tool axis given by angle β. Thus we can determine the value of distance D from equation 6.5 in the range $R_o \leq D \leq R_o + R_i\cos(\theta)$. From the above relationship, we can see that the $R_i\cos(\theta)$ ranges from 0 to R_i, which means the angle θ has a range $(0 \leq \theta \leq \frac{\pi}{2})$. The cases when $(\theta = 0)$ and $(\theta = \frac{\pi}{2})$ are considered separately, thus for this case the range for angle θ is restricted to $(0 < \theta < \frac{\pi}{2})$.

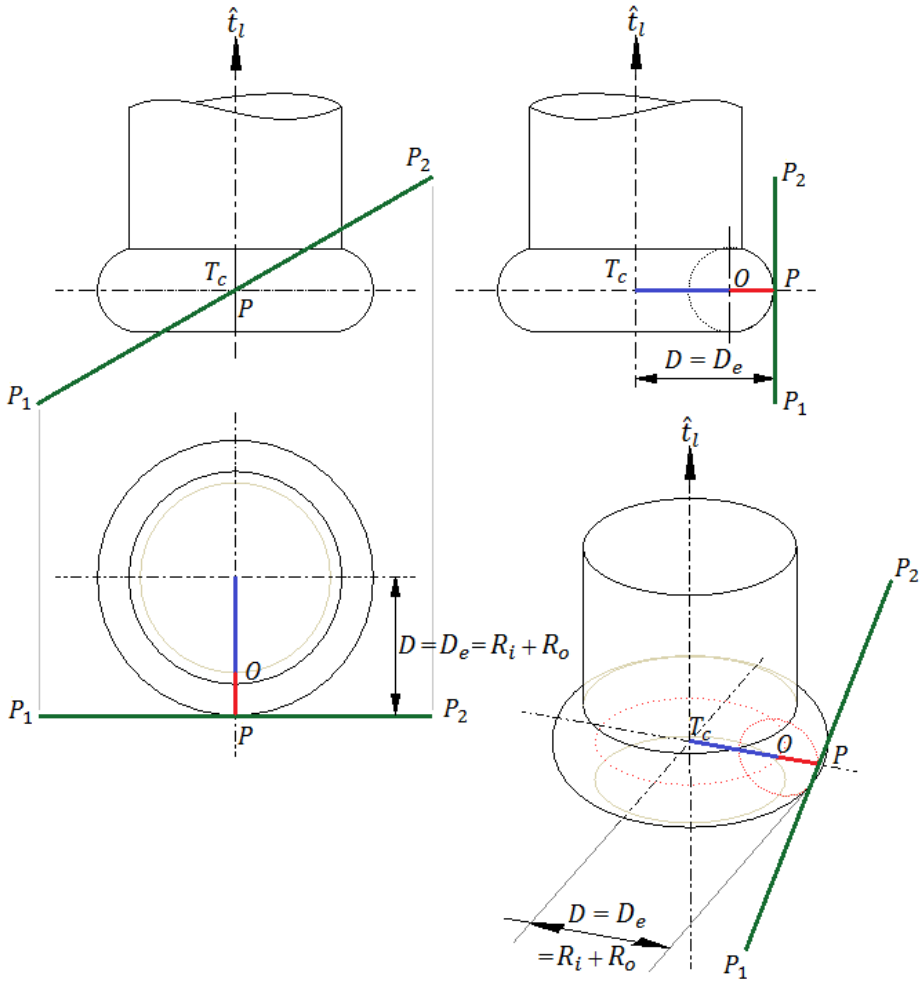

Figure 6.8: Category D, case 2: the point of contact of inclined edge and radiused end mill cutter when ($D_e = R_i + R_o$)

Case (2): When $D_e = R_i + R_o$, the edge will be tangent to the outer most circle of the radiused end mill (of radius $R_i + R_o$) contained in a plane normal to tool axis and centered at T_c, as shown in figure 6.8. Thus in this case, the angle θ will be zero irrespective of the slope of the edge with respect to the tool axis. The distance of point of contact P from tool axis will be given by magnitude of vector $|P - T_c|$ which can also be written as:

$$D = D_e = R_i + R_o \qquad 6.12$$

Case (3): The relationship between the tool and the edge, when $0 < D_e < R_o$, is shown in figure 6.9. The figure shows the front view, top view and an isometric view. The orthogonal coordinate system L_1 is located at the tool center T_c and can be seen in the three views of figure 6.9. In this frame, L_1, the X_1axis lies along the shortest distance vector $\hat{S}_d$ as described in equation 6.7 and the Z_1axis lies along the tool axis. The isometric view shows the contour

of the sectioned surface generated by a plane containing the edge $\overline{P_1P_2}$ and parallel to tool axis. The sectioned surface of radiused end milling cutter has two symmetrically located curved profiles with its center C_{p11} and C_{p12}. The centers have coordinates $(D_e, D_1, 0)$ and $(D_e, -D_1, 0)$ as measured from the origin of an orthogonal coordinate frame L_1. The middle region of sectioned profile is a rectangle of width $2D_1$ and height $2R_i$ as shown in figure 6.9.

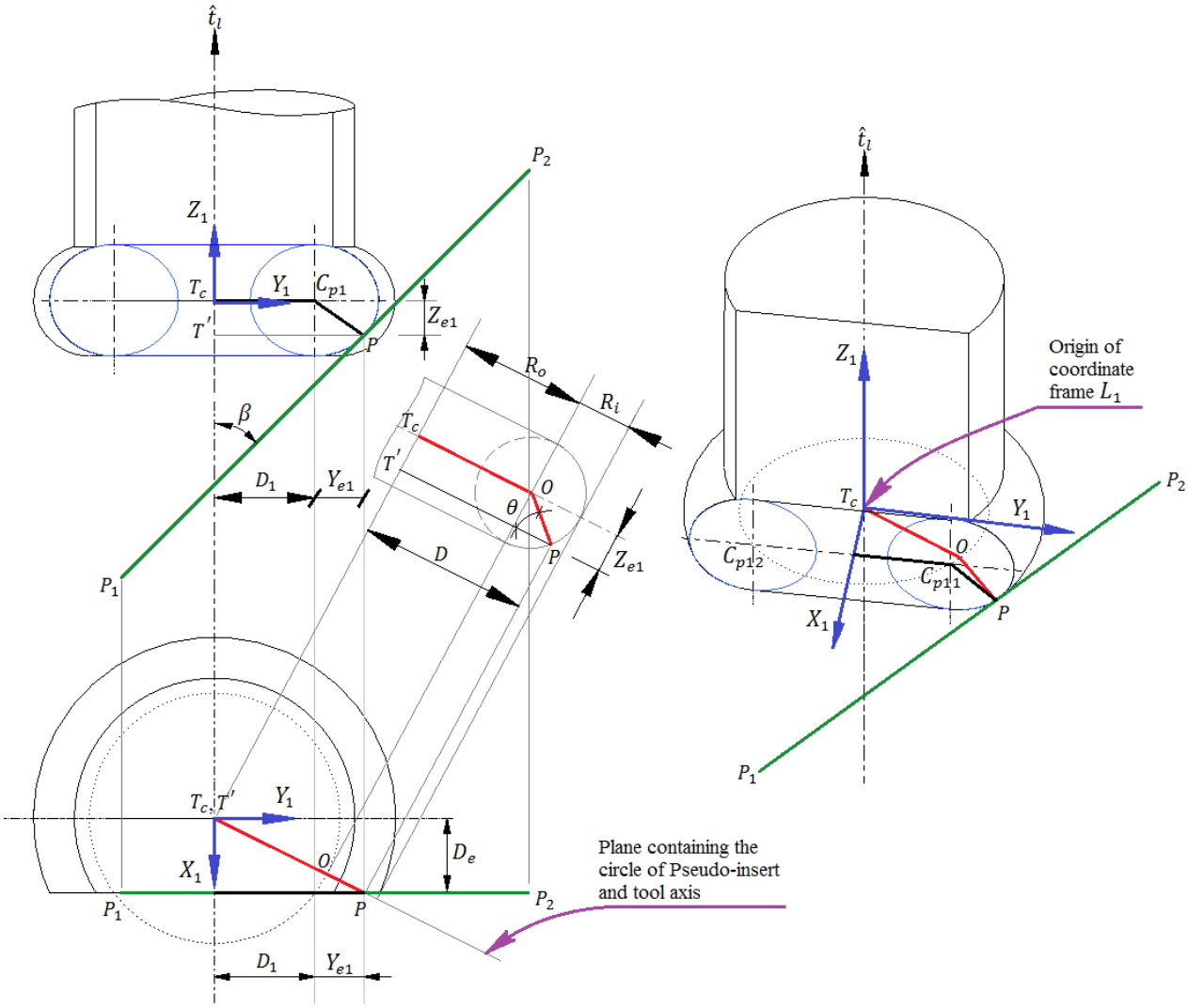

Figure 6.9: Category D, case 3: point of contact of an inclined edge and torus when $(R_o \leq D_e < R_i + R_o)$, and shape of sectioned surface generated by plane parallel to tool axis and containing the inclined edge. Orthonormal coordinate frame (shown in blue) $L_1 = \{X_1, Y_1, Z_1\}$ with origin at T_c

An edge $\overline{P_1P_2}$ will be tangent to the lower quarter arc of the curved profile at a point P as shown in red color in figure 6.9. The point of contact on the edge can be determined in this case because the geometry of the position of line and tool axis is known. Thus, depending upon the position of the edge in 3D space, it will touch the lower quarter of curved profile only on one of two curved profiles of the sectioned surface. The point of tangency of the edge with respect to the center of the curved sectioned profile C_{p1} can be expressed by two

components Y_{e1} and Z_{e1}, which are as measured from the point C_{p1} along the Y-axis and the Z-axis of the orthonormal coordinate frame L_1 as shown in figure 6.9.

Here,

$$Y_{e1} = \left\{\sqrt{\left(D^2 - {D_e}^2\right)} - D_1\right\}$$

$$Z_{e1} = R_i \sin(\theta)$$

and $D = \{R_o + R_i \cos(\theta)\}$ and is measured in the X_1Y_1-plane of frame L_1 frame as the distance of point of contact to the tool center T_c. D_1 is a constant given by :

$$D_1 = \sqrt{{R_o}^2 - {D_e}^2}$$

As shown in figure 6.9 the equation of tangency of edge $\overline{P_1P_2}$ with the lower half curve of the sectioned tool profile is given as:

$$\frac{dZ_{e1}}{dY_{e1}} = c_1 \qquad 6.13$$

where c_1 is defined as, $c_1 = \tan\left(\frac{\pi}{2} - \beta\right)$. Using the relationship of D, Y_{e1} and Z_{e1}, the equations 6.13 can also be rewritten as:

$$c_1 = \frac{\frac{d}{d\theta}[R_i \sin(\theta)]}{\frac{d}{d\theta}\left[\sqrt{\{\{R_o + R_i \cos(\theta)\}^2 - {D_e}^2\}} - D_1\right]} \qquad 6.14$$

The equation 6.14 can be reduced to:

$$\cos(\theta)\sqrt{\{R_o + R_i \cos(\theta)\}^2 - {D_e}^2} = -c_1 . \sin(\theta)\{R_o + R_i \cos(\theta)\}$$

Squaring both sides of above equation and simplifying the terms we get:

$$\{{c_1}^2 - (1 + {c_1}^2)\cos^2(\theta)\}\{R_o + R_i \cos(\theta)\}^2 + {D_e}^2 \cos^2(\theta) = 0 \qquad 6.15$$

The above transcendental equation is not conducive to a closed form solution but in section 6.4.2, this equation is solved numerically for θ.

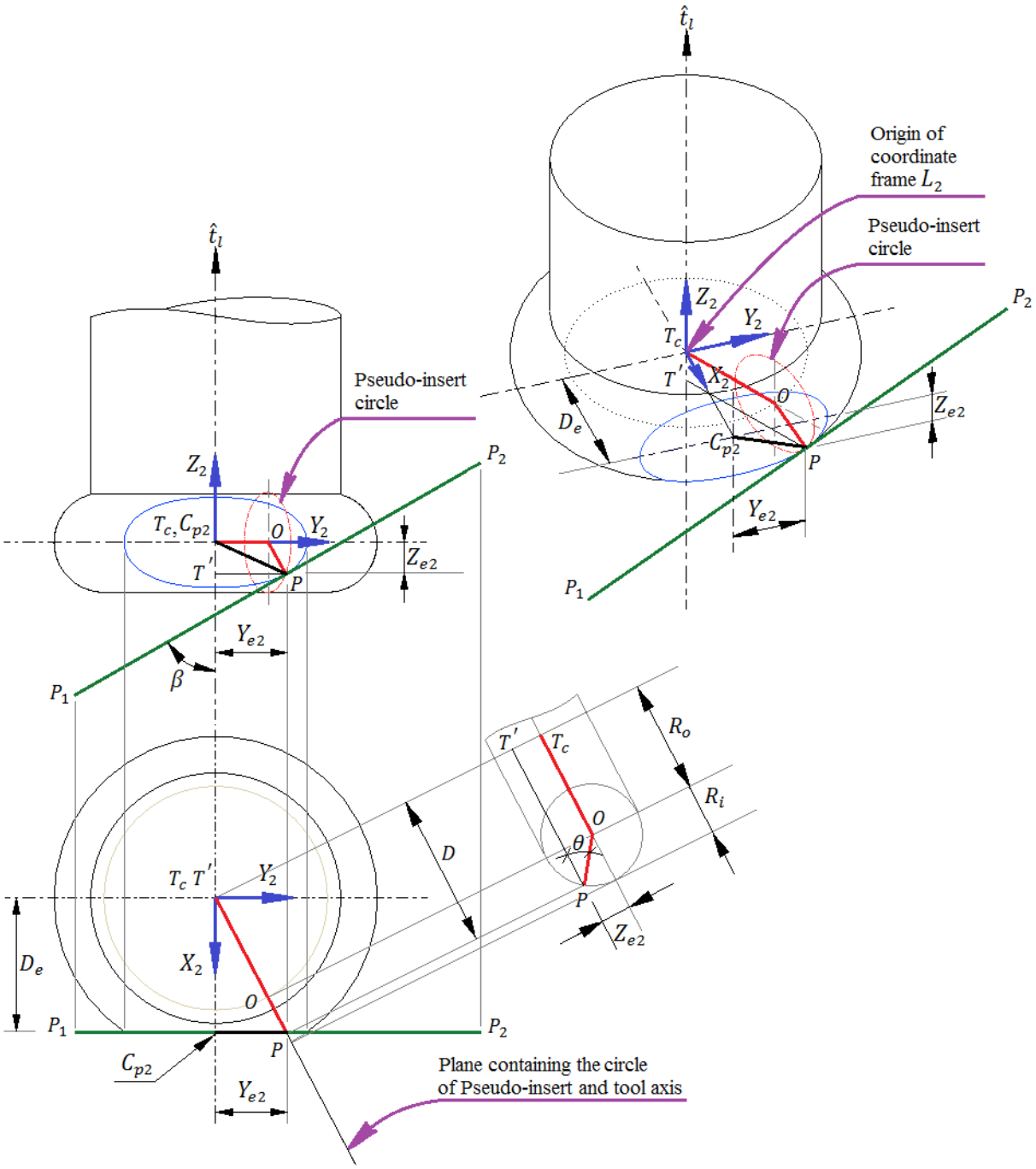

Figure 6.10: Category D, case 4: point of contact of an inclined edge and radiused end mill when ($D_e = R_i + R_o$). The figure shows the cross-section of a toroidal tool sectioned by a plane parallel to tool axis and contains the edge. Orthonormal coordinate frame (shown in blue) $L_2 = \{X_2, Y_2, Z_2\}$ with origin at T_c

Case (4): When $(R_o \leq D_e < R_i + R_o)$, as shown in figure 6.10, the center of the curved sectioned surface generated with plane parallel to tool axis and containing edge $\overline{P_1P_2}$ will be located at point C_{p2} having coordinates (D_e, 0, 0) measured in frame L_2 attached at tool center T_c. The direction of L_2's axes and its origin are defined as for L_1. The edge $\overline{P_1P_2}$ will be tangent to the lower half of the sectioned surface profile as shown in figure 6.10. The point

of tangency of the edge with the curved sectioned profile is given by two components Y_{e2} and Z_{e2} as measured from the point C_{p2} along the X_2-axis and the Z_2-axis of coordinate frame L_2. In this case,

$$Y_{e2} = \sqrt{\left(D^2 - {D_e}^2\right)}$$

$$Z_{e2} = R_i \sin(\theta)$$

and $D = R_o + R_i \cos(\theta)$ and is measured in the X_2Y_2 plane of orthonormal frame L_2 as the shortest distance between the point of contact of edge on radiused end mill and tool axis.

As shown in figure 6.10, the equation of tangency of edge $\overline{P_1P_2}$ with the sectioned profile of the radiused end mill generated by the section plane containing the edge and parallel to tool axis is given as:

$$\frac{dZ_{e2}}{dY_{e2}} = c_2 \qquad 6.16$$

Where c_2 is defined as $c_2 = \tan\left(\frac{\pi}{2} - \beta\right)$. Using the expressions for D, Y_{e2} and Z_{e2}, the equation 6.16 can be rewritten as:

$$\frac{\frac{d}{d\theta}[R_i \sin(\theta)]}{\frac{d}{d\theta}\left[\sqrt{\{R_o + R_i \cos(\theta)\}^2 - {D_e}^2}\right]} = c_2 \qquad 6.17$$

The above equation is reduced to

$$c_2 . \frac{d}{d\theta}\left[\sqrt{\{R_o + R_i \cos(\theta)\}^2 - {D_e}^2}\right] = \frac{d}{d\theta}[R_i \sin(\theta)] \qquad 6.18$$

As the expression for scalar c_1 and c_2 are identical, thus the equation 6.18 reduces to equation 6.15. This means the mathematical model for case (3) and (4) are identical and the same algorithm can be used to solve for θ in the two cases. Simplifying the above equation and incorporating $c_1 = c_2 = c$ results in:

$$\{c^2 - (1 + c^2)\cos^2(\theta)\}\{R_o + R_i \cos(\theta)\}^2 + {D_e}^2 \cos^2(\theta) = 0 \qquad 6.19$$

Note that the equation 6.19 is identical to equation 6.15 of case 3. Thus the same mathematical model needs to be solved to determine the value of angle θ for case (3) and case (4).

6.4 IMPLEMENTATION OF THE EDGE–TORUS TANGENCY

Most of the implementation of the edge-torus tangency method described in the section 6.3 is straightforward: in steps (i) and (ii), the formulas for D_e and β are used as given in equations 6.6 and 6.8; step (iii) uses the value of β to select between four categories of edges to compute the point of contact P and/or the tool center T_c that results in the tangential contact:

- Category A edges make contact with the tool at either P_1 or P_2; such edges are not considered for analysis during the edge testing rather the solution for point of contact is obtained from one of its two vertices and the handling of such cases is given in chapter 4.
- Category B is handled directly with equation 6.9 and 6.11.
- Category C uses the value of D to directly compute point of contact P.
- Category D has four subcases, two of which (cases 1 and 2) are special cases where the computation of P and T_c is straightforward; cases 3 and 4 require additional work to determine the value of θ and are the focus of the remainder of this section.

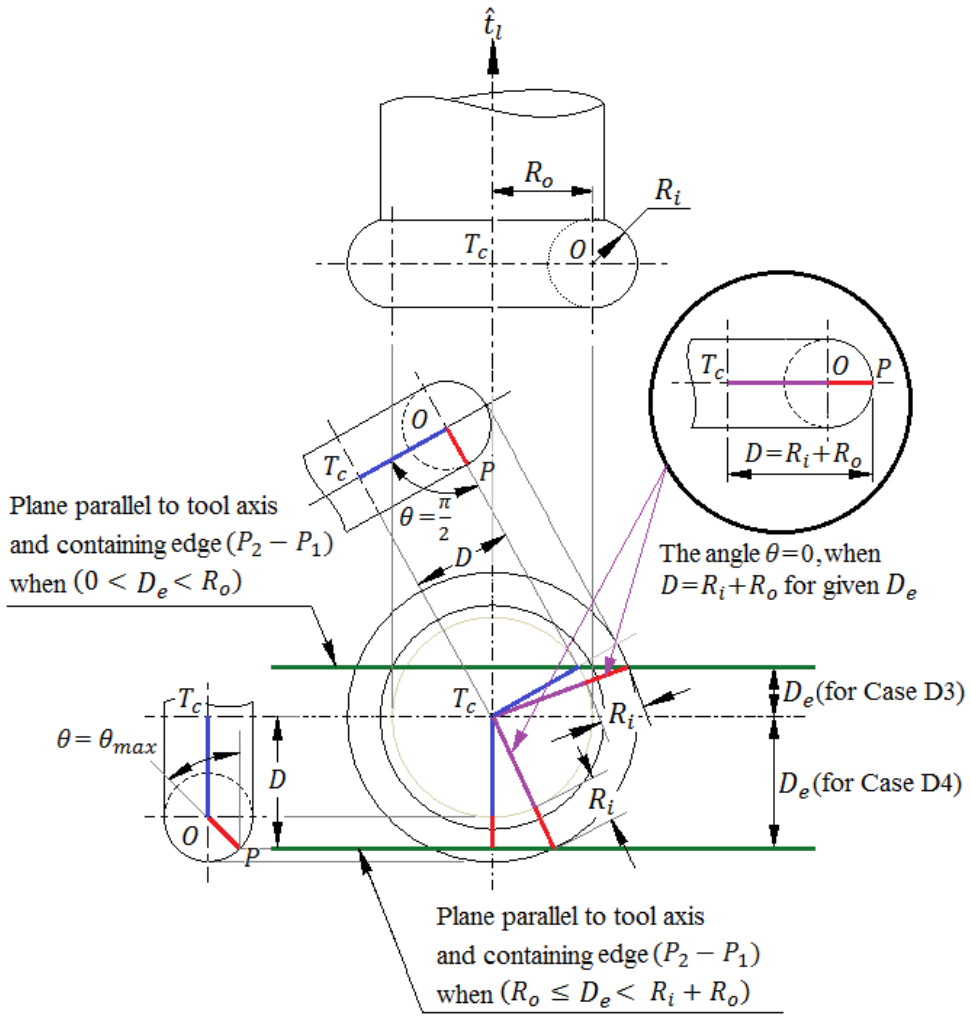

Figure 6.11: The range of angle θ in case $(0 < D_e < R_o)$ and $(R_o \leq D_e < R_i + R_o)$

6.4.1 Determining the angle θ

Cases 3 and 4 of category D require additional consideration to find the parameters of equation 6.19. For a given location of tool axis and an edge of the triangulated surface, all parameters in equation 6.19 are constants except for the angle θ. The equation 6.19 can be solved using Bisection method to determine the value of angle θ.

There can be two possible solution of the equation 6.19 over the range $\left(-\frac{\pi}{2} \leq \theta \leq \frac{\pi}{2}\right)$. As shown in figure 6.11 the range of the angle θ can be easily determined for case (3) and case (4). This will help in reducing the number of iterations required in Bisection method.

When the shortest distance from edge to tool axis is in the range $(0 < D_e < R_o)$, the value of θ is in the range of $\left(0 < \theta < \frac{\pi}{2}\right)$ as shown in figure 6.11. When angle $\theta = 0$ and $\theta = \frac{\pi}{2}$ are special cases that only occur when $\beta = 0$ and angle $\beta = \frac{\pi}{2}$ and are discussed in section 6.3.2 category A and in section 6.3.2 category B, respectively.

When the distance of the edge from the tool axis is in the range of $(R_o \leq D_e < R_i + R_o)$, the range of the angle θ will be $(0 < \theta < \theta_{max})$, where the value of θ_{max} is shown in figure 6.11 and it can be determined as: $\theta_{max} = \cos^{-1}\left(\frac{D_e - R_o}{R_i}\right)$.

Similarly, for case (4) when $(R_o \leq D_e < R_i + R_o)$ with $\beta = 0$, we have $\theta = 0$. This means such an edge is parallel to tool axis, and the solution for cutter location can be determined form vertex check as proposed in section 6.3.2 category A. Thus such an edge is not considered for analysis in category D4. Similarly, when $\beta = \frac{\pi}{2}$, we have $\theta = \theta_{max}$. In this case, the edge is normal to tool axis. Though the point of contact can be found out for this case, but using the concept as illustrated in section 6.3.2 category C.

6.4.2 Determining the point of contact P and cutter location point T_c

For category D, cases 3 and 4, after determining angle θ for an edge, the value of distance D between point P and a point T' on tool axis can be calculated using equation 6.5. Given that the tool axis passes through known points T_1 and T_2 as shown in figure 6.5, the location of the point of contact P on edge $\overline{P_1P_2}$ and T' on tool axis T_a can be determined by solving a

quadratic equation to find the two points on edge $\overline{P_1P_2}$ whose projected distance on to the tool axis is D.

In particular, if we write following equations:

$$P = P_1 + t\,.(P_2 - P_1) \qquad 6.20$$

The roots of the following equation can be determined

$$(P_1^2 - P_2^2).(P_1^2 - P_2^2)t^2 + 2\,(T_1^2 - P_1^2).(P_1^2 - P_2^2)t + (T_1^2 - P_1^2).(T_1^2 - P_1^2) - D^2 \qquad 6.21$$

and substitute into equation 6.20 to find the closest point on edge $\overline{P_1P_2}$ to the tool axis, where P_1^2, P_2^2, and T_1^2 are the points P_1, P_2, and T_1 (respectively) projected into a plane perpendicular to the tool axis (in particular, T_1^2 will have coordinates $[0, 0]$).

Once location of T' is known, tool center T_c can be found by:

$$T_c = T' + \hat{t}_l\,.\{R_i sin(\theta)\} \qquad 6.22$$

$$\beta = \cos^{-1}\left[\frac{(P_2 - P_1).(T_2 - T_1)}{|(P_2 - P_1)||(T_2 - T_1)|}\right] \qquad (6.8)$$

$$c_1 = \tan\left(\frac{\pi}{2} - \beta\right)$$

$$\theta_a = 0;\ \theta_b = 90$$

$$A = F_{19}(\theta_a)$$

$$B = F_{19}(\theta_b)$$

while $(abs(A - B) > \epsilon)$ {

$$C = F_{19}\left(\frac{\theta_a + \theta_b}{2}\right)$$

update $A,\ \theta_a$ or $B,\ \theta_b$

}

$$D = R_o + R_i \cos(\theta) \qquad (6.5)$$

solve for P with (6.21) and (6.20)

$$T' = [0, 0, P_x]$$

$$T_c = T' + R_i sin(\theta).\hat{t}_l \qquad (6.22)$$

Figure 6.12: Pseudo-code for edge-torus tangency, category D, cases 3 and 4. F_{19} is the evaluation of the left-hand side of equation 6.19. Equations numbers are given at the right for some lines of code

6.4.3 Pseudo-code for new edge-torus algorithm

The algorithm for categories A, B, and C is straightforward, as is the code for category D, cases 1 and 2. The algorithm for category D, cases 3 and 4 is more involved; fortunately, both cases share the same code. In particular, for both cases, the value of angle θ which satisfies equation 6.19 is numerically searched. From the computed value of angle θ, the value of

distance D can be determined using equation 6.5. Then by finding the roots of the equation 6.21 we can solve for point P by finding the points on edge $\overline{P_1P_2}$ that are a distance D from the tool axis. T' is the projection of P onto the tool axis, and then the location of tool center T_c can be determined using equation 6.22.

Figure 6.12 gives pseudo-code for the edge-torus tangency computation. Note that the pseudo-code assumes that we are working in a coordinate frame where the Z-axis aligns with the tool axis.

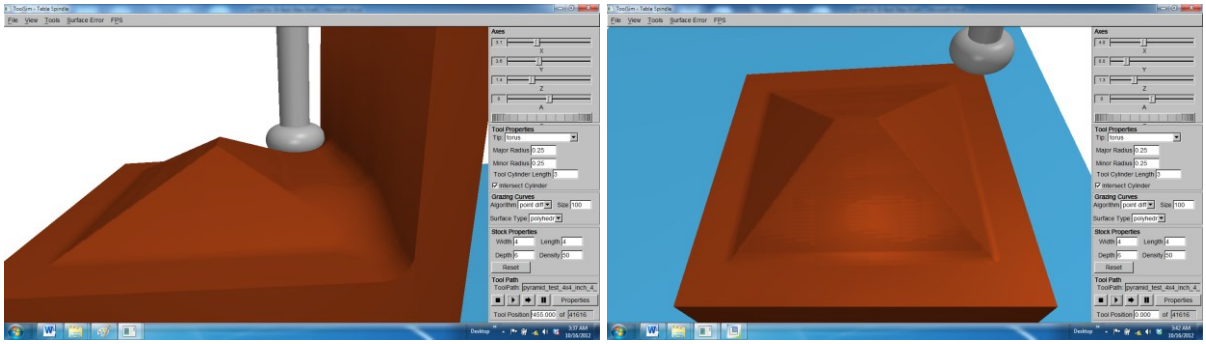

Figure 6.13: A machine simulation results for faceted pyramid model machined using the new edge-torus algorithm (during machining)

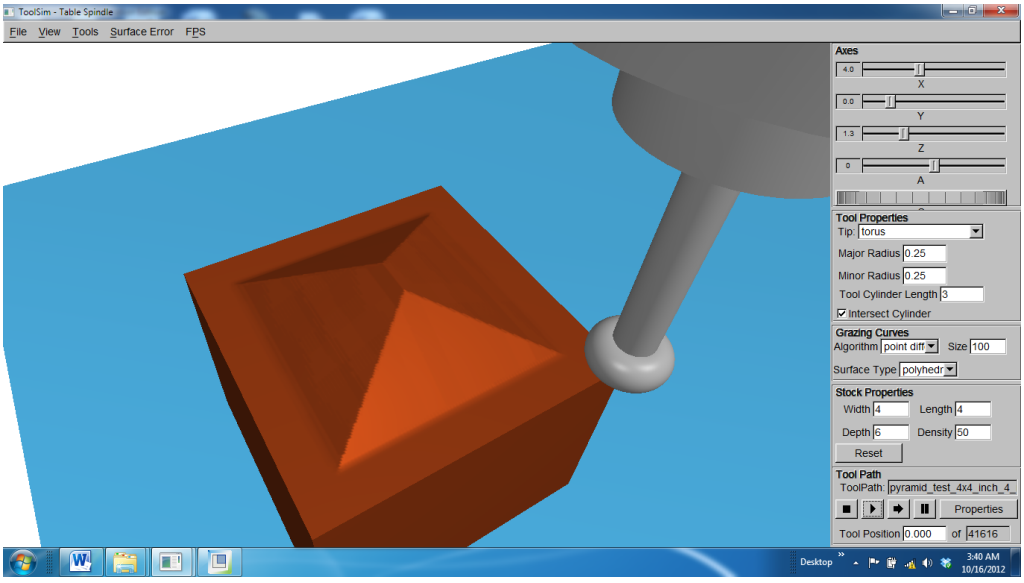

Figure 6.14: A machine simulation results for faceted pyramid model machined using the new edge-torus algorithm (after machining)

6.5 Results and discussions

The mathematical model of new edge-torus approach has been implemented in Visual C++ programming environment. The method was tested on a triangulated surface modeling a pyramid shown in figure 6.1 and on the triangulated tensor product Bezier patch shown in figure 5.16.

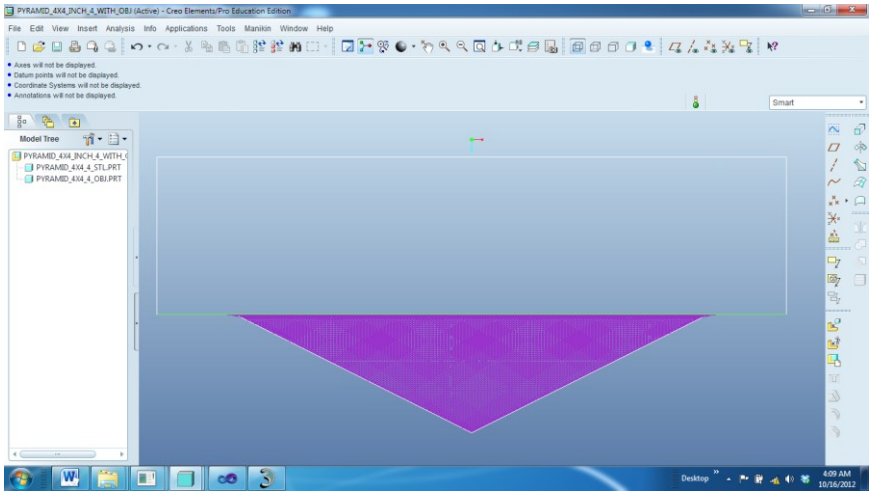

(a)

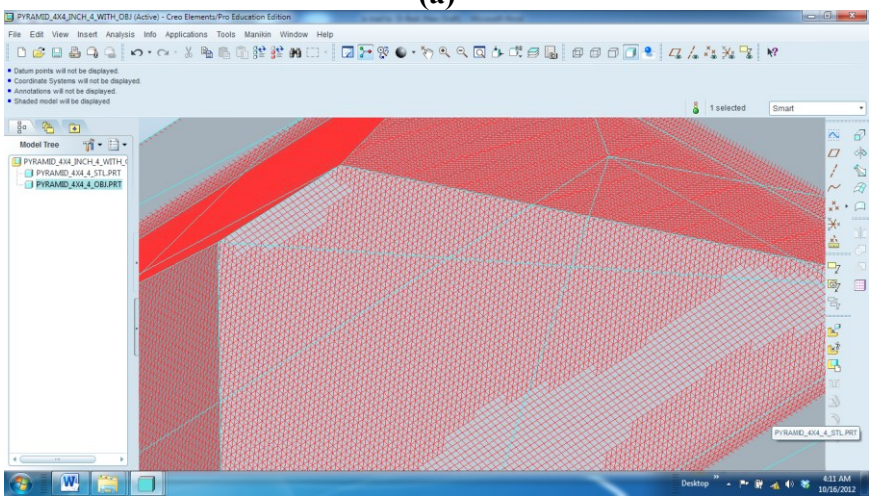

(b)

Figure 6.15: Comparison of simulation output (OBJ data) with original STL pyramid model in Pro-E CAD, (a) view showing slanted faces of pyramid projected as lines, and (b) view showing output from custom simulator compared with edges of STL model

The part model shown in figure 6.1 has been machined in a customized 3D simulator developed by Mann et al. [92], with the radiused end mill cutter of shaft diameter having $R_o = R_i = 6.35$ mm with 3-axis toolpath generated using the new edge-torus tangency model implemented within the numerical DTM algorithm (the tool-axis angle is not rotated rather kept vertical). The side feed distance and feed forward distances are taken 1.0 mm. The simulated results from the new toolpath algorithm are shown in figures 6.13 and 6.14. It is observed during machining simulations that the tool movements were smooth when the tool traveled over edges, planes or vertices. The gouges and other artifacts seen in figure 6.2 (machined with the method of Chuang et al. [33]) are not present with the new edge-torus method. The tool was positioned on and around edges with the same accuracy as the earlier method that required finding the roots of an eight-order equation; further comparison to the eight-order method of Patel et al. [58] is discussed at the end of this section.

The output of the machined surfaces of pyramidal model from the custom simulator was saved in object (.obj) data format and was compared with the original STL model in Pro-E CAD environment by superimposing the two in assembly mode. The output data in object (.obj) format for machined part is shown in figure 6.15(a) in the purple color while the STL part model is shown with the white boundary. The figure 6.15(b) shows the enlarged view of the machined surfaces (highlighted in red color) over five edges of input STL model (four slant edges and one horizontal edge). The results shown in figure 6.13, 6.14 and 6.15 demonstrate the accuracy of the proposed edge-torus tangency algorithm for determination of the point of contact of radiused end milling cutter with an edge of triangulated surface model.

The developed algorithm is tested for 5-axis tool positioning on a model of Bezier surface approximated with 20,000 triangulated facets. The design of the Bezier surface model is the same as shown in figure 5.16. The triangulation for Bezier surface is generated using a custom program developed in Visual C++ environment using the same control points as mentioned in table 5.1 in chapter 5. The Bezier surface is discretized at parametric interval of 0.01 along both parametric direction and the data points thus generated are used to create the triangulation data. The numerical DTM approach for 5-axis tool positioning (presented in chapter 5) with the new edge-torus tangency algorithm was used for the generation of the NC toolpath data. The toolpath data used in this study comprises of 20 zigzag passes with sidestep of 5.08mm and feed forward distance of 0.5 mm. The tool parameters used for radiused end milling cutter are $R_o = 6.7$ mm and $R_i = 6.0$ mm.

The figures 6.16(a) to 6.16(e) below shows the results of simulation for selected toolpath plotted in a custom 5-axis simulation environment developed within Maple^{TM} environment. In these simulations the radiused end mill is modelled as a torus. The shank of the tool and the flat bottom disc are ignored. The figures 6.16(a) to 6.16(e) show the Bezier surface from a point of view located below the surface (bottom view). In these views, the protrusion of the toroidal tool, if any, would be clearly visible. Figure 6.16(e) shows some of the tool positions used to machine the overall surface. Figures 6.16(a) to 6.16(e) show a near circle protruding below the Bezier patch. Even after zooming onto one tool position, the protruding circle stays as a line. This protrusion is an outcome of the plotting software used within Maple^{TM} Graphics. The protrusions also demonstrate that the DTM method produces a tool position that places the cutting surface in close proximity to the desired surface.

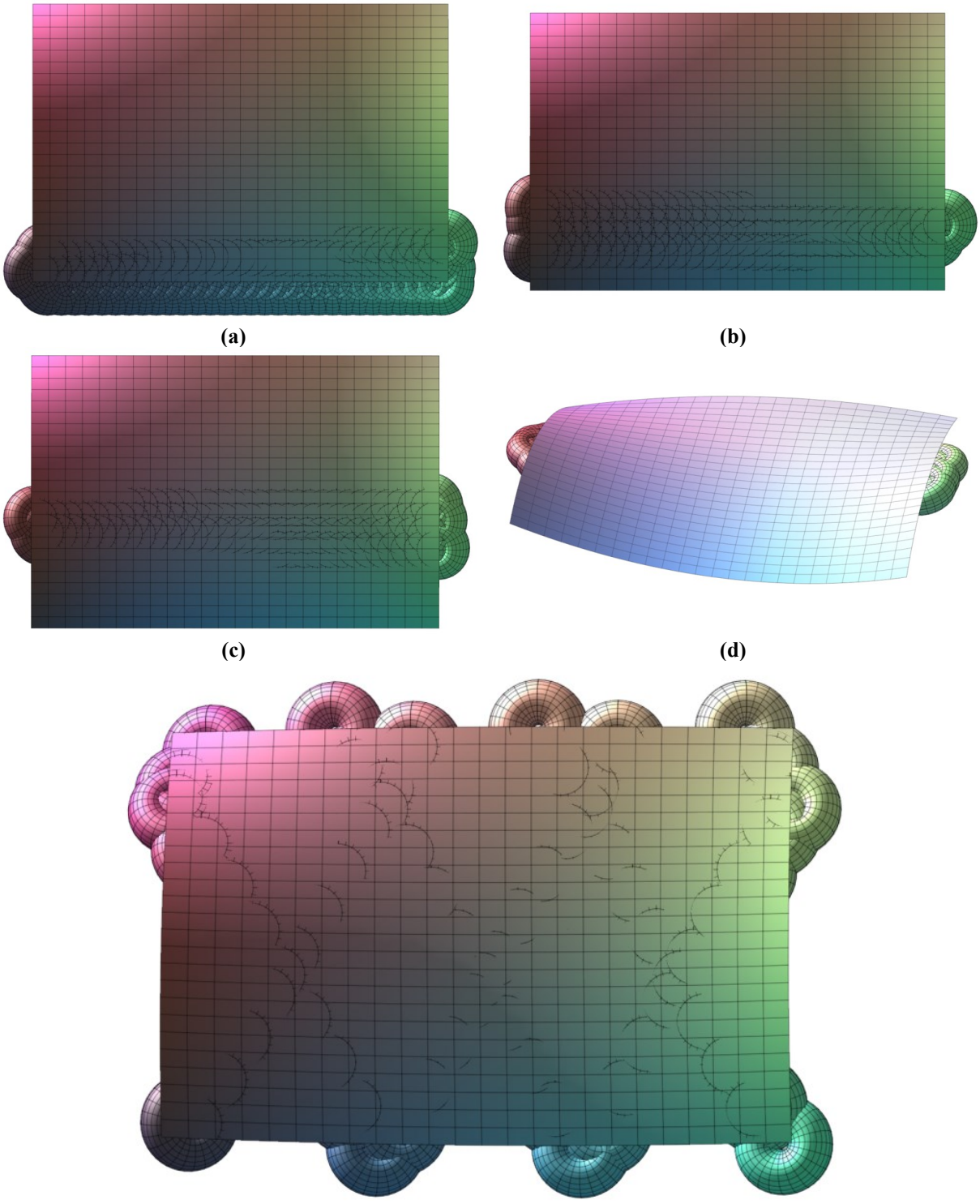

(a) **(b)** **(c)** **(d)** **(e)**

Figure 6.16 (a-e): 5-axis machining simulation of a Bezier surface in a custom Maple™ graphics simulator. The tool modelled as a torus is slightly visible from below the surface.

The edge-torus method presented in chapter 5, requires finding the roots of a degree 8 equation having 78 terms [65]. By appropriate change of basis, this equation can be simplified to a degree 4 equation having 28 terms; while much smaller than 78 terms, it is still a challenge to implement, although the coding task can be eased somewhat by using a symbolic algebra package such as Maple™ to generate the 28 terms.

Table 6.1: Average iterations before we get converged solution for the point P using the new edge-torus model and the Patel et al.[58] model for user specified tolerances for angle θ given by ε_θ (in radians) and non-dimensional parameter s given by ε_s.

ε_θ (in radians)	$\cos(\varepsilon_\theta)$ (shown here to indicate the level of accuracy achieved in cosine of ε_θ)	n_θ (average number of iterations before getting the final value of θ)	ε_s	n_s (average iterations before getting final value of s)
0.1	0.995	5	0.00001	24
0.01	0.99995	8	0.000001	27
0.001	0.9999995	10	0.0000001	30
0.0001	0.999999995	14	0.00000001	34
0.00001	0.99999999995	18	0.000000001	37
0.000001	0.9999999999995	21	0.0000000001	41
0.0000001	0.999999999999995	24	0.00000000001	44

In comparison, the new edge-torus tangency method proposed here is straightforward to implement without the use of a symbolic algebra package (as apparent from pseudo-code presented in figure 6.12). Since the method of Patel et al. [58], searches for a value of parameter s used to define a line between two end vertices (equivalent to parameter t in equation 6.20) and the proposed method searches for the value of θ, we used the error in D (the distance from P to the tool axis) to compare the number of iterations as both methods compute D based on either θ or s. On an edge of the pyramid test part shown in figure 6.1, the new method required two to three times fewer iterations than required by the method of Patel et al. [58] to achieve the same error in D. The detailed comparison of new edge-torus algorithm with the method of Patel et al. [58] in terms of number of iterations required before we get the desired level of accuracy in the value of θ and s is given table 6.1, where the comparison metrics used is precision achieved in the value of $\cos(\theta)$ compared to accuracy of parameter s. Furthermore, comparing Matlab implementations of both methods, the new edge-torus tangency method ran 33 % faster than the Patel et al. [58] method, with the root finding method dominating the run times of both methods.

Thus the new method of edge-torus tangency is faster and easier to implement than earlier methods. The edge-torus tangency computation was prototyped in Maple and Matlab, and integrated into a Visual C++ implementation of the drop-and-tilt method of the authors [65] for 5-axis tool positioning, which drops a toroidal tool onto a triangulated surface with multiple points of contacts. The 3-axis and 5-axis toolpaths generated by this Visual C++ implementation was used to verify the developed technique, which proved the accuracy and efficiency of the method.

CHAPTER 7
CONCLUSIONS AND FUTURE SCOPE

7.1 CONCLUSIONS

The work presented in this thesis work focused on multipoint 5-axis tool positioning for machining of sculptured surfaces. Most methods formulated the 5-axis tool positioning problem as a multi-dimensional optimization, in which two rotations and the vector position are determined in one step. This perspective complicates the math model and made multipoint methods unusable for industry. To use MPM in industry we proposed three innovations. First idea was to simplify the computational complexity of sculptured surfaces by taking it in triangulated format. Though triangulated data in STL data format is quite popular and is used for many manufacturing activities, its use in 5-axis toolpath planning is rare. The second innovation was to divide the tool positioning in two steps. The tool is dropped and subsequently rotated. This simplified the mathematical formulations greatly and lead to development of a method that could be implemented in Visual C++ and thus can be used for 5-axis toolpath planning for larger parts as are found in industry. The details of the developed 5-axis tool positioning method are given in chapter 4 and 5. Thirdly, we introduced a simpler way of finding edge-torus tangency, thereby speeding the computations of multipoint toolpath algorithm as detailed in chapter 6.

The multipoint 5-axis tool positioning approach named as “Drop and Tilt Method” or DTM was developed for machining of triangulated models and was implemented in Maple^{TM} to test the accuracy of the proposed mathematical model. The details of the mathematical procedure and the test results are presented in chapter 3. It was found that the developed DTM method in its original form is quite complicated and as such it is not suitable for implementation as a standalone application. Thus another approach called numerical DTM was developed to solve the problem of computational complexity as well as to enhance the computational efficiency of 5-axis tool positioning. The numerical DTM used the concept of tool rotation about pseudo-insert axis taken from DTM method and implemented in conjunction with a generalized tool drop method within a Bisection algorithm for finding the 5-axis tool positioning for triangulated models. The detailed procedure for generalized tool drop algorithm is presented in chapter 4, whereas in chapter 5 the detailed procedure evolved for numerical DTM method is explained along with the details of its testing and validation.

While implementing the 5-axis tool positioning for triangulated surfaces it is found that the most intricate component of tool positioning using DTM method was the tool positioning over the edges of the triangulated facets. Thus the various methods developed for positioning a radiused end mill over the edges of the triangulated/STL surfaces were examined and some of them were implemented to check accuracy as well as efficiency. A need was felt at this point to find a new method for edge-torus tangency which can enhance the overall computational efficiency of the 5-axis tool positioning algorithm. The new method for edge-torus tangency was developed which is found better compared to the other available methods. The details of the mathematical procedure along with the testing validation of the new edge-torus algorithm for 3-axis and 5-axis tool positioning are presented in chapter 6.

Following conclusions are drawn from the present work on tool positioning for 5-axis machining of faceted surfaces using generalized radiused end mill:

1. The methods available for determining the gouge free NC toolpath data for 3-axis and 5-axis surface machining using radiused end mill cutter are quite complicated and computationally expensive. The use of higher order algebraic, parametric or composite parametric surface representation for complex/sculptured surfaces models further adds to the complexity to determine the cutter contact point (CC) for 3-axis machining and cutter contact point & orientation for 5-axis machining.
2. The complex sculptured surface whether represented by algebraic, parametric or composite parametric model can be easily converted into STL/ faceted/ triangulated data format to user specified accuracy. Faceted surface representation can be conveniently used to reduce the computational complexity for determining the gouge-free cutter contact point for a generalized radiused end mill for 3-axis machining by using the tool drop approach.
3. The concept of tool drop approach used in 3-axis NC toolpath positioning has been extended successfully in this work to determine gouge-free and accurate tool orientation for 5-axis machining of faceted surface models using a new multipoint machining methodology. The developed approach has been termed as Drop and Tilt Method (DTM). The analytical DTM algorithm uses the concept of tool rotation about the axis through the center of pseudo-insert at the first point of contact (between radiused end mill cutter and faceted surface) to determine the gouge-free 5-axis tool orientation. Several examples

have been used to prove the accuracy, reliability and repeatability of the DTM concept and are published in Duvedi et al.[63].

4. The only drawback of the analytical DTM approach is that it needs solution of higher order mathematical equations to determine the gouge-free multipoint tool position for 5-axis machining. Use of commercial solvers like Maple^{TM} takes significantly longer time to solve for each tool-position. Thus, the concept developed for 5-axis tool positioning was enhanced for numerical implementation in Visual C++ environment. The developed numerical approach for 5-axis tool positioning is independent of toolpath data and machine kinematics. Hence, the developed algorithm can be conveniently used with any suitable toolpath strategy and all kinds of 5-axis machine tools irrespective of the machine kinematics.
5. The generalized 3-axis tool drop algorithm is used as the basis for developing analytical DTM approach and subsequently numerical implementation of DTM approach for 5-axis NC tool positioning. The 3-axis tool positioning algorithm is used to determine the gouge-free first point of contact between radiused end mill tool and faceted surface, which is further used to determine the gouge free second cutter contact point and hence the tool orientation for 5-axis tool positioning.
6. The DTM method helps achieve the best proximity of tool to the machined surface. The two contact points define a strip that lies very close to the desired surface. If the strip meets the tolerance requirements than the side step for the next pass is larger than the width of the strip. The larger side step results in fewer passes to machine the whole surface.
7. The developed methods were verified using custom NC simulators and with machined samples. Both methods produced identical results and helped prove the viability of the techniques in machining complex curved parts.
8. While developing the numerical technique for implementing DTM it was discovered that the edge-torus tangency problem resulted in a higher order equation that was challenging to solve. To address this, a new method was developed to determine the point of contact between edge of the triangulated surface and the toroidal tool. The new method has added to the efficiency of the developed DTM algorithm. The developed edge-torus tangency method is faster as compared to the previously available methods Duvedi et al. [69]. This is especially advantageous as the number of edges to be evaluated in a convex region is almost three times as compared to the number of facets to be tested and it further ensures smooth motion of tool when it traverses over an edge of the faceted surface.

9. Toolpaths have been generated for a wide variety of parts. The pyramid part shows the smooth transition of motion of the radiused end mill cutter from one CL point to next CL point in 5-axis machining. Moreover the tool motion over the edges and the vertices is also very smooth owing to the accurate computation of tool location and orientation. The Bezier surface shows that the method can handle complex surfaces with large number of triangles and with a mixed topology of convex and concave sections.
10. The spherical part is machined using a circular contour offset toolpath strategy [65], while the other parts are machined using the zig-zag toolpaths [63, 65-67, 69]. Thus the developed NC tool positioning algorithm developed for 3-axis and 5-axis machining is computationally simpler, accurate and faster for determining the gouge free NC tool positioning. The global and local tool-work piece interference checking is also included in the algorithm.

7.2 FUTURE SCOPE

The work on 5-axis tool positioning for triangulated model can be expanded considering the following aspects.

1. Error estimation and computation of side step and feed forward step for user defined surface error values can be incorporated to minimize the machining time. Thus a multi-objective optimization for reducing the scallops and maximizing the side step values/ cut width and feed forward steps can be carried out.
2. Determination of 5-axis tilt angle and determination of best angle of tool rotation towards the faceted part to maximize the tool proximity to the fated surface can be done.
3. An effective method for path smoothening to generate the jerk free NC toolpath data for 5-axis machining can be developed and used with this algorithm.
4. An effective method to avoid the multiple testing of the edges and the vertices while dropping the tool in generalized 3-axis tool positioning can be implemented to improve further the efficiency of the developed DTM approach.
5. The faceted part surfaces can have totally random orientation of the triangulated facets and the areas of the triangulated facets used to approximate the various part models that can be single surface patch, multiple surface patches with C_o, C_1 or higher surface continuities. In the verification of the proposed model the tool can very effectively move between convex, concave facet orientations.
6. This method is totally independent of the surface continuity of the original surface to generate the 5-axis NC toolpath data. This aspect can be investigated in future studies.

APPENDIX – A

POINT OF CONTACT OF RADIUSED END MILL WITH A TRIANGULAR FACET

A triangular facet can have three possible orientations with respect to tool axis, which can be defined using the orientation of the surface normal of facet with respect to the tool axis. In case when surface normal of facet is perpendicular to the tool axis, the algorithm proceeds to analyze the three edges and the three vertices of such a facet in order to determine the first point of contact. Thus the triangular facets which are analyzed under triangle check are triangular facet with surface normal parallel and inclined to tool axis.

A.1 Point of contact with a triangular facet normal to tool axis

A triangular facet $\Delta P_1P_2P_3$ in tool shadow, having its unit surface normal $\hat{n}$ parallel to the tool axis $\hat{t}_l$, such that $\hat{n} \times \hat{t}_l = 0$, will touch the flat bottom of a radiused end mill tool only if the tool axis lies inside the boundary of such a facet (as shown in figure A.1(a)) or when the shortest distance of at least one of the vertices of this facet from the tool axis is less than equal to R_o (as shown in figure A.1(b)). Thus these facets will have to be subjected to two tests before proceeding to determine the tool location data. If the facet under consideration does not pass any of these two tests then we proceed to test the edges of such facet.

To determine whether the tool axis passes through the boundary of the facet or not, we first determine a point T_{bc} which represents the center of circular bottom surface of radiused end mill when the tool bottom rests on a facet perpendicular to tool axis. As shown in figure A.1(a), the point T_{bc} is given as:

$$T_{bc} = T_1 + \{(P_1 - T_1).\hat{t}_l\}.\hat{t}_l \qquad \text{A.1}$$

The point T_{bc} should satisfy the following equation if it lies inside the triangular facet $\Delta P_1P_2P_3$:

$$T_{bc} = P_1 + s.(P_2 - P_1) + t.(P_3 - P_1) \qquad \text{A.2}$$

If the location of T_{bc} satisfies the constraint on the scalars s, t such that $0 \leq s, t \leq 1$, and $0 \leq s + t \leq 1$, then the tool axis passes through the triangular facet and we can proceed further to find the tool center.

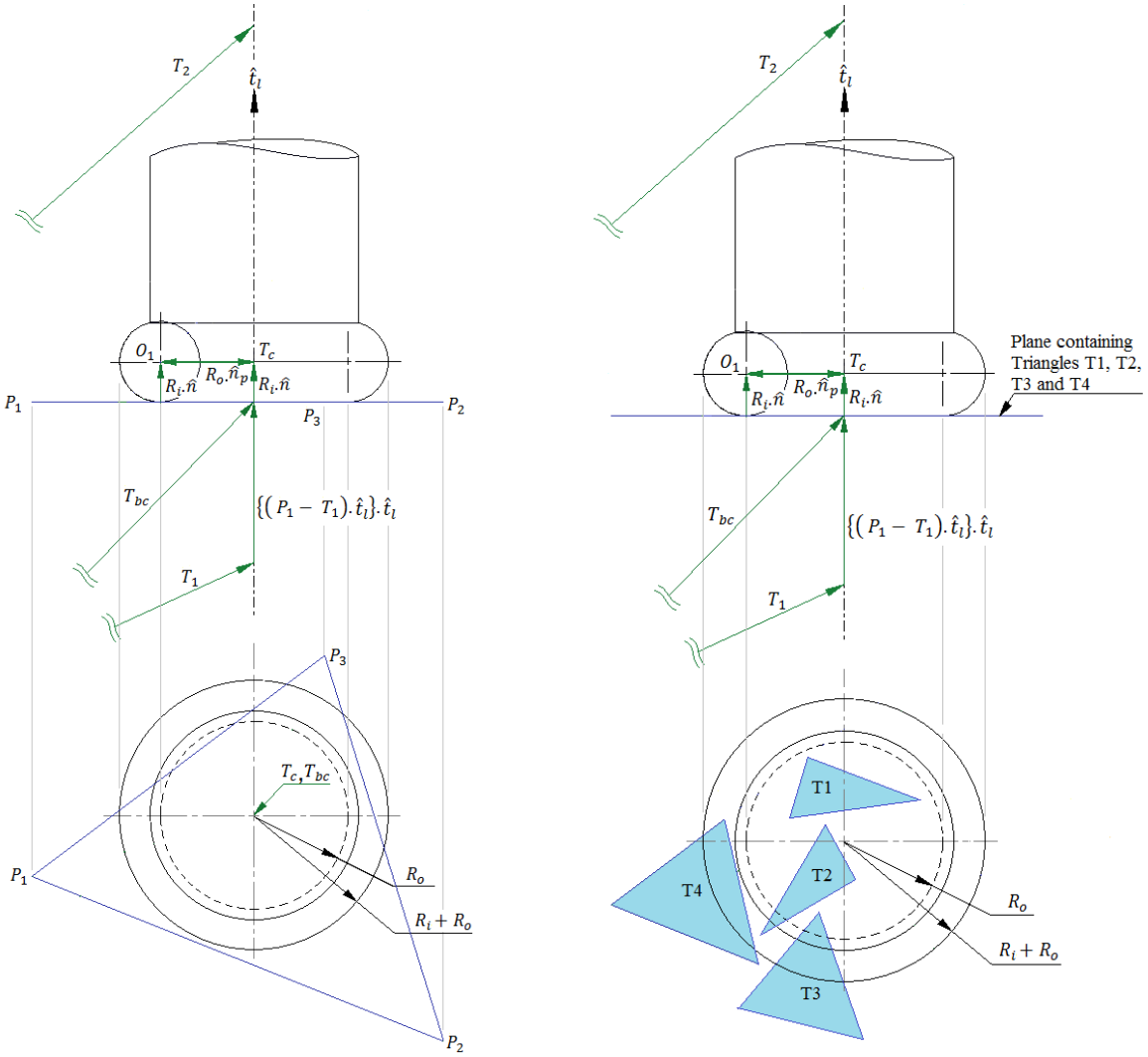

Figure A.1: Facet with surface normal parallel to tool axis: (a) when tool axis lies inside the boundary of triangular facet, and (b) when facets under tool shadow but positioned away from tool axis

For certain smaller triangular facets touching the flat bottom of radiused end mill, the tool axis may not pass through the facet boundary. As shown in figure A.1(b), the facets marked as T1, T2, and T3 are contained in a plane perpendicular to tool axis, which has three, two and one vertex respectively touching the flat bottom of toroidal tool. Such facets has to be considered to find the location of tool center in tool drop algorithm, whereas the facet T4 can be avoided for triangle check as all its vertices are placed away from flat bottom of radiused end milling tool, and such facets will be analyzed in edge or the vertex check cases.

Thus, if $|T_{bc} - P_1| \leq R_o$, or $|T_{bc} - P_2| \leq R_o$, or $|T_{bc} - P_3| \leq R_o$, the algorithm considers the facet to compute the tool center location.

If any of the above two conditions, whether tool axis lying inside the boundary of the triangular facet or at least one of the vertex of the facet is under flat bottom of tool, then the

location for tool center T_c can be determined from the projection of any one of vertex of the facet on tool axis as given below:

$$T_c = T_1 + \{(P_1 - T_1).\hat{t}_l\}.\hat{t}_l + R_i.\hat{n}$$

Because, in the present case the unit surface normal $\hat{n}$ is parallel to $\hat{t}_l$, thus the above equation is rewritten as:

Or, $$T_c = T_1 + \{(P_1 - T_1).\hat{t}_l + R_i\}.\hat{t}_l \quad \text{A.3}$$

The tool center location can also be expressed as:

$$T_c = T_1 + h.(T_2 - T_1) \text{ , where } 0 \leq h \leq 1 \quad \text{A.4}$$

Using equations A.3 and A.4, the parameter h can be we expressed as:

$$h = |\{(P_1 - T_1).\hat{t}_l + R_i\}.\hat{t}_l|/|(T_2 - T_1)|$$

If h lies between 0 and 1, it is a valid solution for the tool center in 3-axis tool drop found from a facet normal to tool axis. Further the value of parameter h is compared to evaluate the highest location of the tool center to determine the gouge free tool location from all facets under tool shadow.

The facets which are orthogonal to the tool axis and which satisfy the above two criteria have a surface contact with the bottom of toroidal tool. It is always better to have the maximum surface contact of tool with the required machined surface to get the best surface finish and highest material removal rate. Thus if the highest value of tool center in tool drop is obtained from a facet perpendicular to tool axis, such cases are not considered for tool axis rotation in 5-axis tool positioning algorithm. While, for 3-axis tool positioning the location of highest tool center point T_c is sufficient.

A.2 Point of contact with a triangular facet inclined to tool axis

When $\hat{n}.\hat{t}_l \neq 0$ and $\hat{n} \times \hat{t}_l \neq 0$, the triangular facet $\Delta P_1P_2P_3$ having unit surface normal $\hat{n}$ is inclined to the tool axis $\hat{t}_l$. When dropped along $\hat{t}_l$ from point T_2 towards T_1, the toroidal tool will touch at the plane of triangulated facet at a unique point P. This point of contact with inclined triangular facet is accepted as valid if and only if it lies within the bounds of the facet, as shown in figures A.2. In this case the tool center location T_c is given by equation A.4.

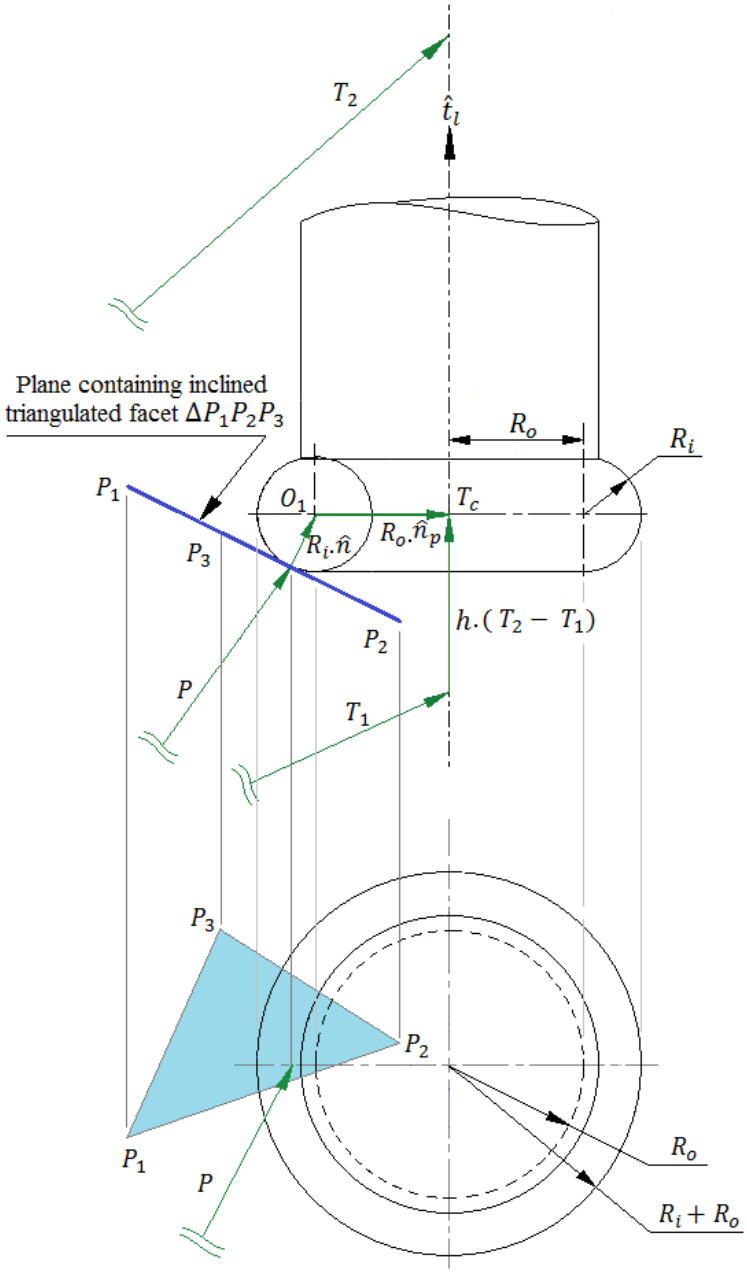

Figure A.2: Point of contact of toroidal tool with an inclined triangular facet

Further, the location of center of radiused end mill T_c can also be determined as:

$$T_c = P + R_i.\hat{n} + R_o.\hat{n}_p \qquad \text{A.5}$$

where, P is a point on the plane of the triangular facet, given by:

$$P = P_1 + s.(P_2 - P_1) + t.(P_3 - P_1)\,, \qquad \text{A.6}$$

such that $0 \leq s, t \leq 1$ and $\hat{n}_p$ is the projection of surface normal $\hat{n}$ in a plane perpendicular to tool axis $\hat{t}_l$, given by:

$$\hat{n}_p = \frac{\hat{n} - \hat{t}_l \cdot (\hat{n} \cdot \hat{t}_l)}{|\hat{n} - \hat{t}_l \cdot (\hat{n} \cdot \hat{t}_l)|}$$

The equations A.4, A.5 and A.6 can be combined as:

$$T_1 + h.(T_2 - T_1) = P_1 + s.(P_2 - P_1) + t.(P_3 - P_1) + R_i.\hat{n} + R_o.\hat{n}_p \quad \text{A.7}$$

The linear simultaneous equation A.7 can be solved for h, s and t. If value of h, s and t lie between 0 and 1, along with another constraint that $0 \leq s + t \leq 1$ then the point of contact is a valid solution. Using values of h, s and t in equation A.4 and A.6, the tool center location T_c and first point of contact P can be determined.

If a valid point of contact is found from the present facet then the edges and vertices of the facet are not evaluated, and next facet from list of facets under tool shadow is selected for finding the tool contact with it. This process is repeated until all triangles in tool shadow are processed. The highest of all estimated point of contacts is retained as the gouge free point of contact.

In case the valid point of contact is determined from the planer triangle, the values of the parameters namely T_1, T_2, $\hat{n}, \hat{n}_p, P$, h, T_c, and O_1 are passed to the 5-axis numerical DTM algorithm (see section 5.2). The location of center of pseudo-insert O_1 as shown in figure A.2 is determined as:

$$O_1 = P + R_i.\hat{n} \quad \text{A.8}$$

In tool drop algorithm, if the valid point of contact is not obtained from a facet, then the three edges of the facet are analyzed followed by the examination of three vertices of the triangular facet to ensure the error free determination of highest valid point of contact between tool and triangulated surface. The stepwise procedure used to determine the point of contact from the edges and vertices is explained in the appendix B and C respectively.

APPENDIX – B
POINT OF CONTACT OF A RADIUSED END MILL WITH AN EDGE

The edges which are not parallel to tool axis $\hat{t}_l$ and are located from tool axis such that $D_e \leq R_i + R_o$, are the only candidate edges that need to be analyzed to determine the valid point of contact between them and the dropping tool (see section 4.2.2). Else, testing an edge can be skipped.

For all edges which satisfies the above said two criteria, we check whether the edge is positioned normal to tool axis or not. An edge is normal to tool axis if $(P_2 - P_1).\hat{t}_l = 0$ and depending upon its shortest distance from tool axis such an edge can touch the flat bottom of tool or the radiused corner of the tool. As discussed in section 4.2.2, to determine the solution for tool drop as well as 5-axis tool positioning for edges perpendicular to tool axis, these edges are classified into two separate categories based on its shortest distance from tool axis: edges with $0 \leq D_e \leq R_o$ and edges with $R_o < D_e \leq R_i + R_o$.

The edges for which $0 < (P_2 - P_1).\hat{t}_l < 1$, are classified as edges inclined to tool axis. The line containing such edges will always touch the radiused corner of the toroidal tool if the shortest distance $D_e \leq R_i + R_o$. But for such edges, the point of contact is considered as valid if it lies within the vertices bounding the edge under consideration.

The mathematical model used to determine the location of tool center and unique point of contact for edges normal to tool axis and inclined to tool axis are explained in following sub sections:

B.1 Point of contact with an edge normal to tool axis, with $0 \leq D_e \leq R_o$

These edges can be imagined as the boundary edges of the various triangles which are normal to tool axis, shown in figure A.1 in annexure A, and satisfy the criteria that $0 \leq D_e \leq R_o$.

For such an edge, touching the flat bottom of radiused end mill tool, the location for tool center T_c, with respect to reference point on tool footprint T_1 can be determined from the projection of any one of its vertex taken on the tool axis, as given below:

$T_c = T_1 + h.(T_2 - T_1)$, where $0 \leq h \leq 1$ B.1

The parametric height of tool center h can be found as given below:

$$h = |(P_1 - T_1).\hat{t}_l + R_i|/|(T_2 - T_1)| \quad \text{B.2}$$

If value of h lies between 0 and 1, then T_c represents a valid solution for the tool center with respect to an edge which is normal to tool axis.

If the highest value of tool center is found form such an edge perpendicular to tool axis, then the edge has a line contact with the flat bottom of tool. Though these cases are not considered in numerical DTM implementation to find the 5-axis tool rotation, but they are required for accurate implementation of tool drop algorithm to obtain the gouge free 5-axis tool positions and orientations.

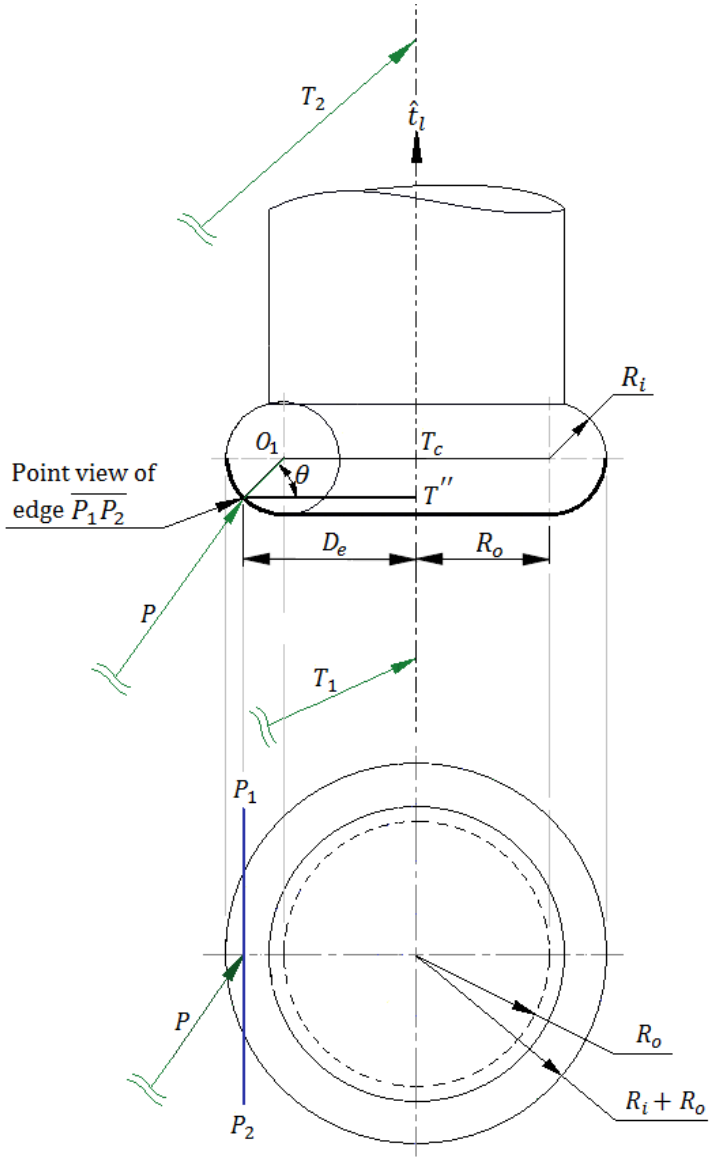

Figure B.1: Point of contact with an edge $\overline{P_1P_2}$ normal to tool axis when $R_o < D_e \leq R_i + R_o$

B.2 Point of contact with an edge normal to tool axis, with $R_o < D_e \leq R_i + R_o$

These edges can also be considered as if contained in a plane perpendicular to the tool axis, especially similar to as an edge of triangulated facet T4 shown in figure A.1(b) in annexure A, which satisfy the criteria that $R_o < D_e \leq R_i + R_o$. Such edges will touch the radiused corner of the radiused tool at a point P, which can be determined as discussed below:

As shown in figure B.1, the location for point of contact P, tool center T_c and a point showing the projection of P on tool axis at T'' can be determined as given below:

$$P = P_1 + s.(P_2 - P_1) \quad \text{B.3}$$

$$T'' = T_1 + h''.(T_2 - T_1) \quad \text{B.4}$$

Where, $(0 \leq s, h'' \leq 1)$

The parameter h'' can be calculated as given below:

$$h'' = |(P_1 - T_1).\hat{t}_l|/|(T_2 - T_1)| \quad \text{B.5}$$

The shortest distance D_e between edge $\overline{P_1P_2}$ and tool axis $\hat{t}_l$ is already known. Thus we can solve the following equation to get the exact value of s:

$$|T'' - P| = D_e \quad \text{B.6}$$

If the value of s and h'' satisfied the criteria that $0 \leq s, h'' \leq 1$, then a valid point of contact exists between tool and the edge under consideration. Therefore, the value of other parameters like $\hat{n}_p$, and θ can be determined as:

$$\hat{n}_p = (T'' - P)/|T'' - P| \quad \text{B.7}$$

$\theta = \cos^{-1}\{(D_e - R_o)/R_i\}$, with a condition that $(0° < \theta < 90°)$ B.8

Thus the value of T_c is obtained as:

$$T_c = T'' + (R_i \sin\theta).\hat{t}_l \quad \text{B.9}$$

The parameter h is required to evaluate the highest location of tool center to determine the gouge free tool location from all facets under tool shadow, and is found as:

$$h = h'' + (R_i \sin\theta)/|(T_2 - T_1)| \quad \text{B.10}$$

If value of h determined from above equation satisfies the criteria that $0 \leq h \leq 1$, the point of contact and tool center locations are considered valid. Thus the center of center of pseudo-insert O_1, and the unit surface normal $\hat{n}$ through P and O_1 are determined as:

$$O_1 = T_c - R_o.\hat{n}_p \quad \text{B.11}$$

$$\hat{n} = (O_1 - P)/|O_1 - P| \quad \text{B.12}$$

As such edges will have a point of contact on radiused corner of the tool, thus the values of variables $T_1, T_2, \hat{n}, \hat{n}_p, P, h, T_c$ and O_1, determined from above equations, are passed for 5-axis algorithm (see section 5.2) to determine the multipoint tool orientation.

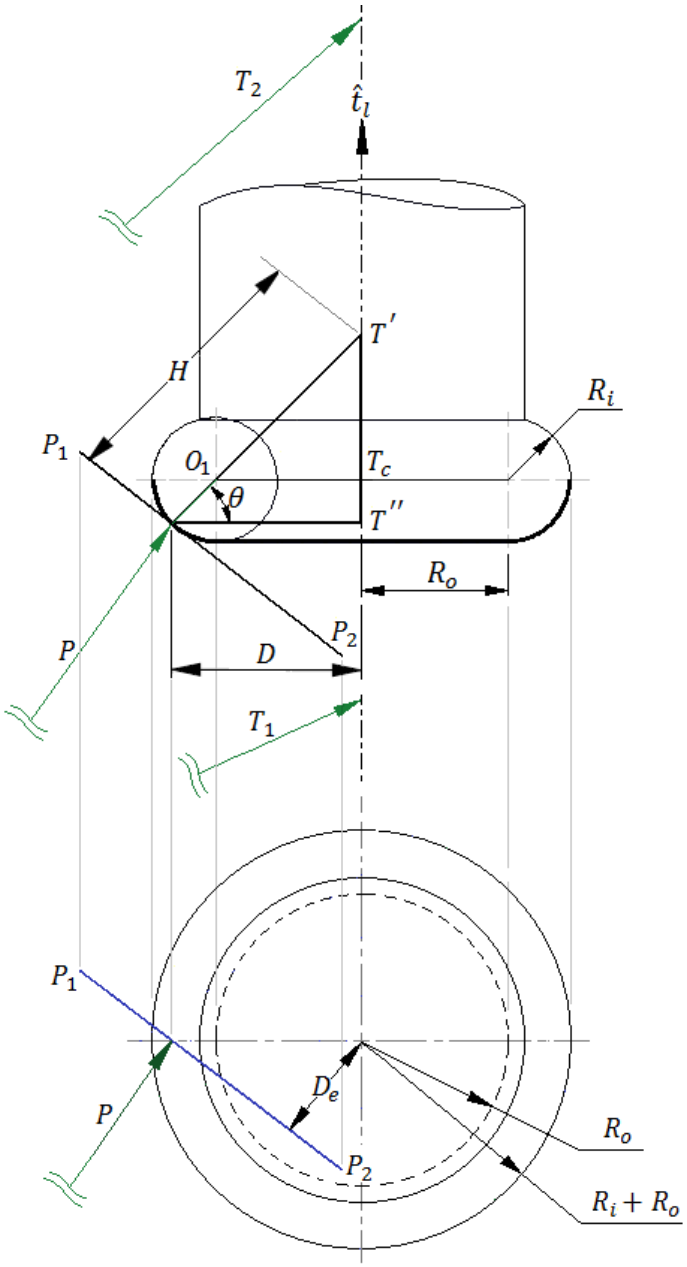

Figure B.2: Point of contact of radiused end mill with an edge $\overline{P_1P_2}$ inclined to tool axis

B.3 Point of contact with an edge inclined to tool axis, with $0 \leq D_e \leq R_i + R_o$

A toroidal tool descending on an edge $\overline{P_1P_2}$ which is neither parallel nor perpendicular to the tool axis $\hat{t}_l$, will touch the radiused corner of the tool tangentially if and only if its shortest distance D_e from the tool axis is such that $0 \leq D_e \leq R_i + R_o$.

To determine the point of contact, let T_1 represent the reference point on tool footprint and T_2 be another point on default tool axis $\hat{t}_l$ passing through T_1 as shown in figure B.2. The variables T_c, T' and T'', as shown in figure B.2, are used to compute the point of contact P between tool and inclined edge $\overline{P_1P_2}$. The point T_c represent the tool center location when descending toroidal tool touches the edge at P. The point T' lie on tool axis such that $(T' - P)$ is a line passing through the center of pseudo-insert O_1 through the point of contact at P. Also T'' is a point on tool axis such that $(T'' - P)$ is a line normal to tool axis $\hat{t}_l$ as shown in figure B.2. Thus, the point of contact P, tool center T_c, points T' and T'' can be expressed as:

$$P = P_1 + s.(P_2 - P_1)$$
$$T_c = T_1 + h.(T_2 - T_1)$$
$$T' = T_1 + h'.(T_2 - T_1)$$
$$T'' = T_1 + h''.(T_2 - T_1)$$

Where, $(0 \leq s, h, h', h'' \leq 1)$. These conditions ensure that the point of contact between tool and triangulated surface on an inclined edge lies on the segment $\overline{P_1P_2}$. For further analysis, the following equations can be derived:

$$(T' - P) \cdot (P_2 - P_1) = 0 \qquad \text{B.13}$$
$$(T'' - P) \cdot (T_2 - T_1) = 0 \qquad \text{B.14}$$

Using the expansions of P, T_c, T' and T'', the equation B.13 and B.14 can be rewritten as:

$$(h'.\vec{A}_1 - s.\vec{A}_2 + \vec{A}_3).\vec{A}_2 = 0$$
$$(h''.\vec{A}_1 - s.\vec{A}_2 + \vec{A}_3).\vec{A}_1 = 0$$

Or,

$h' = a_0.s + a_1$ B.15

$h'' = a_2.s + a_3$ B.16

where; $a_0 = \frac{\vec{A}_2 \,.\, \vec{A}_2}{\vec{A}_1 \,.\, \vec{A}_2}$, $a_1 = -\frac{\vec{A}_2 \,.\, \vec{A}_3}{\vec{A}_1 \,.\, \vec{A}_2}$, $a_2 = \frac{\vec{A}_1 \,.\, \vec{A}_2}{\vec{A}_1 \,.\, \vec{A}_1}$, and $a_3 = \frac{\vec{A}_1 \,.\, \vec{A}_3}{\vec{A}_1 \,.\, \vec{A}_1}$

with $\vec{A}_1 = (T_2 - T_1)$, $\vec{A}_2 = (P_2 - P_1)$ and $\vec{A}_3 = (T_1 - P_1)$

Let, D is the shortest distance between point of contact on radiused end mill and tool axis as shown in figure B.2, and is give as:

$D = |T'' - P|$

and,

$D^2 = a_4.s^2 + a_5.s + a_6$ B.17

where, $a_4 = (\vec{A}_5.\vec{A}_5)$, $a_5 = 2.(\vec{A}_4.\vec{A}_5)$, $a_6 = (\vec{A}_4.\vec{A}_4)$

with, $\vec{A}_4 = (\vec{A}_3 + a_3.\vec{A}_1)$ and $\vec{A}_5 = (a_2.\vec{A}_1 - \vec{A}_2)$

Similarly, the variable H shown in figure B.2 can be determined as:

$H = |T' - P|$

and,

$H^2 = a_7.s^2 + a_8.s + a_9$ B.18

where, $a_7 = (\vec{A}_7.\vec{A}_7)$, $a_8 = 2.(\vec{A}_6.\vec{A}_7)$, $a_9 = (\vec{A}_6.\vec{A}_6)$

with, $\vec{A}_6 = (\vec{A}_3 + a_1.\vec{A}_1)$ and $\vec{A}_7 = (a_0.\vec{A}_1 - \vec{A}_2)$

Since D is the distance of point P on the surface of the radiused tool from axis of the tool having radius of insert R_i and offset radius measured from insert center up to tool axis is R_o, then as shown in figure B.2 the value of D is also given by:

$D = (R_i \cos\theta + R_o)$ B.19

Also from figure B.2, we can write as:

$$\cos\theta = D/H \quad \text{B.20}$$

Combining equation B.19 and B.20, we get:

$$D = R_i \frac{D}{H} + R_o$$

or,

$$DH = R_i D + R_o H \quad \text{B.21}$$

Squaring both sides of equation B.21, and rearranging the terms we get:

$$2R_i R_o DH = D^2H^2 - {R_i}^2D^2 - {R_o}^2H^2 \quad \text{B.22}$$

Squaring equation B.22 again, and rearranging the similar terms, gives:

$$D^4(H^4 + {R_i}^4 - 2{R_i}^2H^2) + H^4({R_o}^4 - 2{R_o}^2D^2) - 2{R_i}^2{R_o}^2D^2H^2 = 0 \quad \text{B.23}$$

Substituting equations B.17 and B.18 for D^2 and H^2 respectively gives us an 8th order equation in terms of parameter s. The C code for finding the roots of the 8th order equation in s is developed using Maple™ symbolic algebra package, and implemented in the overall program code of the tool drop algorithm and hence in the 5-axis numerical DTM code.

If the solution obtained for parameter s is such that $0 \leq s \leq 1$, then it is accepted as valid point of contact, else it is discarded and the tool drop algorithm proceed for finding solution from other edges of triangulated facet. From the valid value of parameter s the parameters h', h'' and point P can be determined. Hence the location of reference point T' and T'' on tool axis, and the location of tool center T_c can also be determined.

The location of tool center T_c can be used to determine the tool height parameter h, which is given as:

$$h = |T_c - T_1|/|T_2 - T_1| \quad \text{B.24}$$

If the solution for highest location of tool center T_c is obtained from an inclined edge, compared to all facets or edges or vertices in tool shadow, then the location of the point of contact P is obtained between the inclined edge and the radiused corner of the tool. Thus we

can implement the concept of tool rotation about the pseudo-insert axis to find the 5-axis tool positioning using numerical implementation of DTM.

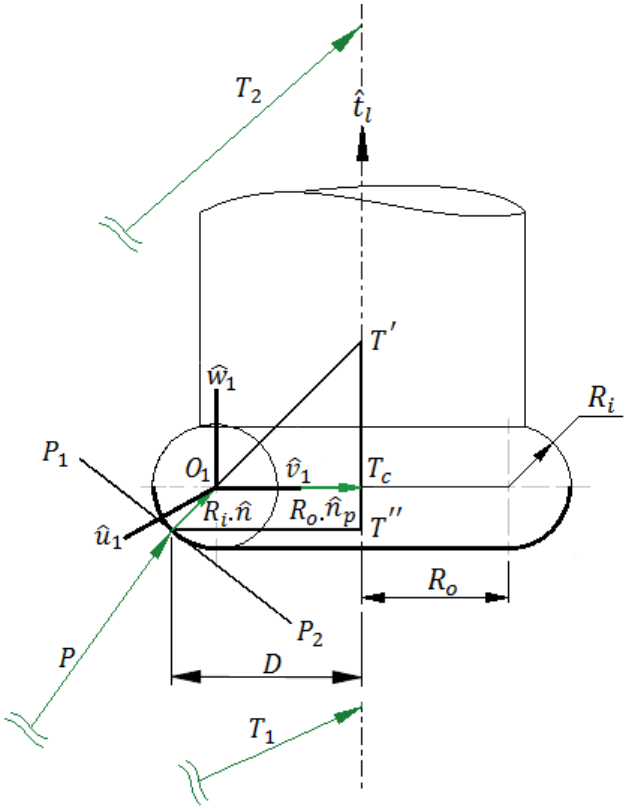

Figure B.3: Surface normal and center of pseudo-insert for inclined edge $\overline{P_1P_2}$ touching radiused end mill

The location of center of pseudo-insert O_1 through first point of contact P on the inclined edge can be determined as shown in figure B.3, and is given as:

$$O_1 = P + R_i.\hat{n} \quad \text{B.25}$$

Where, $\hat{n} = (T' - P)/|T' - P|$ B.26

Also, $\hat{n}_p = (T'' - P)/|T'' - P|$ B.27

Thus the values of variables T_1, T_2, $\hat{n}$, $\hat{n}_p, P, h, T_c$ and O_1determined from a valid inclined edge are passed as input to numerical DTM method to determine the 5-axis tool positioning and orientations (given in section 5.2).

APPENDIX – C

POINT OF CONTACT OF A RADIUSED END MILL WITH A VERTEX

A vertex P will touch the descending toroidal cutter along tool axis $\hat{t}_l$ only when its shortest distance D_v from tool axis is such that $0 \leq D_v \leq R_i + R_o$ (see section 4.2.3,). Thus the vertices which do not satisfy this condition are not analyzed. Depending upon the value of shortest distance of vertex from tool axis it can touch the tool at the radiused cutting edge of the tool or at the circular flat bottom of the tool as discussed earlier in section 4.2.3. If the location of tool center determined with respect to a vertex is highest compared to other facets or edges or vertices lying under tool shadow, then for given toolpath footprint location the current vertex is the valid point of contact between tool and the triangulated/STL surface. The location of tool center T_c with respect to a vertex can be determined as given below:

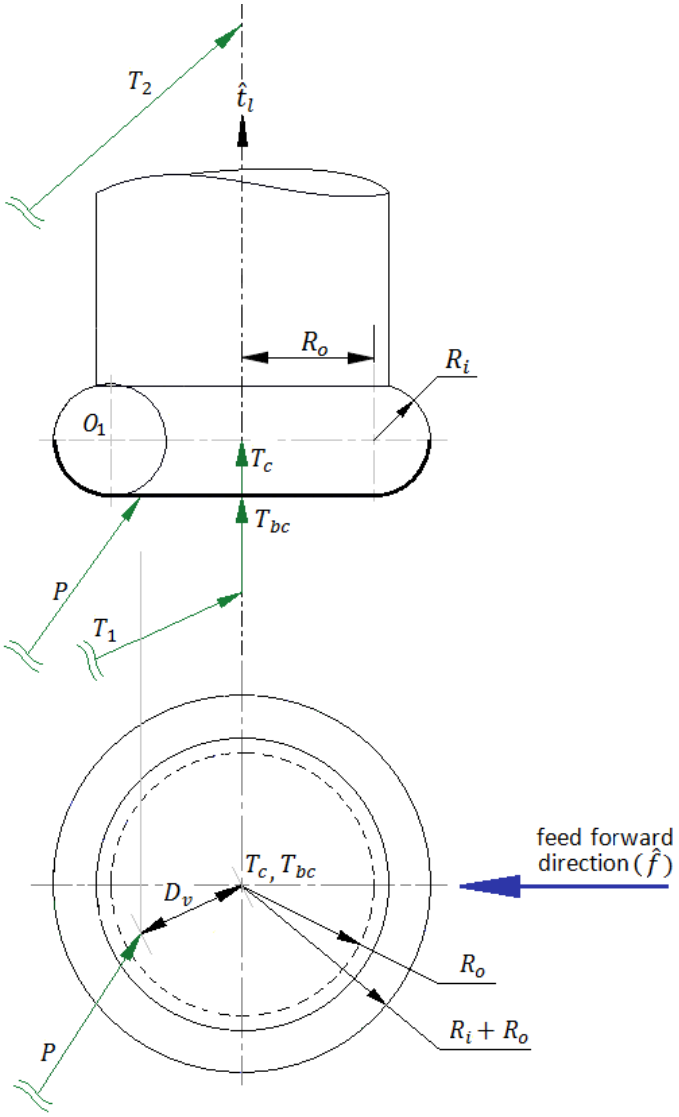

Figure C.1: Vertex touching flat bottom of tool at distance D_v from tool axis $\hat{t}_l$

C.1 Point of contact with a vertex when $0 \leq D_v \leq R_o$

This case is shown in figure C.1, where a vertex P touches the flat bottom of tool. In this case the tool center location is found as:

$$T_c = T_1 + h.(T_2 - T_1) \quad \text{C.1}$$

where, $(0 \leq h \leq 1)$, and for a given vertex P the value for h is determined as:

$$h = \{(P - T_1).\hat{t}_l + R_i\}/|(T_2 - T_1)| \quad \text{C.2}$$

If value of h lies between 0 and 1 then it is a valid solution for the tool center in tool drop with respect to a vertex lying under tool shadow.

Also, the location of tool bottom center T_{bc} is determined as given below:

$$T_{bc} = T_1 + \{(P_1 - T_1).\hat{t}_l\}.\hat{t}_l \quad \text{C.3}$$

These vertices touch the flat circular bottom of radiused end mill. Thus, even though the highest tool center location may be obtained from such vertices, they are not used as the first point of contact for finding the 5-axis tool rotation using numerical DTM method. For effective 5-axis toolpath planning for triangulated surfaces such raised vertices cannot be avoided, thus for 5-axis tool positioning in such cases the tool axis is not rotated. However, this analysis is used in tool drop algorithm for determining the gouge free tool positions for 3-axis and 5-axis numerical DTM algorithm (within a Bisection algorithm).

C.2 Point of contact with a vertex when $R_o < D_v \leq R_i + R_o$

A vertex P will touch at the radiused corner of a dropping toroidal tool along tool axis $\hat{t}_l$, when the vertex is located with respect to tool axis so that $R_o < D_v \leq R_i + R_o$. Such a case is shown in figure C.2. In this case, the location of tool center T_c and a vector on tool axis T'' are determined as:

$$T_c = T_1 + h.(T_2 - T_1) \quad \text{C.4}$$

$$T'' = T_1 + h''.(T_2 - T_1) \quad \text{C.5}$$

where, $(0 \leq h, h'' \leq 1)$, and the values of h and h'' are determined as given below:

$$h = \{(P - T_1).\hat{t}_l + R_i.\sin\theta\}/|(T_2 - T_1)| \quad \text{C.6}$$

$$h'' = \{(P - T_1).\hat{t}_l\}/|(T_2 - T_1)| \quad \text{C.7}$$

where, the value of angle θ is determined as:

$\theta = \cos^{-1}\{(D_v - R_o)/R_i\}$, such that $(0° < \theta < 90°)$

If the value of h and h'' satisfied the criteria that $0 \leq h, h'' \leq 1$, then the point of contact is considered as valid.

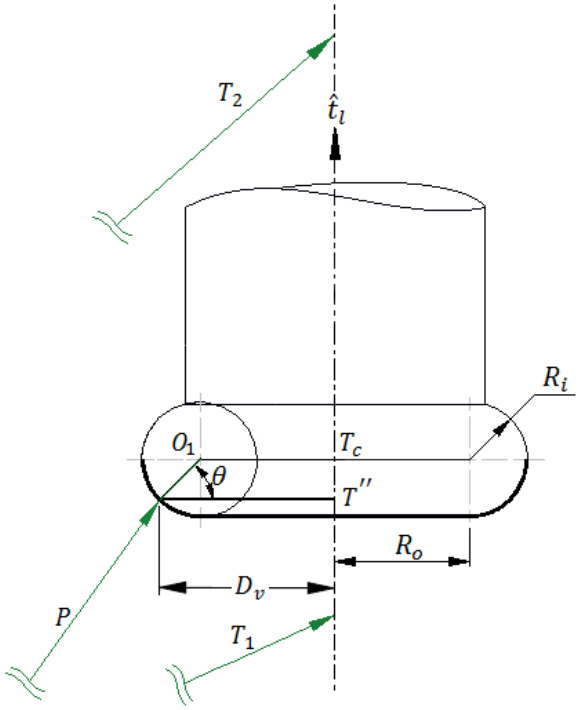

Figure C.2: A raised vertex on triangulated surface touching radiused corner of toroidal tool

When the highest tool center location is determined from a vertex touching the radiused corner of the tool, we can use the value of T_c for 3-axis tool positioning, whereas for 5-axis tool positioning the concept of numerical DTM method is used. In this case, the vertex P touching the radiused corner of the tool is the point of contact itself as shown in figure C.2. The unit projection vector $\hat{n}_p$, the center of pseudo-insert O_1 through point of contact P and hence the unit surface normal $\hat{n}$ can be found as:

$$\hat{n}_p = (T'' - P)/|T'' - P| \quad \text{C.8}$$

$$O_1 = T_c - R_o.\hat{n}_p \quad \text{C.9}$$

$$\hat{n} = (O_1 - P)/|O_1 - P| \quad \text{C.10}$$

Further the values of T_1, T_2, $\hat{n}$, $\hat{n}_p$, P, h, T_c, and O_1 are used as input to determine the 5-axis tool positioning using numerical DTM method using the procedure described in section 5.2.2.

REFERENCES

[1]. Warkentin A., Ismail F., and Bedi S. (2000) Comparison between multipoint and other 5-axis tool positioning strategies, International Journal of Machine Tools and Manufacture, Elsevier, 40(2):185-208

[2]. Rao N., Ismail F., and Bedi S. (1997) Tool path planning for five-axis machining using the principal axis method, Internation+al Journal of Machine Tools and Manufacture, Elsevier, 37(7):1025-1040

[3]. Rao N., Bedi S., and Buchal R.(1996) Implementation of the principal-axis method for machining of complex surfaces, Int. Journal of Advanced Manufacturing Technology, Springer-Verlag London, 11(4):249-257

[4]. Bedi S., Gravelle S., and Chen Y. (1997) Principal curvature alignment technique for machining complex surfaces, Journal of manufacturing Science and Engineering, 119(4B):756-765

[5]. Warkentin A., Ismail F., and Bedi S. (1998) Intersection approach to multi-point machining of sculptured surfaces, Computer Aided Geometric Design, Elsevier, 15(6):567-584

[6]. Gray P., Ismail F., and Bedi S. (2004) Graphics-assisted rolling ball method for 5-axis surface machining, Computer-Aided Design, Elsevier, 36(7):653-663

[7]. Gray P., Bedi S., and Ismail F. (2005) Arc-intersect method for 5-axis tool positioning, Computer-Aided Design, Elsevier, 37(7):663-674

[8]. Hosseinkhani Y., Akbari J., and Vafaeesefat A. (2007) Penetration–elimination method for five-axis CNC machining of sculptured surfaces, Int. Journal of Machine Tools and Manufacture, Elsevier, 47:1625-1635

[9]. Dong Z., Li H. and Vickers G. W. (1993) Optimal rough machining of sculptured parts on a CNC milling machine, Journal of Engineering for Industry, Transactions of the ASME, 115(4):424-432

[10]. Lai J.-Y., and Wang D.-J. (1994) A strategy for finish cutting path generation of compound surfaces, Computers in Industry, Elsevier, 25:189-209

[11]. You C.-F., and Chu C.-H. (1995) An automatic path generation method of NC rough cut machining from solid models, Computers in Industry, Elsevier, 26:161-173

[12]. Dragomatz D., and Mann S. (1997) A classified bibliography of literature on NC milling path generation, Computer-Aided Design, Elsevier, 29(3):239-247

[13]. Hwang J. S., and Chang T. C. (1998) Three-axis machining of compound surfaces using flat and filleted endmills, Computer-Aided Design, Elsevier,30(8):641-647

[14]. Warkentin A., Ismail F., and Bedi S. (2000) Multi-point tool positioning strategy for 5-axis machining of sculptured surfaces, Computer Aided Geometric Design, Elsevier, 17:83-100

[15]. Rao N., Ismail F., and Bedi S. (2000) Integrated tool positioning and tool path planning for five-axis machining of sculptured surfaces, Int. Journal of Production Research, Taylor & Francis, 38(12):2709-2724

[16]. Spence A. D., Abrari F. and Elbestawi M. A. (2000) Integrated solid modeller based solutions for machining, Computer-Aided Design, Elsevier, 32:553-568

[17]. Fleisig R.V. and Spence A. D. (2001) A constant feed and reduced angular acceleration interpolation algorithm for multi-axis machining, Computer-Aided Design, Elsevier, 33:1-15

[18]. Byrne G., Dornfeld D., and Denkena B. (2003) Advancing cutting technology, CIRP Annals - Manufacturing Technology, Elsevier, 52 (2):483-507

[19]. Jun C.-S., Cha K., and Lee Y. S. (2003) Optimizing tool orientations for 5-axis machining by configuration-space search method, Computer-Aided Design, Elsevier, 35(6):549-566

[20]. Lasemi A., Xue D., and Gu P. (2010) Recent development in CNC machining of freeform surfaces: A state-of-the-art review, Computer aided Design, Elsevier, 42:641-654

[21]. Li H., and Feng H.-Y. (2004) Efficient five-axis machining of freeform surfaces with constant scallop height tool paths, International Journal of Production Research, Taylor & Francis, 42(12): 2403-2417

[22]. Li H., Tutunea-Fatan O. R. and Feng H.-Y. (2007) An improved tool path discretization method for five-axis sculptured surface machining, Int. Journal of Advanced Manufacturing Technology, Springer, 33:994-1000

[23]. Makhanov S. S. (2010) Adaptable geometric patterns for five-axis machining: a survey, International Journal of Advanced Manufacturing Technology, Springer, 47:1167-1208

[24]. Fard M. J. B., and Feng H.-Y. (2010) Effective determination of feed direction and tool orientation in five-axis flat-end milling, Journal of Manufacturing Science and Engineering, ASME, 132:1-10

[25]. Zhou, Sheng Y., Yang Xu J., and Chen Z. C. (2011) Vector calculation for tool envelope surface in five-axis NC machining, Advanced Materials Research, 314:1242-1245

[26]. Fard M. J. B., and Feng H.-Y. (2011) New criteria for tool orientation determination in five-axis sculptured surface machining, International Journal of Production Research, Taylor & Francis, 49(20):5999–6015

[27]. Lin Z., Fu J., Shen H., and Gan W. (2014) An accurate surface error optimization for five-axis machining of freeform surfaces, International Journal of Advanced Manufacturing Technology, Springer, 71:1175-1185

[28]. Gilles P., Cohen G., Monies F., and Rubio W. (2014) Machining strategy in five-axis milling using balance of the transversal cutting force, Int. Journal of Advanced Manufacturing Technology, Springer, 72:1377-1387

[29]. Kim Y.-J., Elber G., Bartoň M. and Pottmann H. (2015) Precise gouging-free tool orientations for 5-axis CNC machining, Computer-Aided Design, Elsevier, 58:220-229

[30]. Vickers G. W. (1977) Computer-aided manufacture of marine propellers, Comp-Aided Design, 9(4):267-274.

[31]. Balasubramaniam M., Laxmiprasad P., Sarma S., and Shaikh Z. (2000) Generating 5-axis NC roughing paths directly from a tessellated representation, Computer aided Design, Elsevier, 32:261-277

[32]. Cho J. H., Kim J. W., and Kim K. (2000) CNC tool path planning for multi-patch sculptured surfaces, International Journal of Production Research, Taylor & Francis, 38(7):1677-1687

[33]. Chuang C. -M., Chen C. -Y., and Yau H. -T. (2002) A reverse engineering approach to generating interference-free tool paths in three-axis machining from scanned data of physical models, International Journal of Advanced Manufacturing Technology, Springer-Verlag London, 19:23-31

[34]. Xu X. J., Bradley C., Zhang Y. F., Loh H. T., Wong Y. S. (2002) Tool-path generation for five-axis machining of free-form surfaces based on accessibility analysis, International Journal of Production Research, Taylor & Francis, 40(14):3253-3274

[35]. Jun C.-S., Kim D.-S., and Park S. (2002) A new curve-based approach to polyhedral machining, Computer-Aided Design, Elsevier, 34:379-389

[36]. Park S. C. (2004) Sculptured surface machining using triangular mesh slicing, Computer-Aided Design, Elsevier, 36:279-288

[37]. Chen Z. C., Dong Z., and Vickers G. W. (2003) Automated surface subdivision and tool path generation for 3 ½ ½-axis CNC machining of sculptured parts, Computers in Industry, Elsevier, 50:319-331

[38]. Lauwers B., Kiswanto G. and Kruth J. P. (2003) Development of a five-axis milling tool path generation algorithm based on faceted models, CIRP Annals - Manufacturing Technology, Elsevier, 52(1):85-88

[39]. Zhou Z. D., Zhou J. D., Chen Y. P., Ong S. K., and Nee A. Y. C. (2003) Geometric simulation of NC machining based on STL models, CIRP Annals - Manufacturing Technology, Elsevier, 52(1):129-134

[40]. Kaplan C. S., Bedi S., Mann S., Israeli G., and Poon G. (2004) A new paradigm for woodworking with NC machines, Computer-Aided Design, Elsevier, 4:1-10

[41]. Yau H. -T., Chuang C. -M., and Lee Y. S. (2004) Numerical control machining of triangulated sculptured surfaces in a stereo lithography format with a generalized cutter, International Journal of Production Research, Taylor & Francis, 42(13):2573–2598

[42]. Ahn S.-H., Kim D.-S., Chu W.-S., and Jun C.-S. (2005) MIMS: web-based micro machining service, International Journal of Computer Integrated Manufacturing, Taylor & Francis, 18(4):251-259

[43]. Chuang C.-M., and Yau H.-T. (2005) A new approach to z-level contour machining of triangulated surface models using fillet end mills, Computer-Aided Design, Elsevier, 37(10):1039–1051

[44]. Kim S.-J., and Yang M.-Y. (2005) Triangular mesh offset for generalized cutter, Computer-Aided Design, Elsevier, 37:999-1014

[45]. Lee D.-Y., Kim S.-J., Kim H.-C., Lee S.-G., and Yang M.-Y. (2006) Incomplete two-manifold mesh-based tool path generation, International Journal of Advanced Manufacturing Technology, Springer, 27:797-803

[46]. Qu X., and Stucker B. (2006) Raster milling tool-path generation from STL files, Rapid Prototyping Journal, Emerald, 12(1):4-11

[47]. Yuwen S., Dongming G., Zhenyuan J., and Haixia W. (2006) Iso-parametric tool path generation from triangular meshes for free-form surface machining, International Journal of Advanced Manufacturing Technology, Springer, 28:721-726

[48]. Bu Y., Sun Q., Chen X., Chen Q., and Zhang X. (2007) Research on the algorithm of tool path rapid generation for NC machining of molar prosthesis, Computer-Aided Design and Computer Graphics, IEEE, 525-528

[49]. Kim S.-J., and Yang M.-Y. (2007) Incomplete mesh offset for NC machining, Journal of Materials Processing Technology, Elsevier, 194:110-120

[50]. Kiswanto G., Lauwers B., and Kruth J. P. (2007) Gouging elimination through tool lifting in tool path generation for five-axis milling based on faceted models, International Journal of Advanced Manufacturing Technology, Springer, 32:293-309

[51]. Manos N. P., Bedi S., Miller D. and Mann S. (2007) Single controlled axis lathe mill, International Journal of Advanced Manufacturing Technology, Springer-Verlag, 32:55-65

[52]. Chen T., and Shi Z. (2008) A tool path generation strategy for three-axis ball-end milling of free-form surfaces, Journal of Materials Processing Technology, Elsevier, 208:259-263

[53]. Lee S.-G., Kim H.-C., and Yang M.-Y. (2008) Mesh-based tool path generation for constant scallop-height machining, International Journal of Advanced Manufacturing Technology, Springer, 37:15-22

[54]. Lu J., Cheatham R., Jensen C. G., Chen Y., and Bowman B. (2008) A three-dimensional configuration-space method for 5-axis tessellated surface machining, International Journal of Computer Integrated Manufacturing, Taylor & Francis, 21(5):550-568

[55]. Poon G., Gray P. J., Bedi S., and Miller D. (2008) Architecture for direct model-to-part CNC manufacturing, Systemics, Cybernetics and Informatics, 4(1):14-18

[56]. Yang D. O., and Feng H.-Y. (2008) Machining triangular mesh surfaces via mesh offset based tool paths, Computer-Aided Design and Applications, Taylor and Francis, 5(1-4):254-265

[57]. Li W., Yin Z., Huang Y., Wu T., and Xionga Y. (2010) Tool path generation for triangular meshes using least-squares conformal map, International Journal of Production Research, Taylor & Francis, 49(12):3653-3667

[58]. Patel K., Bolaños G. S., Bassi R., and Bedi S. (2011) Optimal tool shape selection based on surface geometry for three-axis CNC machining, International Journal of Advanced Manufacturing Technology, Springer, 57:655-670

[59]. Tapie L., Mawussi B., and Bernard A. (2012) Topological model for machining of parts with complex shapes, Computers in Industry, Elsevier, 63:528-541

[60]. Sortino M., Belfio S., Motyl B., and Totis G. (2013) Compensation of geometrical errors of CAM/CNC machined parts by means of 3D workpiece model adaptation, Computer-Aided Design, Elsevier, 48:28-38

[61]. Azzam N., Chaves-Jacob J., Boukebbab S., and Linares J.-M. (2014) Adaptation of machining toolpath to distorted geometries: application to remove a constant thickness on rough casting prosthesis, International Journal of Advanced Manufacturing Technology, Springer, 72:1073-1083

[62]. Bolaños G. S., Bedi S., and Mann S. (2014) A topological-free method for three-axis tool path planning for generalized radiused end milled cutting of a triangular mesh surface, International Journal of Advanced Manufacturing Technology, Springer, 70(9-12):1813-1825

[63]. Duvedi R. K., Bedi S., Batish A., Mann S. (2014) A multipoint method for 5-axis machining of triangulated surface models, Computer-Aided Design, Elsevier, 52:17–26. DOI: 10.1016/j.cad.2014.02.008

[64]. Huertas-Talón J. L., García-Hernández C., Berges-Muro L., and Gella-Marín R. (2014) Obtaining a spiral path for machining STL surfaces using non-deterministic techniques and spherical tool, Computer-Aided Design, Elsevier, 50:41-50

[65]. Duvedi R. K., Bedi S., Batish A., and Mann S. (2015) Numeric implementation of drop and tilt method of 5-axis tool positioning for machining of STL surfaces, International Journal of Advanced Manufacturing Technology, Springer-Verlag London, 78:1677-1690, DOI: 10.1007/s00170-014-6636-3

[66]. Duvedi R. K., Batish A., Bedi S., and Mann S. (2015) Scallop height of 5-axis machining of large triangles with a flat end mill, Computer Aided Design and Applications, Taylor and Francis, Published online: 29 April 2015, DOI: 10.1080/16864360.2015.1033334

[67]. Duvedi R. K., Bedi S., Batish A., and Mann S. (2015) A method for simplifying edge-torus tangency in drop-tilt method for 5axis machining of triangulated surfaces, Accepted in 4th International Symposium on NC Machining (CNCM 2015) held at HKUST, Hong Kong, China in June 3-5, 2015

[68]. Xu J., Sun Y., and Zhang L. (2015) A mapping-based approach to eliminating self-intersection of offset paths on mesh surfaces for CNC machining, Computer-Aided Design, Elsevier, 62:131-142

[69]. Duvedi R. K., Bedi S., Batish A., and Mann S. (2015) The edge-torus tangency problem in multipoint machining of triangulated surface models, Accepted for publication in International Journal of Advanced Manufacturing Technology, Springer-Verlag London, on 1st July, 2015

[70]. Lin C.-Y., Hwang Y.-Y., and Lai J.-Y. (1997) Interference-free cutting-path generation based on scanning data, International Journal of Advanced Manufacturing Technology, Springer, 13:535-547

[71]. Kawabe S., Kimura F., and Sata T. (1980) Generation of NC commands for sculptured surface machining from 3-coordinate measuring data, CIRP Annals - Manufacturing Technology, Elsevier, 29(1):369-372

[72]. Feng H.-Y., and Teng Z. (2005) Iso-planar piecewise linear NC tool path generation from discrete measured data points, Computer-Aided Design, Elsevier, 37:55-64

[73]. Teng Z., Feng H.-Y.and Azeem A. (2006) Generating efficient tool paths from point cloud data via machining area segmentation, International Journal of Advanced Manufacturing Technology, Springer, 30:254-260

[74]. Chui K. L., Chiu W. K., and Yu K. M. (2008) Direct 5-axis tool-path generation from point cloud input using 3D biarc fitting, Robotics and Computer-Integrated Manufacturing, Elsevier, 24:270-286

[75]. Makki M., Lartigue C., Tournier C., and Thiébaut F. (2008) Direct duplication of physical models in discrete 5-axis machining, Virtual and Physical Prototyping, Taylor & Francis, 3(2):93-103

[76]. Mehta N. K., Pandey P. C., and Chakravarti G. (1983) An investigation of tool wear and the vibration spectrum in milling, Wear, Elsevier, 91(2):219–234

[77]. Bedi S., Ismail F., Mahjoob M. J., and Chen Y. (1997) Toroidal versus ball nose and flat bottom end mills, International Journal of Advanced Manufacturing Technology, Springer-Verlag London, 13:326-332

[78]. Jenson C. G., Red W. E., and Pi J. (2002) Tool selection for five-axis curvature matched machining, Computer-Aided Design, Elsevier, 34:251-266
[79]. Senatore J., Segonds S., Rubio W., and Dessein G. (2012) Correlation between machining direction, cutter geometry and step-over distance in 3-axis milling: Application to milling by zones, Computer-Aided Design, Elsevier, 44:1151-1160
[80]. Khan M. R., and Tandon P. (2013) Mathematical modeling of a generic multi-profile form milling cutter, Proceedings of the Institution of Mechanical Engineers, Part C: Journal of Mechanical Engineering Science, 227(5):1036–1046
[81]. Khan M. R., and Tandon P. (2013) Parameterized geometric design of a generic form milling cutter, Computer Aided Design & Applications, 10(5):757-765
[82]. Lacalle L. N. Lopez de, and Lamikiz A. (2008) Sculptured surface machining, Machining Fundamentals and Recent Advances, Springer London, Chapter 8:225-248
[83]. Marshall S., and Griffiths J. G. (1994) A new cutter-path topology for milling machines, Computer Aided Design, Elsevier, 26(3):204-214
[84]. Park S. C., and Choi B. K. (1999) Tool-path planning for direction-parallel area milling, Computer-Aided Design, Elsevier, 32:17-25
[85]. Kim B. H., and Choi B. K. (2002) Machining efficiency comparison direction-parallel tool path with contour-parallel tool path, Computer-Aided Design, Elsevier, 34:89-95
[86]. You C.-F., and Chu C.-H. (1997) Tool-path verification in five-axis machining of sculptured surfaces, International Journal of Advanced Manufacturing Technology, Springer, 13:248-255
[87]. Mann S., and Bedi S.(2002) Generalization of the imprint method to general surfaces of revolution for NC machining, Computer-Aided Design, Elsevier, 34(5):373–378
[88]. Li C., Mann S., and Bedi S. (2005) Error measurements for flank milling, Computer-Aided Design, Elsevier, 37(14):1459–1468
[89]. Reddy N. S. K., and Rao P. V. (2005) Selection of optimum tool geometry and cutting conditions using a surface roughness prediction model for end milling, The International Journal of Advanced Manufacturing Technology, Springer, 26 (11-12):1202–1210
[90]. Reddy N. S. K., and Rao P. V. (2005) A genetic algorithmic approach for optimization of surface roughness prediction model in dry milling, International Journal of Machining Science & Technology, Taylor & Francis, 9(1):63-84
[91]. He Y., and Chen Z. (2014) Optimising tool positioning for achieving multi-point contact based on symmetrical error distribution curve in sculptured surface machining, International Journal of Advanced Manufacturing Technology, Springer-Verlag London, 73:707-714
[92]. Mann S., Bedi S., Israeli G., and Zhou X. (L.) (2010) Machine models and tool motions for simulating five-axis machining, Computer-Aided Design, Elsevier, 42:231-237
[93]. Xu X.W., and Newman S.T. (2005) Making CNC machine tools more open, interoperable and intelligent—a review of the technologies, Computers in Industry, Elsevier, 57:141-152
[94]. Moriwaki T. (2008) Multi-functional machine tool, CIRP Annals - Manufacturing Technology, 57:736-749
[95]. Zeid I. (1991) CAD/CAM theory and practice, McGraw-Hill
[96]. Piegl L., and Tiller W. (1995) Curve and surface basics, Springer

[97]. Farin G. (2002) Curves and surfaces for CAGD, Morgan Kaufmann, 5th edition
[98]. Duncan J. P., and Mair S. G. (1993) Sculptured surfaces in engineering and medicine, Cambridge University Press, Cambridge, UK.
[99]. Austin S., Jerard R., and Drysdale R. (1997) Comparison of discretization algorithms for NURBS surfaces with application to numerically controlled machining, Computer-Aided Design, 29(1):71-83.
[100]. Qu X. and Stucker B. (2003) A 3D surface offset method for STL-format models, Journal of Rapid Prototyping, Emerald, 9(3): 133–141.
[101]. Kim S.-J., and Yang M.-Y. (2006) A CL surface deformation approach for constant scallop height tool path generation from triangular mesh, International journal of advance manufacturing technology, 28:314–320
[102]. Hwang J. S. (1992) Interference-free tool-path generation in the NC machining of parametric compound surfaces, Computer-Aided Design, 24:667–676
[103]. Chen Z. C., Vickers G. W. and Dong Z. (2004) A new principle of CNC tool path planning for three-axis sculptured part machining - a steepest-ascending tool path, Journal of Manufacturing Science and Engineering, 126:515-523
[104]. Huang Y. and Oliver J. H. (1992) Non-constant parameter NC tool path generation on sculptured surfaces, ASME Journal of Computer in Engineering, 1:411-419
[105]. Suh S. H., Lee B. E., Chung D. H., and Cheon S. U. (2003) Architecture and implementation of a shop-floor programming system for STEP-compliant CNC, Journal of Computer-Aided Design, Elsevier, 35:1069–1083
[106]. Gray P. J., Bedi S. and Mann S. (2003) A new paradigm for numerically controlled machines", Virtual Concept, Biarritz, France, 128-134
[107]. Gray P. J., Poon G., Israeli G., Bedi S., Mann S., and Miller D. (2005) Model to part: a road map for the CNC machine of the future, 7th International Conf. on Adv. Manuf. Systems and Technology, Udine, Italy
[108]. Broomhead P., and Edkins M. (1986) Generation NC data at the machine tool for the manufacture of free-form surfaces, International Journal of Production Research, 24(1):1-14
[109]. Chen Y.J., and Ravani B. (1987) Offset surface generation and contouring in computer-aided design, ASME Journal of Mechanisms, Transmissions & Automation in Design, 109:132-142
[110]. Cho H. D. and Yang M. Y. (1995) A study on the five-axis end milling for sculptured surfaces", KSME Journal, 9(4): 428-437
[111]. Cho J. H., Kim J. H. and Kim K. (2000) CNC tool path planning for multi-patch sculptured surfaces, International Journal of Production Research, Taylor and Francis, 38(7):1677-1687
[112]. Choi B. K., Lee C. S., Hwang J. S. and Jun C. S.(1988), Compound surface modeling and machining, Computer-Aided Design, 20:126–136
[113]. Chung Y. C., Park J. W., Shin H. and Choi B. K.(1998) Modeling the surface swept by a generalized cutter for NC verification, Computer-Aided Design, 30:587–594
[114]. Choi B. K., Kim D. H. and Jerard R. B. (1997) C-space approach to tool-path generation for die and mold machining, Computer-Aided Design, 29:657–669
[115]. Lee E. (2003) Contour offset approach to spiral tool path generation with constant scallop height, Computer-Aided Design, Elsevier, 35: 511–518

[116]. Choi B. K., and Jerard R. B. (1998) Sculptured surface machining - theory and applications, Dordrecht, Kluwer Academic Publishers
[117]. Jensen C.G., Anderson D.C. (1996) A review of numerically controlled methods for finish-sculpture-surface machining. IIE Transactions, 28(1):30-39.
[118]. Hatna A., Grieve R.J., Broomhead P. (1998) Automatic CNC milling of pockets: geometric and technological issues. Computer Integrated Manufacturing Systems, 11(4):309-330.
[119]. Hu P., Tang K., Lee C-H. (2013) Global obstacle avoidance and minimum workpiece setups in five-axis machining, Computer-Aided Design, 45: 1222-1237
[120]. Tang T. D. (2014) Algorithms for collision detection and avoidance for five-axis NC machining- A state of the art Review, Computer-Aided Design, 51: 1-17